Mathematical Modelling of Fluid Flow and Heat and Pollutant Transport in a Porous Medium with Embedded Objects

Khadija Tul Kubra

Institute of Natural and Mathematical Sciences

Massey University, Albany, New Zealand

A thesis submitted in partial fulfilment of the requirements for the degree of

Doctor of Philosophy (PhD) in Mathematics

May 2018

Abstract

How does heat and/or pollutant transfer from objects embedded in the ground depend on their size, shape and burial depth, and how does the dispersion of heat and/or pollution in groundwater aquifers depend on the soil properties, the speed of the groundwater flow, etc.? In detail, the aims of present study are:

- To investigate how the size, shape and position of an object or set of solid or partially pervious objects, e.g., fluid tanks, pipes, etc., embedded in a porous medium affect the local speed and shape of the flow.

- If heat is ejected from the solid objects e.g., fuel storage cylindrical tanks, radioactive waste reservoirs in deep geological formations, etc., and/or a pollutant is released from, or removed by, the pervious object, e.g., septic tanks, disposal of drums of contaminants, etc., how does the subsequent dispersal through a groundwater aquifer depend on the various parameters involved (e.g., the object size, object's burial depth, perviousness of the object, the aquifer's depth, the fluid flow rates, etc.)?

- What is the effect of the non-homogeneity in matrix properties (e.g. permeability or hydraulic conductivity) on fluid flow, pollutant and heat transport rates?

This study pursues answers to these questions. The porous medium fluid flow equations, and the advection-dispersion equations that model the heat and/or species transport, have coefficients that depend mainly on depth. Generally, analytic solutions are not possible. In order to investigate the effects of various objects of different shapes embedded in a porous medium, I have developed numerical algorithms and used some special mathematical techniques for two-dimensional models, namely conformal mappings within the framework of complex analysis.

The velocity potential and (2-D) stream function satisfy Laplace's equation. Central and one-sided finite difference methods are applied to solve this equation subject to a chosen combination of constant-head or constant-flux boundary conditions. Results are discussed for various embedded shapes in homogeneous and layered groundwater aquifers. A Matlab command "contour" is used to depict the streamlines and equipotential lines, and the resulting temperature or pollutant concentrations.

Steady-state and time-dependent forced convection heat/pollutant transfer from some cylinders embedded in groundwater are explored numerically using finite difference methods. The results show that the size, shape, position, perviousness and burial depth of the cylinder affect the pressure drop, as well as the pollutant and/or heat transfer. Moreover advection and dispersion depend on the permeability structure and the fluid speed.

Acknowledgements

I have no words to express my deepest sense of gratitude to the Almighty Allah (God), who enabled me to complete this thesis.

Next, I am extremely grateful to my supervisors Robert McKibbin and Winston L. Sweatman whose knowledge, inspiration, guidance, suggestions and encouragement helped me all along during my research work. I am deeply indebted to my supervisor Robert McKibbin who gave me the opportunity to work for the *Mathematical modelling of fluid flow and heat and pollutant transport in a porous medium with embedded objects.*

Also, my sincere thanks are due to Government College University Faisalabad, Pakistan for granting me with a doctoral scholarship under *Faculty Development Program* (FDP), and Massey University for providing me with the best learning facilities, healthy environment and opportunities for research.

I wish to record my deepest obligations to my beloved father Abdul Rashid, respected mother Shamshad Begum, lovely sisters and brothers for their prayers for my success and unfailing support. I am greatly obliged to Almighty Allah (God) for having them in my life.

I would be unfair if I don't mention my fellow PhD colleagues and friends in New Zealand who have been encouraging me with their worthwhile suggestions, discussions, and support not only in my studies but also in various other fields. Special thanks to all my well wishers, family members and teachers.

Finally, I avail this opportunity to thank my dear husband Sana Ullah Lehre, and my sweet children, Umama Gul Gaity and Moeez Hassan for their prayers and moral support throughout my studies and stay in New Zealand. I also welcome to my new born baby Muhammad Ali Obaid Lehre during my PhD studies.

Contents

Nomenclature

Symbol	Units	Description
Bi	[-]	Biot number
c	[J kg^{-1} K^{-1}]	specific heat
C	[kg m^{-3}]	concentration of pollutant in the fluid
D	[m^2 s^{-1}]	tensor coefficient of mechanical dispersion of a dissolved pollutant while it flows in the porous media
D	[m^2 s^{-1}]	scalar coefficient of mechanical dispersion of a dissolved pollutant while it flows in the porous media
D_{th}	[m^2 s^{-1}]	thermal diffusion/dispersion coefficient
g	[m s^{-2}]	gravitational acceleration
h	[m]	height of the vertical wall
k	[m^2]	isotropic permeability of the porous medium
K	[m s^{-1}]	hydraulic conductivity
n	[-]	porosity of the porous media
Nu_f	[-]	time-mean average fluid Nusselt number
Nu_s	[-]	time-mean average solid Nusselt number
P	[kg m^{-1} s^{-1}]	mass flux of a pollutant
p	[kg m^{-1} s^{-2}]	absolute pressure of the fluid
Q	[m^2 s^{-1}]	total flux through the whole aquifer per unit width of the aquifer, subscripts L, R and I stand for flux in, flux out, and net flow across the pervious rectangular/cuboidal cross section, respectively
Ra	[-]	Rayleigh number

Re	[-]	Reynolds number
t	[s]	time
T	[K]	temperature
$\mathbf{V}$	[m s^{-1}]	average three-dimensional Darcy velocity vector of fluid $\mathbf{V}=(u,v,w)$

Greek Symbols

α	[m]	dispersion length (dispersivity) of the porous medium
α_L	[m]	longitudinal dispersivity
α_T	[m]	transversal dispersivity
α_{th}	[m]	coefficient of thermal diffusion/dispersion
β_{ps}	[m]	coefficient of pressure difference (which is a measure of resistance of the object's surface to flow through it)
ϕ	[m]	two- and three-dimensional velocity potential function
Φ	[m^2 s^{-1}]	$\Phi = K\phi$
$\gamma = \alpha_L/\alpha_T$	[-]	ratio of longitudinal to transverse dispersivity
κ_{ms}	[W m^{-1} K^{-1}]	thermal conductivity
ω_{ps}	[s^{-1}]	constant of proportionality
μ	[kg m^{-1} s^{-1}]	dynamic viscosity of the fluid
ρ	[kg m^{-3}]	density of water (constant)
ψ	[m]	two-dimensional stream function
Ψ	[m^2 s^{-1}]	$\Psi = K\psi$
σ	[-]	coefficient of thermal advection
ξ, η	[m]	transformed coordinates

Subscripts

e	effective
f	fluid
ˆ	transformed variable
I	internal
L	left

m	mixture (formation+fluid)
ms	mixture saturated
ps	porous surface
R	right

Chapter 1

Introduction

Transport phenomena within porous media[1] is a subject of common interest and has emerged as a distinct field of study. The mechanism of fluid flow in a porous medium relates to many problems crucial to engineering, applied science and industry, e.g., groundwater hydrology, reservoir engineering, soil science, soil mechanics and chemical engineering. For example, civil engineers manage the water flow in aquifers, transmission of moisture through and under engineering constructions, advection and dispersion of pollutants (or tracers) in aquifers and prediction of stresses under engineering systems. Movement of water and solute transport in the root zone in the soil is tackled by agricultural engineers. Chemical engineers face problems related to heat and mass transfer in packed-bed reactor columns, solid catalyzed reactions and drying phenomena. Flow of oil, water and gas in petroleum reservoirs, and recovery of fuels from underground oil and gas reservoirs are encountered in reservoir engineering. In all these examples, one or more quantities that are additive over volume, mass, momentum and energy are transported through the solid or liquid phase of a porous medium domain. In such a domain, the solution of a transport problem means to determine the spatial and temporal distributions of state variables. *State variables* include velocity, mass density and pressure of a fluid phase, concentration of a solute and stress in the solid skeleton [12].

---

[1] A material that contains pores (voids) is called a porous medium (or a porous material). The skeletal portion of the material is often called the "matrix" or "frame". Normally, the pores are filled with a fluid (liquid and/or gas). Generally, the skeletal material is a solid, but in many occasions, foam like substances are also considered as porous media.

Dissertation topic and motivation of the study

This thesis deals with the mathematical modelling of incompressible fluid flow and transport of pollutant/heat released from leaky/hot bodies embedded in homogeneous[2] and non-homogeneous aquifers. The reason for undertaking the study of pollutant transport in groundwater aquifers leaking from some underground buried formations (e.g., septic tanks, drums of contaminants, leaky swimming pools, broken sewerage pipes, etc.), is that groundwater pollution is one of the major threats to public health in the whole world. Water quality has deteriorated during the last few decades not only in my home country Pakistan but all over the globe. Regarding drinking water quality, Pakistan ranks at number 80 among 122 nations [8].

Drinking water quality is poorly monitored and managed all over the country. Drinking water sources, both surface and groundwater are contaminated not only by human activities but also by agrochemicals, and industrial and municipal wastes. A frequent violation in drinking water quality parameters set by WHO (World Health Organisation) is observed.

In Pakistan, the area near to my locality, Ghulam Muhammad Abad, Faisalabad is notorious for its poor quality of drinking water. Sewerage pipes are quite old and cracked at many places. As a result of which, groundwater is polluted severely by this contaminated water and people ignorantly are forced to drink this polluted water, which results in the form of many health problems, e.g., a high rate of hepatitis, cholera, and many other infectious and fatal bacterial diseases of small intestine, etc.

The Government of Pakistan has established some organisations/acts to improve drinking water quality. Among them are: Ministry of Environment, Pakistan; NWFP, North West Frontier Province (former name of Khyber Phakhtoonkhwa Province); NWQM, National Water Quality Monitoring; PAK-EPA, Pakistan Environmental Protection Agency: PCRWR, Pakistan Council for Research in Water Resources: and PEPO, Pakistan Environmental Protection Ordinance [8].

As a researcher, I want to contribute my expertise at a national and international level. The prime applications of this research would be: special emphasis on major pollutants, sources of

---

[2]A porous medium domain is said to be *homogeneous* with respect to its *permeability*, if the *permeability* is the same at all its points. If not, the domain is called heterogeneous, or *non-homogeneous* [11].

pollution, remediation of different pollutants, and the consequent health problems.

A project in Japan is working on the possibility of re-use of buried cylindrical tanks. Once, these cylinders are used for fuel storage at motor vehicle service stations, and afterwards would be re-used as thermal repositories connected to space heating systems, e.g., utility stores, in Japan [34]. The study of heat transport from underground buried cylindrical tanks is motivated by the above project. To seek new resources of energy, this project should be initialised in other countries as well, specially in the developing ones.

In this work, the phenomenon of pollutant and heat transport in groundwater aquifers works on a similar basis. In both cases, it is assumed that fluid is incompressible and Darcy's law is applicable. The only difference between these two models is that: transport of heat occurs for solid objects, whereas, transport of pollutant takes place for pervious bodies embedded in a porous medium.

Porous medium

The concept of porous media is used in many areas of applied science and engineering, e.g., filtration, mechanics (acoustics, geomechanics, soil mechanics, rock mechanics), engineering (petroleum and geothermal engineering, bio-remediation, construction engineering), geosciences (hydrogeology, petroleum geology, geophysics), biology and biophysics, material science, etc. [11]. Soil, sand, fissured rock, cemented sandstone, Karstic limestone, man-made materials such as cements and ceramics, foam rubber, zeolites, bread, biological tissues (e.g. bones, wood, cork), lungs and kidneys are some examples of natural and artificial porous media. Some additional examples of porous medium domains include aquifers[3], petroleum reservoirs which provide oil and/or gas, sand filters for purifying water, packed-beds in the chemical engineering industry and the root zone in agriculture [12]. The aquifer, is the porous medium domain explored by the ground water hydrologist, and the oil reservoir, is the porous medium domain investigated by the reservoir engineer [11].

The *porosity n* is the major characteristic of a porous medium, which is defined as the ratio of volume of the void spaces (U_v) to the bulk volume (U_b) of a porous medium, averaged over a

---

[3]A geological formation, or a stratum, that contains water with a considerable amount of water passing through it [11].

suitably-sized representative elementary volume (REV) [11]:

$$n = \frac{U_v}{U_b} = \frac{U_b - U_s}{U_b},$$

(1.1)

where U_s is the volume of solids within U_b. Other properties of the medium are permeability, hydraulic conductivity, transmissivity, tensile strength and electrical conductivity, etc.

Mathematical modelling

Several types of mathematical models have been used to investigate groundwater flow problems. These models can be distinguished into analogue and mathematical models; the latter can be solved using analytical and numerical techniques [44]. Hydrologists usually use mathematical models to analyse groundwater flow problems. These models contain a set of differential equations along with initial and boundary conditions whose solutions demonstrate the groundwater flow. The mathematical models are usually solved using a mixture of analytical and numerical techniques. Modelling the physics of three different media like solids, fluids and porous media is an important area in engineering and mathematical problems. Due to the complexity and non-linear nature of fluid flow in porous media, direct experimentation methods are often used to investigate the nature of the fluid flow in a porous medium.

Almost all mathematical models are composed of a set of partial differential equations (PDE's) with appropriate initial and boundary conditions within and on the porous medium's boundaries, layer interfaces, and on the object's surfaces. Generally, analytic solutions are not possible. Numerical modelling of the problem is established on the basis of the assumption that if the flow is incompressible then the velocity potential satisfies Laplace's equation. Hence, the governing equation, in terms of velocity potential for two- and three-dimensional flows, is Laplace's equation, which is discretized together with boundary conditions, using finite-difference methods. For some geometries, a two-dimensional formulation allows the use of a stream function (a complementary function that also satisfies Laplace's equation). Here, Matlab is used to compute approximations to the velocity potential and stream function. The

Matlab command "contour" is used to depict the equipotential lines[4] and streamlines[5], and all the contour lines are equally spaced. All the modelling is done numerically by my own computer coding and no special Matlab package/subroutine is used to solve the equation.

Both three-dimensional (XYZ, where the xy-plane is horizontal and the positive z-axis is aligned vertically upwards) and two-dimensional (XZ) Cartesian coordinate systems are used. Because of the rectangular meshes used, it is laborious to model the problems for shapes of higher complexity, such as ellipses, circles, polygons and irregular objects embedded in porous media. To overcome this difficulty, a special mathematical technique of complex analysis, namely conformal mapping, has been used for the solution of fluid and pollutant/heat flow (two-dimensional problems) in the porous media. For a homogeneous porous medium, the basis of the complex potential is that the two-dimensional velocity potential and stream function for steady and unsteady flow are both harmonic functions. Since harmonic functions remain harmonic under conformal mappings, transformation of complicated flow boundaries into regular flow geometries allows the use of a standard method.

This work - an outline

This work is composed of seven chapters, with the current one being the introduction of the thesis. The reader is led to comprehend the meanings of the various parameters and coefficients involved in the explanation of flow problems in porous media. The concept of velocity potential, stream function and conformal transformation is also introduced in this chapter. Mathematics has substantial implementations in the field of advanced engineering mathematics, partial differential equations, vector analysis, Cartesian tensor analysis, fluid mechanics and elements of the theory of functions. Obviously, it is not possible to review every example of each subject treated. Although I discuss the topic in general, the surfaces are restricted to simply-shaped objects, thus excluding chemical and electrochemical surfaces.

---

[4] The lines/surfaces where the velocity potential is constant are referred to as *equipotential lines/surfaces or isobars*.

[5] The lines for which the stream function is constant are referred to as *streamlines*.

In Chapter 2, a background of the topic is included. Nusselt[6], Peclet[7], and Reynolds[8] numbers are introduced. A comparison of *LTE* (one-equation energy model)[9] and *LTNE* (two-equation energy model)[10] models is also discussed in detail.

Chapter 3 deals with the mathematical modelling of the problem, conceptual models are represented in the form of mathematical formulations. The equations of conservation of mass, momentum and energy in a continuum give a good start to the next step and the motion equations describe the behaviour of the fluid flow for the general case of an isotropic and homogeneous aquifer. Modelling is initiated with the equation of motion for an incompressible fluid, starting from its two-dimensional form and then extending the idea to three-dimensional flow in homogeneous aquifers.

Due to the limitation on analytical solutions, most of the results are simulated numerically. A relationship between the stream function and the piezometric head is also added in that chapter. Once the continuity or mass conservation equations have been established, the next natural step is to examine the initial and boundary conditions on a porous medium domain as well as on the objects embedded in it. For two- and three-dimensional cases, rectangular and cuboidal homogeneous aquifers, respectively are discussed. The effects of the presence of impermeable/pervious rectangular and triangular objects on fluid flow are investigated. It is demonstrated that the flow rates are affected not only by the parameter β_{ps} (which is a measure of resistance of the object's surface to flow through it), but also by the geometries and positions of the objects embedded in aquifers. However, the results remain unaltered for different domain sizes. Afterwards, the problem is approximated by a Hele-Shaw cell[11].

Chapter 4 deals with the fluid flow in two- and three-dimensional non-homogeneous aquifers.

---

[6]In heat transfer at a boundary (surface) within a fluid, the Nusselt number (Nu) is the ratio of convective to conductive heat transfer across (normal to) the boundary. In this context, convection includes both advection and diffusion.

[7]The Peclet number is defined to be the ratio of the rate of advection of a physical quantity by the flow to the rate of diffusion of the same quantity driven by an appropriate gradient.

[8]The Reynolds number is defined as the ratio of inertial forces to viscous forces and consequently quantifies the relative importance of these two types of forces for given flow conditions.

[9]In a local thermal equilibrium (*LTE*) energy model it is supposed that within a representative elementary volume (REV), the solid and fluid phase have the same temperature.

[10]In this model, both fluid and solid are assigned individual local temperatures, as a result of which heat transfer occurs between the two phases.

[11]This term is usually used for cases in which a fluid is injected between (from above or below) two parallel flat impervious plates separated by a small gap. It occurs when a less viscous fluid is injected displacing a more viscous one or vice versa. The governing equation of Hele-Shaw flows is similar to that of the inviscid potential flow and to the flow of fluid through a porous medium (Darcy's law).

The porous media that constitute aquifers and oil reservoirs are rarely homogeneous with respect to their permeability. A non-homogeneous aquifer may be composed of several parallel layers of different texture. In this work, it is assumed that, within each layer, the properties of the medium remain uniform. The groundwater flow within each layer is considered to be due to a pressure gradient across each layer. Transfer of the pollutant may occur across the layer interfaces as well as along the strata.

Various cases are discussed in the absence and presence of impermeable and pervious objects embedded in the non-homogeneous aquifers. The conceptual model starts with the assumption that the non-homogeneous aquifer system is composed of horizontal and vertical layers of different thicknesses. Because of recharge or pumping of groundwater, there is a large variation in the value of dynamic pressure[12] in each sub-layer. For horizontally layered aquifers, for the vertical movement of the water, the vertical speed and the dynamic pressure have an equal value above and below the interface. In fact, there is no barrier at horizontal interfaces and they are just sitting between the sub-layers, so the pressure is continuous across the boundary. However, for a vertically layered non-homogeneous aquifer, the dynamic pressure and horizontal speed of fluid on the interface have a value equal to that of the adjacent layers.

Moreover, a short discussion about the permeable objects, whose permeability is different from the outer porous media is also added. The conceptual model is justified by graphical representation of contouring plots of equipotential and streamlines. Lastly, the modelling is continued for the motion of fluids in three-dimensional aquifers.

Chapter 5 presents the transport phenomena of waste disposal in deep geological formations in both homogeneous and non-homogeneous porous media. In each case, the discussion leads to the construction of a complete mathematical model of the problem. Advection and dispersion of the pollutant in the vicinity takes place due to motion of the underground water and the permeability structure of adjacent layers, respectively. A general comparison of the cases:

1. when dispersion depends on fluid speed and direction,

---

[12]The kinetic energy per unit volume of a fluid particle is called dynamic pressure.

2. when dispersion depends upon fluid speed only, and

3. when dispersion is uniformly constant,

have been discussed for various values of the parameters.

In Chapter 6, heat flow from buried cylindrical tanks submerged in groundwater is modelled. A complex variable technique, namely conformal mapping, is introduced for both fluid and heat flow. The transformed problem is then solved numerically subject to the mapped boundary conditions in the $\xi\eta$-plane. This model is based on the assumptions that: the groundwater flow speed is very slow, cold water is entering in the region from the upstream boundary and passes by the cylinder which is assumed to be kept at a constant temperature; no heat is generated by the system and the cylinder is completely buried in the ground. Elliptic and diamond-shaped cylinders are considered. It is found that the shape and burial depth of the cylinder, the thickness of the aquifer, permeability structure of the medium, and the positions of the upstream and downstream boundaries have a great impact on predicted fluid and heat fluxes.

In Chapter 7, a summary of the theoretical background in the form of mathematical models is discussed, a short conclusion and some future proposals are also recommended there.

Finally, for the justification of the mathematical models, derivations and calculations for some mathematical equations are added in the form of Appendices. An analytic solution for the derivation of time-dependent as well as steady-state heat equations from the xz-plane to the transformed $\xi\eta$-plane is also included in Appendix A.

Figure 1.1 is the schematic diagram of rectangular porous media with one inlet and one exit, that are enclosed in an envelope marked by a blue boundary. In these porous media, there are embedded various cylinders of different cross-sections. Water enters from the left-hand side upstream boundary, passes through the porous medium with embedded objects at various positions and leaves from the right-hand side exit. The objects may be impermeable, pervious, or be kept at constant temperature.
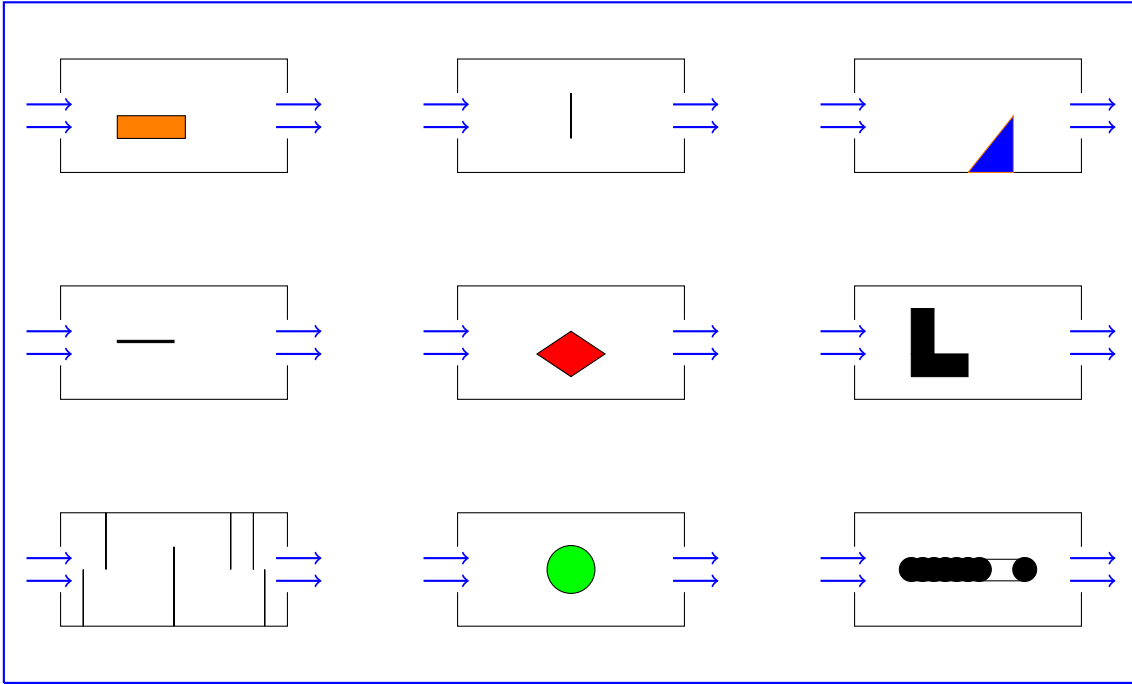
Figure 1.1: *Some cross-sections of cylinders, that will be investigated in the thesis, embedded in rectangular porous mediums (thick black lines), with one entrance and one exit. The outer thick blue boundary just serves as an envelope for these porous media.*

Figure 1.2 illustrates the example of fluid flow in a multilayered aquifer with two impermeable rectangular cylinders mounted at different positions. The aquifer is composed of two layers of different permeabilities, the top layer is ten times more permeable than the lower one. The separation zone between these two regions is marked by a dashed black line which is called the interface. Refraction in streamlines and equipotential lines can be seen along this interface. Water is entering and leaving the aquifer from upstream (marked by red line on L.H.S) and downstream (blue line on R.H.S) boundaries respectively.
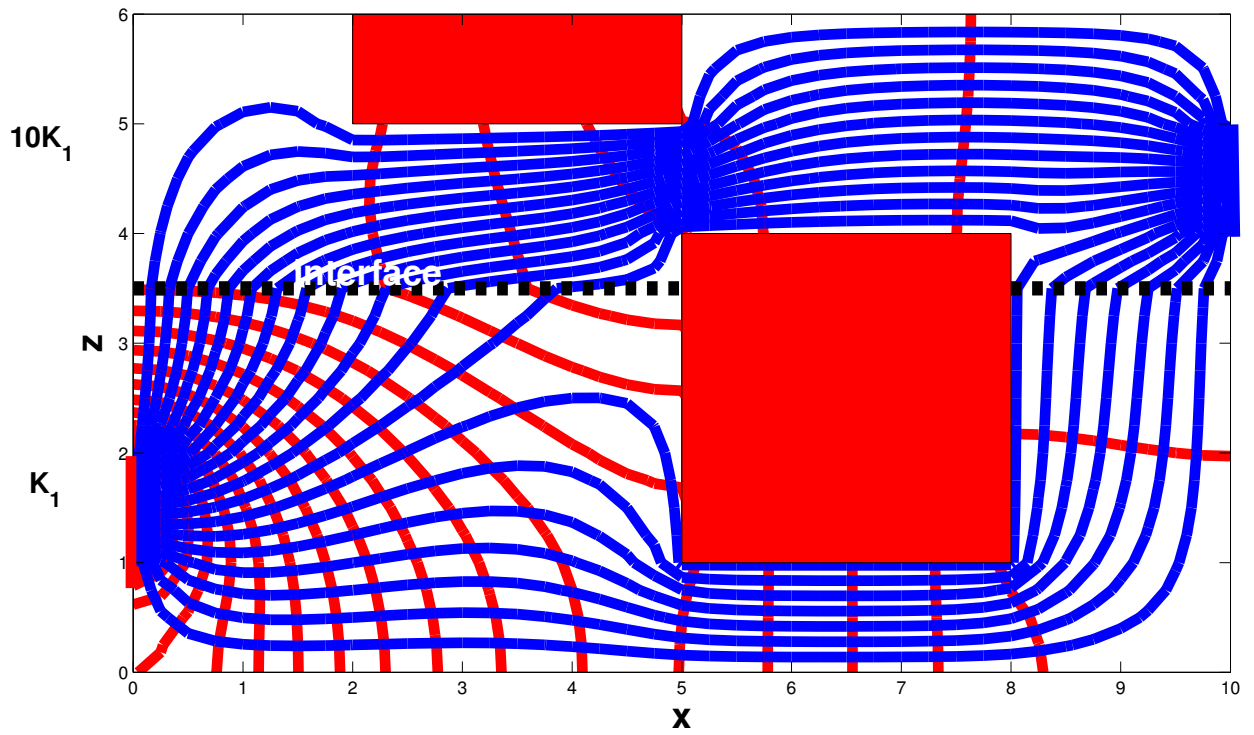
Figure 1.2: *Example of the numerical solution for the velocity potential ϕ (red lines) and stream function ψ (blue lines) with two rectangular objects (prisms) embedded in a layered porous medium with inflows and outflows. This is a typical example of what will be investigated later.*

Chapter 2

Background

Modelling heat and mass transfer from embedded objects in porous media has been a topic of great interest for researchers of geophysics and engineering for the last three decades or so. An extensive range of solution techniques are available for the solution of fluid flow and transport problems in porous media incorporating numerical and analytical techniques. When it is the matter of solving a realistic field problem, due to limitations on analytic solutions, it becomes challenging for the scientists to achieve their goals. Currently, such problems become practicable numerically by the advent of super computers.

Steady and non-steady groundwater flow problems can be solved by the finite difference method, which was first proposed by 20th century scientists (Southwell,1940; Forsythe and Wasow, 1960; Fox, 1962; Kantorovich and Krylov, 1964), who used it for the solution of engineering problems [13]. In this study, we will focus our attention on the finite difference method to solve two- and three-dimensional flow problems of incompressible flow, pollutant and heat transfer from/to objects embedded in groundwater. We will deal with various flow problems with the help of velocity potentials and stream functions.
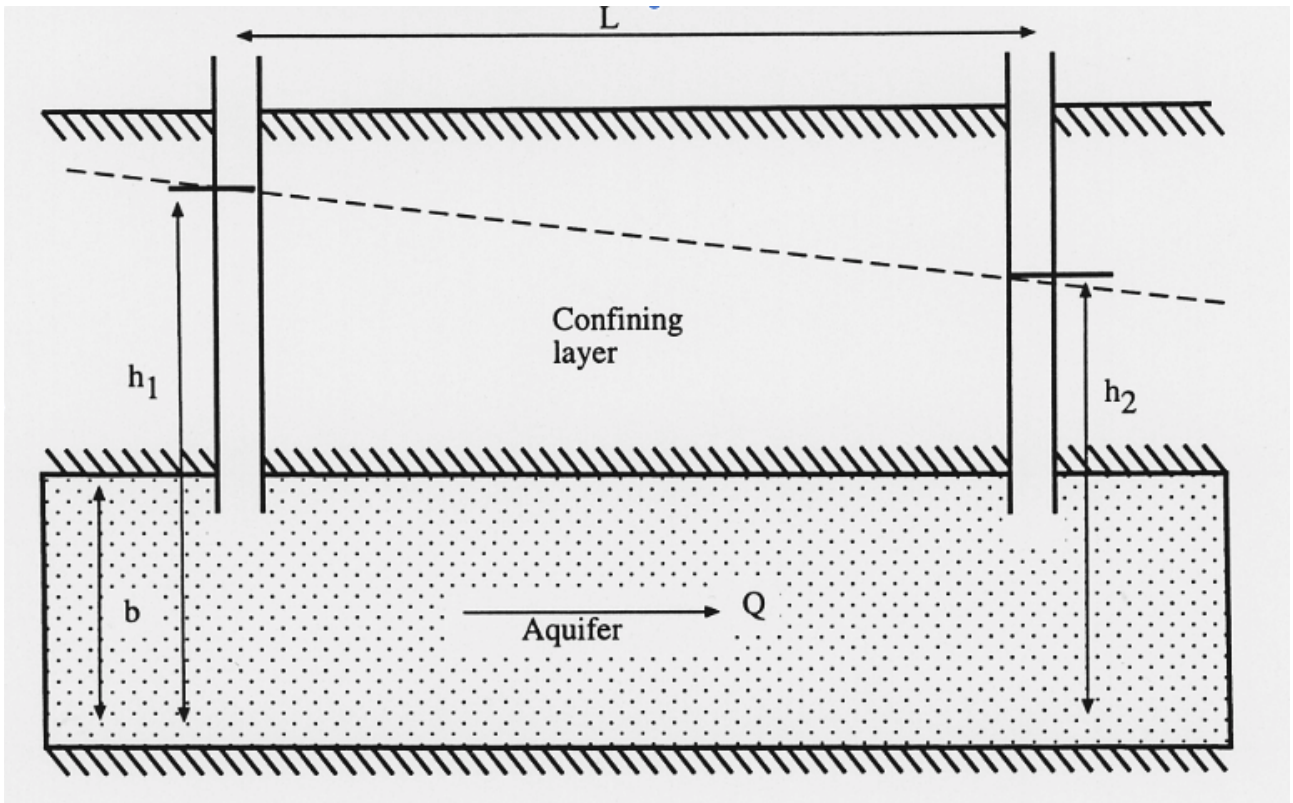
Figure 2.1: *Schematic diagram of Darcy's law in groundwater aquifers. Here, Q $[m^2 s^{-1}]$ is the fluid flux, and h_1, h_2 in [m] are the piezometric heads in the two wells. Later on, the symbols ϕ_1 and ϕ_2 are used as piezometric heads.*

Henry Darcy was a French hydraulic engineer who pioneered the modelling of fluid flow in saturated porous media and proposed several theories about groundwater flow [20]. Darcy's law[1] was based on the results of experimental data on the flow of water through beds of sands. An interesting factor about this law is that it is analogous to Fourier's law[2] in the field of heat conduction, Ohm's law[3] in the field of electricity, or Fick's law[4] in diffusion theory.

After the introduction of Darcy's model, several extensions and modifications were made by researchers of various disciplines including chemical, mechanical and civil engineering. There has been considerable work published in the field of convective heat and pollutant transfer

---

[1]In 1856, Henry Darcy deduced that flow rate in porous media is proportional to head loss and inversely proportional to the length of the flow path, i.e., $Q \propto (-dh/L)$, $dh = h_2 - h_1$, see Figure 2.1.

[2]Fourier's law, states that the time rate of heat transfer through a material is proportional to the negative gradient in the temperature and to the area, at right angles to that gradient, through which the heat flows.

[3]Ohm's law postulates that the current through a conductor between two points is directly proportional to the voltage difference across the two points. Introducing the constant of proportionality, the resistance R, the mathematical formulation of the law is that $I = \frac{V}{R}$, where I is the current through the conductor in units of amperes, V is the voltage measured across the conductor in units of volts, and R is the resistance of the conductor in units of ohms.

[4]Fick's law states that the diffusion flux goes from regions of high concentration to regions of low concentration, with a magnitude that is proportional to the concentration gradient.

in porous media stimulated by a large number of geophysical and engineering applications. Nield and Bejan [39] comprehensively reviewed the phenomenon of thermally-driven convection in porous media. It is well established that using porous media with higher thermal conductivity can increase heat transfer.

Some analytical, numerical and experimental review articles and monographs have been produced by, for example, Cheng [16], Tien and Vafai [51], Kakac *et al.* [27], Ingham and Pop [24], Vafai [53], Pop and Ingham [42]. All these studies demonstrate the concept of heat transfer in porous media. However, a lot of work on the above stated topic has dealt with either convection near plane walls or in channels filled with porous medium.

To date little work has been published on convective heat and pollutant (or tracers) transfer from heated bodies of higher complexity or leaking structures buried in porous media, such as a tank filled with liquid or gas, a pipe, building foundations, cylinders embedded in porous media, etc.

Chemical species such as tracers or dissolved pollutants are dispersed by flow in groundwater aquifers. Soluble compounds are not only advected downstream together with fluid flow but are spread in all directions. This happens mainly due to the phenomenon of mechanical dispersion of fluid flow in complex porous formations. The aquifer may be composed of several different layers of non-uniform thickness. However, when a rock system contains different layers, the average permeability of the system can be measured for some simple flow cases.

Many researchers, for example Van Herwaarden [54] investigated fluid flow and pollutant transport in porous media. In his study, he found that the horizontal and vertical coefficients of dispersion are proportional to the fluid speed. Moreover he found that the solution obtained by asymptotic approximations only depends on the point of intersection of the boundary with the streamline leading away from the stagnation point, and not on the particular shape of the boundary. Burr *et al.* [15] examined the field-scale transport of reactive and nonreactive groundwater solutes in a statistically anisotropic aquifer by means of high-resolution, three-dimensional numerical solutions of the steady state flow and transient advection-dispersion equations. In this analysis, a relationship was established between fluid velocity, longitudinal and transversal plume spreading of reactive and non-reactive solutes transport and the results

were verified with those available in the literature. Moreover, it was also explored that the longitudinal macrodispersivity of a reactive solute could be enhanced comparative to that of a nonreactive one through heterogeneous aquifers.

McKibbin [32] published an interesting study using simplified layered models to discuss the parallel discretization of groundwater confined aquifers of different physical properties. Afterwards, McKibbin [33] formulated the coupled mass-balance equation for multi-layered systems in confined[5] aquifers. The latter work was extended more generally by Ali *et al.* [4, 5, 6, 7] when pollutant transport in phreatic[6] and confined aquifers were taken into consideration. In this study, some simplified modelling of pollutant transport as well as pollutant remediation in one- and two-dimensional homogeneous and non-homogeneous aquifers was presented. The pollutant remediation model of this study was for the remediation strategy called In Situ Chemical Oxidation (ISCO) and the reaction between pollutant and remediation agent was taken to be of order two.

Jourak *et al.* [26] studied the longitudinal (D_L) and transverse (D_T) dispersion coefficients for flow through randomly packed beds of discrete monosized spherical particles. The derived values of D_L and D_T in the 3-D packed beds of spheres are in good agreement with those available in the literature at low Peclet numbers. It was found that, as the porosity decreases, D_L and D_T also decrease at very low Peclet numbers. However, the effect of porosity at high Peclet numbers was negligible. Moreover, changing the pore structure from random to perturbed hexagonal close-packed packing shows higher values of D_L and D_T at low Peclet numbers. However, at higher Peclet numbers ($Pe_m > 2$), because in the case of an ordered structure there is lower irregularity of the flow front, so the resulting D_L and D_T have lower values as compared to the system that had been packed randomly.

Singh *et al.* [48] derived the analytical solution for solute transport along the unsteady groundwater flow in a semi-infinite porous medium by the Laplace Transformation Technique. For predicting the contamination concentration profiles in the different geological formations such as aquitards and aquifers, an exponentially decreasing, sinusoidal, asymptotic, and algebraic sigmoid form of velocity expression are taken into account. These geological formations are

---

[5]Confined aquifers are those which are bounded above and below by impermeable layers of clay that prohibits water seepage into the aquifer.

[6]Phreatic aquifers are those which are not confined above.

composed of gravel, sand and sandy clay and solute concentration for these materials is predicted for their average porosities. Later on, Singh *et al.* [49] mathematically modelled the solute transport in finite aquifers. A comparison between analytical and numerical solution was given for contaminant concentration for two different time domains and the results of the model were verified with those available in the literature. Dalwadi *et al.* [19] presented a mathematical model about chemical agent removal by reaction with an immiscible cleanser. Their study demonstrates how different features of a cleanser affect the speed of decontamination. Moreover, they found that the changing cleanser concentration affects the removal time of a chemical agent and using a more potent cleanser may not enhance the removal time of the agent.

Heat transfer from a circular cylinder submerged in a fluid saturated porous media has many experimental implementations such as compact heat exchangers, nuclear reactors, solar power collectors and in radioactive waste containers in deep geological structures, where the waste serves as a large heat source. The studies to date underpin the usefulness of using mathematical modelling to investigate fluid flow and heat transport in a porous medium with embedded objects. Moreover, most of the studies published on this particular topic have been extensively investigated by using either free (natural or buoyant)[7] or mixed (combination of forced[8] and free) convection. Typical examples of the free or mixed convection are the pioneering work of Merkin [35], Cheng [17], Ingham and Pop [25], Badr and Pop [9], Pop and Cheng [41], Zhou and Lai [60] and Saeid [46], whereas, forced convection has been given less attention by researchers. Garimella and Schlitz [21] analysed experimentally the enhancement of forced convection heat transfer in a rectangular duct from discrete heat sources with water and FC-77. Generally, fluorocarbon liquids (e.g., FC-72, FC-86, FC-77, etc.) are considered to be the most suitable liquids for direct immersion cooling. It was found that the Nusselt number data from FC-77 coolant are higher than those from water coolant.

Most of the studies presented so far on forced convection have applied Darcy's law to build a relationship between flow velocities and the applied pressure gradient. Pop & Yan [43] and

---

[7]Natural convection is a process, or type of heat transfer, in which the fluid motion is caused only by density differences in the fluid occurring due to temperature gradients but not produced by any external source (like a pump, fan, suction device, etc.).

[8]Forced convection is a mechanism, or type of heat transfer in which fluid motion is produced by an external source (like a pump, fan, suction device, etc.).

Sano [47] applied this model to explore analytic solutions of the energy equation for large and small Peclet number. Kimura [29] analytically and numerically investigated transient forced convective heat transfer from a circular cylinder in a saturated porous medium. The Nusselt number was calculated analytically at transient and steady-states. It was found that the length of the transient periods generally decrease with increasing Peclet numbers. Layeghi and Nouri-Borujerdi [30] numerically computed the thermal field around the cylinder; it was found to vary with the porosity of the porous medium and not with the permeability. The steady-state problem was studied for Peclet number ≤ 40 with constant Prandtl number equal to 1.

Several other authors have applied other types of Darcy model. Murty *et al.* [37], for example, used the Darcy-Brinkman-Forchheimer (DBF) model and presented streamlines and equipotential lines for a single Prandtl and certain ranges of Darcy and Reynolds number; it was found that the heat transfer is not effected much by the Forchheimer extension of Darcy's equations. J. Thevenin and D. Sadaoui [50] used the Darcy-Brinkman model to analyse the conditions of the enhancement of heat transfer over a circular cylinder immersed in porous medium and observed the influence of various local and mean Nusselt numbers with certain ranges of the Reynolds, Darcy and Peclet numbers on streamlines and isotherms. It was found that the permeability of the porous medium has no influence on the temperature field whereas, it has strong effects on the velocity field.

One- and two-equation energy models which are referred to as local thermal equilibrium (LTE) and local thermal non-equilibrium ($LTNE$) models, respectively, are used by many researchers. It appears that the LTE model was used in all the above studies, i.e., within a representative elementary volume (REV), the temperature of the solid and fluid phase is considered to be the same. However the LTE assumption is rejected by several authors due to the fact that when advection and conduction techniques vary significantly in transferring heat, the temperature difference between solid and fluid phase also increases significantly. Pop & Cheng [41] also noticed that when the particle size in the solid porous matrix is similar to, or more than, the thermal boundary layer thickness, the LTE model may not be applicable. To overcome these difficulties, a $LTNE$ model is introduced. According to this model, local temperatures are assigned independently to the solid and fluid phases during heat transfer.

The two-equation energy model has been applied by Rees *et al.* [45] and Wong *et al.* [57]. Gazy

et al. [3] and Gazy [2] included Darcian affects, i.e. combining the effects of solid boundaries, inertia and thermal dispersion with the *LTNE* assumptions to analyse time-dependent forced convection heat transfer from a single cylinder and then from banks of four circular cylinders, immersed in a horizontal packed bed of spherical particles. In the first study [3], it was found that using the one-equation energy model there is a continuous increase in Nu_f (time-mean average fluid Nusselt number) against κ_r (solid/fluid thermal conductivity ratio); however, the two-equation energy model predicts that relationship between Nu_f against κ_r (for $\kappa_r > 10$) is completely produced by the Biot number Bi ($B_i = hL/\kappa_s$, where h is the convection heat transfer coefficient, L is the characteristic length scale, κ_s is the thermal conductivity of the solid medium). Also, Bi is directly proportional to Nu_s (time-mean average solid Nusselt number) and inversely proportional to Nu_f. Moreover, the effect of Reynolds number Re on Nu_f is much higher than that of κ_r and Bi due to the effect of thermal dispersion.

In the later study [2], a numerical investigation was made to find the characteristics of fluid flow and forced convection heat transfer around a bank of four circular cylinders, in two alignments; staggered and in-line, embedded in a different metallic or non-metallic porous horizontal channel. It was found that both Nu_f and $Nu_{f\phi}$ (steady-state local fluid Nusselt number) have a significant dependence on Re_D (Reynolds number, D stands for cylinder diameter), SP (Spacing parameter), and the type of cylinder bank alignment. However, the variation of Nu_f (steady-state average fluid Nusselt number) with SP is unaltered with varying κ_r. Moreover, the results show that, the staggered arrangement of cylinders is highly recommended from practical and economical aspects due to a high level of thermal performance in construction of actual tubular heat exchangers. In addition, it is evident that heat transfer increases as a result of thermal dispersion and this effect is more dominant than that of spacing between cylinders and the type of the porous material used.

A three-dimensional mixed convection in a fluid saturated cubic porous medium with an isothermally heated cubic body embedded at its centre is examined by Krishna Murthy *et al.* [36] for various values of the Rayleigh number and for several geometries of the hot object for different injection/suction velocities. In their study, they found that when $Ra < 100$, a three-dimensional symmetry of flow as well as temperature distribution is visible. However, for $Ra > 100$, the three-dimensional symmetry to the four vertical planes, is replaced by a two-dimensional sym-

metry for flow and temperature fields. Moreover, with an increase in Ra beyond 100, mixed heat transfer and descending expansion of thermal plumes are observed in the lower half of the cuboidal porous media as well as under the hot body.

Applications of this research are not only in groundwater hydrology, it could be extended to any field relating to heat and mass transfer in porous media. Recently, a novel possible application of my research is found in heat transfer in skin cancer treatment, and it would be innovative for future PhD students. In this study, Casey *et al.* [40] developed a mathematical model for obtaining an optimal temperature distribution in a 3-D triple-layered rectangular skin structure with an embedded countercurrent vasculature comprised of seven-level blood vessels, arteries and veins and a tumor appearing in the subcutaneous area. The tumor tissue is injected with gold nano-shells with an optimized laser intensity. Numerical results show that, within the pain tolerance limit of the patients, the tumor tissue can be heated and maintained above 42 °C while the temperature of the surrounding healthy tissue remains low enough in order to keep it from being damaged.

It is very interesting to note that the concept of leaky objects embedded in two- and three-dimensional, homogeneous and non-homogeneous groundwater aquifers, is my own and original contribution. I reviewed the literature, but found very little about leaky bodies with finite dimensions embedded in groundwater aquifers. So far, no work has been reported on three-dimensional forced convection heat/pollutant transfer from leaky/hot objects embedded in fluid-saturated cubic porous media. In this study, an example of pollutant transport in a three-dimensional aquifer is included in Chapter 5. The only concerns at this stage, are to find a relationship between longitudinal and transversal dispersivities and to obtain their effects on the shape of pollutant plumes. Further study will focus on three-dimensional forced convection pollutant/heat transport in a porous medium with embedded objects, where two-dimensional slices may be taken to explore the effects of various parameters on pollutant/heat plumes.

The main objective of the present study is to mathematically model:

1. fluid flow in a porous medium in which there are embedded one or more impermeable and pervious two- and three-dimensional objects (e.g. a tank, a pipe, building foundations in a groundwater aquifer),

2. the transport of heat or a pollutant (or tracer) that is injected into a groundwater aquifer together with a fluid source that may be associated with the object(s) (e.g., heat from a tank, pollution from a leaking pipe, injected waste water, or that removed by pumping or leaking),

3. the effects of longitudinal and transversal dispersivities on shape of the pollutant plume, and to establish a relationship between them.

The concentration of the pollutant will vary laterally and vertically because of advection by the fluid, mechanical dispersion by the flow in the porous matrix, and interlayer transfer across the layer interfaces. All of these aspects will depend on the mechanical parameters of the matrix system (including layer thicknesses, porosities, permeabilities and dispersivities) as well as background pressure gradient, etc.

The modelling will include cases where there is significant fluid injection into, and/or withdrawal from, an aquifer system. The presence or otherwise of a background flow due to a natural pressure gradient will also be considered. The mathematical models will be solved using a mixture of analytical (using conformal transformations) and numerical techniques. The most popular equation to describe the flow of fluids through porous media has famously been described by Darcy's law [20].

Darcy's law is adequate for studying a substantial class of flows through porous media; however, this law does not help to solve all problems. One example is a flow wherein the range of pressure involved is very large and high pressure gradients are at play [28]. To overcome this difficulty, a new formulation which involves a relationship between pressure and pressure gradients is included in Chapter 3. This relationship is derived by taking into account Darcy's law and will be discussed in detail for various values of the parameters involved in the formulation.

Chapter 3

Fluid Flow Model for a Homogeneous Aquifer

The objective of this chapter is to develop the mathematical models that describe transport phenomena in homogeneous aquifers in which there are embedded various cylinders of different shapes. To achieve this goal, we start with a short analysis of some basic concepts of continuum mechanics. Furthermore, we establish balance equations for several substantial quantities of interest. Expressions for fluxes are introduced that come into view in the balance equations. Finally, after the discussion of the nature of boundaries, models for discussion include potential flow[1] in a two- and a three-dimensional homogeneous aquifer in the:

1. absence of impermeable and pervious objects,

2. presence of impermeable objects of different sizes and shapes, placed at various positions in the aquifer, and

3. presence of pervious objects with the pressure inside different from those at the inlet and outlet.

The first model will give a comparison for fluid flow in groundwater aquifers without impermeable and pervious objects. This modelling will include examples of fluid flow in aquifers with one or more entrances and exits, and give measurements for pressure and fluid flow rates.

---

[1]The flow of an inviscid (ideal) incompressible fluid is known as *potential flow*.

In the second model, study of impermeable buried cylindrical tanks will be extended for modelling of heat transfer. In Chapter 6, I will look at the cases when one or more impermeable objects are embedded in the groundwater and will explore the effects of their size, shape, burial depth, and their position on fluid flow and heat transport rates.

Modelling about pervious objects embedded in groundwater aquifers for model three will be helpful in the study of groundwater pollution (pollutant leaking from septic tanks, disposals of drums of contaminants, etc.) in Chapter 5. Examples of leaky cylinders which are completely buried in the groundwater and pollutant which are leaking from the whole surface of the cylinder or from a part of the cylinder will be discussed in detail for various values of the parameters involved.

The development of mathematical models for each case is discussed below.

3.1 Eulerian coordinate systems

By *Eulerian* we mean information (pressure, say) at a position relative to some "zero" position or *origin*. By coordinate systems we mean methods to measure space. One example of Eulerian coordinate systems is the Cartesian (x, y, z) (in case of 2D, (x, y)) system for a box, as shown in Figure 3.1. It should be noted that all the coordinate system axes are orthogonal.
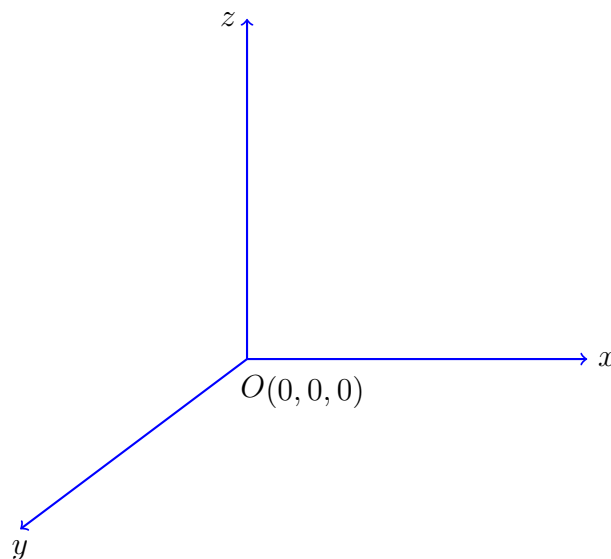
Figure 3.1: *Cartesian coordinate system.*

Using a three-dimensional Cartesian coordinate system XYZ, where the xy-plane is horizontal

and the positive z-axis is aligned vertically upwards as shown in Figure 3.1, we will discuss the fluid flow through a homogeneous porous medium. For the two-dimensional case, a rectangular domain, and for the three-dimensional case a cuboidal domain, are used.

3.2   Three-dimensional modelling of aquifers

The visualisation of two- and three-dimensional flow and vector fields is one of the major tasks in scientific visualisation. In general, flow through aquifers is three-dimensional. Darcy's law[2] gives the specific discharge (or specific volume flux) $\mathbf{V}$ $(\text{m}^3/\text{s})/\text{m}^2$ through a surface perpendicular to the flow velocity vector whose components are given as:

$$\mathbf{V}(x, y, z) = u(x, y, z)\mathbf{i} + v(x, y, z)\mathbf{j} + w(x, y, z)\mathbf{k}. \tag{3.1}$$

Generally in the three-dimensional case, the continuity equation (conservation of fluid mass equation) for a fluid with uniform density, is expressed by:

$$\nabla \cdot \mathbf{V} = \mathbf{0}, \quad \text{implies} \tag{3.2}$$

$$\frac{\partial u}{\partial x} + \frac{\partial v}{\partial y} + \frac{\partial w}{\partial z} = 0. \tag{3.3}$$

According to Darcy's law, the velocity vector $\mathbf{V}(x, y, z)$, where z is vertical, is proportional to gradient of dynamic pressure. The momentum equation for the water flow is Darcy's law:

$$\mathbf{V}(x, y, z) = \frac{k}{\mu}(-\nabla p + \rho \mathbf{g}), \tag{3.4}$$

where k [m^2] is the *intrinsic permeability*, μ [kg m^{-1} s^{-1}] is the *fluid dynamic viscosity*, ρ [kg m^{-3}] is the *fluid density*, p [kg m^{-1} s^{-2}] is the *absolute pressure of the fluid*, and $\mathbf{g} = (0, 0, -g)$

---

[2]Darcy velocity is the volume flow rate of water per unit area through a cross-sectional area perpendicular to the flow direction.

[m s^{-2}] is the *gravitational acceleration.* Hence, the velocity components are expressed by:

$$u(x, y, z) = \frac{k}{\mu}\left(-\frac{\partial p}{\partial x}\right), \tag{3.5}$$

$$v(x, y, z) = \frac{k}{\mu}\left(-\frac{\partial p}{\partial y}\right), \tag{3.6}$$

$$w(x, y, z) = \frac{k}{\mu}\left(-\frac{\partial p}{\partial z} - \rho g\right). \tag{3.7}$$

The piezometric level, or head, ϕ (the level to which water will rise in a well that penetrates a groundwater aquifer) is referred to here as the velocity potential which is defined by:

$$\phi = \left(\frac{p}{\rho g} + z\right). \tag{3.8}$$

Then the components of velocity in terms of ϕ are written as:

$$u(x, y, z) = -\frac{\rho g k}{\mu}\frac{\partial \phi}{\partial x}, \tag{3.9}$$

$$v(x, y, z) = -\frac{\rho g k}{\mu}\frac{\partial \phi}{\partial y}, \tag{3.10}$$

$$w(x, y, z) = -\frac{\rho g k}{\mu}\frac{\partial \phi}{\partial z}. \tag{3.11}$$

3.3 Two-dimensional modelling of aquifers

In the case where the flow has negligible dependence on y, the equation of continuity gives

$$\frac{\partial u}{\partial x} + \frac{\partial w}{\partial z} = 0. \tag{3.12}$$

As we are assuming that flow is two-dimensional, so it is convenient to introduce another function, which is plausible only for such a case and is the so-called stream function $\psi(x, z)$ [m]. The function $\psi = \psi(x, z)$ is a measure of total flow and components of velocity in terms of the stream function can be defined as:

$$u(x, z) = \frac{\rho g k}{\mu}\frac{\partial \psi}{\partial z}, \tag{3.13}$$

$$w(x, z) = -\frac{\rho g k}{\mu}\frac{\partial \psi}{\partial x}. \tag{3.14}$$

In terms of components of velocity the two-dimensional velocity potential is:

$$u(x, z) = -\frac{\rho g k}{\mu}\frac{\partial \phi}{\partial x}, \qquad (3.15)$$

$$w(x, z) = -\frac{\rho g k}{\mu}\frac{\partial \phi}{\partial z}. \qquad (3.16)$$

The functions (ϕ, ψ) satisfy the Cauchy-Riemann (C-R) equations; they are related to each other by:

$$\frac{\partial \phi}{\partial x} = -\frac{\partial \psi}{\partial z}, \qquad (3.17)$$

$$\frac{\partial \phi}{\partial z} = \frac{\partial \psi}{\partial x}. \qquad (3.18)$$

Also both ϕ and ψ are harmonic, i.e. they each satisfy Laplace's equation. As $\mathbf{V} = -(k\rho g/\mu)\nabla\phi$, and $\nabla \times \mathbf{V} = -(k\rho g/\mu)(\nabla \times \nabla\phi) \equiv \mathbf{0}$ for irrotational flow. Also, the flow is incompressible, so $\nabla \cdot \mathbf{V}=0$, implies $\nabla^2\phi = 0$, and for the two-dimensional case, $\nabla^2\psi = 0$.

We will deal with various flow problems with the help of velocity potential ϕ and stream function ψ. The stream function gives a good representation of fluid flows, and the velocity potential is the tool used to calculate potentials across the flow.

3.4 Elliptic PDE on rectangular domain, separation of variables for velocity potential $\phi(x, z)$
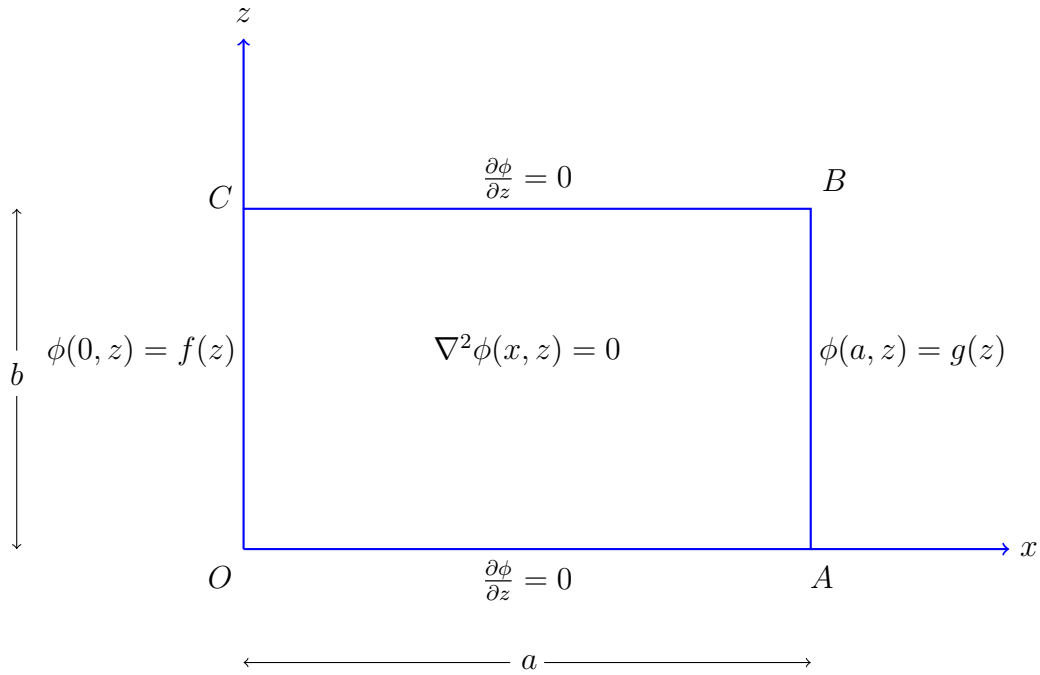
Figure 3.2: *Schematic diagram of porous domain for ϕ.*

An analytical solution for velocity potential $\phi(x, z)$ is found by using the separation of variables technique. The following problem is discussed for Laplace's equation in terms of the velocity potential.

The boundary value problem for $\phi(x, z)$ with impervious lower and upper boundaries and prescribed flow speeds on the vertical boundaries is:

$$\frac{\partial^2 \phi}{\partial x^2} + \frac{\partial^2 \phi}{\partial z^2} = 0, \quad 0 < x < a, \quad 0 < z < b, \tag{3.19}$$

$$\frac{\partial \phi}{\partial z}(x, 0) = 0, \quad 0 < x < a, \tag{3.20}$$

$$\frac{\partial \phi}{\partial z}(x, b) = 0, \quad 0 < x < a, \tag{3.21}$$

$$\phi(0, z) = f(z), \quad 0 < z < b, \tag{3.22}$$

$$\phi(a, z) = g(z), \quad 0 < z < b. \tag{3.23}$$

Solution

By using the method of separation of variables, let $\phi(x, z) = X(x)Z(z)$, then Laplace's equa-

tion (3.19) can be written as:

$$X''Z + XZ'' = 0, \qquad (3.24)$$

$$\text{which implies} \quad \frac{X''}{X} = \frac{-Z''}{Z}. \qquad (3.25)$$

Since the two sides of Equation (3.25) are functions of different variables, we conclude that they must be constant, which we set to be α_C (say), i.e.,

$$\frac{X''}{X} = \frac{-Z''}{Z} = \alpha_C. \qquad (3.26)$$

Homogeneous boundary conditions (3.20)-(3.21) implies $Z'(0) = Z'(b) = 0$.

Therefore $X(x)$ and $Z(z)$ must satisfy

$$X'' - \alpha_C X = 0, \qquad (3.27)$$

$$Z'' + \alpha_C Z = 0, \qquad (3.28)$$

$$Z'(0) = 0, \qquad (3.29)$$

$$Z'(b) = 0. \qquad (3.30)$$

Here, we need to find a number α_C and a nonzero solution. For this constant α_C, we have three cases:

Case 1 α_C=0.

Equation (3.27) has a general solution:

$X = A + Bx.$

Whereas, Equation (3.28) gives the general solution:

$Z = C + Dz.$

This solution satisfy the boundary conditions (3.29)-(3.30). Hence the solution for Z reduces to:

$Z = C.$

Since

$$\phi(x, z) = X(x)Z(z), \tag{3.31}$$

we have

$$\phi(x, z) = A_0 + B_0 x. \tag{3.32}$$

Case 2 $\alpha_C = -\lambda^2$, $(\lambda > 0)$.

Equations (3.27)-(3.30) become:

$$X'' + \lambda^2 X = 0, \tag{3.33}$$

$$Z'' - \lambda^2 Z = 0, \tag{3.34}$$

$$Z'(0) = 0, \tag{3.35}$$

$$Z'(b) = 0. \tag{3.36}$$

For case 2, only the trivial solution exists, i.e.,

$$\phi(x, z) = 0. \tag{3.37}$$

Case 3 $\alpha_C = \lambda^2$, $(\lambda > 0)$.

Equations (3.27)-(3.30) become

$$X'' - \lambda^2 X = 0, \tag{3.38}$$

$$Z'' + \lambda^2 Z = 0, \tag{3.39}$$

$$Z'(0) = 0, \tag{3.40}$$

$$Z'(b) = 0, \tag{3.41}$$

We find that the general solution to Case 3 is:

$$\phi(x, z) = (A \cosh \lambda x + B \sinh \lambda x)(C \cos \lambda z),$$

where, $\lambda = \frac{n\pi}{b}$.

After inserting the value of λ,

$$\phi(x, z) = (A_2 \cosh \frac{n\pi x}{b} + B_2 \sinh \frac{n\pi x}{b}) \cos \frac{n\pi z}{b}.$$

By superposing the solutions of all cases, we find that

$$\phi(x, z) = A_0 + B_0 x + \sum_{n=1}^{n=\infty} \left[A_n \cosh \frac{n\pi x}{b} + B_n \sinh \frac{n\pi x}{b} \right] \cos \frac{n\pi z}{b}. \qquad (3.42)$$

(3.42) is the solution of Laplace's equation with real numbers A_n and B_n. We want to choose A_n and B_n such that $\phi(x, z)$ in Equation (3.42) satisfies the non-zero boundary conditions (3.22)-(3.23):

$$\phi(0, z) = A_0 + \sum_{n=1}^{n=\infty} A_n \cos \frac{n\pi z}{b} = f(z),$$

and

$$\phi(a, z) = A_0 + B_0 a + \sum_{n=1}^{n=\infty} \left[A_n \cosh \frac{n\pi a}{b} + B_n \sinh \frac{n\pi a}{b} \right] \cos \frac{n\pi z}{b} = g(z), \qquad (3.43)$$

where

$$A_0 = \frac{1}{b} \int_0^b f(z) dz,$$

$$A_n = \frac{2}{b} \int_0^b f(z) \cos \frac{n\pi z}{b} dz,$$

$$A_0 + B_0 a = \frac{1}{b} \int_0^b g(z) dz,$$

and

$$A_n \cosh \frac{n\pi a}{b} + B_n \sinh \frac{n\pi a}{b} = \frac{2}{b} \int_0^b g(z) \cos \frac{n\pi z}{b} dz.$$

A_0, B_0, A_n and B_n can be solved by Quadrature methods.

3.4.1 Corollary

If in the non-homogeneous boundary conditions i.e., in Equations (3.22)-(3.23), we replace $f(z)$ by a constant ϕ_L and $g(z)$ by ϕ_R, hence,

$$\phi(0, z) = \phi_L, \quad \text{and} \quad \phi(a, z) = \phi_R,$$

implies

$$A_0 = \phi_L, \ B_0 = \frac{(\phi_R - \phi_L)}{a}, \ A_n = 0, \quad \text{and} \quad B_n = 0.$$

So the Equation (3.42) reduces to a linear function:

$$\phi(x, z) = \phi_L + \frac{(\phi_R - \phi_L)x}{a}, \tag{3.44}$$

where ϕ_L and ϕ_R are the values of head on left- and right-hand side of the domain respectively.

3.5 Modelling two-dimensional flow in aquifers in absence of objects

As part of the hydrologic cycle, it is always significant to discuss the motion of groundwater. The movement of groundwater always takes place from natural and artificial recharge zones to those of natural and artificial discharge. For the flow modelling in an aquifer, the dependent variable is the velocity potential $\phi(x, z)$ as discussed in Section 3.2, with the governing (balance) equation and suitable initial and boundary conditions within a control box. Here, the control box is in the form of a rectangular region with area ab, where a is the aquifer's length and b is its height, respectively. A more rigorous way for discretization of the solution domain is discussed in the following subsection.

3.5.1 Discretization of the solution domain
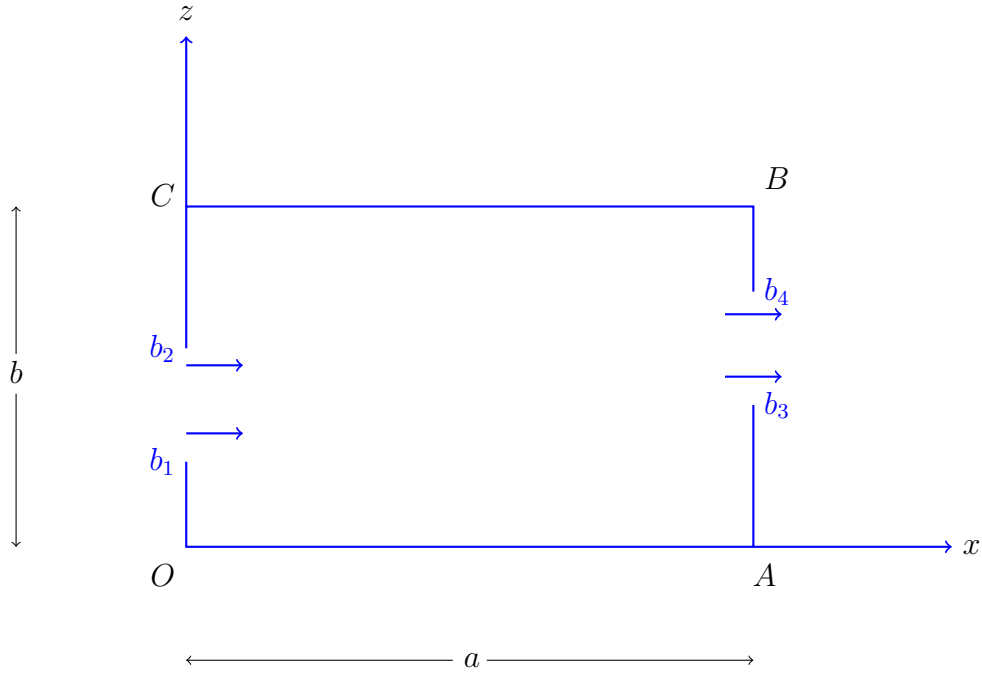
Figure 3.3: *Schematic diagram of the physical domain.*

The solution domain is in the form of a rectangular box $OABC$ having a height b and width a as shown in Figure 3.3. The entrance b_1b_2 is on the left hand side and the exit b_3b_4 is on the right hand side of the domain. The thick blue lines represent the solid impermeable walls of the domain, the x-axis is taken along the horizontal direction, while the (vertical) z-axis is aligned normal to it.

The domain will be equipped with a solution grid comprising $k = 1, ..., N + 1$ equally-spaced points and $j = 1, ..., M + 1$ in the x- and z-directions respectively. The increments in the x- and z-direction are given by the constant difference between their two consecutive values, i.e., $dx = x(2) - x(1)$; and $dz = z(2) - z(1)$.

Along the line Ob_1b_2C, $k = 1$ or $x_1 = 0$, while line Ab_3b_4B represents $k = N + 1$ or $x_{N+1} = a$. Similarly, the line OA corresponds to $j = 1$ or $z_1 = 0$ and along line CB, $j = M + 1$ or $z_{M+1} = b$.

In order to locate the points b_1, b_2, b_3 and b_4, the indices j_{b_1}, j_{b_2}, etc. are assigned respectively with the assumption that $j_{b_1} < j_{b_2}$ and $j_{b_3} < j_{b_4}$.

3.5.2 Complete statement of mathematical flow model

Prior to the development of any mathematical model, it is necessary to conduct a set of relevant assumptions that incorporate our conceptual model. Conceptual models provide a pathway for the understanding of real systems under consideration. This model comprises the following characteristics which are relevant to the problem:

1. Describe a complete format of the flow domain required for the construction of the model.

2. Specify the flow pattern (laminar or turbulent flow), that will pass through the geometrical configuration.

3. Set out the assumptions about matrix properties relevant to the homogeneity/non-homogeneity (e.g., permeability or hydraulic conductivity) and isotropy/anisotropy of the domain, which affect the transport and storage procedure in the flow domain.

4. Develop an understanding about the sources and sinks of water within the flow regime.

5. Specify state variables (usually, $\phi(x, z)$, and $\psi(x, z)$, etc.).

6. Form a partial differential equation (PDE) with respect to the state variables defined in (6).

7. Identify the numerical value of the coefficients of the PDE stated in (7).

8. Specify initial/boundary conditions in terms of state variables appearing in (6), It is worthwhile to mention that no initial condition is specified for the steady flow.
   Taking into account the assumptions set out for the construction of the conceptual model, every mathematical model needs to be *well-posed*. By a *well-posed boundary value problem*, we mean a system subject to the following conditions:

   (a) a unique solution of the problem must exist,

   (b) the solution must be stable, i.e., a small alteration in the initial or boundary conditions should leave little impact on the solution, otherwise the problem should be considered as *ill-posed*.

3.5.3 Mathematical description of the velocity potential problem

Figure 3.4 shows the governing Laplace's equation $\nabla^2\phi(x, z) = 0$, and initial and boundary conditions for a two-dimensional potential flow in terms of the velocity potential $\phi(x, z)$. It is assumed that flow in the porous medium is governed by Darcy's law, and therefore inertial, thermal expansion, and fluid buoyancy effects are neglected. Following are the initial and boundary conditions for ϕ.

The opening in the upstream boundary, namely, section b_1b_2, and opening in the downstream boundary, namely, section b_3b_4, have a scaled dynamic pressure which is hydrostatic i.e., Dirichlet-type boundary conditions, $\phi(0, z) = \phi_L$, and $\phi(a, z) = \phi_R$ are specified in these sections.

Since no water can pass across the solid impermeable boundaries of the domain so, Neumann-type boundary conditions are stated there. Hence, normal components of the velocity are taken to be zero there, i.e., $w = \partial\phi/\partial z = 0$ along OA and CB and $u = \partial\phi/\partial x = 0$ along vertical solid boundaries of the domain.
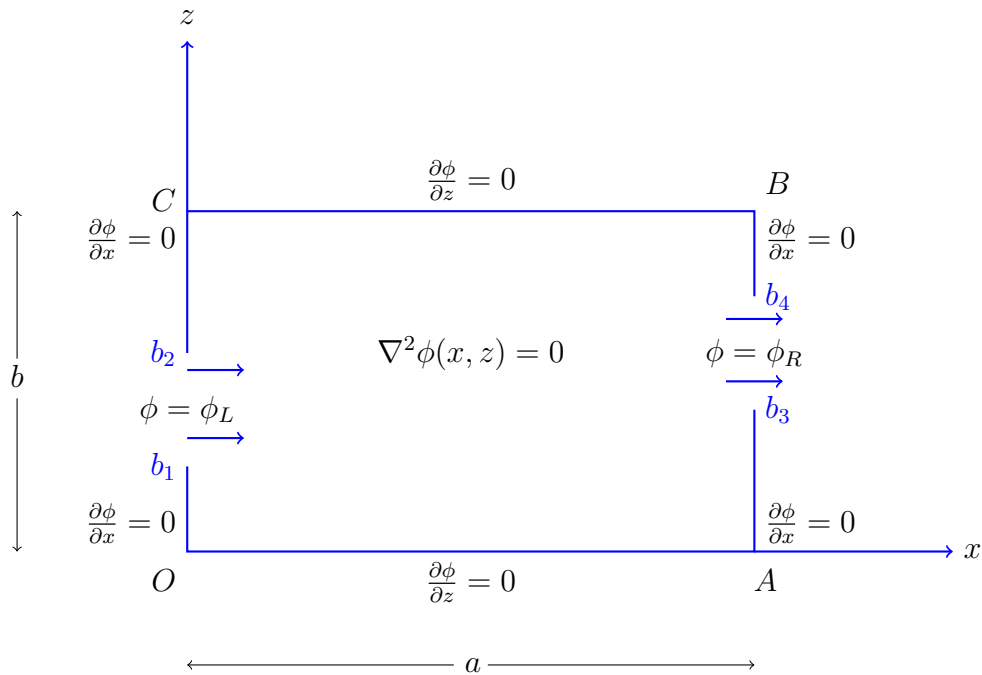
Figure 3.4: *Schematic diagram of the physical domain for ϕ.*

3.5.4 Mathematical description of the stream function problem
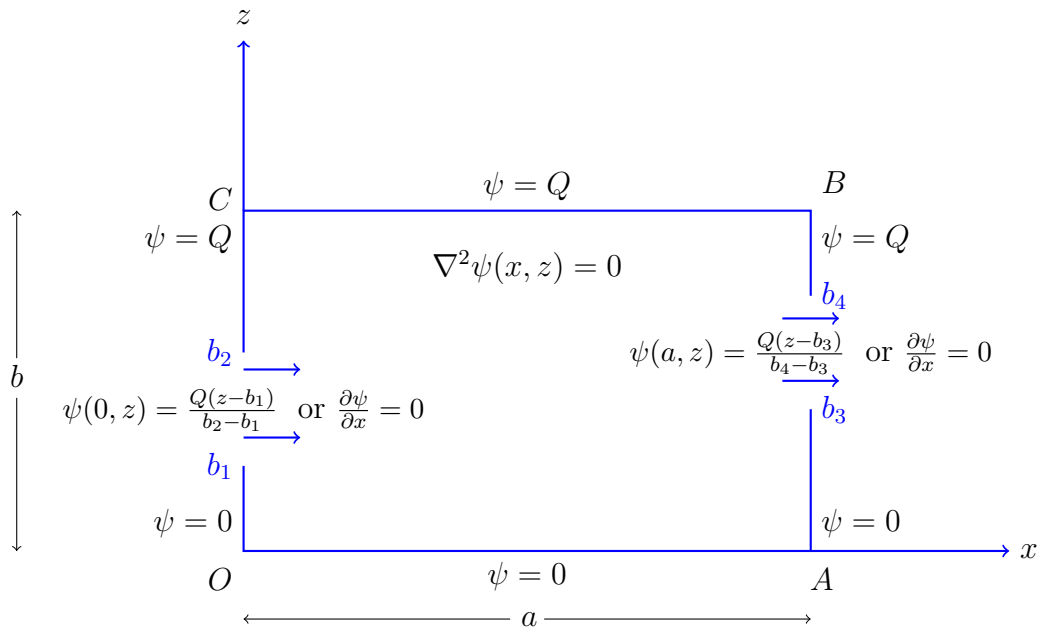
Figure 3.5: *Schematic diagram of the physical domain for ψ.*

A short discussion about streamlines was provided in Chapter 1, now a detailed analysis of the topic is discussed here. The flow velocity $\mathbf{V}$ at any point of a streamline is tangent to the line, i.e., no water can flow across the streamline, but water flows along the direction of streamline. Moreover, the quantity of water remains constant between any two streamlines and is measured by the difference in the values of the stream function on that pair of streamlines. Figure 3.5 shows the governing Laplace's equation $\nabla^2\psi(x,z) = 0$, and the boundary conditions for a two-dimensional potential flow in terms of the stream function $\psi(x,z)$ of the flow within a rectangular domain with one entrance and one exit. The solution domain is rectangular having width a and height b.

In the beginning of the research work, for both the analytic and numerical solutions, the opening in the upstream boundary, namely, section b_1b_2, has a value $\psi(0,z) = Q(z - b_1)/(b_2 - b_1)$, and the opening in the downstream boundary, namely, section b_3b_4, has a value $\psi(a,z) = Q(z - b_3)/(b_4 - b_3)$. Afterwards, along these cross-sections (i.e., along b_1b_2 and b_3b_4), the assumption of horizontal flow is taken into account, therefore the vertical velocity component, $w = -\partial\psi/\partial x = 0$ is assigned there.

The solid boundary b_1OAb_3 corresponds to a streamline of flow since for ideal flow a flow particle entering the domain at b_1 will be transported along b_1OAb_3. We select streamline b_1OAb_3

to correspond to $\psi(x, z) = 0$. The solid boundary b_2CBb_4 is also a streamline of the flow corresponding to the value of the unit discharge Q (the discharge per unit width perpendicular to the flow plane), i.e., $\psi(x, z) = Q$ along b_2CBb_4.

3.5.5 Analytical solution for stream function $\psi(x, z)$

Solve Laplace's equation $\nabla^2\psi(x, z) = 0$ subject to the boundary conditions:

$$\psi(x, 0) = 0, \quad 0 < x < a,$$
$$\psi(x, b) = Q, \quad 0 < x < a,$$

$$\psi(0, z) = \begin{cases} 0, & 0 \leq z \leq b_1, \\ \frac{Q(z - b_1)}{b_2 - b_1}, & b_1 < z < b_2, \\ Q, & b_2 \leq z \leq b, \end{cases}$$

$$\psi(a, z) = \begin{cases} 0, & 0 \leq z \leq b_3, \\ \frac{Q(z - b_3)}{b_4 - b_3}, & b_3 < z < b_4, \\ Q, & b_4 \leq z \leq b, \end{cases}$$

where Q is the unit discharge.

The analytical solution of Laplace's equation $\nabla^2\psi(x, z) = 0$ with these boundary conditions is found by the method of separation of variables as discussed in Section 3.4:

$$\psi(x, z) = \frac{Qz}{b} + \sum_{n=1}^{\infty} \left[A_n \cosh\frac{n\pi x}{b} + B_n \sinh\frac{n\pi x}{b} \right] \sin\frac{n\pi z}{b}, \tag{3.45}$$

where,

$$A_n = \frac{2}{b} \int_0^b \left[\psi(0, z) - \frac{Qz}{b} \right] \sin\frac{n\pi z}{b} dz,$$

and

$$A_n \cosh \frac{n\pi a}{b} + B_n \sinh \frac{n\pi a}{b} = \frac{2}{b} \int_0^b \left[\psi(a, z) - \frac{Qz}{b} \right] \sin \frac{n\pi z}{b} dz.$$

A_n and B_n can be solved by quadrature methods.

3.5.5.1 Fluid flow illustration for analytic solution for $\psi(x, z)$

Figure 3.6 shows the graphical representation of analytic solution (given by Equation (3.45)) for stream function $\psi(x, z)$. The flow domain is rectangular with one entrance, marked by a red line on the left-hand side and one exit, marked by a blue line on the right-hand side. Fluid flow lines are visible going from left to right through the porous medium domain. The value of stream function is constant on each streamline and this value remains constant between each pair of streamlines. The validity of this analytic solution is verified by the numerical solution of $\psi(x, z)$ which is illustrated in Figure 3.10a and a detailed analysis about the graph of streamlines is given in Subsection 3.5.7. To make the exact comparison between the two solutions, both results are calculated for similar boundary conditions, identical geometry and same values of the parameters involved.
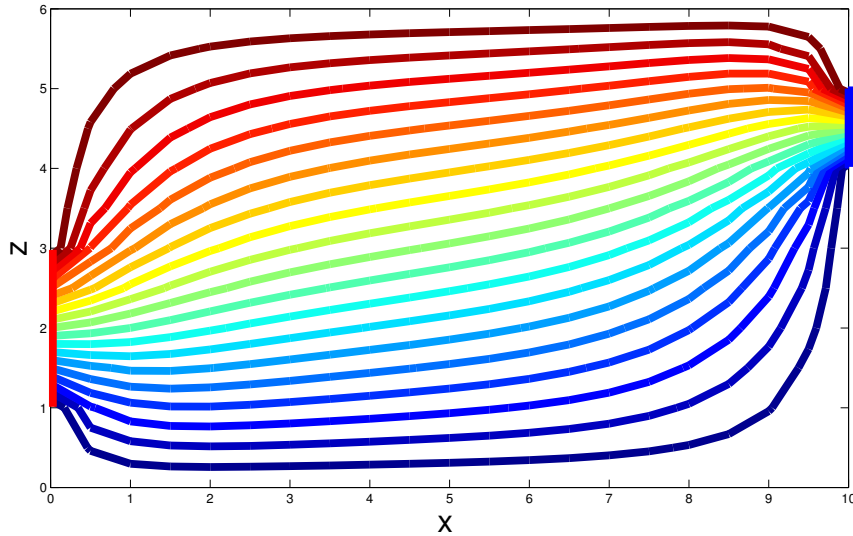
Figure 3.6: *Example of the analytic solution for the stream function ψ with inflows and outflows.*

3.5.6 Fluid flow illustrations for velocity potential $\phi(x, z)$

Different techniques have been used to investigate flow problems numerically. Some of them are: finite difference method, finite element method, boundary integral method, boundary element method, panelisation method, etc. Among them, the finite difference and finite element methods are widely used in fluid dynamics research [56]. In both these methods a system of nodal points is superimposed over the problem domain. The distribution of nodes make it possible to differentiate between these two methods. The finite difference nodes are usually taken in the form of a regular grid where nodes can be block-centred or mesh-centred (Figure 3.7), whereas the finite element methods can have an irregular distribution of nodes which are connected together to form triangular sub-areas called elements [56].
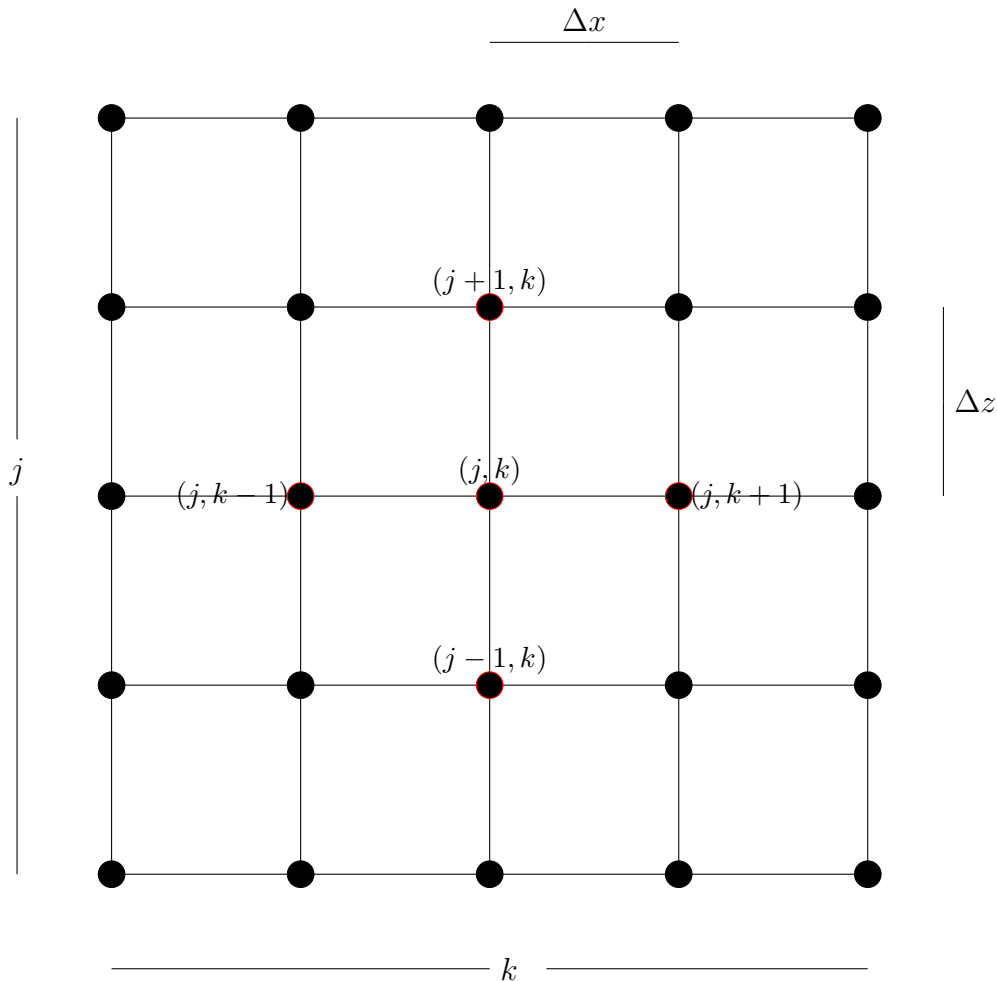
Figure 3.7: *Finite difference grid of nodes.*

To demonstrate the numerical method, consider an example of an incompressible fluid flowing in a homogeneous, isotropic confined aquifer in the absence of sources or sinks. The

numerical solution of Laplace's equation $\partial^2\phi/\partial x^2 + \partial^2\phi/\partial z^2 = 0$ should be satisfied for all the interior points of the flow domain. On the boundaries of the domain, boundary conditions are specified as discussed in Subsection 3.5.3. MATLAB was used to find the solution through an implicit solution scheme for Laplace's equation. The discretization of the solution domain is presented in Subsection 3.5.1. The solution is shown graphically by using the function *contour* in Figure 3.8. Computer code of some numerical methods will be included in Appendix B.

Tests were performed for four different physical domains according to the positions and number of their upstream and downstream boundaries to ensure that the nature of the numerical results obtained remains unaltered. For all the graphs with more than one entrance and exit, all the entrances are connected to the same reservoir with pressure is equal to one, and all the exits are connected to the same reservoir with pressure is equal to zero.

Graphs illustrate that water flows in a direction opposite to the dynamic pressure gradient, i.e., water flows from the area of higher pressure ($\phi = 1$, shown by red lines) to that of the lower pressure ($\phi = 0$, shown by blue lines), and the value of pressure along equipotential lines (isobars) remains constant. The darkest red lines in each of the figures are all of the same pressure and the darkest blue lines are similarly all at the same pressure, but lower than that in the case of red lines. The lines from blue to red go up in steps of $0 : 0.05 : 1$. Moreover, the fluid velocity at every point of an equipotential line is normal to the line, i.e., no water can flow along equipotential lines, but water flows across the equipotential lines.
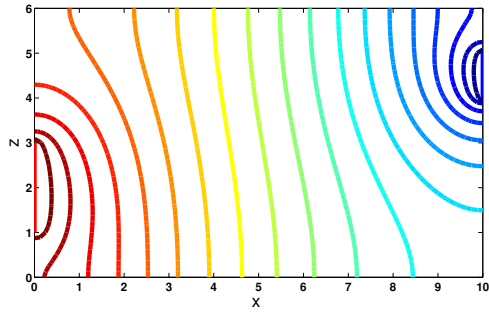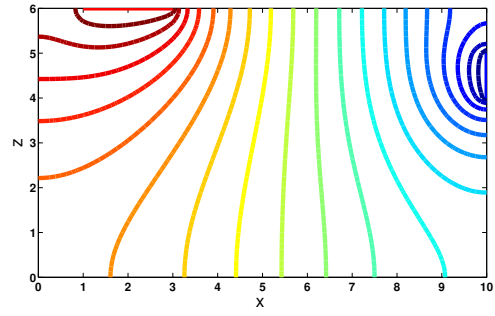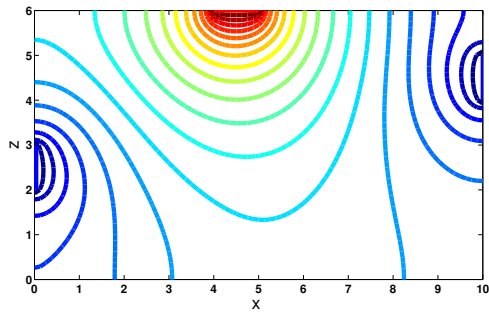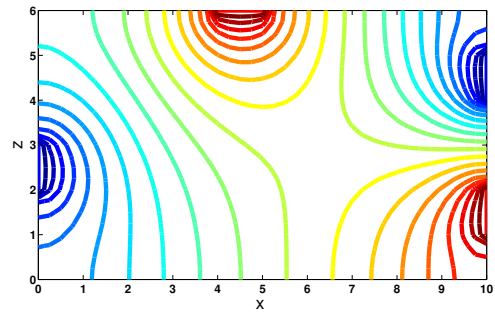
Figure 3.8: *Illustration of numerical solution for the velocity potential $\phi(x, z)$, with $\phi = 1$ in the entrance(s), and $\phi = 0$ in the exit(s). Darkest red lines are $\phi = 1$ and darkest blue lines are $\phi = 0$. In all the graphs, the contours are equally spaced and the lines are all at 5 percent intervals between the highest and lowest pressure. Graph of isobars with (a) one entrance on L.H.S and one exit on R.H.S; (b) one entrance on top boundary and one exit on R.H.S; (c) one entrance on top and two exits on L.H.S and R.H.S; (d) two entrances, one on the top boundary and a second on R.H.S and two exits, first on L.H.S and second on R.H.S.*

3.5.7 Fluid flow for stream function $\psi(x, z)$ without an object
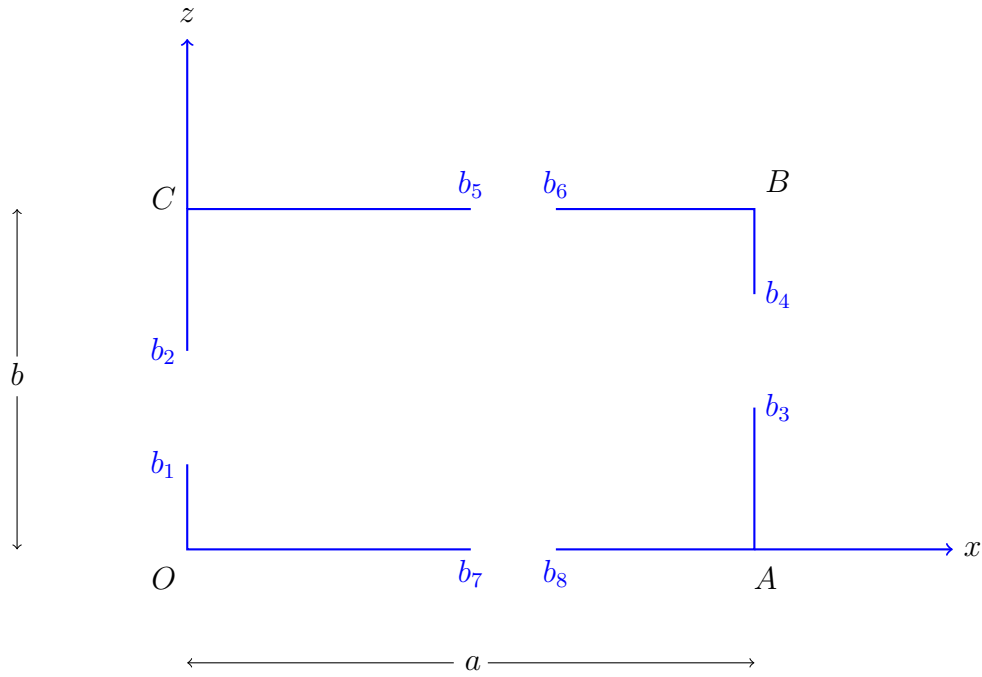
Figure 3.9: *Schematic diagram of the physical domain.*

After the solution of velocity potential $\phi(x, z)$, the next goal is to calculate the net flow across the flow domain. If $b_1 b_2$, $b_3 b_4$, $b_5 b_6$ and $b_7 b_8$, are openings in the L.H.S (OC), R.H.S (AB), top boundary (CB) and bottom boundary (OA), respectively, as shown in Figure 3.9 in the flow domain, then the fluxes in these directions are given by the following four integrals, calculated using quadrature formulae

$$Q_{left} = \frac{-k\rho g}{\mu} \int_{b_1}^{b_2} \frac{\partial \phi}{\partial x}(0, z) \, dz,$$

$$Q_{right} = \frac{-k\rho g}{\mu} \int_{b_3}^{b_4} \frac{\partial \phi}{\partial x}(a, z) \, dz,$$

$$Q_{top} = \frac{-k\rho g}{\mu} \int_{b_5}^{b_6} \frac{\partial \phi}{\partial z}(x, b) \, dx,$$

$$Q_{bottom} = \frac{-k\rho g}{\mu} \int_{b_7}^{b_8} \frac{\partial \phi}{\partial z}(x, 0) \, dx.$$

Within computational error, the net flux across the domain should be zero; this provides a check on the method.

In Section 3.3, it was discussed that the functions (ϕ, ψ) satisfy the Cauchy-Riemann equations

and they relate to each other in this way:

$$-\frac{\partial \phi}{\partial x} = \frac{\partial \psi}{\partial z}, \quad -\frac{\partial \phi}{\partial z} = -\frac{\partial \psi}{\partial x}.$$

After the calculations of fluxes along the openings and for the sake of assigning boundary conditions there in terms of stream function ψ, we use the above Cauchy-Riemann equations. Figure 3.5 shows the governing Laplace's equation $\nabla^2 \psi(x, z) = 0$, and the boundary conditions for a two-dimensional potential flow in terms of the stream function $\psi(x, z)$. The numerical solution (a finite difference scheme is used) to the problem is represented subject to the fluxes calculated in terms of the velocity potential $\phi(x, z)$.

The resulting contour lines demonstrate the streamlines of the flow as illustrated in Figure 3.10 for four different domains in respect of the different position and number of their upstream and downstream boundaries. The water enters the domain from entrance(s) and flows out through the exit(s) along the streamlines (routes which a water particle will travel under absolutely advective motion).

The different colours of the streamlines show that, in accordance with the boundary conditions, the minimum value of the stream function is on the bottom, as shown in Figure 3.10a and 3.10b i.e., where $\psi(x, 0) = 0$ (where streamlines has blue colour). The stream function increases towards the top (red streamlines). Moreover, in the narrower region of the aquifer (i.e., in entrance(s) and exit(s)), where fluid speed is greater, streamlines are closer to each other and they spread apart in the regions of lower speed of the fluid.

In addition, for the cases where there are more than one entrance and exit, e.g., in Figure 3.10c and 3.10d, the results are verified by the law of conservation of mass, i.e., $\sum Q_{in} = \sum Q_{out}$.
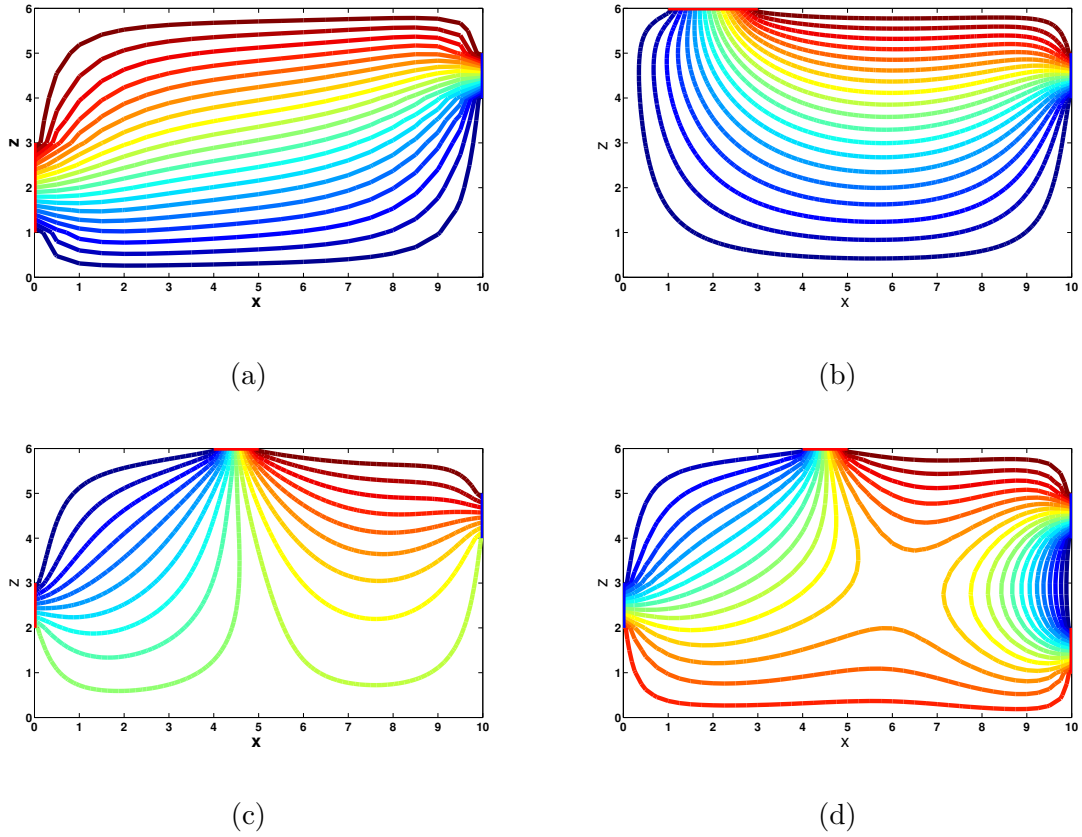
Figure 3.10: *Graph of numerical solution for the stream function $\psi(x, z)$, with (a) one entrance on L.H.S and one exit on R.H.S; (b) one entrance on top boundary and one exit on R.H.S; (c) one entrance on top and two exits, with one on L.H.S and second on R.H.S; (d) two entrances, one on the top boundary and second on R.H.S (lower) and two exits, first on L.H.S and second on R.H.S (upper).*

Another analysis is undertaken for four different domains with the same upstream and downstream lengths and positions, but with different spatial length resolutions in terms of streamlines. Table 3.1 demonstrates the details of these four domains, where $b_1 b_2$, is the entrance, $b_3 b_4$ is the exit, M is the number of rows, N is the number of columns and Q is the unit discharge. Figure 3.11 shows that the numerical results obtained so far are independent of the spatial grid resolutions. Other numerical experiments showed that increasing the grid resolution did not improve the results.

Table 3.1: *Four physical domains with their upstreams and downstream lengths for different mesh resolutions.*

Domain	b_1	b_2	b_3	b_4	M	N	Q
M_1	1	3	4	5	20	12	4
M_2	1	3	4	5	40	24	4
M_3	1	3	4	5	80	48	4
M_4	1	3	4	5	160	96	4
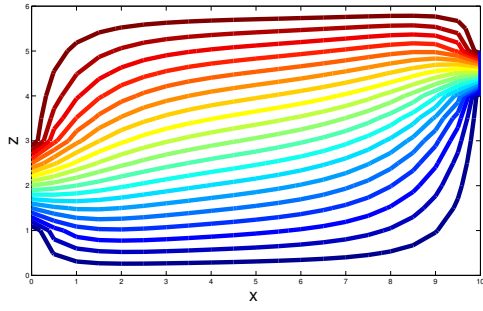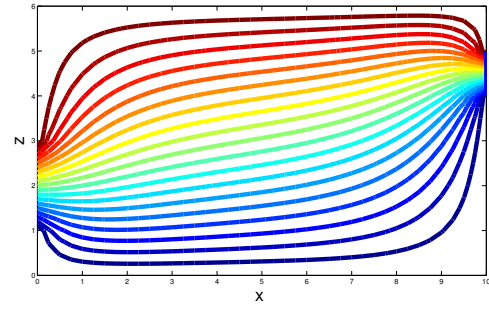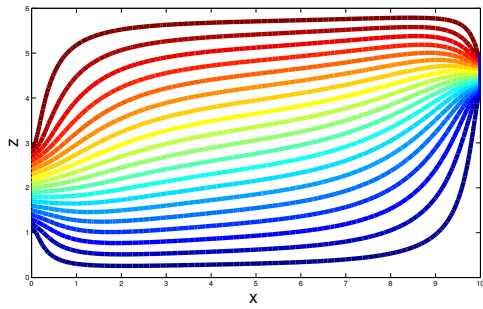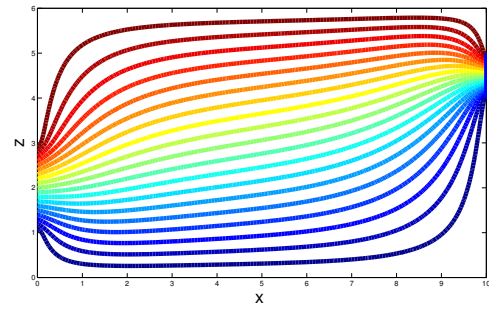
Figure 3.11: *(a) - (d) Graphs of numerical solution for 4 physical domains with different resolutions with their upstream and downstream lengths, for stream function ψ.*

3.6 Modelling two-dimensional flow in aquifers in the presence of impermeable objects

The problem under consideration is to find the steady-state flow around a rectangular impermeable object immersed in a rectangular aquifer, as shown in Figure 3.12.
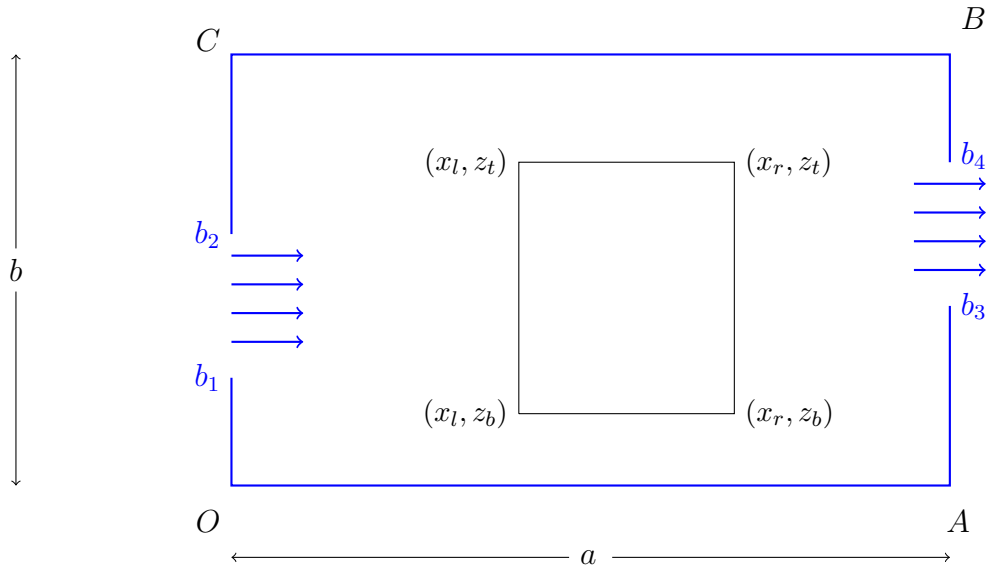
Figure 3.12: *Schematic diagram of the physical domain with embedded impermeable object.*

Together with the assumptions discussed in Section 3.5, we set some extra assumptions for the object embedded in groundwater:

- The object is completely impermeable, i.e., a solid tank(s) or pipe(s), building foundations, rocks, etc.

- No heat is generated by the object.

- Fluid buoyancy effects are neglected.

Based on these assumptions, the system has a two-dimensional governing Laplace's equation in terms of velocity potential ϕ and stream function ψ. The discussion about the boundary conditions on the object and illustration of the numerical results in terms of ϕ and ψ are given separately in the following subsections.

3.6.1 Fluid flow for velocity potential $\phi(x, z)$ in the presence of impermeable objects

The main purpose of this study is to elaborate the behaviour of equipotential lines through a porous medium in which there are embedded solid impermeable objects. A possible combination of boundary conditions for the rectangular object are shown in Figure 3.13.

(x_l, z_t) $\frac{\partial \phi}{\partial z} = 0$ (x_r, z_t)

$\frac{\partial \phi}{\partial x} = 0$ $\frac{\partial \phi}{\partial x} = 0$

(x_l, z_b) $\frac{\partial \phi}{\partial z} = 0$ (x_r, z_b)
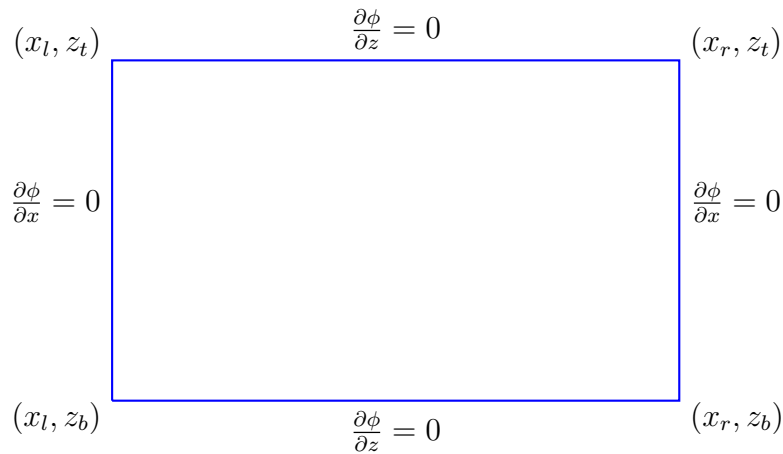
Figure 3.13: *Schematic diagram of boundary conditions for ϕ on an impermeable rectangular object.*

As no fluid passes through the solid boundaries of the impermeable object, so, the normal components of velocity are taken as zero on the four walls of the rectangular object and this object serves as a streamline for the flow. Figure 3.14a shows that all pressure lines strike normally to the solid walls of the rectangular cross-sections of the cylinder and water alters its steady hydrodynamic behaviour in the presence of embedded underground solid objects. The flow pattern varies for the different geometries and positions of the embedded objects.

If instead of placing a rectangular object, a very thin vertical impermeable wall is placed in the porous media, as shown in Figure 3.14b, the flow assumes a pattern similar to that discussed for the rectangular one.

In Figure 3.14c, a number of solid vertical walls are mounted on the bottom and top of the rectangular domain; pressure lines strike normally to these walls. In addition, it seems that the greatest pressure drop occurs in the first and second "chambers" and then the pressure gradient weakens as fluid flows further downstream. This is because the second pair of walls (in this pair, from left to right, one is at the first position on the bottom and the other is at the second position on the top) have a relatively smaller "gate" than the others.
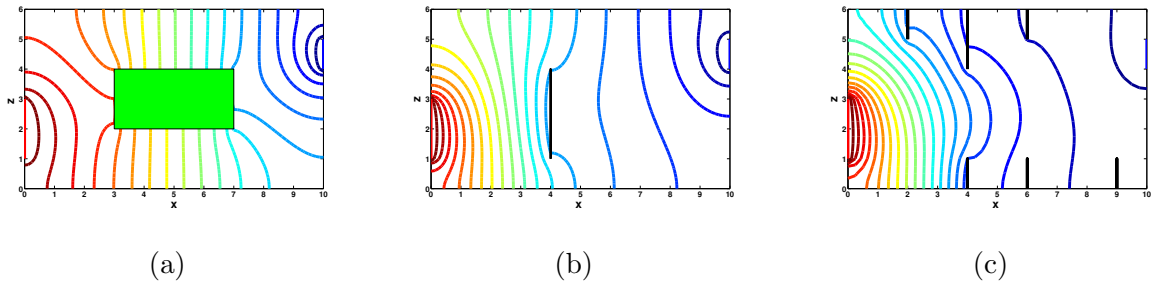
Figure 3.14: *Graphs of numerical solution of velocity potential with embedded impermeable (a) rectangular object; (b) vertical wall; (c) different vertical walls mounted at bottom and top of domain.*

3.6.2 Fluid flow for stream function $\psi(x, z)$ in the presence of impermeable objects: some examples

In this section, the study will be extended in terms of the stream function ψ for a selection of triangular and rectangular impermeable solid objects placed at various positions of the aquifer. Following are the possible boundary conditions for ψ on a rectangular object, where Q_c is the constant amount of the unit discharge along all the boundaries of the object. This is just to experiment to find out what kind of flows we will get for a variety of object shapes.
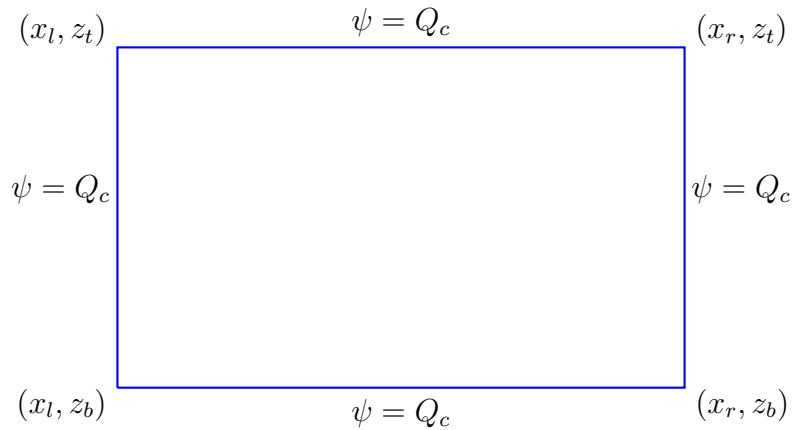
Figure 3.15: *Schematic diagram of impermeable rectangular object for ψ.*

As discussed before the presence of solid objects embedded inside groundwater significantly alters the steady hydrodynamic behaviour inside the medium. This argument is more significantly evident in the illustrations of ψ (which is the representation of pathways of water). For the illustrations, consider the following cases:

If a vertical impermeable wall is embedded inside the porous medium as illustrated in Fig-

ure 3.16a, then this wall behaves as a streamline, as the value of the stream function remains constant everywhere on this wall.

Figure 3.16b shows a rectangular object placed at the bottom of a rectangular domain. Since the value of stream function ψ is zero at the lower boundary, the whole object would be considered as a streamline corresponding to the value $\psi = 0$.

Now, if two adjacent rectangles are attached to the upper boundary of the rectangular domain, then since the value of ψ is Q [m^2 s^{-1}] at the top boundary, so the value of the stream function is $\psi = Q$ [m^2 s^{-1}] at every point on the surfaces of these two rectangular objects.

Owing to the rectangular mesh size in the finite difference method, a triangular object is positioned so that points on its sloping surface coincide with mesh points. The value of the stream function is $\psi = 0$ at every point of this triangular object as shown in the Figure 3.16d.

In Figure 3.16e, a number of impermeable vertical walls are placed on the top and bottom of the rectangular domain which serve as streamlines of the flow, and we can see an interesting pattern of fluid flow between these walls. Actually, there is no particular motivation to discuss such kinds of objects embedded in the aquifers, but the motivation is to investigate the different kinds of flow patterns for different combinations of objects embedded inside the aquifer.

In summary, if some of the above results are combined together, Figure 3.16f depicts the change of hydrodynamic flow pattern in the presence of underground solid objects.
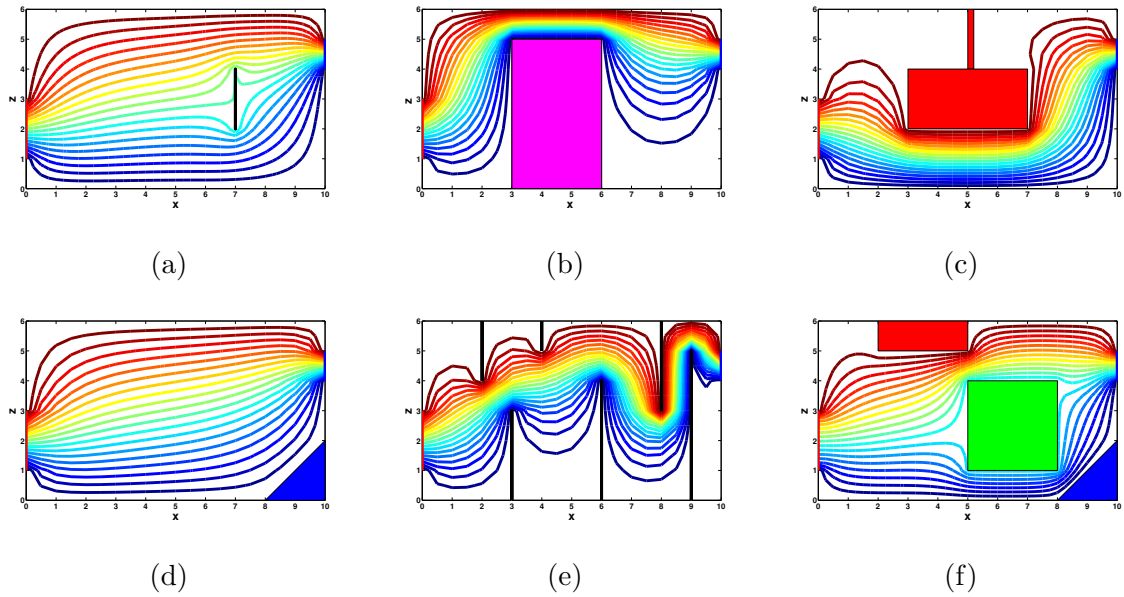
Figure 3.16: *Graphs of the numerical solution of the stream function with embedded in it (a) an impermeable vertical wall; (b) a rectangular object placed on the bottom; (c) two rectangular objects hanging on the top; (d) a triangular object placed at the bottom; (e) various vertical impermeable walls mounted at the bottom and top of the domain; (f) a triangular object placed at the bottom, one rectangle mounted on the top and a second one hanging in the middle of the aquifer.*

3.6.3 Stream function for flow past impermeable objects when there are more than one entrance and/or exit

The problem considered in this part represents fluid flow passing through two rectangular objects immersed in a horizontal, rectangular porous medium having;

1. two entrances and one exit,

2. one entrance and two exits,

3. two entrances and two exits.

One of the rectangular objects is attached to the upper wall and the other is hanging in the porous domain. The value of the stream function is $\psi = Q$ [m^2 s^{-1}] at every point of the rectangular objects attached at the top and the value of the stream function on the rectangular object immersed within the rectangular domain is a constant. This constant value on this rectangular object is obtained by using a relaxation technique.

It is noticeable in Figure 3.17a that out of the total flow Q, $Q_1 = 1$ [m^2 s^{-1}] units of fluid enters from the lower upstream boundary and $Q_2 = 3$ [m^2 s^{-1}] units of fluid enters from the

upper entrance. Since flux in should be equal to flux out, so, a total $Q = Q_1 + Q_2$ [m^2 s^{-1}] units of fluid leaves the domain from the single exit on the R.H.S, which is evident from the greater number of streamlines passing through the downstream boundary.

If on the other hand, a negative value is assigned to the inflow from one of the entrances, e.g. $Q_2 = -0.5$ [m^2 s^{-1}] (say), then the entrance discussed earlier in the L.H.S will be converted into an exit, as shown in Figure 3.17b, and instead of water entering, it starts to leave the porous media.

Figure 3.17c illustrates $Q_1 = 2$ [m^2 s^{-1}] and $Q_2 = 4$ [m^2 s^{-1}] units of fluid entering from the lower and the upper entrances on the L.H.S respectively, and since *inflow=outflow*, so $Q_3 = 3$ [m^2 s^{-1}] and $(Q - Q_3)$ [m^2 s^{-1}] units of fluid leave the porous media from the lower and upper exits on the R.H.S respectively.

The trapezoidal rule is used to calculate the fluid flow rates through the inlets and exits and the numerical results confirm the above said argument.

| (a) | (b) | (c) |
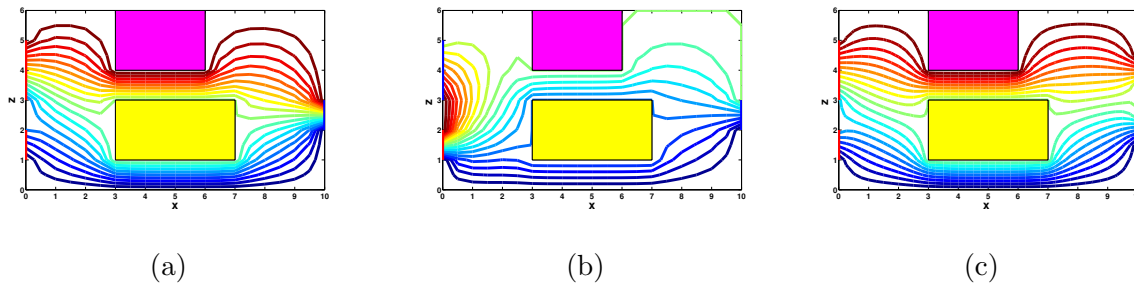
Figure 3.17: *Graphs of the numerical solution of the stream function with two rectangular objects embedded in it, with (a) two entrances on L.H.S, and one exit on R.H.S; (b) with one entrance on L.H.S and two exits, one on L.H.S and second on R.H.S; (c) with two entrances on L.H.S and two exits on R.H.S.*

3.6.4 Flow grid display

For two-dimensional flow, one may be interested to find a relationship between stream function ψ and velocity potential ϕ.

From the Cauchy-Riemann equations, the velocity components of the flow in terms of the velocity potential and stream function are related to each other by

$$u = -\frac{\partial \phi}{\partial x} = \frac{\partial \psi}{\partial z}, \quad w = -\frac{\partial \phi}{\partial z} = -\frac{\partial \psi}{\partial x}. \tag{3.46}$$

Since along an isobar, ϕ is constant, i.e., let $\phi = C$. It follows that:

$$d\phi = \nabla\phi \cdot ds = \frac{\partial\phi}{\partial x}dx + \frac{\partial\phi}{\partial z}dz = 0. \tag{3.47}$$

In Equation (3.47), the displacement ds occurs along a line of constant velocity potential. Inserting Equations (3.46) into Equations (3.47), we get:

$$-udx - wdz = 0. \tag{3.48}$$

Hence, the gradient of equipotential lines is given by

$$\left(\frac{dz}{dx}\right)_{\phi=C} = -\frac{u}{w}. \tag{3.49}$$

Along a streamline the stream function does not change (i.e., $d\psi = 0$), let $\psi = D$. It follows that:

$$d\psi = \nabla\psi \cdot ds = \frac{\partial\psi}{\partial x}dx + \frac{\partial\psi}{\partial z}dz = 0. \tag{3.50}$$

Making use of Equation (3.46) into Equation (3.50), we get:

$$-wdx + udz = 0. \tag{3.51}$$

Hence the gradient of the streamlines is given by

$$\left(\frac{dz}{dx}\right)_{\psi=D} = \frac{w}{u}. \tag{3.52}$$

Multiplying Equations (3.49) and (3.52) with each other, we find:

$$\left(\frac{dz}{dx}\right)_{\phi=C}\left(\frac{dz}{dx}\right)_{\psi=D} = -1. \tag{3.53}$$

showing that equipotential lines and streamlines are orthogonal to each other. The stream function is able to be calculated from (3.46) when the velocity potential is given and vice versa. As equipotential lines and streamlines cross each other at 90 degrees, so both sets of lines form

an orthogonal grid, (known as the flow grid) as shown in Figure 3.18a.

The presence of impermeable objects within the domain preserves the property of orthogonality as well. An example of a flow grid for the whole problem domain when an impermeable rectangular object is inside the aquifer, is shown in Figure 3.18b.

<div align="center">(a)   (b)</div>
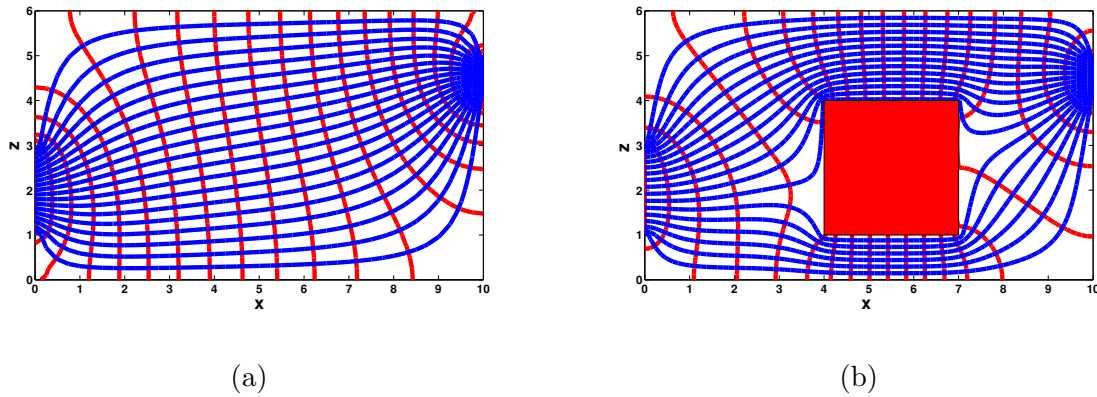
Figure 3.18: *Flow grid display of numerical solution for the equipotential lines (red) and streamlines (blue) (a) without an object; (b) with an impermeable object.*

3.7 Modelling two-dimensional flow in aquifers in the presence of a leaky rectangular cylinder

The flow into or from a pervious structure embedded in a porous media is one of great significance in many areas of engineering and science. Major examples include petroleum and geothermal engineering, manufacturing process of advanced composites, radioactive waste containers, geosciences (hydrogeology, petroleum geology), septic tanks and disposal of drums of contaminants, etc.

Although Darcy's law [20] is sufficient to describe the flow of fluid through porous media, there are however certain situations in which Darcy's equation cannot be applied. One such example is a flow through the boundaries of a pervious block and where certain pressures and pressure gradients are applied inside.

To deal with such situations, we need a more advanced flow model which precisely describes appropriate boundary conditions for the pervious boundaries of the objects. Several modifications have been made in Darcy's law to model such problems. Most of the models comprise the situations in which pervious blocks are partially embedded in the overall system. In this

study, the definition of boundary conditions on the pervious walls of the embedded objects is discussed.

The objective of the present study is to propose suitable boundary conditions on the surface of a pervious object, and analyse the solution for various values of the parameters involved. Assuming the same governing equation (Laplace's equation) and the outer boundary conditions for the rectangular porous medium, as discussed in Section 3.5, a pervious tube with rectangular cross-section is now supposed to be embedded in the porous medium. To describe the boundary conditions on the walls of this pervious structure, we proceed as follows;

To calculate values of the pressure gradients on the boundaries of the pervious surface, we start with Darcy's law on the boundaries outside the object. The flow into the object is

$$u_n \;=\; -\frac{\rho g k_{ps}}{\mu}\left(\frac{\partial \phi}{\partial n}\right)_{ps}. \tag{3.54}$$

Also, for the pervious boundary,

$$u_n \;\propto\; (\phi_{ps} - \phi_I), \tag{3.55}$$

$$\text{implies} \quad u_n \;=\; \omega_{ps}(\phi_{ps} - \phi_I), \tag{3.56}$$

in which ω_{ps} [s^{-1}] is a *measure of resistance of the object's pervious surface to flow through it*, and ϕ_I [m] is *the constant pressure inside the object*. It is assumed that the pervious object is full of water at a constant pressure.

Combining Equation (3.54) and Equation (3.56), we get,

$$u_n = -\frac{\rho g k_{ps}}{\mu}\left(\frac{\partial \phi}{\partial n}\right)_{ps} \;=\; \omega_{ps}(\phi_{ps} - \phi_I), \tag{3.57}$$

$$\text{implies} \quad -\left(\frac{\partial \phi}{\partial n}\right)_{ps} \;=\; \frac{\omega_{ps}\mu}{\rho g k_{ps}}(\phi_{ps} - \phi_I), \tag{3.58}$$

$$\text{implies} \quad -\left(\frac{\partial \phi}{\partial n}\right)_{ps} \;=\; \frac{\beta_{ps}}{k_{ps}}(\phi_{ps} - \phi_I), \tag{3.59}$$

in which,

$$k_{ps} = \frac{K_{ps}\mu}{\rho g}, \tag{3.60}$$

where, k_{ps} [m^2], and K_{ps} [cm s^{-1}] or [m day^{-1}] are respectively the *intrinsic permeability* and *hydraulic conductivity* of the porous medium, μ [kg m^{-1}s^{-1}] is *the dynamic viscosity*, ρ [kg m^{-3}] is *fluid density*, g [m s^{-2}] is *acceleration of gravity*, ϕ_I is the *pressure inside the rectangular cross-section*, and $\beta_{ps} = \omega_{ps}\mu/\rho g$.

The boundary conditions in terms of $(\partial\phi/\partial n)_{ps}$ along the four pervious walls of the rectangular cross-section are illustrated by the following schematic diagram:
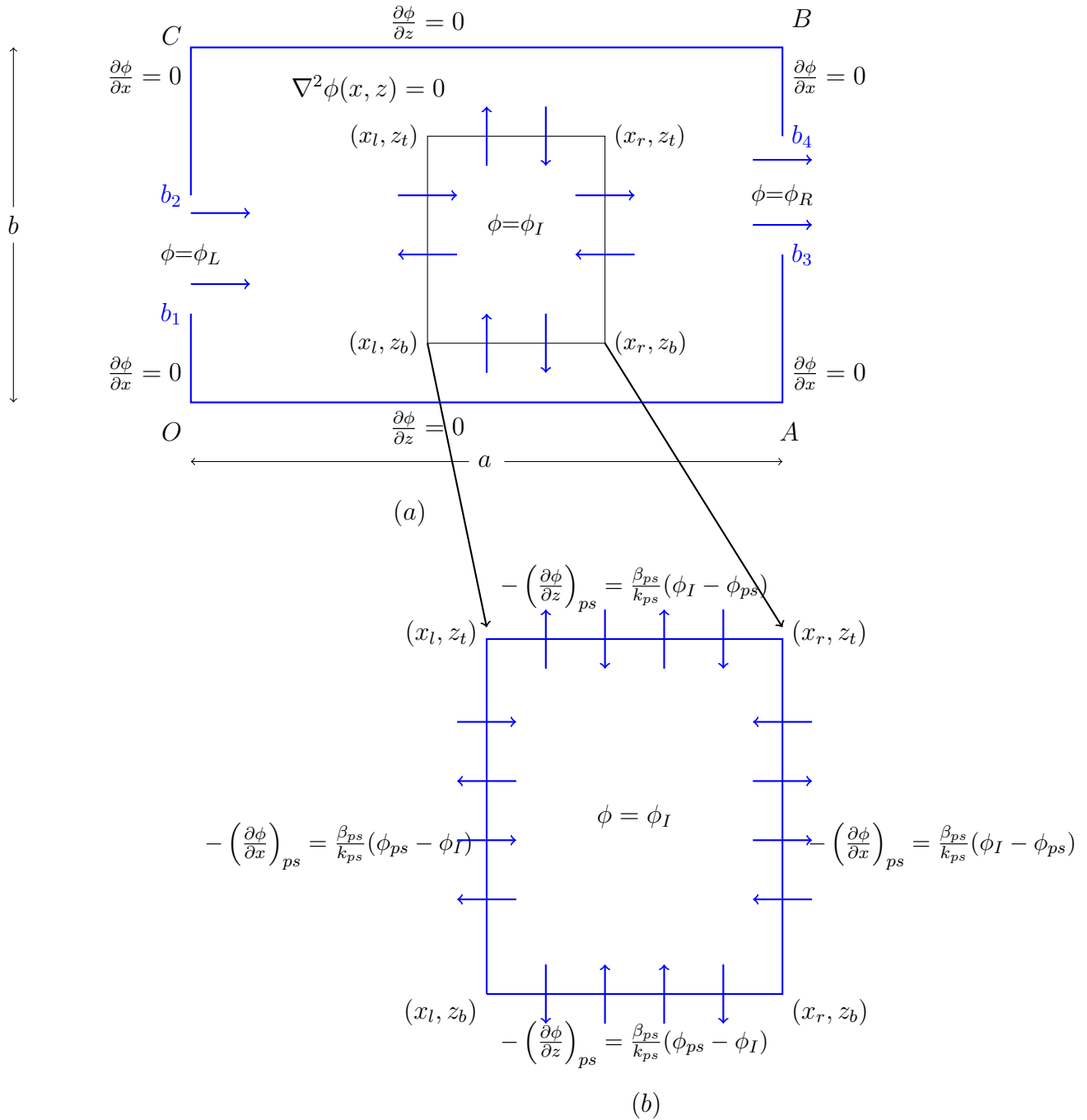
Figure 3.19: *Schematic diagram of the (a) physical domain for ϕ with a pervious septic tank embedded in the homogeneous porous media; (b) rectangular cross-section of a pervious septic tank.*

3.7.1   Illustrations

Consider a septic tank, which is connected to some continuous source of fluid and is kept at a constant dynamic pressure inside. The tank is embedded in a homogeneous aquifer, which is further connected to two reservoirs of water, one on the left-hand side and the other on the right-hand side. Fluid is ejected or sucked by this leaky tank depending upon the amount of fluid inside and the level of water in the two reservoirs. The schematic diagram of the setup is shown in Figure 3.19. This example is presented only for the discussion of fluid flow, transport of pollutant will be discussed in Chapter 5.

In this particular situation, the aquifer is connected to two different reservoirs, with fixed values of the dynamic pressures on left- and right-hand sides as $\phi_L = 1$ and $\phi_R = 0$, respectively. Numerical simulations are performed for four different values of ϕ_I, which represents the value of constant pressure inside the tank, but with a fixed value of the permeability parameter $\beta_{ps} = 3$. At the end, two contour plots are added for $\beta_{ps} = 3$, and $\beta_{ps} = 0$ to give the comparison between pervious and impermeable objects. It should be noted that, in all the graphs of Figure 3.20, the outline of the rectangular cross-sections is drawn to mention their exact position in the porous medium, and the colour of the boundaries of rectangles is selected to match with the value of ϕ_I inside.

In the first illustration, the value of ϕ_I inside the pervious rectangular cross-section is taken as $\phi_I = 5$, which is larger than the values of the pressures in the two openings of the aquifer, so the fluid inside the tank exerts a larger pressure on the outside fluid; as a result of which, water is ejecting outside through these two openings. This effect is evident from the filled graphics in Figure 3.20a by the red colour in the neighbourhood of the tank and blue colours in the two openings.

In Figure 3.20b, the value of ϕ_I inside the pervious object/tank is taken as $\phi_I = 1$, which is equal to the value of pressure in the left-hand side opening, $b_1 b_2$, as a result of which a larger pressure is observed by the red area in the surrounding of the tank. This pressure is exerted by the fluid inside the object and the fluid coming from the left-hand side reservoir. Figure 3.20c illustrates the value of ϕ_I equal to the value of ϕ on the right-hand side opening, $b_3 b_4$. Since the pressure on the object and on the right-hand opening is less than the pressure

on the left-hand side opening, so more pressure is exerted by the fluid coming through the left-hand opening to the fluid in the remaining area of the domain, which is visible by the greater blue area on R.H.S of the domain and in the neighbouring area of the object.

The behaviour of lower pressure inside the object is determined by Figure 3.20d, where the value of ϕ_I is taken as -1, which is less than that in the left-hand side opening, b_1b_2 and right-hand opening, b_3b_4. This situation shows the example when water is being sucked by the tank from the incoming water through the two openings. Since the pressure in the object is less than from the two openings, but the pressure in the left-hand opening is greater than that in the right-hand opening, so more pressure is exerted by the fluid coming from the left-hand reservoir to the fluid in the remaining part of the domain. A lighter red colour is also visible in the right-hand side opening, showing a relatively larger pressure there than that in the tank.

(a)

(b)

(c)

(d)
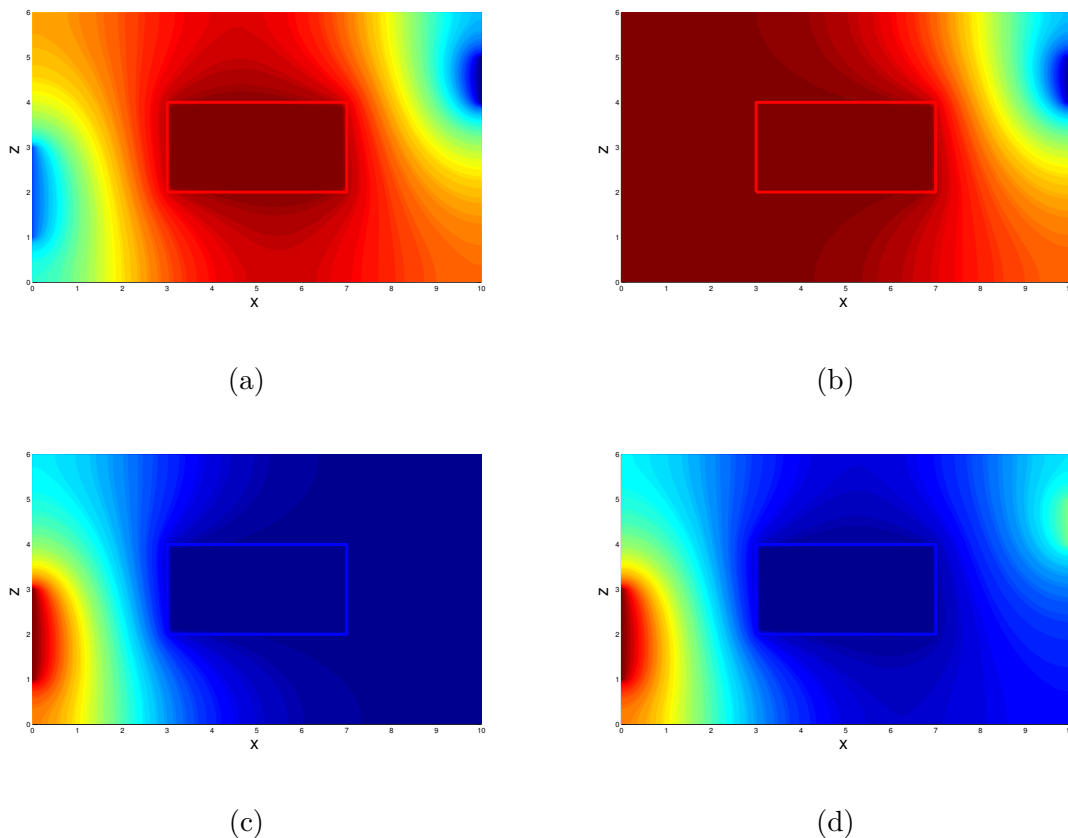
Figure 3.20: *Filled contour plots of numerical solution for $\phi(x,z)$ with a leaky cylinder embedded in a homogeneous porous medium, for $\beta_{ps} = 3$, $\phi_L = 1$, $\phi_R = 0$, and for (a) $\phi_I = 5$; (b) $\phi_I = 1$; (c) $\phi_I = 0$; (d) $\phi_I = -1$.*

The value β_{ps} is a measure of resistance of the object's pervious surface to flow through it.

This will be discussed in detail in Sections 3.9 and 3.10 and illustrated by Figure 3.23. However, here we will take only two examples for the sake of comparison between pervious and impervious objects. The colour of the cylinders is taken randomly to match with the value of ϕ_I inside.

In Figure 3.21a, the value of β_{ps} is taken as $\beta_{ps} = 3$, and the value of pressure inside the pervious rectangular cross-section is taken as $\phi_I = 5$, which is larger than the pressures in the left- and right-hand sides openings. Since the object is pervious with a larger pressure inside, so the fluid inside the object pushes the outside fluid towards the two openings; this is evident from the red lines near the object in Figure 3.21a. On the other hand, Figure 3.21b shows the result of the case when the value of $\beta_{ps} = 0$ (it doesn't matter what would be the value of ϕ_I inside the object), as a result of which, the pervious object becomes completely impermeable and isobars are visible striking normally to the solid boundaries of the tank. The contour plot in Figure 3.21b looks similar to the graph for the impermeable object as illustrated in Figure 3.14a, where the isobars strike normally to the solid walls of the surface.

(a)   (b)
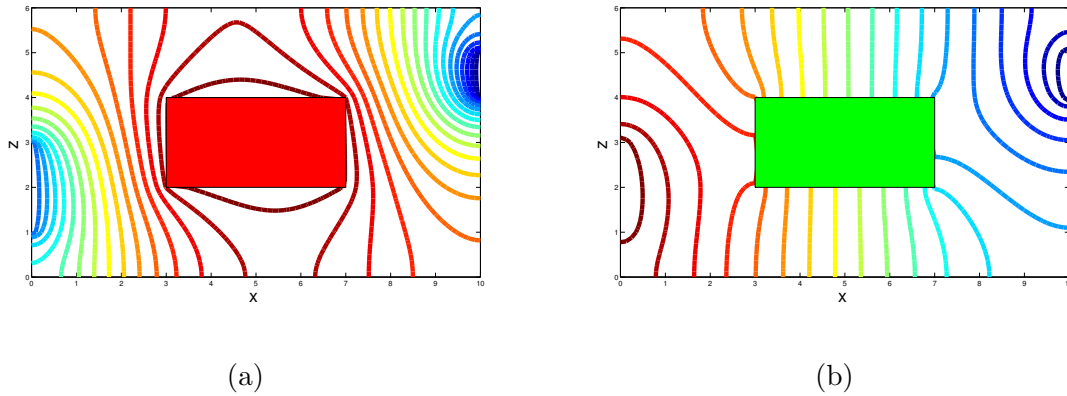
Figure 3.21: *Contour plots of $\phi(x,z)$ for a leaky cylinder with rectangular cross-section for $\phi_L = 1$, $\phi_R = 0$, $\phi_I = 5$, and for (a) $\beta_{ps} = 3$; (b) $\beta_{ps} = 0$.*

3.8 Calculation of the net flow along the four boundaries of the rectangular cross-section using the Trapezoidal rule

We can also calculate the net flow Q_I [m^2 s^{-1}] out of the cylinder by calculating the separate outward flows across the four boundaries of rectangular cross-section (by using Trapezoidal rule), i.e., $Q_I = -Q_{left} + Q_{right} - Q_{bottom} + Q_{top}$.

The results are verified if $Q_I = Q_R - Q_L$, or $Q_R = Q_L + Q_I$, where Q_L [m^2 s^{-1}] and Q_R [m^2 s^{-1}] are the values of the flux in the left- and right-hand side openings respectively. The value of Q_I clarifies whether the water is injected into or withdrawal from this pervious object. If Q_I is negative, then water is being sucked by the object, and the positive value of Q_I represents the withdrawal of water from the pervious cylinder.

Table 3.2: *Verification of the net flows across the leaky tube of rectangular cross-section embedded in a porous medium with $\phi_L = 2$ [m] and $\phi_R=1$ [m].*

β_{ps}	ϕ_I	Q_L	Q_R	Q_I	$Q_R - Q_L$	*relative error*
	0	1.9418	-0.8460	-2.7345	-2.7878	0.0191
	-1	2.9080	-1.7014	-4.5207	-4.6094	0.0192
3	1	0.9756	0.0095	-0.9482	-0.9661	0.0185
	2	0.0094	0.8649	0.8380	0.8555	0.0205
	5	-2.8891	3.4313	6.1967	6.3204	0.0196
	0	2.0298	-0.8871	-2.8245	-2.9169	0.0317
	-1	3.0418	-1.7800	-4.6686	-4.8218	0.0318
10	1	1.0178	0.0058	-0.9804	-1.0120	0.0312
	2	0.0058	0.8986	0.8637	0.8929	0.0327
	5	-3.0303	3.5773	6.3960	6.6076	0.0320
	0	2.0681	-0.9048	-2.8470	-2.9729	0.0423
	-1	3.0998	-1.8141	-4.7054	-4.9140	0.0424
100	1	1.0363	0.0045	-0.9886	-1.0318	0.0419
	2	0.0045	0.9138	0.8699	0.9093	0.0433
	5	-3.0908	3.6418	6.4452	6.7326	0.0427

3.9 A vertical pervious thin wall

In this part we will discuss the case of taking an infinitesimally thin vertical wall in a homogeneous porous domain. The pressure gradients on L.H.S and R.H.S of this wall are denoted by

$\partial \phi^- / \partial x$ and $\partial \phi^+ / \partial x$ respectively, and can be found by the formulae,

$$-\left(\frac{\partial \phi^-}{\partial x}\right)_{ps} = \frac{\beta_{ps}}{k_{ps}}(\phi_{kB_1}^- - \phi_{kB_2}^+), \tag{3.61}$$

$$-\left(\frac{\partial \phi^+}{\partial x}\right)_{ps} = \frac{\beta_{ps}}{k_{ps}}(\phi_{kB_1}^- - \phi_{kB_2}^+). \tag{3.62}$$

where β_{ps} is a measure of resistance of the object's surface to flow through it, as discussed in Section 3.7, $\phi_{kB_1}^-$, and $\phi_{kB_2}^+$ are the values of pressures on L.H.S and R.H.S of the wall respectively.

The solution is obtained by using a finite difference formula. In Equation (3.61), a 3-4-1 backward formula and in Equation (3.62), a 3-4-1 forward formula are used for the calculations of pressures ϕ_{kB1}^- and ϕ_{kB2}^+ respectively.

3.9.1   Illustrations

The present section includes some results for different values of parameter β_{ps} to give a comparison between impermeable and pervious wall. Moreover, an analysis is given to show how the perviousness of the wall increases as the value of β_{ps} gets larger.

Figures 3.22a-3.22d comprise examples for the cases when $\beta_{ps} = 0, 5, 50$, and 1000, respectively. Results show that when $\beta_{ps} = 0$, the wall becomes completely impermeable, as shown in Figure 3.22a which is similar to the results of Figure 3.14b for an impermeable wall. Whereas, for $\beta_{ps} > 0$, the wall becomes comparatively more pervious and there is a smaller pressure drop across the pervious wall, as shown in Figures 3.22b and 3.22c. More significant results are shown in Figure 3.22d where a larger value is assigned to β_{ps} (=1000), as a result of which the wall becomes completely pervious and the fluid feels no resistance to flow (as if the wall was not present at all).

(a) $\beta_{ps} = 0$
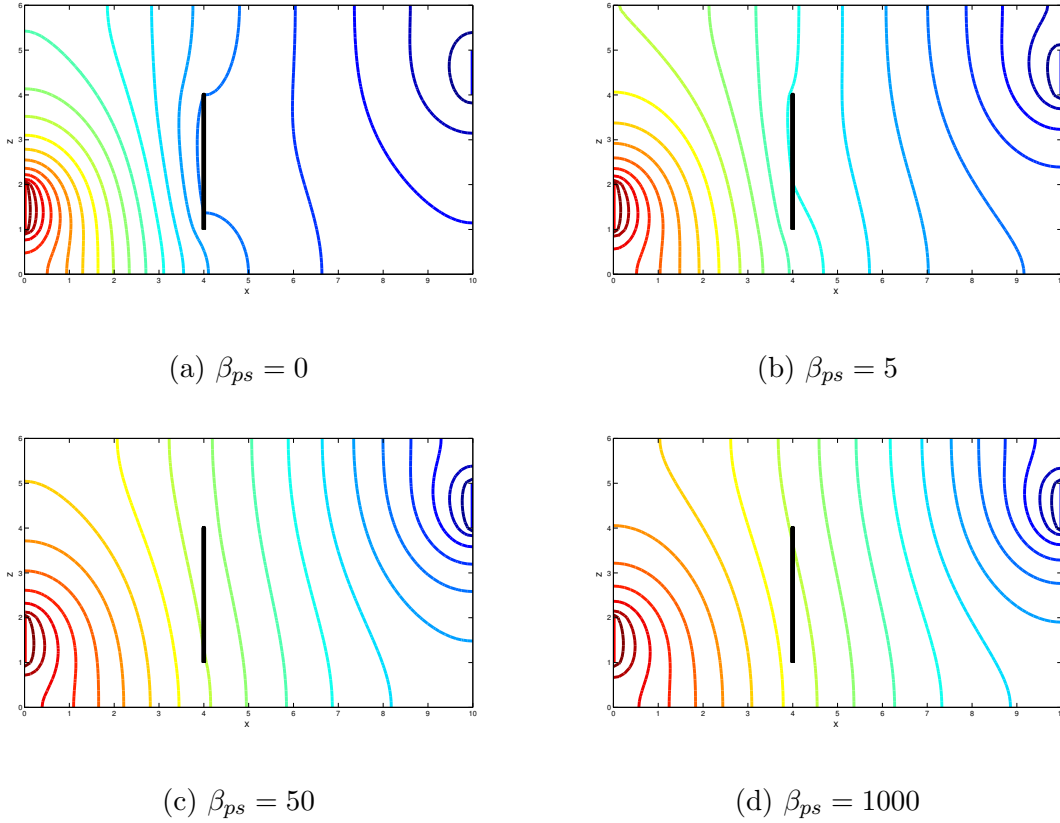
(b) $\beta_{ps} = 5$

(c) $\beta_{ps} = 50$

(d) $\beta_{ps} = 1000$

Figure 3.22: *Contour plots of $\phi(x,z)$ for a vertical thin wall immersed in homogeneous porous media with, $\phi_L = 1$, $\phi_R = 0$, for different values of parameter β_{ps}, with (a) $\beta_{ps} = 0$; (b) $\beta_{ps} = 5$; (c) $\beta_{ps} = 50$; (d) $\beta_{ps} = 1000$.*

3.10 A connection between flux out, height of the pervious wall, h, and parameter β_{ps}

To see the impact of β_{ps} and height of pervious wall on net flow, a numerical study is undertaken for a rectangular domain with width $a = 10cm$ and height $b = 6cm$, at a grid resolution 48×80 for the following parameters:

- h, the height of the vertical pervious wall within the range 0-6,

- the parameter β_{ps}, which is a measure of perviousness of the wall, and

- *flux out Q_R.*

The first analysis is done between Q_R and h, by varying β_{ps} within the range $0 - 1000$, while keeping the wall at the bottom of the system. In Figure 3.23a, it is observed that, when

h is very small, Q_R does not vary significantly, but as the values of h increase, Q_R decreases gradually. It is also observed that when $\beta_{ps} = 0$, the wall becomes completely impermeable and it serves as a barrier for the flow of the fluid; it completely stops the fluid flow at $h = 6$, which is the maximum height of the flow domain. Moreover, for larger values of β_{ps}, the wall becomes more pervious and for very large values of β_{ps} (e.g. $\beta_{ps} = 1000$), this wall becomes almost completely permeable and the flow is little affected by height or even the presence of the wall.

The second analysis is made between Q_R and β_{ps}, for eight different heights of the wall. In Figure 3.23b, it is shown that when the values of β_{ps} increase, the flux out Q_R also increases. In addition, for maximum height of the wall, i.e., at $h = 6cm$, a little amount of water can pass through the wall, while for $h = 0$, there is no variations in the amount of the flow and a constant amount of fluid passes through the domain. As the height of the wall increases, the value of Q_R decreases.
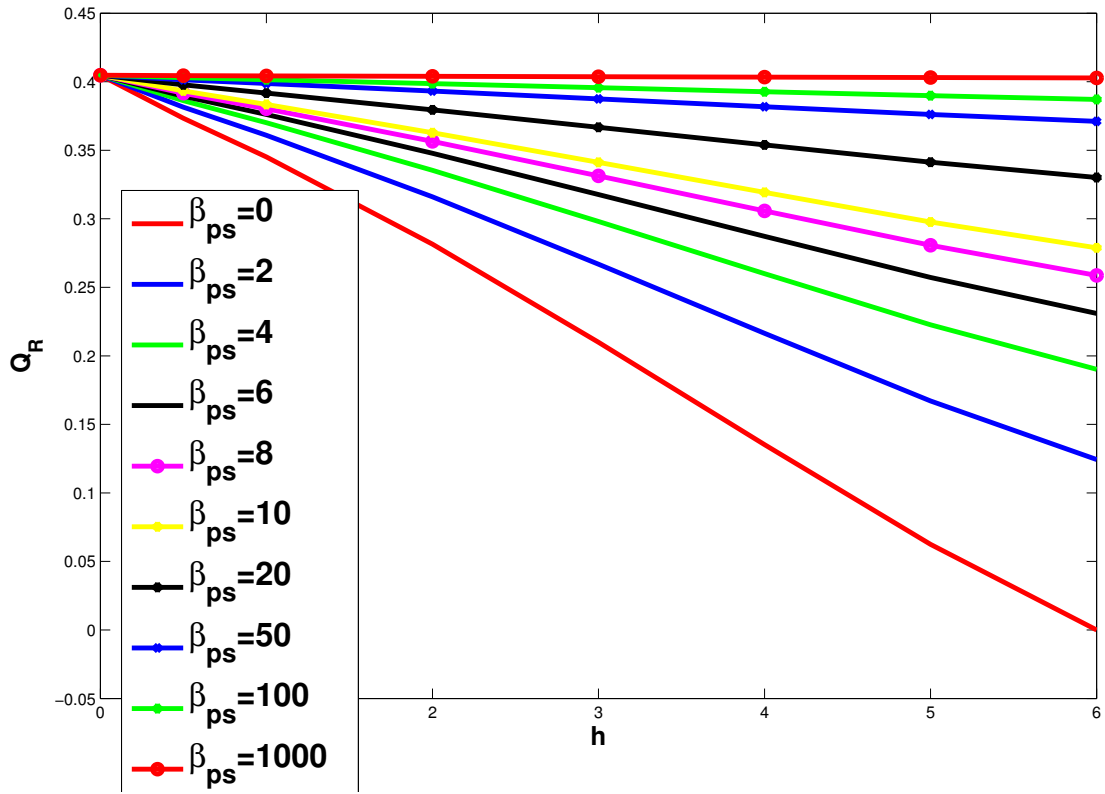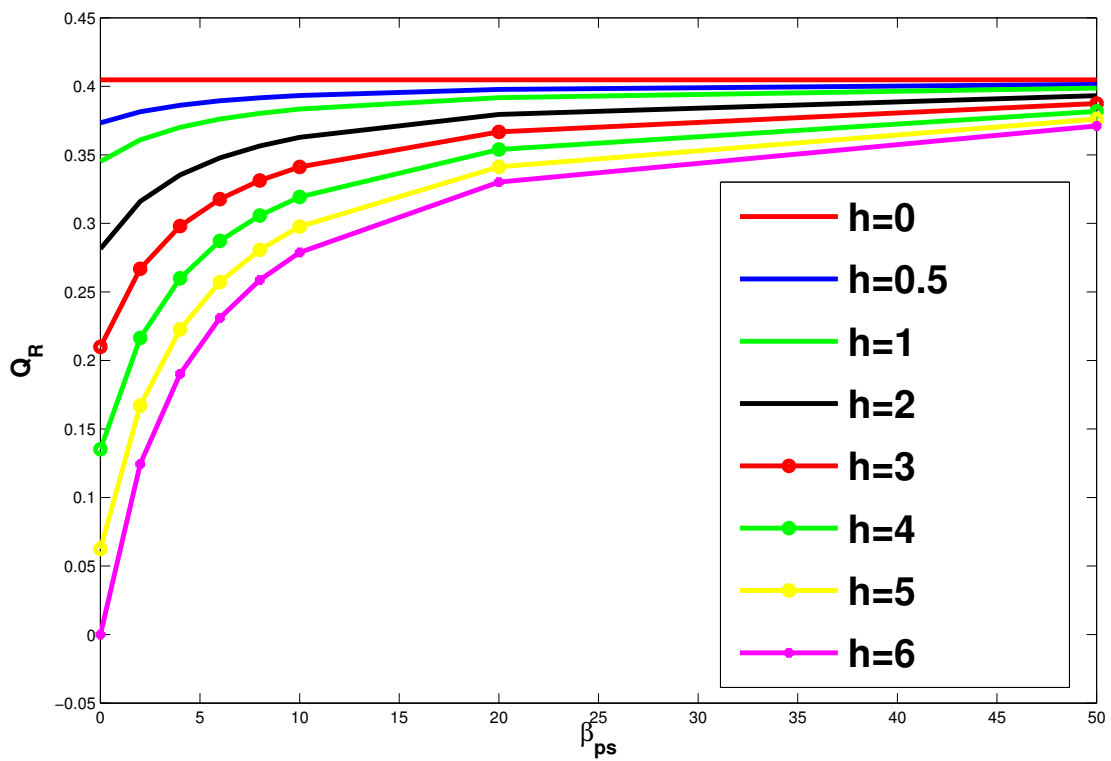
Figure 3.23: *Graphs of (a) h versus Q_R; (b) β_{ps} versus Q_R.*

3.11 Modelling three-dimensional flow

The objective of this part of the study is to formulate a mathematical model based on the conceptual model of any groundwater flow problem for three-dimensional domains. After the discussion of the basic mass balance equation and boundary conditions for three-dimensional flows, the equations will be developed for flow in homogeneous aquifers. Solution of the mathematical model enables one to solve forecasting problems of water levels or piezometric heads in any type of aquifer with precise geometries and properties.

Every mathematical model that describes the transport phenomena of mass and energy in a porous medium domain requires a balance equation of that quantity. In fluid flow problems, this balance equation is considered in the form of a partial differential equation, each term of which represents a change in mass of the fluid per unit volume of porous media per unit time.

3.11.1 Discretization of solution domain
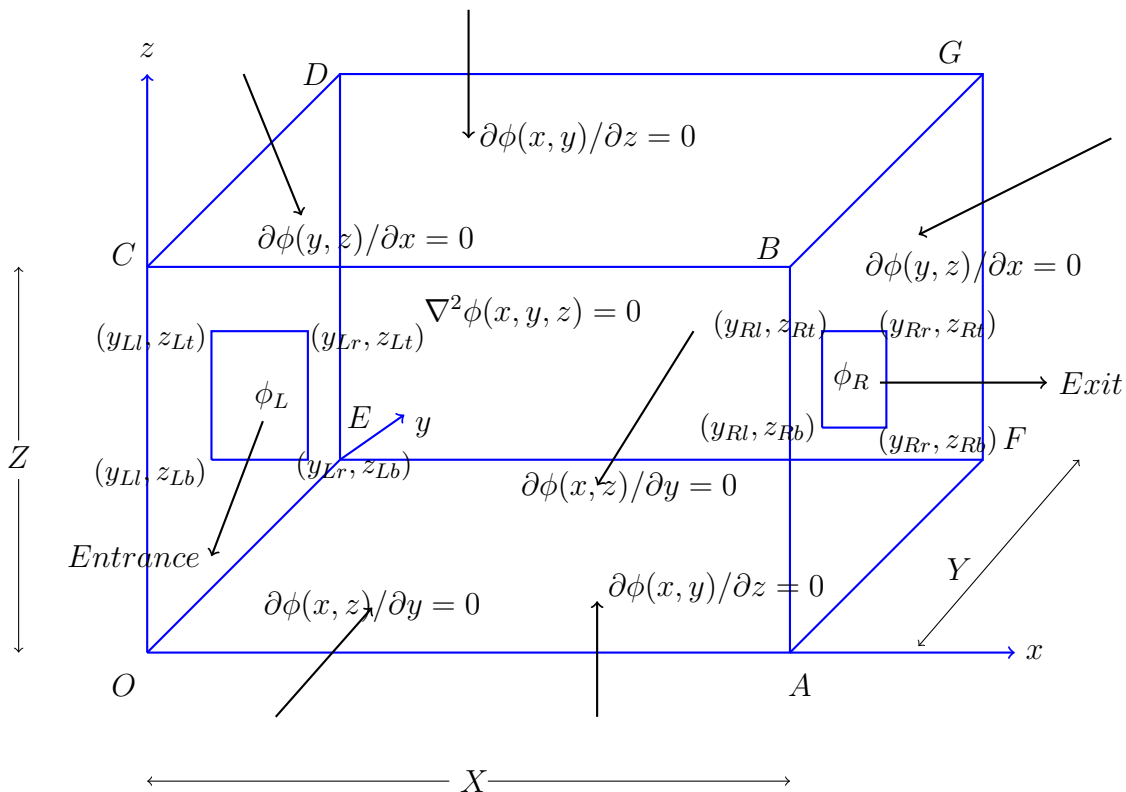
Figure 3.24: *Nomenclature for mass conservation for a control volume for ϕ.*

Consider a control box in the form of a solid rectangular parallelepiped box $OABCDEFG$, having a length X, width Y and height Z. The domain is provided by a solution grid consisting

of I equally-spaced points in the x-direction, J equally-spaced points in the y-direction and K equally-spaced points in the z-direction. The following uses MATLAB terminology.

In the x-direction the increments are represented by $dx = round(\frac{X}{I})$, the increments in the y-direction are given by $dy = round(\frac{Y}{J})$, and the increments in the z-direction are given by $dz = round(\frac{Z}{K})$. The mesh grid is constructed as: $[x, y, z] = meshgrid(xx, yy, zz)$.

In this case, instead of taking the holes in entrance and exits, open rectangular windows are taken in L.H.S and R.H.S of the cube. In this program, windows are located in the yz-plane. The coordinates of the upstream boundary are taken as: (y_{Ll}, z_{Lb}), (y_{Ll}, z_{Lt}), (y_{Lr}, z_{Lb}) and (y_{Lr}, z_{Lt}) and in the downstream boundary are represented as: (y_{Rl}, z_{Rb}) (y_{Rl}, z_{Rt}), (y_{Rr}, z_{Rb}) and (y_{Rr}, z_{Rt}). In order to locate points $y_{Ll}, y_{Lr}, z_{Lb}, z_{Lt}$ in the upstream boundary, we associate them with indices jL_l, jL_r, kL_b, kL_t, respectively, and calculate $jL_l = round(\frac{yL_l}{dy}) + 1$, $jL_r = round(\frac{yL_r}{dy}) + 1$, $kL_b = round(\frac{zL_b}{dz}) + 1$ and finally $kL_t = round(\frac{zL_t}{dz}) + 1$.

Similarly, for the downstream boundary, in order to locate points $y_{Rl}, y_{Rr}, z_{Rb}, z_{Rt}$, we associate them with indices jR_l, jR_r, kR_b, kR_t, respectively, and calculate $jR_l = round(\frac{yR_l}{dy}) + 1$, $jR_r = round(\frac{yR_r}{dy}) + 1$, $kR_b = round(\frac{zR_b}{dz}) + 1$ and finally $kR_t = round(\frac{zR_t}{dz}) + 1$.

3.12 The basic mass balance equation and initial and boundary conditions

As velocity potential $\phi(x, y, z)$ is defined for three-dimensional flows as well, we consider the flow is steady and both water and solid matrix are taken as incompressible, so the governing equation is the *Laplace's equation*

$$\nabla^2 \phi(x, y, z) = \frac{\partial^2 \phi}{\partial x^2} + \frac{\partial^2 \phi}{\partial y^2} + \frac{\partial^2 \phi}{\partial z^2} = 0. \tag{3.63}$$

This basic equation has an infinite number of possible solutions, each one is consistent with a unique case of flow in a porous media domain. To obtain a particular solution from multiple solutions, it is essential to provide additional information besides the basic equation. The additional information together with the partial differential equation determines the mathematical model of a particular problem with the requirement of initial and boundary conditions.

Different boundary conditions correspond to different solutions. Each boundary condition is expressed in the form of a mathematical equation to describe known water fluxes, or known values of state variables on all the boundaries of the domain.

Since no water can pass across the solid impermeable boundaries of the domain, Neumann-type boundary conditions are stated there. Normal components of the velocity are zero on the six solid faces of the box i.e., $\partial\phi/\partial n = 0$ along these faces. The opening in the upstream boundary and opening in the downstream boundary have the scaled dynamic pressure which is hydrostatic i.e., Dirichlet-type boundary condition, $\phi(0, y, z) = \phi_L$, and $\phi(X, y, z) = \phi_R$ are specified in these sections. In detail these boundary conditions are:

$$-\frac{\partial\phi}{\partial x} = 0, \quad \text{on left face excluding inlet,} \tag{3.64}$$

$$-\frac{\partial\phi}{\partial x} = 0, \quad \text{on right face excluding exit,} \tag{3.65}$$

$$-\frac{\partial\phi}{\partial y} = 0, \quad \text{on front face,} \tag{3.66}$$

$$-\frac{\partial\phi}{\partial y} = 0, \quad \text{on back face,} \tag{3.67}$$

$$-\frac{\partial\phi}{\partial z} = 0, \quad \text{on bottom face,} \tag{3.68}$$

$$-\frac{\partial\phi}{\partial z} = 0, \quad \text{on top face,} \tag{3.69}$$

$$\phi(0, y, z) = \phi_L, \quad \text{on injection window,} \tag{3.70}$$

$$\phi(X, y, z) = \phi_R, \quad \text{on suction window.} \tag{3.71}$$

3.13   Three-dimensional flow in the absence of an object

A numerical solution for the dynamic pressure is undertaken for Laplace's equation subject to suitable boundary conditions as shown in Figure 3.24. A simple example is used for illustration. A homogeneous aquifer is taken in the form of a rectangular parallelepiped box with $0 \leq x \leq 10$ [m], $0 \leq y \leq 12$ [m], and $0 \leq z \leq 14$ [m]. The boundary conditions on the upstream and downstream boundaries (at free surfaces of the fluid) are assigned respectively, as follows:

$$\phi(0, y, z) = \phi_L = 2, \quad \phi(X, y, z) = \phi_R = 1, \tag{3.72}$$

and for the boundary conditions on the solid boundaries of the cube, the fact of zero normal velocities is taken into account, i.e., $\partial\phi/\partial n = 0$, where n is the unit vector normal to every side of the box.

Figure 3.25 shows the contour plot of isobars, which provides the same fact as illustrated for two-dimensional aquifers, i.e., water flows in a direction opposite to the dynamic pressure gradient (that water flows along the direction where pressure gradient drops most, because a greater value of pressure, i.e., $\phi_L = 2$ (red) is assigned to the upstream boundary as compared to the downstream boundary, where $\phi_R = 1$ (blue)).
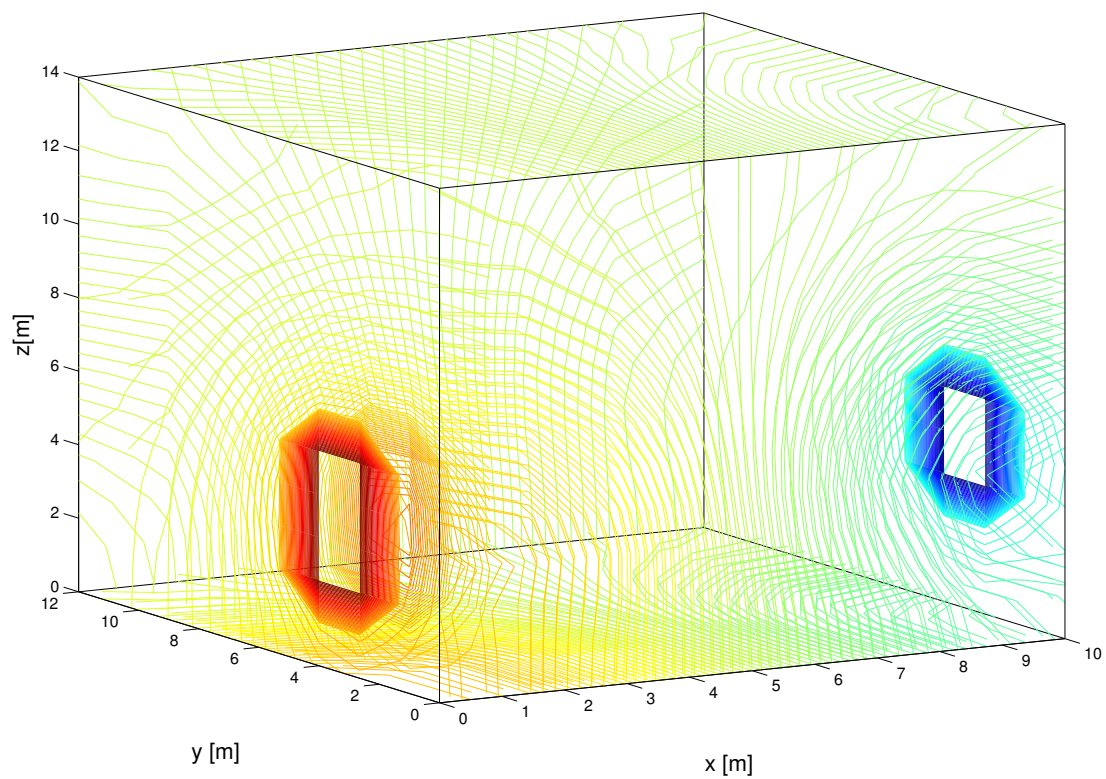
Figure 3.25: *Graphs of velocity potential $\phi(x, y, z)$, with all the contours equally spaced between minimum ($\phi_R = 1$) and maximum ($\phi_L = 2$) values of $\phi(x, y, z)$.*

3.14 Three-dimensional flow in the presence of an impermeable cuboidal object
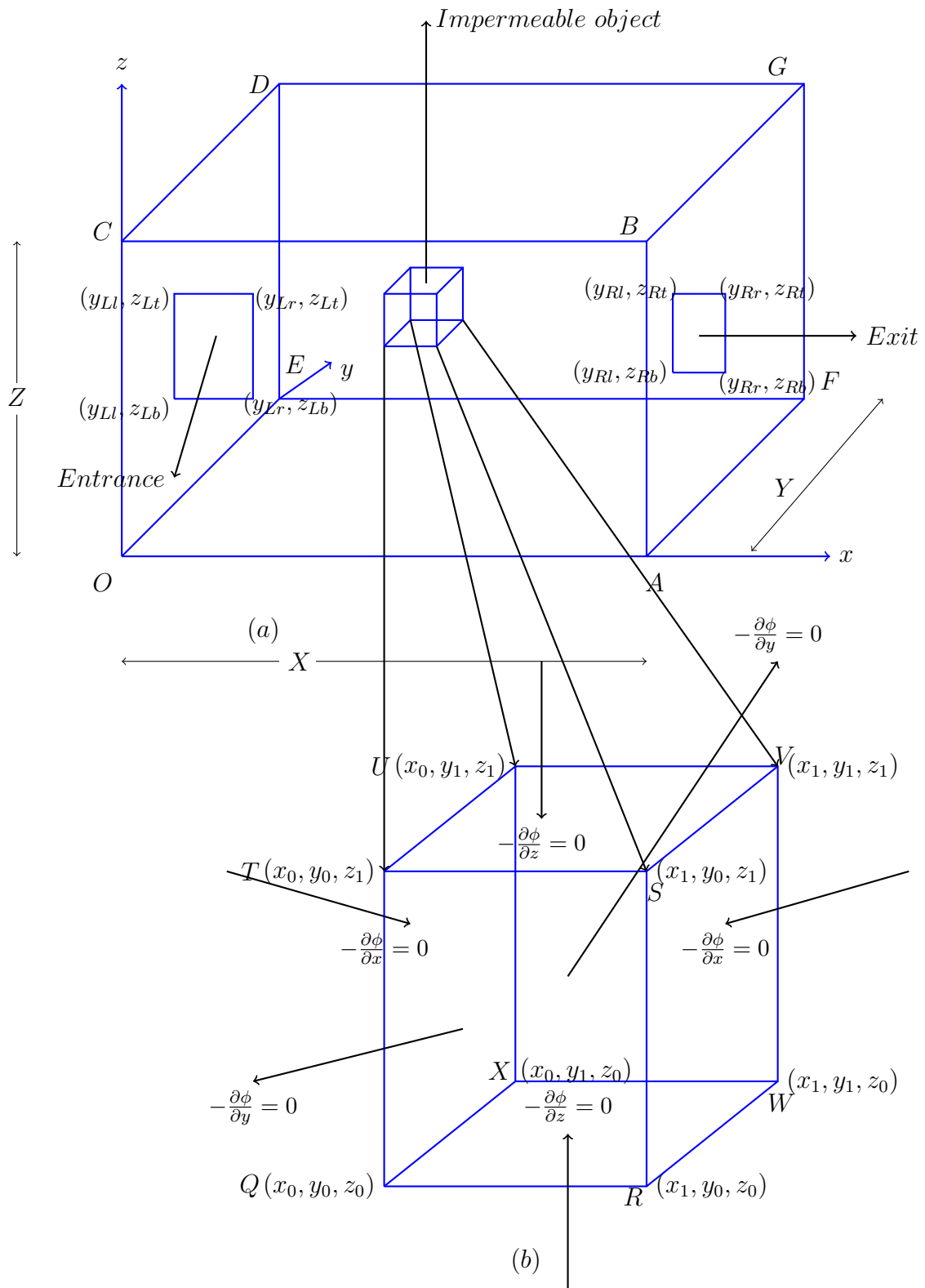
Figure 3.26: *Nomenclature for (a) mass conservation for a control volume for ϕ, with an impermeable cuboidal object embedded in it; (b) schematic diagram of the impermeable object.*

Figure 3.26 represents a three-dimensional cubical porous medium with an impermeable cubical object embedded in it. In analysing the problem, the following assumptions should be considered:

- The cubic porous medium is homogeneous and isotropic.

- No heat generation, or pollutant or tracers occur inside the porous medium.

- No heat generation or pollutant or tracers pass across the cuboidal object.

Based on these assumptions, the governing equation and the boundary conditions on porous media are the same as discussed in Section 3.13. The boundary conditions on the impermeable cuboidal object are assigned with regard to the fact that normal components of the velocities are taken to be zero there.

Figure 3.27a illustrates the results of the numerical simulations. Since the cuboid is impermeable, no fluid can pass across the solid boundaries (walls) of this object. However, it is not clear that equipotential lines strike normal to this object, so an xy-slice of Figure 3.27a is taken and the preservation of normality is illustrated in Figure 3.27b.

(a)   (b)
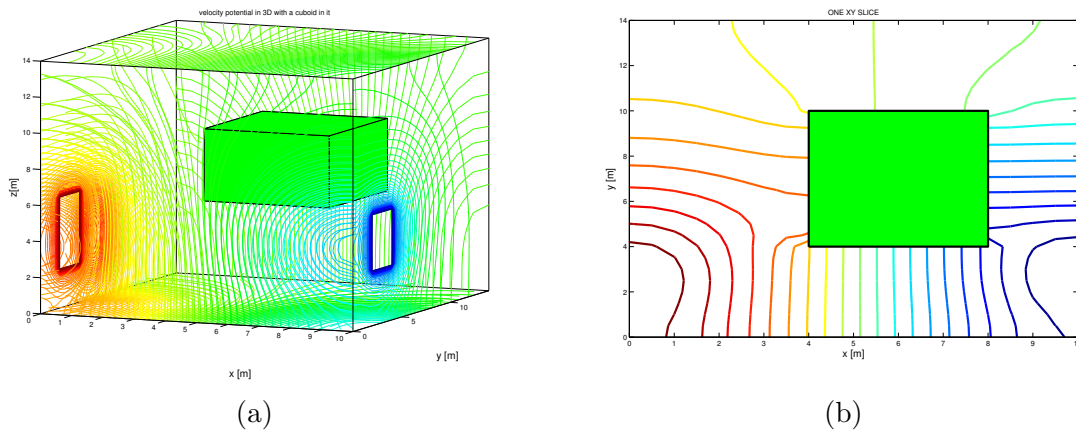
Figure 3.27: *Graphs of velocity potential $\phi(x, y, z)$ with (a) an impermeable cuboid placed in it (b) an xy-slice through the impermeable cuboid*

3.15 Three-dimensional flow in the presence of pervious cuboidal objects
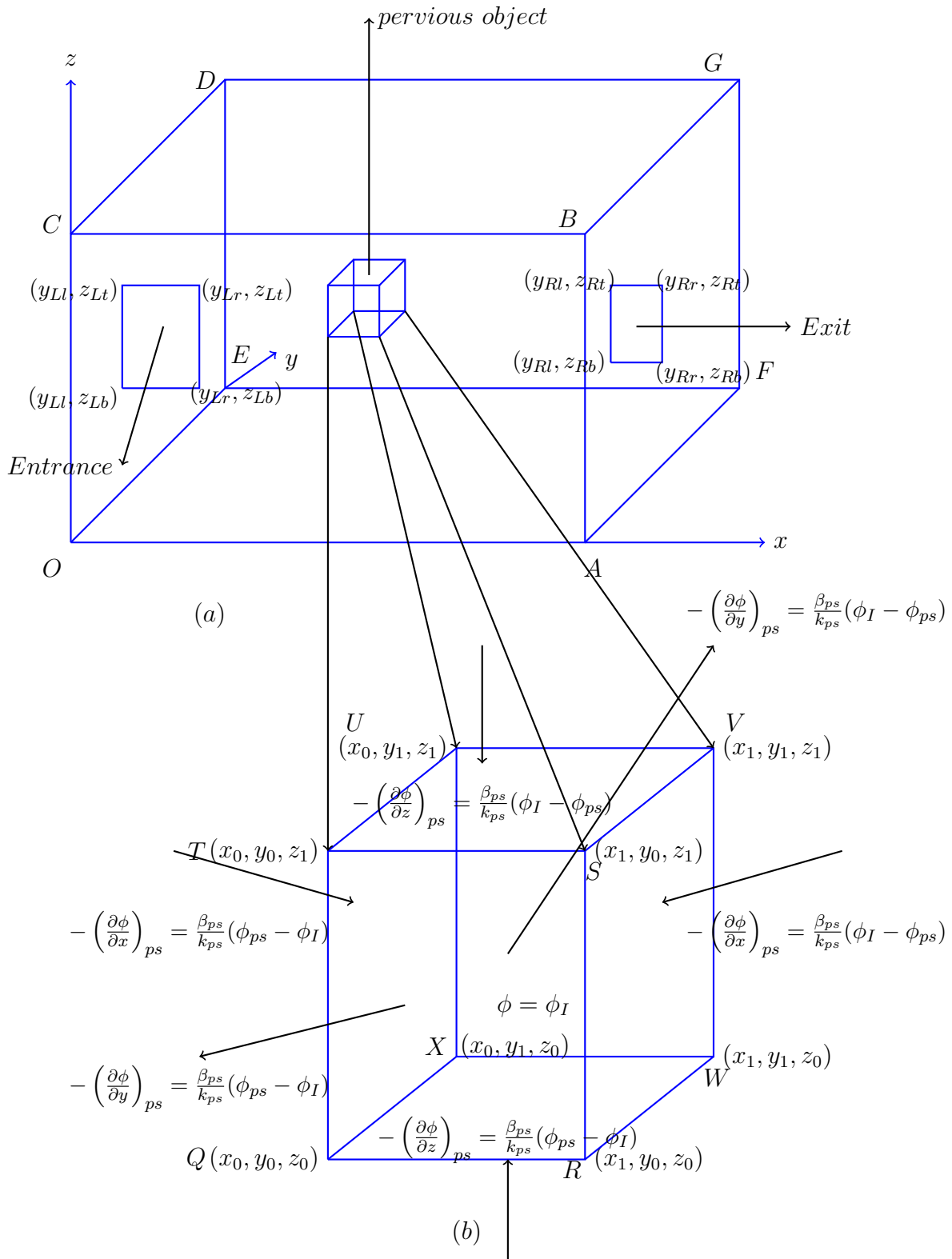
Figure 3.28: *Schematic diagram of (a) $\phi(x, y, z)$ with pervious object embedded in it; (b) an enlarged view of pervious cuboidal object with boundary conditions.*

Figure 3.28 represents a cubical pervious object in a three-dimensional aquifer. Boundary conditions on the surface of the porous enclosure are the same as those discussed in Section 3.12. The following boundary conditions have been considered on the surface of embedded pervious body. These equations have been written in the scaled form of the velocity potential $\phi(x, y, z)$ as:

$$-\left(\frac{\partial \phi}{\partial x}\right)_{ps} = \frac{\beta_{ps}}{k_{ps}}(\phi_{ps} - \phi_I), \quad \text{on left face,} \tag{3.73}$$

$$-\left(\frac{\partial \phi}{\partial x}\right)_{ps} = \frac{\beta_{ps}}{k_{ps}}(\phi_I - \phi_{ps}), \quad \text{on right face,} \tag{3.74}$$

$$-\left(\frac{\partial \phi}{\partial y}\right)_{ps} = \frac{\beta_{ps}}{k_{ps}}(\phi_{ps} - \phi_I), \quad \text{on front face,} \tag{3.75}$$

$$-\left(\frac{\partial \phi}{\partial y}\right)_{ps} = \frac{\beta_{ps}}{k_{ps}}(\phi_I - \phi_{ps}), \quad \text{on back face,} \tag{3.76}$$

$$-\left(\frac{\partial \phi}{\partial z}\right)_{ps} = \frac{\beta_{ps}}{k_{ps}}(\phi_{ps} - \phi_I), \quad \text{on bottom face,} \tag{3.77}$$

$$-\left(\frac{\partial \phi}{\partial z}\right)_{ps} = \frac{\beta_{ps}}{k_{ps}}(\phi_I - \phi_{ps}), \quad \text{on top face,} \tag{3.78}$$

where β_{ps} [m] is a measure of resistance of the object's surface to flow through it, and ϕ_I [m] is the pressure inside the pervious body.

A numerical solution for the governing Laplace's equation together with boundary conditions (3.64)-(3.78) is plotted as contours of isobars in Figure 3.29. In this example, the value of dynamic pressure in the entrance is taken as $\phi_L = 1$ [m], in the exit as $\phi_R = 0$ [m], and inside the body as $\phi_I = 5$ [m] or $\phi_I = -5$ [m].

In Figure 3.29a, the mean dynamic pressure inside the pervious body is higher than that of the neighbourhood area, which is shown by red isobars. But the pressure exerted by the fluid inside the cubic cross-section to the neighbouring area is not visible, so two-dimensional xy- and yz-slices of this cuboid are taken. Figures 3.29b and 3.29c represent higher pressure inside the slices as compared to the upstream and downstream boundaries. On the other hand for a lower value of dynamic pressure, i.e., $\phi_I = -5$ [m], the isobars are visible in the form of blue lines near the object in the Figures 3.29d-3.29f.

(a)   (b)   (c)

(d)   (e)   (f)
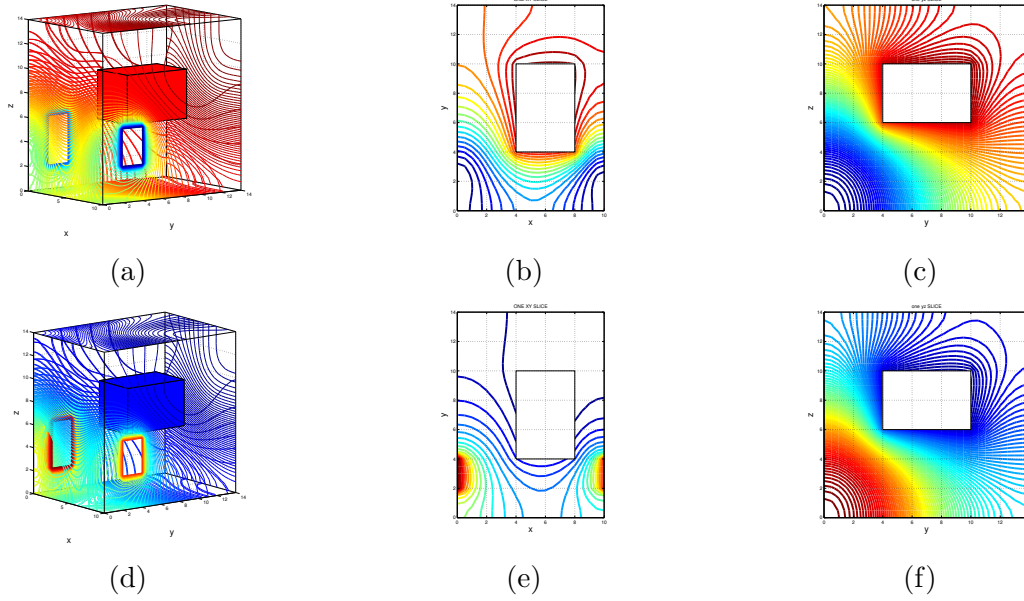
Figure 3.29: *Graphs of ϕ with $\beta_{ps} = 2$, for a cubical aquifer with (a) a pervious cuboid in it with $\phi_I = 5$; (b) an xy-slice of pervious cuboid with $\phi_I = 5$, at z=8; (c) a yz-slice of pervious cuboid with $\phi_I = 5$, at x = 4; (d) a pervious cuboid in it with $\phi_I = -5$; (e) an xy-slice of pervious cuboid with $\phi_I = -5$, at z = 6; (f) a yz-slice of pervious cuboid with $\phi_I = -5$, at x = 6.*

3.15.1 Influence of ϕ_I on fluxes

To give the influence of ϕ_I on net flow, a comparison between ϕ_I and various fluxes through a cubic porous media with a pervious cubical body is given in Figure 3.30. For a positive value of β_{ps} (say $\beta_{ps} = 2$), as ϕ_I turns from negative to positive, flux through the cuboid, Q_I (red line) and flux out through the porous media, Q_R (magenta line) increases significantly, whereas, flux in, Q_L (green line) through the porous media tends to decrease gradually, as illustrated in Figure 3.30a. This is because, for a higher value of ϕ_I, the fluid inside the pervious cuboid exerts a high pressure on the neighbouring fluid, as a result of which, water flows outside the porous media from the exit as well as from the inlet, and the relationship between ϕ_I and fluxes is linear. On the other hand, for a larger magnitude of negative value of ϕ_I, flux in is larger than flux out and flux through cuboid. This shows that more water is entering into the cubical body as compared to leaving it.

In addition, the net flow across the system follows the mass balance law, and results are verified in Figure 3.30b, in which the net flow in (which is equal to flux in, Q_L through the porous media and flux, Q_I passed through cuboid) is exactly equal to flux out Q_R through the porous media i.e., $Q_R = Q_I + Q_L$.

69
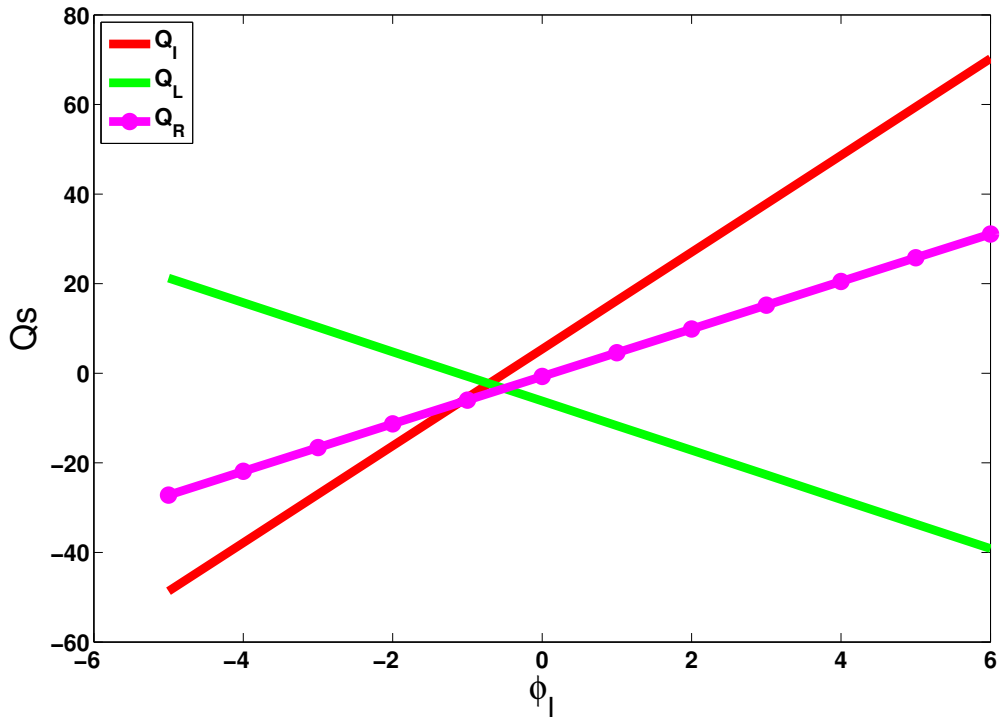
(a)
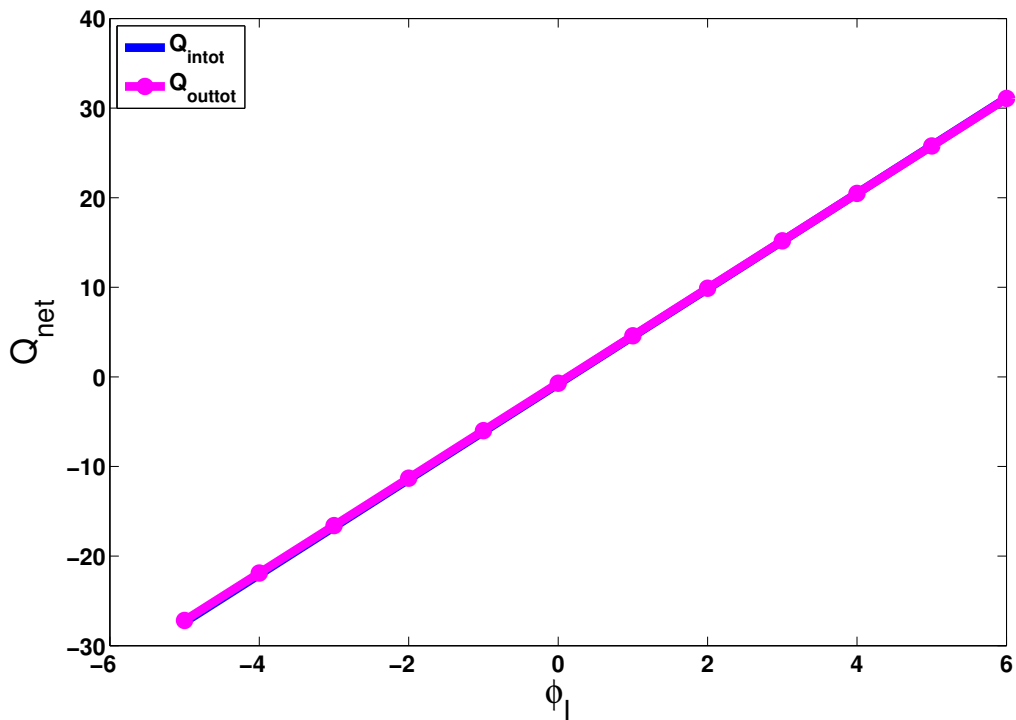
(b)

Figure 3.30: *Illustrations of fluxes for $\beta_{ps} = 2$, $\phi_L = 1$, $\phi_R = 0$, for various values of ϕ_I, graph between (a) ϕ_I and flux through pervious cubic object, flux in through entrance and flux out through exit, and; (b) ϕ_I and net flow in and net flow out.*

3.16 Hele-Shaw cell

The notion of pervious objects enables us to extend our study to various pervious objects embedded inside the porous media. This leads us to elaborate on the idea of a Hele-Shaw cell [10]. In this arrangement of the fluid flow field, inertia forces are neglected.

According to this composition, a two-dimensional flow takes place between two parallel plates, which are separated by an infinitesimally small displacement d. The gap between the plates is partially covered by fluid and partially by stumbling blocks (cylinders) whose generators are perpendicular to the plates. A steady pressure difference is exerted between both the ends of the system, as a result of which, fluid is forced to flow from one end of the layer to the other. In this arrangement, the local velocity and local pressure gradient are related by

$$u \approx -\frac{1}{2\mu}\frac{\partial p}{\partial x}z(d-z), \quad v \approx -\frac{1}{2\mu}\frac{\partial p}{\partial y}z(d-z), \tag{3.79}$$

where the coordinate z is normal to the plane [10]. In 1898, Hele-Shaw proposed the idea that at some constant value of z (or averaged with respect to z (Equation. (3.79)), the value of u and v defines a two-dimensional, irrotational velocity field which also preserves the property of zero normal components on the rigid boundaries of a surface. Thus the Hele-Shaw's steady flow past objects is similar to that of theoretical flow of inviscid fluid with zero vorticity passing through a porous media with embedded objects of the same kind.

The equations governing the Hele-Shaw flows are similar to those of the inviscid potential flow and to the flow of fluid through a porous medium (Darcy's law). For a porous medium, approximations to Hele-Shaw flow are observed in the way that, when groundwater is forced to flow by a pressure gradient exerted by the soil, then each constituent of the water follows a complicated path when it passes through the random arrangement of the interstices. In this case, the interstices function like the parallel plates [10].

Our system is composed of two parallel plates which are joined together in the form of a rectangular porous medium $OABC$, which is connected to two water containers on L.H.S and R.H.S with different scaled dynamic pressures ϕ_L and ϕ_R respectively. Between these plates there are immersed four rectangular pervious objects, which are also connected to a single separate water container whose dynamic pressure ϕ_I is different from that of ϕ_L and ϕ_R, as

shown in Figure 3.31.

Water is forced to flow in the system in this way so that the level of surface at one end of the arrangement is being kept higher than the other by the introduction of liquid there.
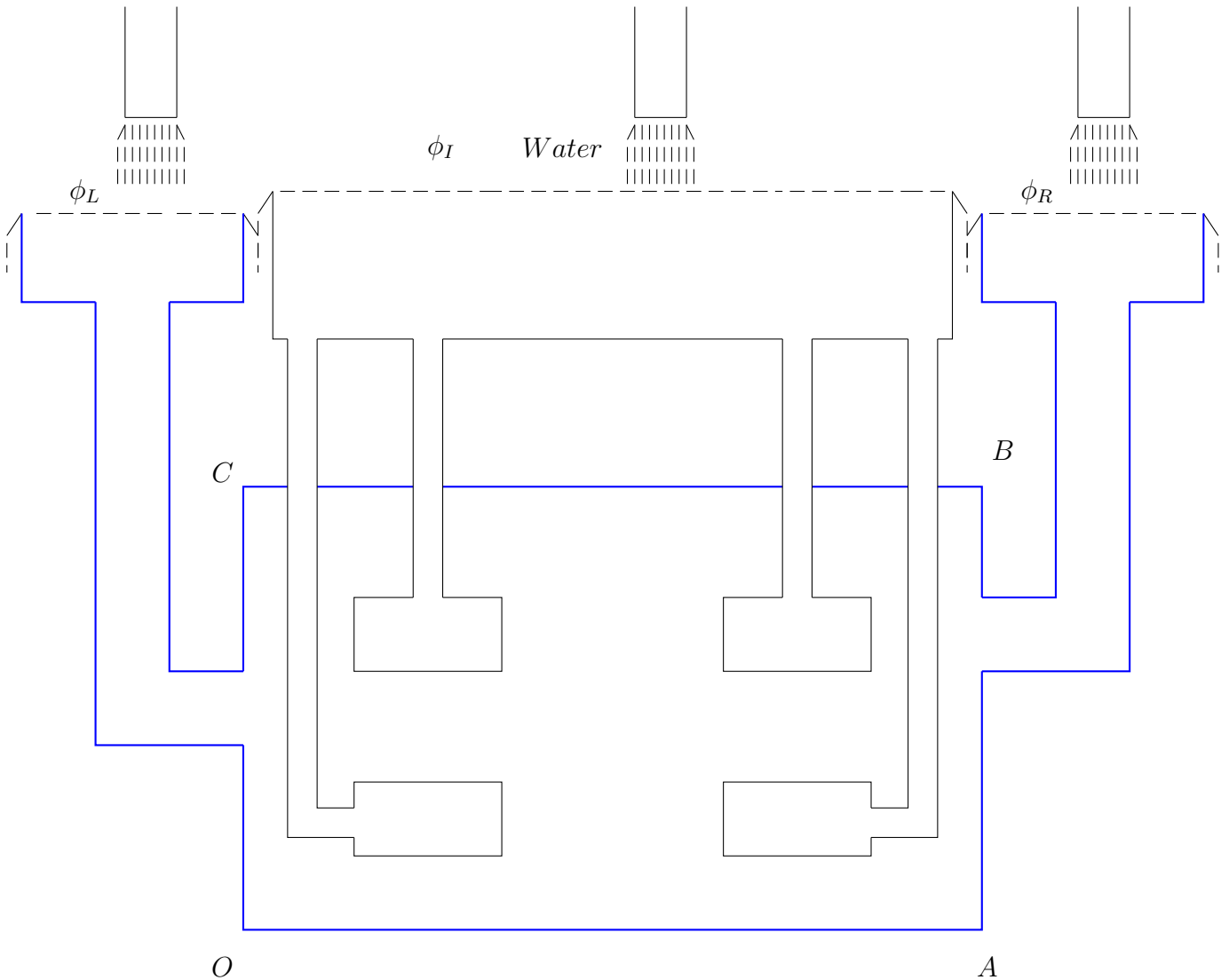
Figure 3.31: *Schematic diagram of the physical domain for Hele-Shaw cell.*

3.16.1 Illustration: a three-dimensional homogeneous aquifer with four pervious cuboidal objects embedded in it, with the same value of ϕ_I

Even though the Hele-Shaw cell is described for two-dimensional flows, here as an illustration, consider a three-dimensional flow past objects in homogenous cubic porous media as shown in Figure 3.32. The governing equation and boundary conditions on the porous media and pervious objects are similar as discussed in Section 3.15.

As water always flows from areas of higher dynamic pressure to those of lower pressure, so the flow of water will depend on the values of ϕ_L, ϕ_R and ϕ_I. In this example, fluid is set in motion by assigning a higher value of $\phi_I = 5$ for the obstacles and by fixing the values of scaled dynamic pressure in the entrance and exit as $\phi_L = 1$, and $\phi_R = 0$, respectively. Four pervious objects of different dimensions are placed in the cube. Figure 3.32a is a simple illustration of equipotential lines (red), which depicts a higher pressure in the neighbourhood of the obstacles and flow of water through the two openings on L.H.S and R.H.S of the porous media.

Since the governing equation and boundary conditions are linear and homogeneous, so the motion of the fluid is reversible and there is a linear relationship between ϕ_I and flux through the cuboids, as illustrated in Figure 3.32b. The graph is plotted for $\phi_L = 1$, $\phi_R = 0$, $\beta_{ps} = 1$ and $\beta_{ps} = 100$, for various values of ϕ_I. As β_{ps} is a measure of the perviousness of a surface, so for non-negative values of ϕ_I, the value of flux through the cuboids increases significantly for a larger value of β_{ps}. Moreover, the value of flux depends also on the dimensions and positions of the cuboids, as is obvious from the plot of flux through the yellow cuboid, which is placed near the exit and has relatively higher dimensions than the others.
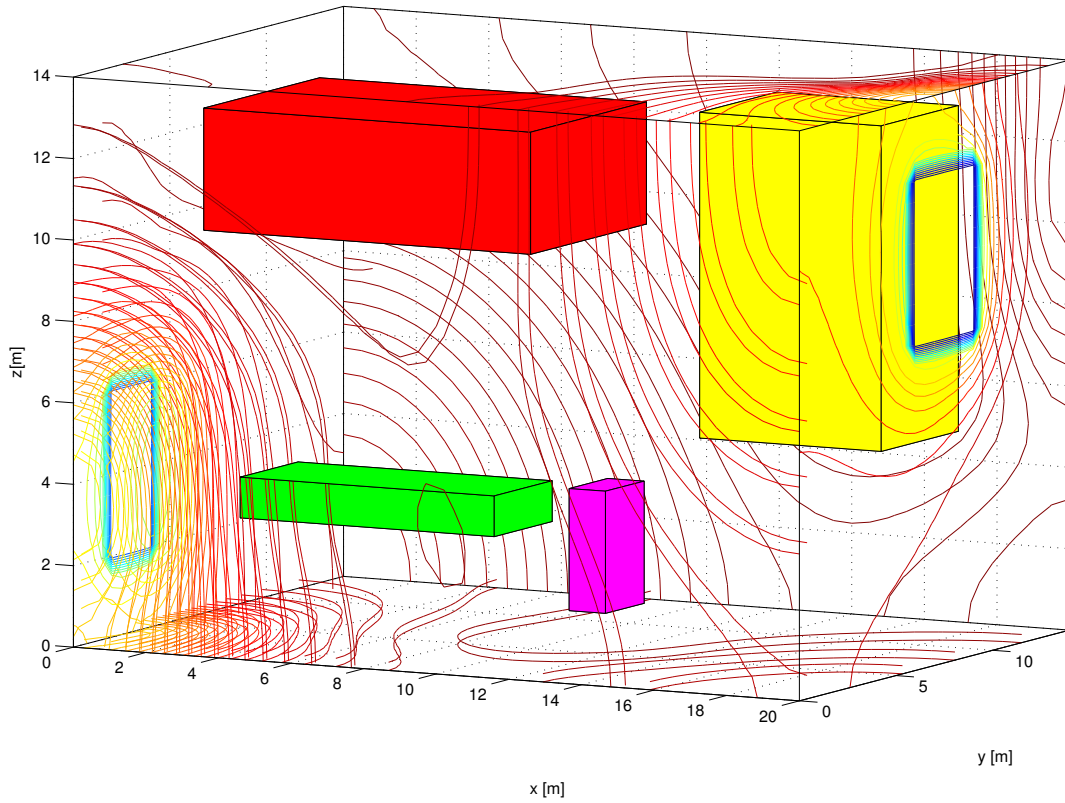
(a)
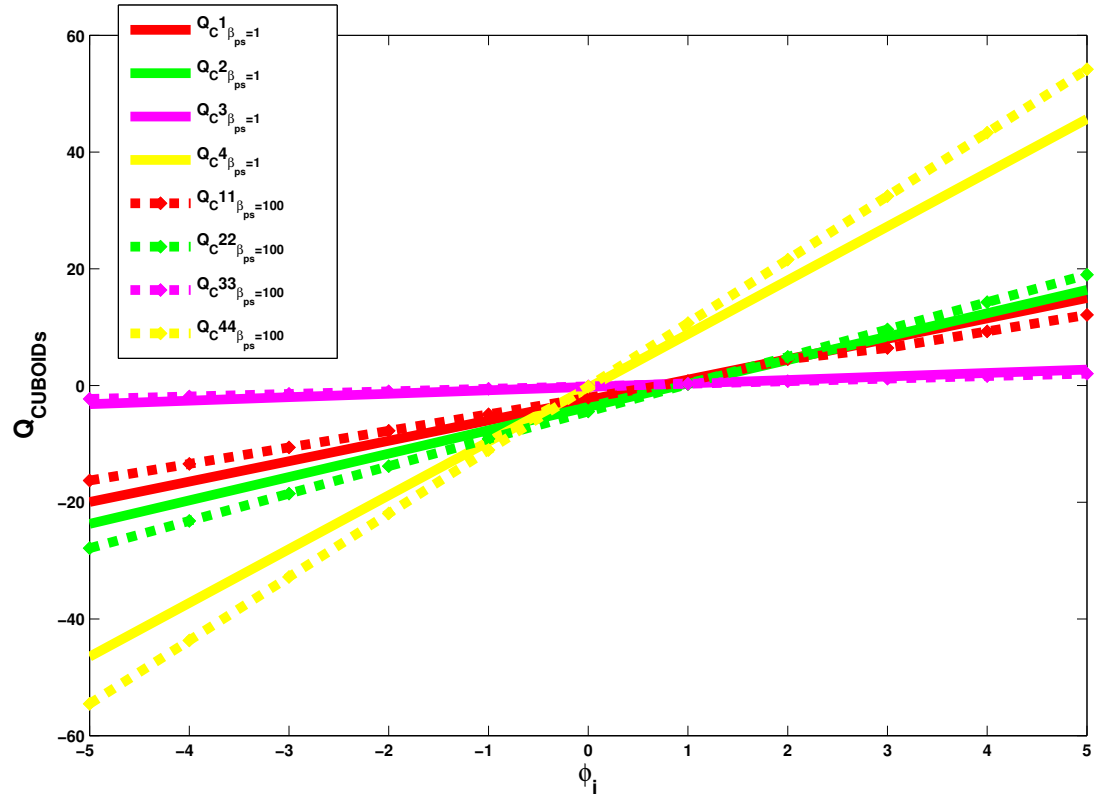
(b)

Figure 3.32: *(a) Isolines of velocity potential in 3D with four pervious cuboids, with $\beta_{ps} = 100$, $\phi_L = 1$, $\phi_R = 0$ and $\phi_I = 5$; (b) Graph of fluxes into (for negative ϕ_I) or out (for positive ϕ_I) of these cuboids for various values of ϕ_I, with $\beta_{ps} = 1$, and $\beta_{ps} = 100$.*

74

3.17 A three-dimensional homogeneous aquifer, with four pervious cuboidal objects embedded in it with different values of ϕ_I

Following the discussion in Subsection 3.16.1, and recalling the idea of Hele-Shaw cell of Section 3.16, here we suppose that all the embedded objects are connected to different water containers with different pressures ϕ_I, $I = I_1, I_2, I_3, I_4$, by introduction of varying amounts of liquid there, as shown in Figure 3.33. It does not matter what are the values of ϕ_i, $i = L, R, I_1, I_2, I_3, I_4$ (L means in the inlet, R means in the exit and I_1, I_2, I_3, I_4, means in the four containers), because on the basis of our previous experiments, it can be deduced readily that, whatever the values and signs of ϕ_i, $i = L, R, I$, the velocity of the water lies in the direction opposite to the scaled dynamic pressure gradient.
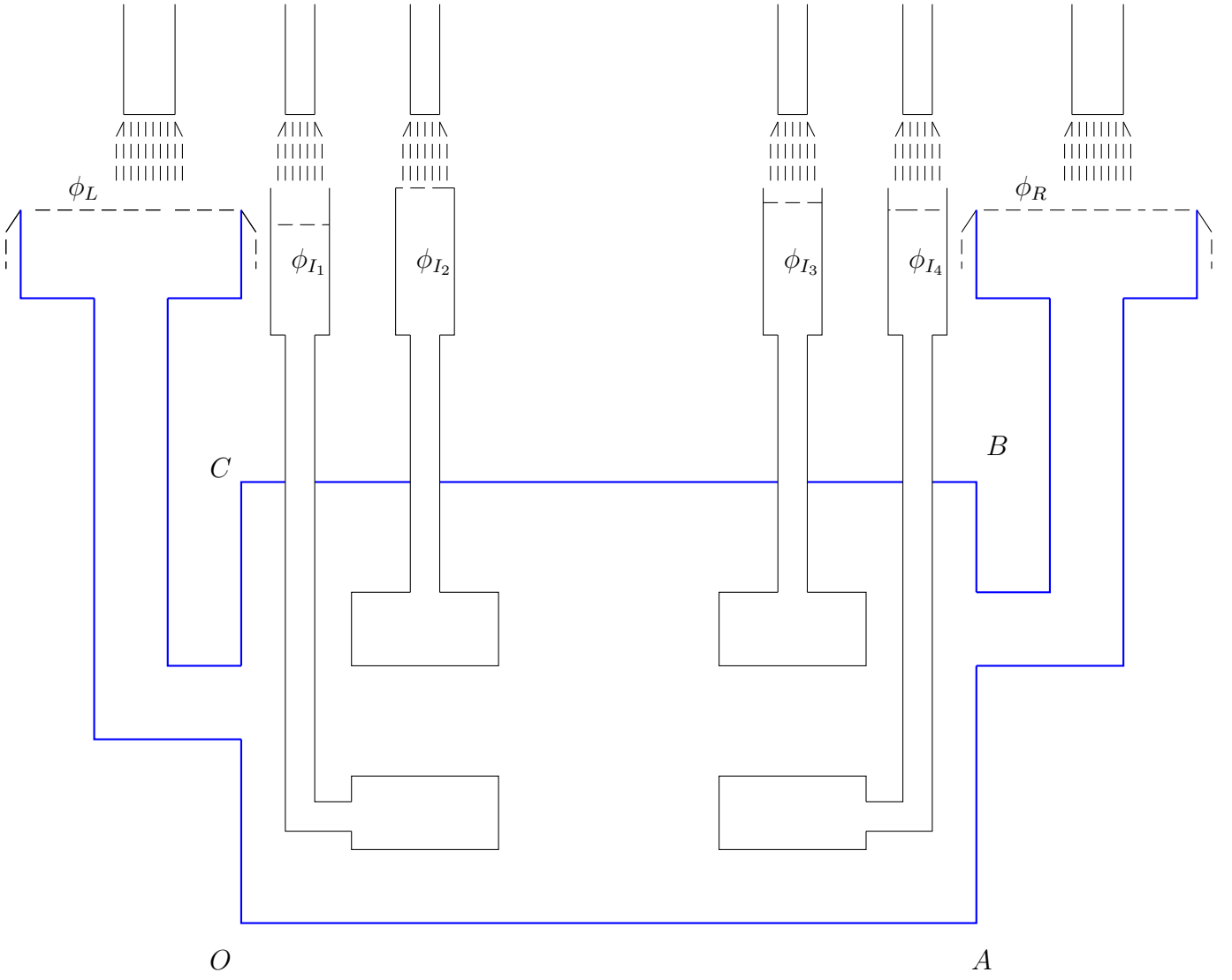
Figure 3.33: *Schematic diagram of the physical domain for Hele-Shaw cell for four different pressures of containers.*

As an illustration, consider Figure 3.34, in which four pervious cuboids with different values of pressure inside are immersed inside a cubic porous media. The values of scaled dynamic pressures in the entrance and exit are kept constant by assigning them the values $\phi_L = 1$ [m] and $\phi_R = 0$ [m], respectively. The values of pressure inside the cuboids are taken as follows:

$$\phi_{I_1} = 0.1 \text{ [m] (red)},$$

$$\phi_{I_2} = 0.5 \text{ [m] (green)},$$

$$\phi_{I_3} = 0.7 \text{ [m] (magenta)},$$

$$\phi_{I_4} = 0.8 \text{ [m] (yellow)}.$$

Since the pressure inside the red cuboid is minimum, so blue equipotential lines can be seen in the neighbourhood of this cuboid. On the other hand, due to the higher pressure in the

yellow cuboid, red isobars are prominent in its neighbouring area.
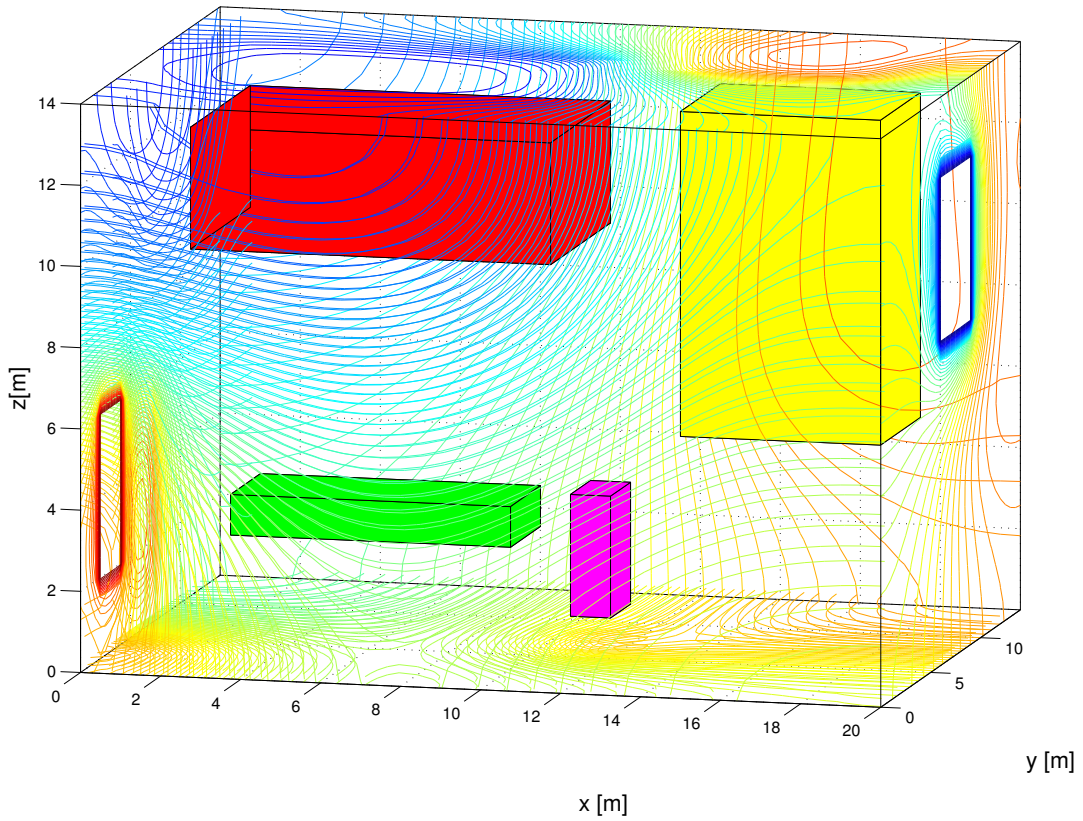
Figure 3.34: *Graph of ϕ in 3D aquifer, with $\beta_{ps} = 2$, $\phi_L = 1$, $\phi_R = 0$ with four pervious cuboids in it kept at different pressures as: $\phi_{I_1} = 0.1$ (red), $\phi_{I_2} = 0.5$ (green), $\phi_{I_3} = 0.7$ (magenta), $\phi_{I_4} = 0.8$ (yellow).*

Chapter 4

Fluid Flow Model for

Non-homogeneous Aquifers

So far in the discussion of permeability, we assumed that the geological formation was homogeneous and isotropic, indicating that the value of *intrinsic permeability, k* was everywhere uniform. However, porous media comprising groundwater aquifers and oil reservoirs are rarely homogeneous regarding to their permeability[1]. To avoid confusion with *intrinsic permeability k*, the *hydraulic conductivity K* may be expressed as:

$$K = \frac{k\rho g}{\mu}, \tag{4.1}$$

where k [m²], K [m day^{-1}], ρ [kg m^{-3}], g [m s^{-2}] and μ [kg m^{-1} s^{-1}] are respectively *the permeability, the hydraulic conductivity of a material, fluid density, gravitational acceleration, and fluid dynamic viscosity.* Table 4.1 represents values of μ, g, and ρ.

Table 4.1: *Parameters used for the simulations.*

Parameters	Values	Units
fluid dynamic viscosity μ	1.002×10^{-3}	[kg m^{-1} s^{-1}]
gravitational acceleration g	9.8	[m s^{-2}]
fluid density ρ	1000	[kg m^{-3}]

Table 4.2 includes representative hydraulic conductivity and respective permeability of ge-

---

[1]Permeability is a measure of the ability of a material (such as rocks or soil) to transmit fluids. This is a property only of the medium and is independent of fluid properties [52].

ological materials. It is worthy to mention that these values are taken as an average of many measurements, which depend on various elements, e.g., fracturing, weathering, burial depth, and solution channels, etc. [52].

Table 4.2: *Representative values of hydraulic conductivity and permeability of some materials. For conversion, see Equation 4.1.*

Material	Hydraulic conductivity K (m/day)	Permeability k (m^2)
Gravel, fine	450	5.3167×10^{-10}
Gravel, medium	270	3.1952×10^{-10}
Gravel, coarse	150	1.7751×10^{-10}
Sand, coarse	45	5.3253×10^{-11}
Sand, medium	12	1.4201×10^{-11}
Sand, fine	2.5	2.9585×10^{-12}
Silt	0.08	9.4671×10^{-14}
Clay	0.0002	2.3668×10^{-16}
Sandstone medium-grained	3.1	3.6685×10^{-12}
Sandstone fine-grained	0.2	2.3668×10^{-13}

Groundwater aquifers are composed of a layered structure of different physical properties, such as *permeability*, *porosity*, *hydraulic conductivity* and *transmissivity*, etc. This layered system has evolved due to various geological processes over different periods of time. It forms a non-homogeneous material composed of layers of different textures [11]. The present chapter will cover a discussion about potential flow in two- and three-dimensional non-homogeneous aquifers considering permeability and hydraulic conductivity as its main characteristics, including analysis of flow:

1. in the absence of an object in two- and multi-layered systems, with different positions of entrance and exit of fluid,

2. in the presence of impermeable objects of different sizes and shapes, placed at various positions in the aquifer,

3. in the presence of a permeable object, whose permeability is different from the outside porous media, and

4. in the presence of pervious objects with pressure inside different from the inlet and outlet.

Two situations arise for a non-homogeneous aquifer: one with the horizontal layered system and the other composed of several vertical layers of different thicknesses and permeabilities. In former system, if a single layer has relatively lower permeability, then the vertical flow is decelerated, but fluid flows smoothly in the horizontal direction by means of a layer of relatively higher permeability.

An example of three horizontal layers is shown in Figure 4.1. This is just an illustration to show an aquifer consisting of three horizontal layers, each independently isotropic, but with different permeabilities and thicknesses. If k_i, d_i and Q_i, $i = 1, 2, 3$, are respectively, the permeability, the thickness and discharge per unit width of aquifer (measured normal to the plane of flow) in each layer, then by Darcy's law, the total discharge, Q, which is the sum of individual discharge rates, Q_i, is given by [11]:

$$Q = \sum_{i=1}^{3} Q_i, \tag{4.2}$$

$$\text{where} \quad Q_i = k_i d_i \frac{\Delta \phi}{a}, \tag{4.3}$$

$$\text{and} \quad \Delta \phi = \phi_L - \phi_R, \tag{4.4}$$

$$\text{so,} \quad Q = \sum_{i=1}^{3} Q_i = \sum_{i=1}^{3} k_i d_i \frac{\Delta \phi}{a}. \tag{4.5}$$
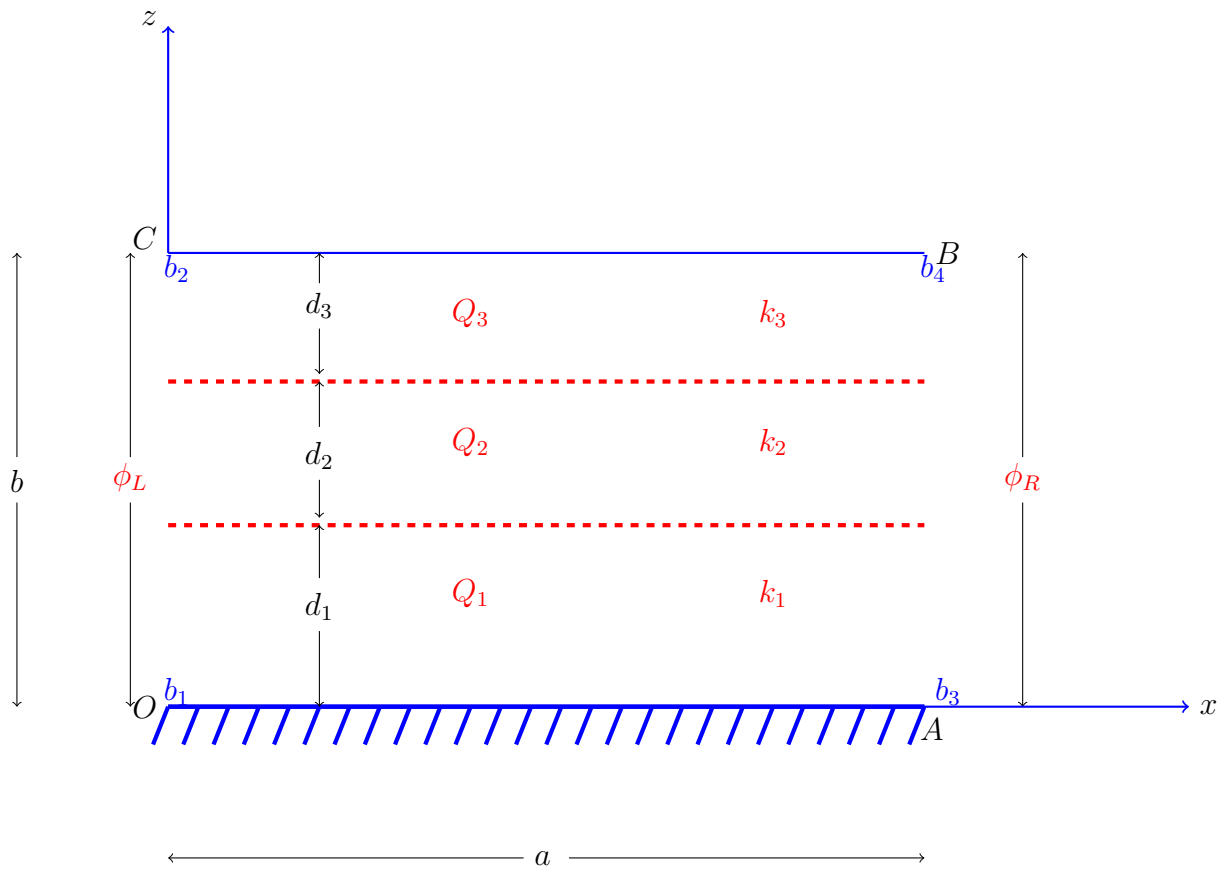
Figure 4.1: *Diagram of 3 horizontal strata in a confined aquifer, each isotropic, with different thicknesses and permeabilities.*

Now consider a second example of flow whose direction is normal to the layer system as shown in Figure 4.2. In this case, the discharge Q, and $\Delta\phi$ is given by,

$$\Delta\phi = \phi_L - \phi_R, \tag{4.6}$$

$$\text{and} \quad a = \sum_{i=1}^{3} a_i, \tag{4.7}$$

$$\text{hence} \quad Q_i = k_i b \frac{\Delta\phi}{a_i}; \tag{4.8}$$

$$\text{where} \quad Q = \sum_{i=1}^{3} Q_i = \sum_{i=1}^{3} k_i b \frac{\Delta\phi}{a_i}; \tag{4.9}$$

$$\text{so,} \quad Q = b\Delta\phi \sum_{i=1}^{3} \frac{k_i}{a_i}. \tag{4.10}$$
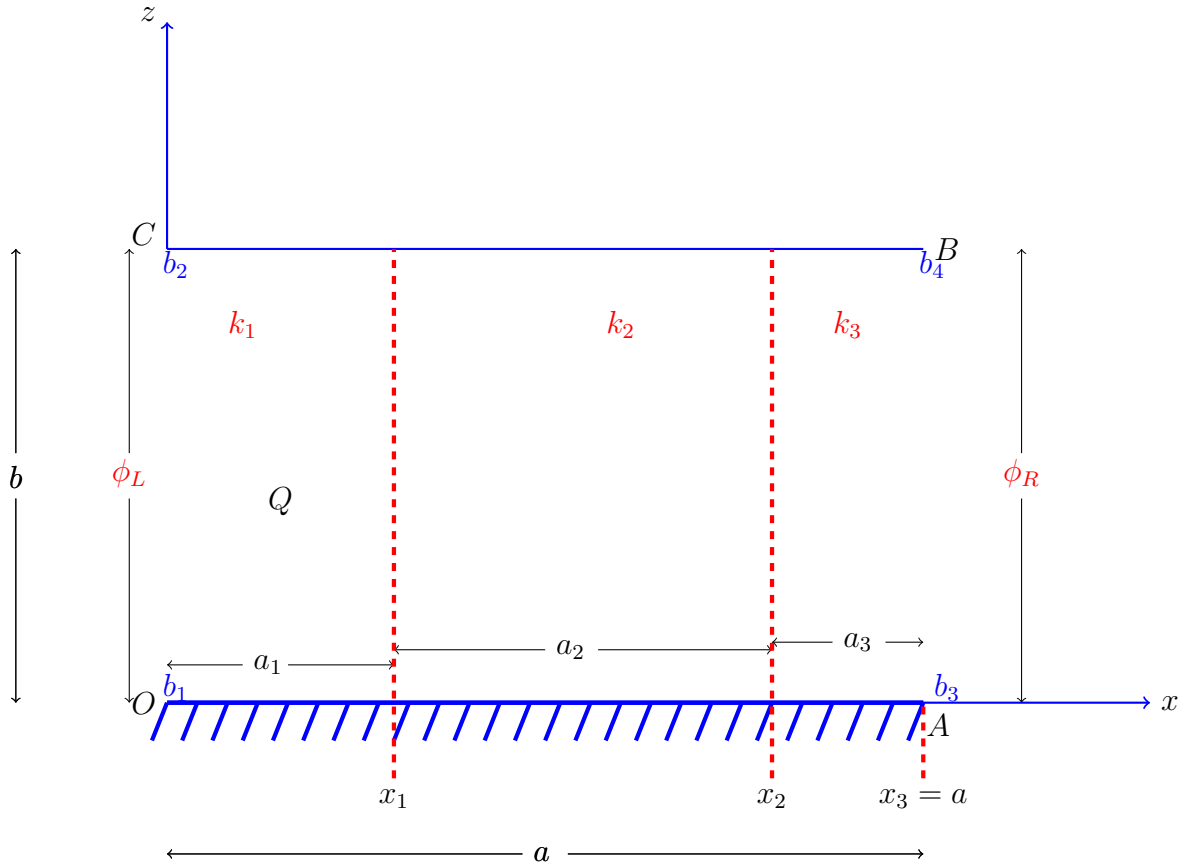
Figure 4.2: *Diagram of 3 vertical strata, each isotropic with different widths and permeabilities.*

4.1 The general motion equation for a non-homogeneous aquifer in terms of $\phi(x, z)$

For two-dimensional flow in an isotropic homogeneous aquifer in the xz-plane, we have $\mathbf{V} = -\nabla \Phi(x, z)$, where $\Phi = K\phi$. However, when the discussion is extended to non-homogeneous, yet isotropic porous media, the above relationship becomes,

$$\mathbf{V} = -K\nabla \phi(x, z) = -\frac{(\rho g k)}{\mu} \nabla \phi(x, z). \tag{4.11}$$

For a non-homogeneous medium, with two materials of different permeabilities k_i, $i = 1, 2$, the components of velocity in terms of piezometric head ϕ are

$$u_1 = -\frac{\rho g k_1}{\mu} \frac{\partial \phi_1}{\partial x}, \quad u_2 = -\frac{\rho g k_2}{\mu} \frac{\partial \phi_2}{\partial x}, \quad w_1 = -\frac{\rho g k_1}{\mu} \frac{\partial \phi_1}{\partial z}, \quad \text{and} \quad w_2 = -\frac{\rho g k_2}{\mu} \frac{\partial \phi_2}{\partial z}, \tag{4.12}$$

where k_1 [m^2], k_2 [m^2], and ϕ_1 [m], ϕ_2 [m], are respectively the permeabilities of the materials and piezometric heads in the two-layer system of a non-homogeneous aquifer.

Based on the same assumptions and same procedure as described for a homogeneous porous medium, another assumption is to be supposed here that the medium is non-homogeneous. To clarify this new assumption we proceed as follows.

Consider a two-dimensional incompressible, steady-state fluid flow in an isotropic non-homogeneous medium in the xz-plane. As a non-homogeneous porous medium contains various layers of different permeabilities, the equation of motion for a two-layered, non-homogeneous incompressible fluid in terms of piezometric head ϕ ($\phi = z + p/\rho g$) [11] is

$$\nabla^2 \phi(x, z) = 0. \tag{4.13}$$

At the vertical interface, $u_1 = u_2$, this implies

$$k_1 \frac{\partial \phi_1}{\partial x} = k_2 \frac{\partial \phi_2}{\partial x}. \tag{4.14}$$

By integrating the above expression, we get

$$\phi_1 = \phi_2. \tag{4.15}$$

For a horizontal interface, $w_1 = w_2$, this implies

$$k_1 \frac{\partial \phi_1}{\partial z} = k_2 \frac{\partial \phi_2}{\partial z}. \tag{4.16}$$

By integrating the above relationship, we have $\phi_1 = \phi_2$. The problem and physical domain are shown in Figure 4.3.
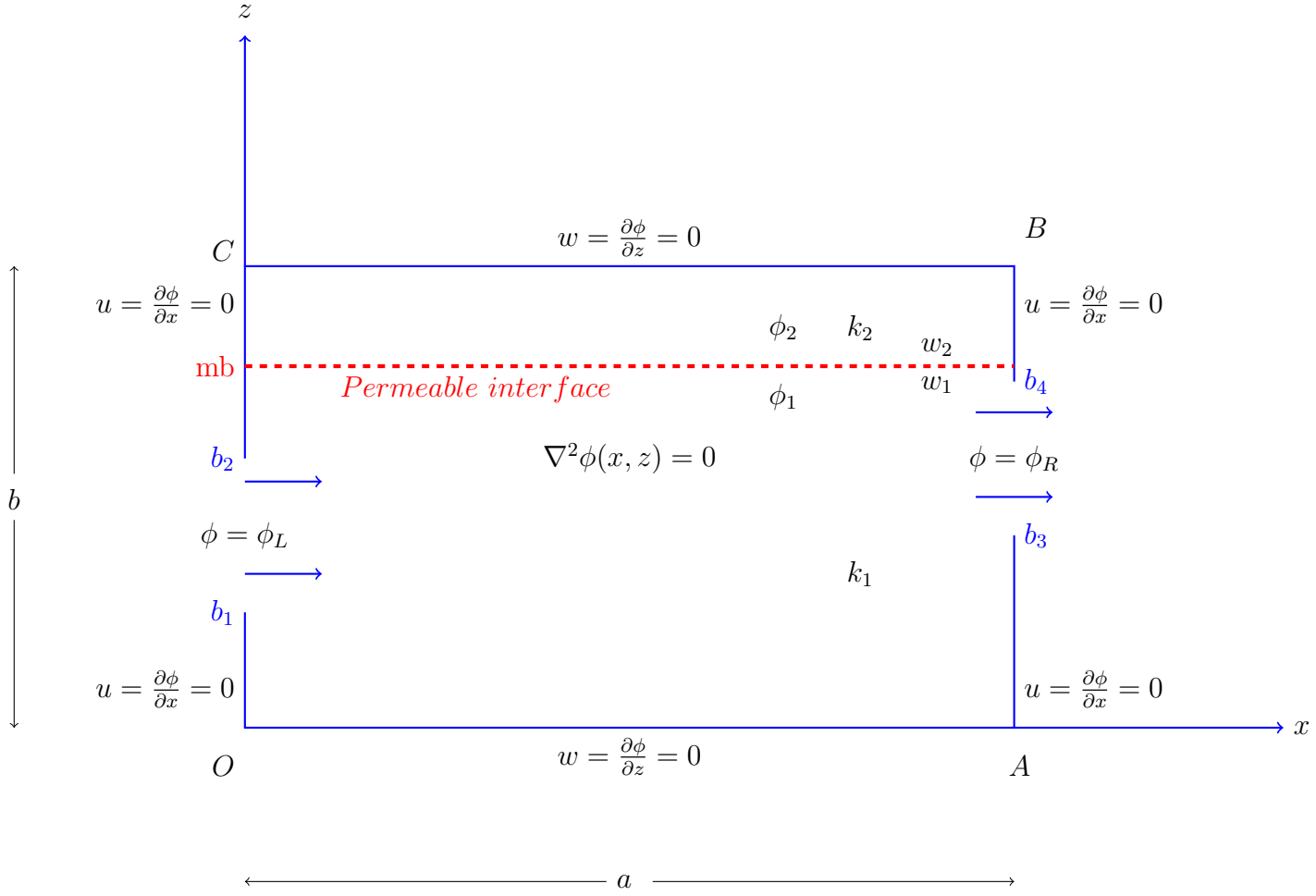
Figure 4.3: *Schematic diagram in terms of ϕ, for a two-layered non-homogeneous aquifer, separated by a horizontal permeable interface.*

4.2 The relationship between ϕ and Φ, ψ and Ψ, and the general motion equation for a non-homogeneous aquifer in terms of $\Psi(x, z)$

In the case of two-dimensional flow in a homogeneous isotropic aquifer, we know that the function $\Psi = \Psi(x, z)$ is constant along streamlines, where $\Psi = K\psi(x, z)$. Moreover, the functions Φ and Ψ, satisfy Cauchy-Riemann conditions for two-dimensional flow in the xz-plane, i.e.,

$$u = -\frac{\partial \Phi}{\partial x} = \frac{\partial \Psi}{\partial z}, \quad w = -\frac{\partial \Phi}{\partial z} = -\frac{\partial \Psi}{\partial x}. \tag{4.17}$$

But, in the case of two-dimensional flow in the xz-plane in an isotropic non-homogeneous aquifer, Equation (4.17) is converted into the form:

$$u = -K\frac{\partial \phi}{\partial x} = \frac{\partial \Psi}{\partial z}, \quad w = -K\frac{\partial \phi}{\partial z} = -\frac{\partial \Psi}{\partial x}. \tag{4.18}$$

For a non-homogeneous medium, with two layers of different materials with hydraulic conductivities, K_i, $i = 1, 2$, the components of velocity become:

$$u_1 = -K_1\frac{\partial \phi_1}{\partial x} = \frac{\partial \Psi_1}{\partial z}, \quad u_2 = -K_2\frac{\partial \phi_2}{\partial x} = \frac{\partial \Psi_2}{\partial z}, \tag{4.19}$$

$$\text{implies} \quad u_1 = -\frac{\rho g k_1}{\mu}\frac{\partial \phi_1}{\partial x} = \frac{\partial \Psi_1}{\partial z}, \quad u_2 = -\frac{\rho g k_2}{\mu}\frac{\partial \phi_2}{\partial x} = \frac{\partial \Psi_2}{\partial z}, \quad \text{and} \tag{4.20}$$

$$w_1 = -K_1\frac{\partial \phi_1}{\partial z} = -\frac{\partial \Psi_1}{\partial x}, \quad w_2 = -K_2\frac{\partial \phi_2}{\partial z} = -\frac{\partial \Psi_2}{\partial x}, \tag{4.21}$$

$$\text{implies} \quad w_1 = -\frac{\rho g k_1}{\mu}\frac{\partial \phi_1}{\partial z} = -\frac{\partial \Psi_1}{\partial x}, \quad w_2 = -\frac{\rho g k_2}{\mu}\frac{\partial \phi_2}{\partial z} = -\frac{\partial \Psi_2}{\partial x}, \tag{4.22}$$

where ϕ_1 [m], ϕ_2 [m], and Ψ_1 [m^2 s^{-1}], Ψ_2 [m^2 s^{-1}], are respectively the piezometric heads and stream functions in a two-layer system.

Since $\mathbf{V} = -K\nabla\phi(x, z)$ and the flow is irrotational, so we have $curl\mathbf{V} = \mathbf{0}$. By inserting Equation (4.18) in terms of Ψ in $(curl\mathbf{V})_y = 0$, we get a parallel differential equation for Ψ

$$\nabla^2\Psi(x, z) = \frac{\partial^2 \Psi}{\partial x^2} + \frac{\partial^2 \Psi}{\partial z^2} = 0, \tag{4.23}$$

which is the governing Laplace's equation for a two-dimensional flow in a non-homogeneous porous media in terms of Ψ. The governing equation and the boundary conditions for the porous medium are shown in Figure 4.4.

Now a discussion about boundary conditions on the interface of two horizontal layers, each individually isotropic, is given below.

Near the horizontal interface, $w_1 = w_2$, so from Equation (4.17) we have,

$$-\frac{\partial \Psi_1}{\partial x} = -\frac{\partial \Psi_2}{\partial x}, \tag{4.24}$$

then by integrating the above expression, i.e.

$$-\int_0^x \frac{\partial \Psi_1}{\partial x}\, dx = -\int_0^x \frac{\partial \Psi_2}{\partial x}\, dx,$$

we get

$$-\Psi_1(x) = -\Psi_2(x), \tag{4.25}$$

implies

$$\Psi_1 = \Psi_2. \tag{4.26}$$

Similarly, for a vertical interface, $u_1 = u_2$, again from Equation (4.17) we have

$$\frac{\partial \Psi_1}{\partial z} = \frac{\partial \Psi_2}{\partial z}, \tag{4.27}$$

integration gives

$$\Psi_1 = \Psi_2. \tag{4.28}$$
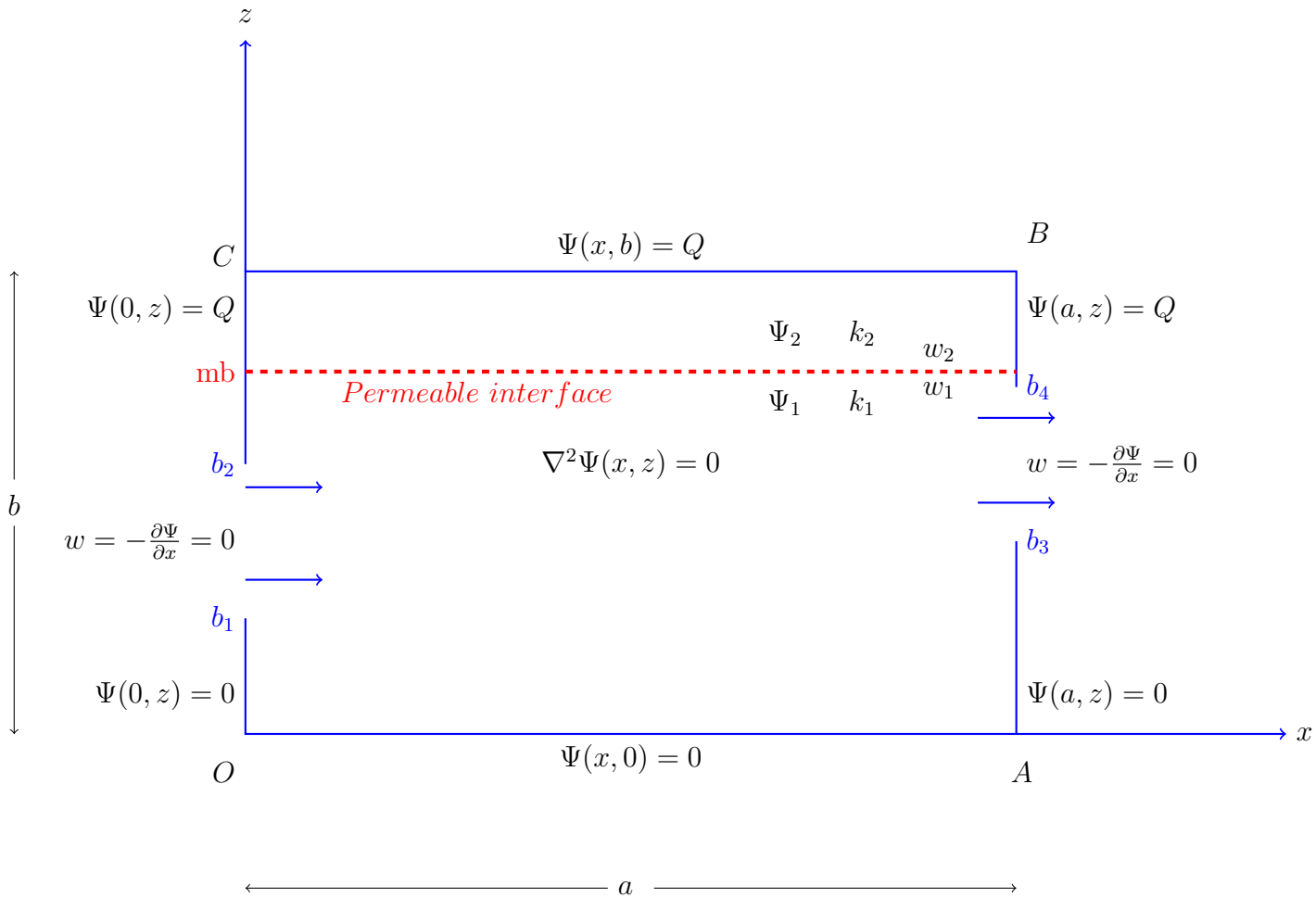
Figure 4.4: *Schematic diagram in terms of Ψ, for a two-layered non-homogeneous aquifer, separated by a horizontal permeable interface.*

4.2.1 Illustrations: fluid flow in a horizontally-layered aquifer in terms of $\phi(x,z)$ and $\Psi(x,z)$ in the absence of objects

Example 4.2.1 *Water is flowing in a two-layer system of a two-dimensional, non-homogeneous, isotropic aquifer, with length, $a = 10$ [m], and a width $b = 6$ [m]. The lower layer is composed of coarse gravel, and the upper layer is made of fine gravel. Values of various parameters involved are shown in Tables 4.2 and 4.1. The opening in the upstream boundary is kept at piezometric head, $\phi_L = 1$ [m], and the opening in the downstream boundary is kept at piezometric head, $\phi_R = 0$.*

(a) If the upstream opening lies in the lower layer, and the downstream opening lies in the upper layer of the system, determine the flow pattern and rate of flow Q. Also consider the reverse case, i.e., when the upstream opening lies in the upper layer and the downstream

opening lies in the lower layer.

(b) *If the upstream opening lies in the upper layer, and the downstream opening lies in the upper layer as well, determine the flow pattern and the rate of flow Q.*

(a) If the upstream opening, lies in the lower layer, and the downstream boundary lies in the upper layer of the system, then the scaled dynamic pressure ϕ is plotted as red contours (isobars) and the stream function Ψ, is plotted as blue contours (streamlines) as shown in Figure 4.5a. A refraction in isobars and streamlines can be seen across the interface (marked by dashed black line). According to the statement, the permeability, k_2 of the upper layer is 3-times greater than that of the lower layer, and the large spacing between the streamlines indicates a lower permeability while in the area of higher permeability the streamlines get closer to each other demonstrating it as a higher fluid speed area. Moreover, within each layer, the isobars and streamlines are orthogonal as they were orthogonal in homogeneous aquifers discussed in Subsection 3.6.4. The total discharge Q [m² s⁻¹], in the upstream and downstream boundaries is given respectively by

$$Q_L = \frac{-k_1 \rho g}{\mu} \int_{b_1}^{b_2} \frac{\partial \phi}{\partial x}(0, z)\, dz = 0.0011[m^2 s^{-1}],$$

$$Q_R = \frac{-k_2 \rho g}{\mu} \int_{b_3}^{b_4} \frac{\partial \phi}{\partial x}(a, z)\, dz = 0.0011[m^2 s^{-1}].$$

Figure 4.5b shows the reverse case, i.e., when the entrance lies in the upper layer, and the exit lies in the lower layer of the system. Interestingly, the total discharge Q [m² s⁻¹], in the upstream and downstream boundaries remains unaltered, and is given respectively by

$$Q_L = \frac{-k_2 \rho g}{\mu} \int_{b_1}^{b_2} \frac{\partial \phi}{\partial x}(0, z)\, dz = 0.0011[m^2 s^{-1}],$$

$$Q_R = \frac{-k_1 \rho g}{\mu} \int_{b_3}^{b_4} \frac{\partial \phi}{\partial x}(a, z)\, dz = 0.0011[m^2 s^{-1}].$$

(b) When both the upstream and downstream boundaries lie in the upper layer, i.e., in the region of higher permeability, the results are shown in Figure 4.5c. As a contrast, the total discharge Q [m² s⁻¹], in the upstream and downstream boundaries, is slightly increased to

the amount 0.0016 [m² s⁻¹] and is given respectively by the formula

$$Q_L = \frac{-k_2 \rho g}{\mu} \int_{b_1}^{b_2} \frac{\partial \phi}{\partial x}(0, z)\, dz = 0.0016 [m^2 s^{-1}],$$

$$Q_R = \frac{-k_2 \rho g}{\mu} \int_{b_3}^{b_4} \frac{\partial \phi}{\partial x}(a, z)\, dz = 0.0016 [m^2 s^{-1}].$$

(a) (b) (c)
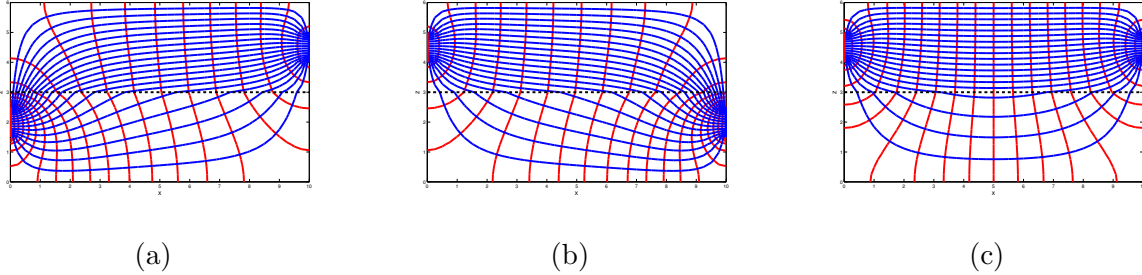
Figure 4.5: *Graphs of the numerical solution for Ψ (blue) and ϕ (red) in a 2D non-homogeneous porous medium: (a) two-layer system, with $k_1 = 1.7751 \times 10^{-10}$, and $k_2 = 3k_1$ respectively the permeabilities of lower and upper layers, with entrance in the lower layer, and exit in upper layer of the system; (b) same as (a), but the entrance lies in the upper layer and the exit lies in the lower layer; (c) same as (a), but both entrance and exit lie in the upper layer.*

Example 4.2.2 *Water is flowing in a three-layer system of a non-homogeneous, isotropic aquifer. The lower layer is composed of coarse sand, the middle layer is formed by fine gravel and the upper layer is made of coarse gravel, values of various parameters involved are shown in Table 4.2 and 4.1. Dimensions of the aquifer are taken as length $= a = 20$ [m], and width $= b = 12$ [m]. Values of piezometric head in the upstream and downstream boundaries are taken to be similar to that of Example 4.2.1. The exit lies in the top layer of the aquifer. What would be the effect on the flow pattern, if the entrance lies in the:*

(a) lower layer,

(b) middle layer,

(c) and top layer of the system?

In the present example, as shown in Figure 4.6 a numerical solution for Laplace's equation is presented for a three-layer non-homogeneous aquifer. The respective boundary conditions on the aquifer in terms of $\phi(x, z)$ and $\Psi(x, z)$ are shown in Figure 4.3 and Figure 4.4. Boundary

conditions on the interface are assigned in accordance with the Sections 4.1-4.2, however, in a three-layer, non-homogeneous system, the boundary conditions for the third layer, in terms of ϕ and Ψ, are assigned respectively as follows.

At the second horizontal interface, $w_2 = w_3$, so we have

$$k_2 \frac{\partial \phi_2}{\partial z} = k_3 \frac{\partial \phi_3}{\partial z}, \tag{4.29}$$

and, since the pressure is continuous,

$$\phi_2 = \phi_3. \tag{4.30}$$

Moreover, in terms of Ψ, near the second horizontal interface, $w_2 = w_3$, so we have

$$-\frac{\partial \Psi_2}{\partial x} = -\frac{\partial \Psi_3}{\partial x}, \tag{4.31}$$

after integration, we get

$$\Psi_2 = \Psi_3, \tag{4.32}$$

where, ϕ_2 [m], ϕ_3 [m], Ψ_2 [m^2 s^{-1}], Ψ_3 [m^2 s^{-1}], and k_2 [m^2], k_3 [m^2] are, respectively, the values of the piezometric head, the stream function and permeabilities for the second and third layers of the system.

(a) Figure 4.6a represents the case when the entrance lies in the lower layer of the aquifer. As the permeability of the bottom layer is 10 times smaller than that of the upper (middle) layer, and $\frac{10}{3}$ times than that of top layer, so vertical movement of the water occurs towards the area of relatively higher permeability, as a result of which fluid speed is highest in the middle layer, which is visible by the greater number of streamlines there. It is interesting to note that, even though the permeability of the top layer is 3-times lower than that of the middle layer, a vertical movement of flow occurs from the middle layer towards the top layer due to the decreasing value of the pressure.

(b) Figure 4.6b represents the case when the entrance lies in the middle layer of the aquifer. Knowing that the permeability of the bottom layer is 10 times smaller than the middle

layer, so downward vertical movement of the water is retarded completely; however, upward movement can occur due to the decreasing pressure gradient of the flow, as a result of which water can easily leave the aquifer from the exit lying in the third layer having relatively lower permeability than that of middle layer.

(c) Figure 4.6c represents the case when the entrance lies in the top layer of the aquifer. As the top layer has 3-times lower permeability than that of the middle layer, so a vertically downward flow can occur towards an area of relatively higher permeability, as well as a horizontal flow due to a decreasing pressure gradient. However, movement of water is completely retarded in the bottom layer of the aquifer, having the lowest permeability.

(a)   (b)   (c)
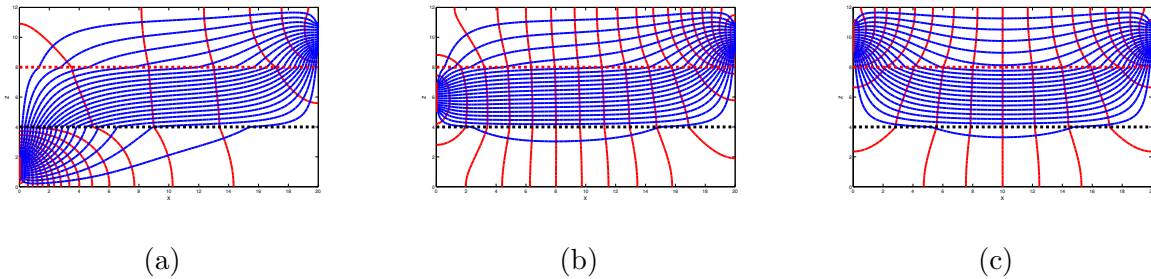
Figure 4.6: *Graphs of the numerical solution for* Ψ *(blue) and* ϕ *(red) in a 2D non-homogeneous, three-layer system, with* $k_1 = 5.3253 \times 10^{-11}$, $k_2 = 10k_1$, *and* $k_3 = \frac{10}{3}k_1 = 3.3k_1$, *respectively the permeabilities in* $[m^2]$, *from bottom to top, and the exit lies in the top layer, with the entrance in the (a) bottom layer; (b) middle layer; (c) top layer of the system.*

4.2.2   Illustrations: fluid flow in a vertically-layered aquifer in terms of $\phi(x, z)$ and $\Psi(x, z)$ in absence of objects

Example 4.2.3 *Repeat Examples 4.2.1 and 4.2.2 for a vertically-layered, non-homogeneous aquifer with the same values of parameters used.*

For the two-layer system, at the vertical interface, since $u_1 = u_2$, so we have

$$k_1 \frac{\partial \phi_1}{\partial x} = k_2 \frac{\partial \phi_2}{\partial x},$$

and, since the pressure is continuous,

$$\phi_1 = \phi_2.$$

In the case of the stream function Ψ, in the two-layer system for a vertical interface, $u_1 = u_2$, so we have,

$$\frac{\partial \Psi_1}{\partial z} = \frac{\partial \Psi_2}{\partial z},$$

after integration, we get

$$\Psi_1 = \Psi_2.$$

Similarly, for a vertical three-layer non-homogeneous system, for the second vertical interface, $u_2 = u_3$, then the boundary condition in terms of $\phi(x, z)$ and $\Psi(x, z)$, are respectively,

$$k_2 \frac{\partial \phi_2}{\partial x} = k_3 \frac{\partial \phi_3}{\partial x},$$

and

$$\frac{\partial \Psi_2}{\partial z} = \frac{\partial \Psi_3}{\partial z},$$

where, ϕ_2 [m], ϕ_3 [m], Ψ_2 [m^2 s^{-1}], Ψ_3 [m^2 s^{-1}], and k_2 [m^2], k_3 [m^2] are, respectively, the values of the piezometric head, the stream function and permeabilities for the second and third layer of the system.

Figure 4.7 shows the results for vertical, two- and three-layer (from left to right), non-homogeneous aquifers.

In the two-layer system, the permeability k_2, of the second layer is 3-times greater than the permeability k_1 of the first layer, so we can note in Figure 4.7a that the greatest pressure drop occurs in the area of highest permeability. However, by changing the positions of entrance and exits, there is not a significant influence on the net flow.

Figures 4.7b and 4.7c, show the plots of isobars and streamlines, for a vertical three-layer system. Let k_1, k_2, and k_3, respectively (from left to right) be the permeabilities of the first, second and third layers. As $k_2/k_1 = 10$, $k_3/k_1 = 10/3$, and $k_3/k_2 = 3$, so fluid flows with lower speed and greater pressure in the first and third layer. However, a greatest pressure drop can

be seen in the middle layer, where fluid speed is greater than that of remaining two layers of the system. To observe the normality condition for the pair (ϕ, Ψ) in a vertical three-layer system, Figure 4.7d illustrates the combined plot of Figures 4.7b and 4.7c, where isobars and streamlines strike with each other orthogonally.

(a)

(b)

(c)

(d)
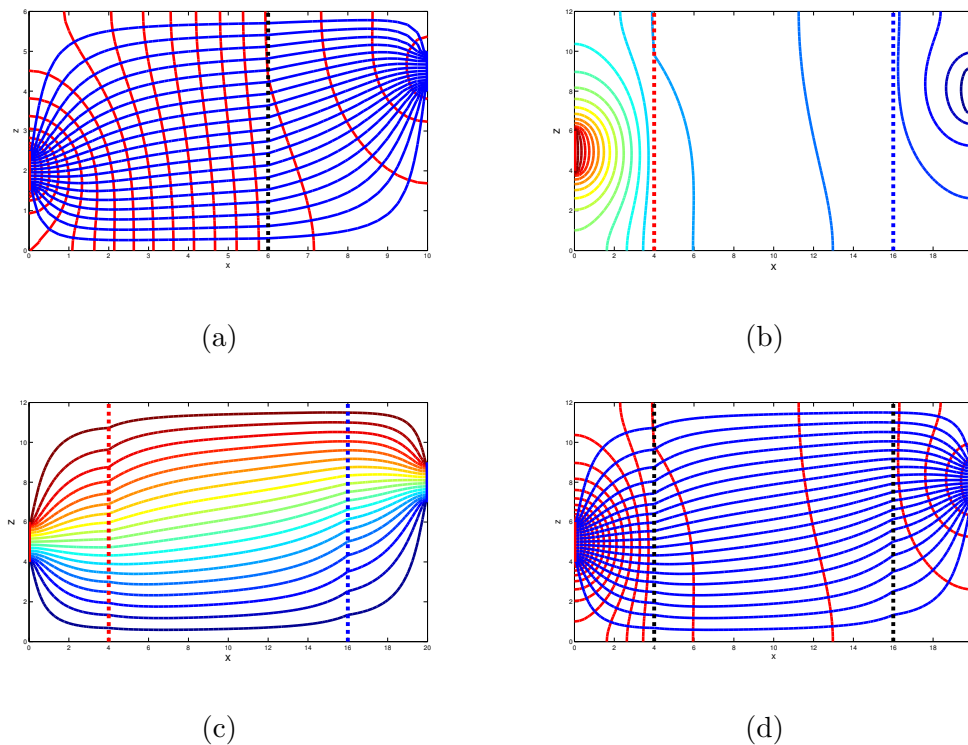
Figure 4.7: *Graphs of the numerical solution of (a) Ψ (blue) and ϕ (red) in 2D non-homogeneous, vertical two-layer system, with $k_1 = 1.7751 \times 10^{-10}$, and $k_2 = 3k_1$ respectively the permeabilities in $[m^2]$, from left to right; (b) ϕ in 2D non-homogeneous, vertical three-layer system, with $k_1 = 5.3253 \times 10^{-11}$, $k_2 = 10k_1$, and $k_3 = \frac{10}{3}k_1 = 3.3k_1$, the permeabilities in $[m^2]$ of the layers from left to right respectively; (c) same as (b), but plot of streamlines only; (d) combining the plots of (b) and (c).*

4.3 Numerical solution for velocity potential $\phi(x, z)$ and stream function $\Psi(x, z)$ in a non-homogeneous porous medium with embedded impermeable objects

Recalling the flow in a homogeneous aquifer with embedded objects in Section 3.6 and following the discussion in Subsections 4.2.1-4.2.2, the present model is of non-homogeneous aquifers with embedded objects. The confined aquifer is composed of horizontal two-layer and vertical two- and three-layer systems with different permeabilities (as values labelled in Figures 4.5,

and 4.7), as shown in Figure 4.8.

A separate graph for a horizontal three-layer system is shown in Figure 4.10 for the sake of comparison with the results presented in Example 4.2.2. The purpose of dividing the non-homogeneous aquifers in horizontal and vertical two- and three-layer systems with embedded impervious objects of various dimensions is to elaborate the effect of these objects on groundwater flow.

In all the graphs of Figure 4.8, and Figure 4.9, it can be seen that water changes its path when it passes underground embedded impervious objects. In addition, it is also evident that position, dimension, burial depth of the embedded objects, and non-homogeneity of the aquifer influence the fluid flow.

(a)   (b)

(c)   (d)
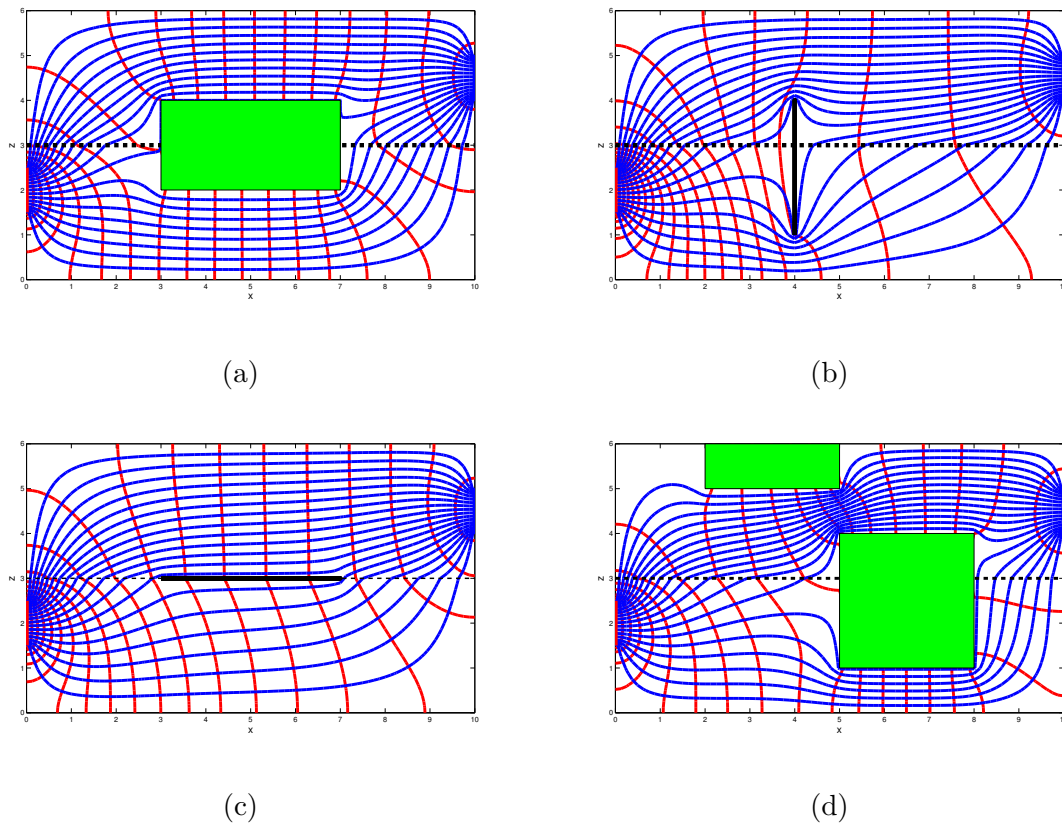
Figure 4.8: *Graphs of isobars (red) and streamlines (blue) in a 2D non-homogeneous porous medium in a horizontal two-layer system, with $k_1 = 1.7751 \times 10^{-10}$, and $k_2 = 3k_1$, respectively the permeabilities of lower and upper layers, with (a) an impermeable rectangular object embedded in it; (b) an impermeable vertical wall embedded in it; (c) an impermeable horizontal wall embedded in it; (d) two impermeable rectangular objects embedded in it.*

<div style="text-align:center">(a)   (b)</div>
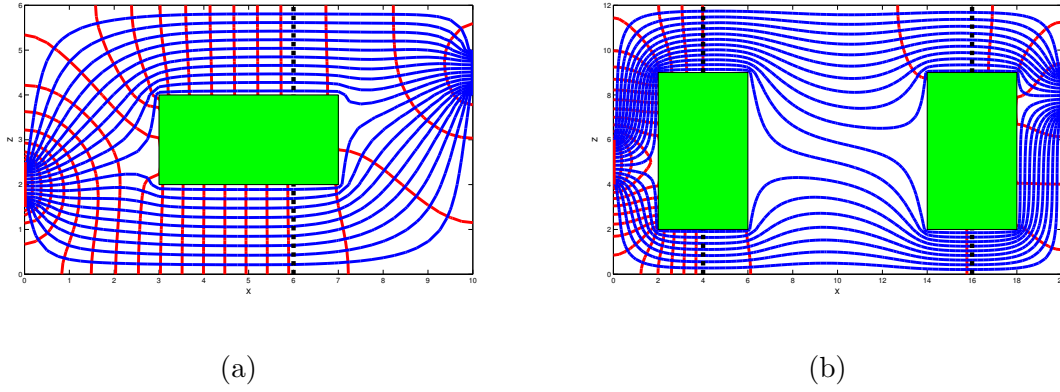
Figure 4.9: *Graphs of isobars (red) and streamlines (blue) in non-homogeneous porous media for a vertical (a) two-layer system with an impermeable rectangular object embedded in it, the values of permeabilities are, $k_1 = 1.7751 \times 10^{-10}$, and $k_2 = 3k_1$, in $[m^2]$, from left to right respectively; (b) three-layer system with two impermeable rectangular objects embedded in it, with $k_1 = 5.3253 \times 10^{-11}$, $k_2 = 10k_1$, and $k_3 = \frac{10}{3}k_1 = 3.3k_1$ in $[m^2]$ from left to right respectively.*

It is well known in the literature [52] that, in the absence of solid objects, water would flow preferentially in the highest permeability region, as verified in Figure 4.6. However, in the presence of solid objects, this may not generally be the case, intuitive results can be achieved as shown in Figure 4.10, where a certain amount of water can be seen flowing all around the object in all layers including the layers of lowest permeability.

It can be concluded that the presence of impermeable objects embedded inside the non-homogeneous aquifers significantly alters the behaviour of water flow. Moreover, it is also concluded that the rate of fluid flowing into and out of the non-homogeneous aquifer is equal in all the cases of Figure 4.10 as discussed above.

<div style="text-align:center">(a)   (b)   (c)</div>
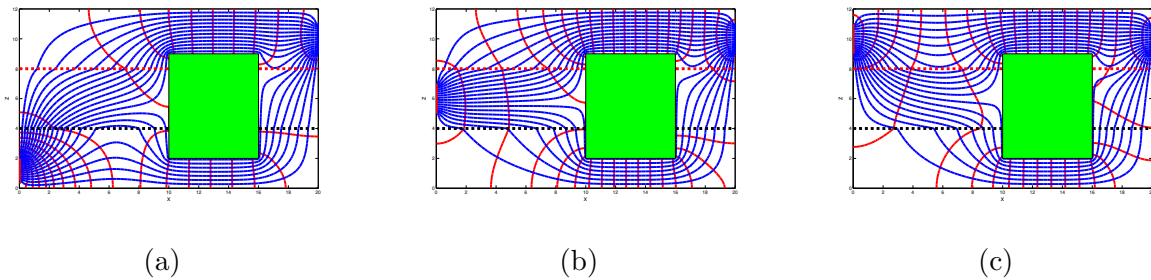
Figure 4.10: *Graphs of the numerical solution for Ψ (blue) and ϕ (red) with a rectangular object embedded in 2D non-homogeneous, three-layer system, with $k_1 = 5.3253 \times 10^{-11}$, $k_2 = 10k_1$, and $k_3 = \frac{10}{3}k_1 = 3.3k_1$, respectively the permeabilities in $[m^2]$, from bottom to top, and the exit lies in the top layer, with the entrance in the: (a) bottom layer; (b) middle layer; (c) top layer of the system.*

4.4 A permeable rectangular cylinder with permeability different from outside

The fundamentals of every mathematical model in the transport of any universal quantity, e.g., mass or energy, inside a porous medium is the balance equation of that quantity [13]. The balance equation may be in the form of a partial differential equation. Here we shall concentrate on the situation of transport of fluid through a semipermeable object placed inside an aquifer.

Consider a control rectangular box placed inside the flow domain in an aquifer. In the present study, fluid enters and leaves the box through its surfaces, and our objective is to write a balance, or a statement of conservation for the mass of fluid entering, leaving, and being stored in the box. The next goal is the discussion of boundary conditions.

Boundary conditions provide a mechanism of interaction between a considered section and its environment. Alternatively, they provide the background of a situation, e.g., known water fluxes or piezometric head, that the outer zone affects the considered one. Despite the fact that in a mathematical model, boundary conditions are stated in mathematical form, their role is to explore some concrete truth in the real world [13].

If k_1 and k_2 are the permeabilities of the aquifer and that of the box respectively, then we can compute pressure (potential) and amount of fluid flow across the semipermeable object with the help of ϕ and Ψ.

Suppose ϕ_1 is the value of pressure in the porous medium whose permeability is k_1, and ϕ_2 is the value of pressure inside the object with permeability k_2. The quantity $k_i(\partial \phi_i/\partial n)$, $i = 1, 2$ denotes the mass flux of the water at the surface of box. Then the boundary conditions in terms of $\phi(x, z)$ for the rectangular object are:

on the bottom and top boundaries of the object, since $w_1 = w_2$, we have

$$k_1 \frac{\partial \phi_1}{\partial z} = k_2 \frac{\partial \phi_2}{\partial z}, \tag{4.33}$$

and on the left-hand and right-hand side boundaries, since $u_1 = u_2$, the boundary conditions are

$$k_1 \frac{\partial \phi_1}{\partial x} = k_2 \frac{\partial \phi_2}{\partial x}. \tag{4.34}$$

If Ψ_1 is the value of the stream function in the porous medium whose permeability is k_1 and Ψ_2 is the value of the stream function inside the object with permeability k_2, then the boundary conditions for the rectangular object in terms of $\Psi(x, z)$ are:

on the bottom and top boundaries of the object, since $w_1 = w_2$, we have

$$\frac{\partial \Psi_1}{\partial x} = \frac{\partial \Psi_2}{\partial x}, \tag{4.35}$$

and on the left-hand and right-hand side boundaries, since $u_1 = u_2$, the boundary conditions are

$$\frac{\partial \Psi_1}{\partial z} = \frac{\partial \Psi_2}{\partial z}. \tag{4.36}$$

To understand the whole phenomenon consider the following example.

4.4.1 Illustrations

Example 4.4.1 *Consider a confined aquifer, composed of coarse sand with dimensions 10×6 [m]. Water is flowing inside the aquifer in which there is embedded a semipermeable box filled with fine gravel. Values of the piezometric head in the entrance and exit are respectively, $\phi_L = 2$ [m] and $\phi_R = 1$ [m]. Determine:*

(a) the flow pattern graphically,

(b) the flow pattern graphically, if the materials in the aquifer and box are replaced by each other.

(a) Consider a homogeneous aquifer with permeability k_1 and a rectangular box placed inside the aquifer with different permeability k_2 (the values of k_1 and k_2 are labelled in Figure 4.11). Suitable boundary conditions on the aquifer are similar to those assigned in Section 3.5,

and on the object are taken in accordance to Section 4.4.

Water is flowing through the aquifer from left to right as the value of piezometric head ϕ_L in the entrance is higher than that in the exit (as evident by red isobars near the entrance and blue near the exit in Figure 4.11a). As the permeability of fine gravel is 10 times higher than that of coarse sand, so water feels less pressure (Figure 4.11a) when it enters through the object and the fluid speed becomes higher in that region (Figure 4.11b).

(b) For the reverse case, as the permeability in the vicinity of the object is 10 times higher than the object, so the water feels a relatively greater pressure while passing through the object, as evident by Figure 4.11c, and fluid flows slowly through the object, as illustrated in Figure 4.11d by the help of streamlines. This is visible by the smaller number of streamlines and the greater number of pressure lines inside the object.

(a)   (b)

(c)   (d)
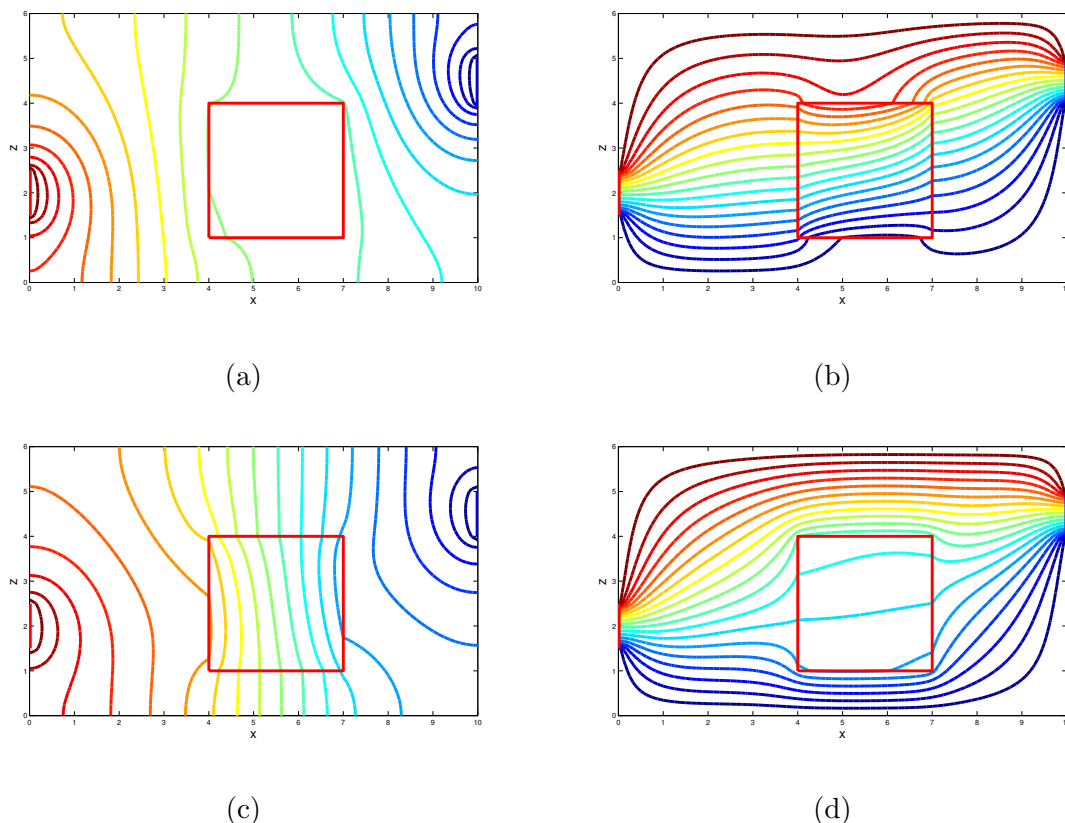
Figure 4.11: *Graphs of a permeable rectangular object with permeability k_2 embedded in a homogeneous porous medium with permeability k_1; the value of the piezometric head in the entrance is $\phi_L = 2$, and that in the exit is $\phi_R = 1$. (a) isobars with $k_1 = 5.3253 \times 10^{-11}$, $k_2 = 10k_1$; (b) streamlines with $k_1 = 5.3253 \times 10^{-11}$, $k_2 = 10k_1$; (c) isobars with $k_1 = 10k_2$, $k_2 = 5.3253 \times 10^{-11}$; (d) streamlines with $k_1 = 10k_2$, $k_2 = 5.3253 \times 10^{-11}$.*

4.5 Modelling two-dimensional flow in aquifers in the presence of a leaky cylinder with rectangular cross-section, placed in a non-homogeneous porous medium

Following the discussion of Section 3.7 for a homogeneous porous medium, in this section fluid flow through pervious objects placed inside a non-homogeneous porous medium is discussed. For a non-homogeneous porous medium, with two layers of different permeabilities k_i, $i = 1, 2$, the gradient of ϕ on the boundaries of the object can be written as:

$$\frac{\partial \phi}{\partial n} = \frac{\omega_{ps}\mu}{\rho g k_1}(\phi_{ps} - \phi_I), \quad \frac{\partial \phi}{\partial n} = \frac{\omega_{ps}\mu}{\rho g k_2}(\phi_{ps} - \phi_I), \tag{4.37}$$

$$\text{implies} \quad \frac{\partial \phi}{\partial n} = \frac{\beta_{ps}}{k_1}(\phi_{ps} - \phi_I), \quad \text{and} \quad \frac{\partial \phi}{\partial n} = \frac{\beta_{ps}}{k_2}(\phi_{ps} - \phi_I), \tag{4.38}$$

where $\beta_{ps} = \omega_{ps}\mu/\rho g$, and ϕ_I is the pressure inside the rectangular cross-section.

The other boundary conditions in terms of ϕ, i.e., on the porous media, are assigned in the same manner as discussed in Subsection 3.5.3. For further explanation, consider the following schematic diagram:
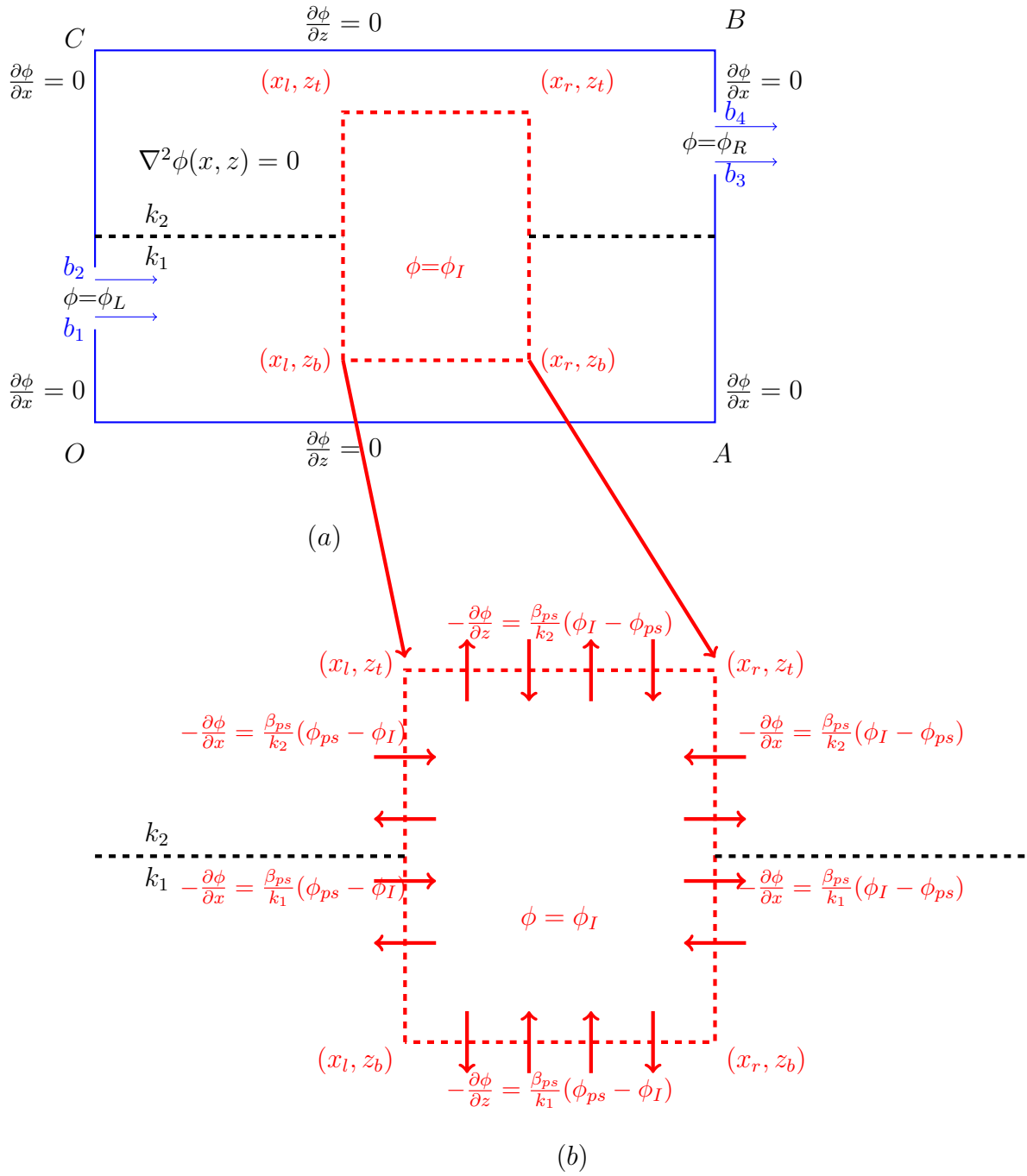
Figure 4.12: *Schematic diagram of the (a) physical domain for ϕ with pervious object embedded in it; (b) pervious rectangular cross-section of the object.*

4.5.1 Illustrations

Results are calculated for a two-layer non-homogeneous aquifer with a pervious object positioned between two layers of different permeabilities. Again, it is assumed that, the value of the scaled dynamic pressure in the entrance is taken to be higher than that of the exit, so fluid flows in the direction of decreasing pressure gradient.

Permeability of the lower layer, k_1 is taken as 10 times higher than that of the top one. In order to make direct comparison between different cases, results are repeated with fixed values of β_{ps} and for a range of values of ϕ_I. Values of various parameters used in the simulation are given in Table 4.3.

Table 4.3: *Parameters used for the simulations*

Parameters	Values	Units
value of ϕ in entrance ϕ_L	1	[m]
value of ϕ in exit ϕ_R	0	[m]
values of ϕ inside the pervious object ϕ_I	-1, 0, 0.5, 1, 5	[m]
value of β_{ps}	1.0224	[m]
value of ω_{ps}	10000000	[s^{-1}]
value of k_1	5.3167×10^{-10}	[m^2]
value of k_2	5.3253×10^{-11}	[m^2]
fluid dynamic viscosity μ	1.002×10^{-3}	[kg m^{-1} s^{-1}]
gravitational acceleration g	9.8	[m s^{-2}]
fluid density ρ	1000	[kg m^{-3}]

The main objective of this section is to highlight the feasibility of placing pervious objects inside a non-homogeneous aquifer which is composed of different materials. It is found that the nature of the results remains unaltered from those previously conducted for homogeneous aquifers, however, the speed of the fluid is noticed to be higher in the layer of higher permeability.

In systems where the value of ϕ_I, is negative or 0, water is being sucked by the object, as shown by Figures 4.13a and 4.13b, indicated by a blue area. For the cases when the value of ϕ_I is taken to be the average value of ϕ_L and ϕ_R (the values of scaled dynamic pressures in the entrance and exit, respectively), some water is being sucked by the object, whereas, in some areas of the aquifer where the pressure is lower than that of ϕ_I, water is being discharged by the object, as illustrated in Figure 4.13c.

For systems where the value of ϕ_I is higher than or equal to the higher value of piezometric head in either the entrance or exit, water is being discharged by the object, which is shown by the red area in the graphs of Figures 4.13d and 4.13e. In order to represent the refraction of the isobars across the interface of the two-layer system, a contour plot of Figure 4.13e is shown

in Figure 4.13f.
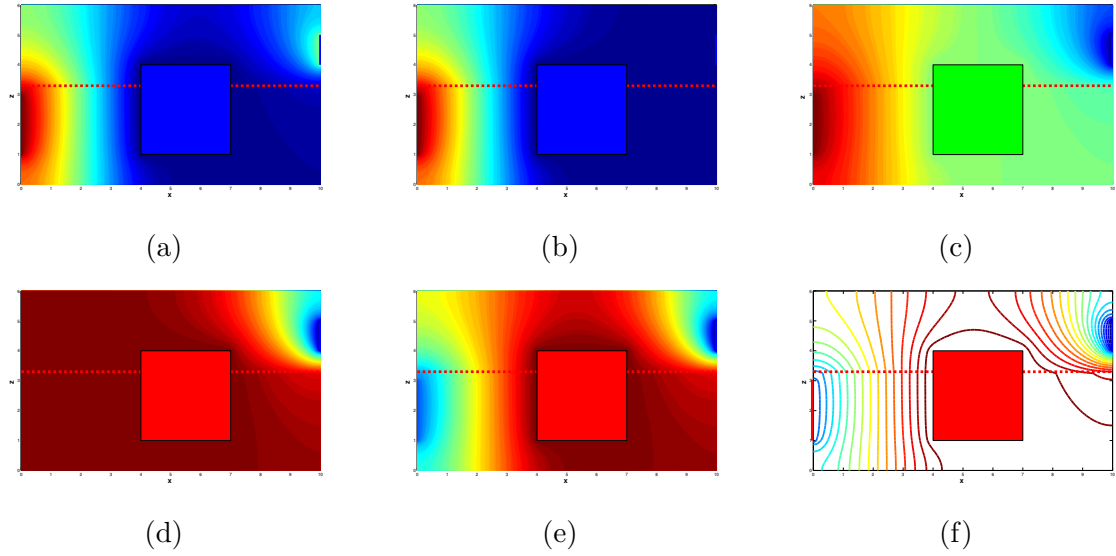
Figure 4.13: *Graphs of $\phi(x,z)$ of a leaky tube with rectangular cross-section in a non-homogeneous porous medium with $\phi_L = 1$, $\phi_R = 0$, $k_1 = 10k_2$, $k_2 = 5.3253 \times 10^{-11}$, for (a) a filled contour plot with $\phi_I = -1$; (b) a filled contour plot with $\phi_I = 0$; (c) a filled contour plot with $\phi_I = 0.5$; (d) a filled contour plot with $\phi_I = 1$; (e) a filled contour plot with $\phi_I = 5$; (f) a contour plot with $\phi_I = 5$.*

4.6 A vertical pervious thin wall placed in a non-homogeneous aquifer

This section includes a discussion about a thin pervious vertical wall embedded in a non-homogeneous porous medium. As the wall is infinitesimally thin, we assume that the value of pressure gradients on L.H.S and R.H.S of the wall are equal and are denoted by $\partial\phi^-/\partial x$ and $\partial\phi^+/\partial x$ respectively, and can be found by the formulae:

$$-\frac{\partial\phi^-}{\partial x} = \frac{\beta_{ps}}{k_1}(\phi_{kB_1}^- - \phi_{kB_2}^+), \quad -\frac{\partial\phi^-}{\partial x} = \frac{\beta_{ps}}{k_2}(\phi_{kB_1}^- - \phi_{kB_2}^+), \tag{4.39}$$

$$-\frac{\partial\phi^+}{\partial x} = \frac{\beta_{ps}}{k_1}(\phi_{kB_1}^- - \phi_{kB_2}^+), \quad -\frac{\partial\phi^+}{\partial x} = \frac{\beta_{ps}}{k_2}(\phi_{kB_1}^- - \phi_{kB_2}^+), \tag{4.40}$$

where β_{ps}, is a measure of perviousness of the wall, k_i, $i = 1, 2$, are the permeabilities of the two layers in the system, $\phi_{kB_1}^-$ and $\phi_{kB_2}^+$ are the values of pressures on L.H.S and R.H.S of the wall respectively.

4.6.1 Illustrations

In this section, some examples for different values of parameters β_{ps}, k_1, and k_2 (where k_1 and k_2 are the permeabilities of the lower and upper layers, respectively) are illustrated. If $\beta_{ps} = 0$, the pervious vertical wall is converted to an impervious wall as indicated in Figures 4.14a and 4.14d, where the pressure lines strike normally to the wall, indicating it as a barrier in the fluid flow path, moreover fewer pressure lines are visible in the region of higher permeability and more lines are present in the less permeable region. However, for a non-zero value of β_{ps}, the wall becomes semi-pervious as shown in Figures 4.14b, 4.14e, and even becomes completely pervious for an extremely large value of β_{ps}, as shown in Figures 4.14c and 4.14f, and fluid flows freely without any resistance.

(a) (b) (c)

(d) (e) (f)
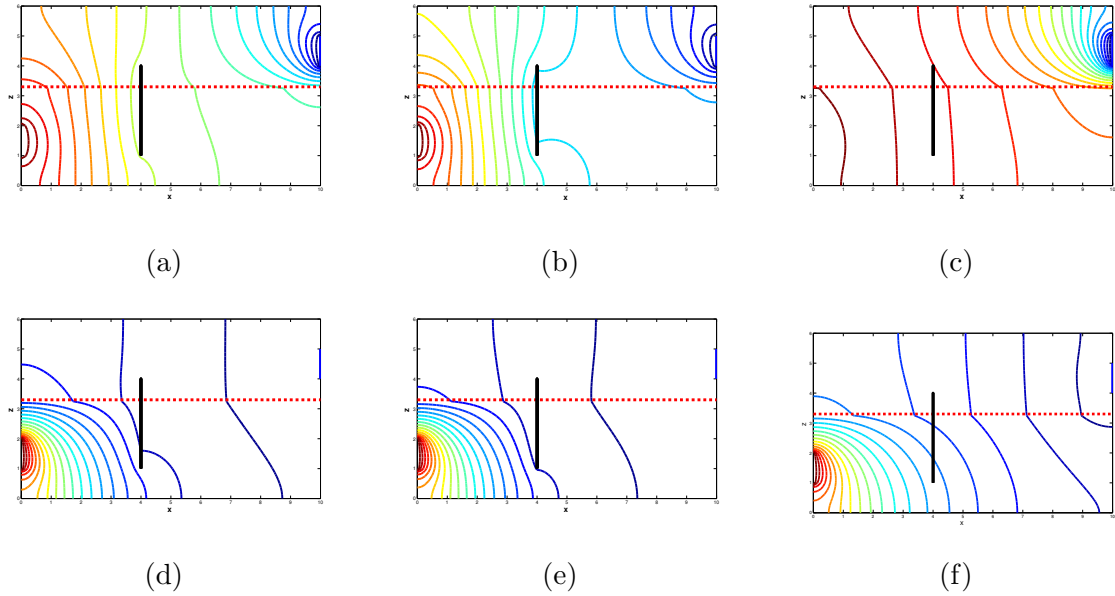
Figure 4.14: *A contour plot for $\phi(x, z)$ of a pervious vertical thin wall placed in a non-homogeneous porous medium, with $\phi_L = 1$, $\phi_R = 0$, (a) $k_1 = 10k_2$, $k_2 = 5.3253 \times 10^{-11}$, $\beta_{ps} = 0$; (b) $k_1 = 10k_2$, $k_2 = 5.3253 \times 10^{-11}$, $\beta_{ps} = 1.0224$; (c) $k_1 = 10k_2$, $k_2 = 5.3253 \times 10^{-11}$, $\beta_{ps} = 1000$; (d) $k_1 = 5.3253 \times 10^{-11}$, $k_2 = 10k_1$, $\beta_{ps} = 0$; (e) $k_1 = 5.3253 \times 10^{-11}$, $k_2 = 10k_1$, $\beta_{ps} = 1.0224$; (f) $k_1 = 5.3253 \times 10^{-11}$, $k_2 = 10k_1$, $\beta_{ps} = 1000$.*

4.7 Modelling three-dimensional flow in a non-homogeneous porous medium, with an embedded cuboid

The study of Section 4.3 is limited to two-dimensional non-homogeneous porous media; here the discussion is extended to a three-dimensional non-homogeneous aquifer.

The governing equation and the boundary conditions on porous media and object are similar to that of the Section 3.14. For a two-layer system with horizontal interface, the boundary condition for this interface in terms of $\phi(x, y, z)$ (where the z-axis is aligned normal to the xy-plane) is

$$k_1 \frac{\partial \phi_1}{\partial z} = k_2 \frac{\partial \phi_2}{\partial z}, \tag{4.41}$$

where k_1 [m^2], k_2 [m^2] and ϕ_1 [m], ϕ_2 [m] are, respectively, the values of permeabilities and piezometric heads in the lower and upper layers of the system.

Some simulations are performed to show the results and a few illustrations are shown in three-dimensional non-homogeneous porous media.

For the illustrations, the value of the scaled dynamic pressure in the entrance and exit are, respectively, $\phi_L = 2$, and $\phi_R = 1$. The permeability of the top layer is taken to be 10 times that of the lower layer, so we can see in Figure 4.15a more isobars in the lower permeability region, however, refractions are not visible across the interface. As the interface is parallel to the xy-plane, so for a xy-slice, refractions across the interface are not visible in Figure 4.15b, hence these refractions are only visible for the vertical, yz- slice in Figure 4.15c.

(a)

(b)

(c)
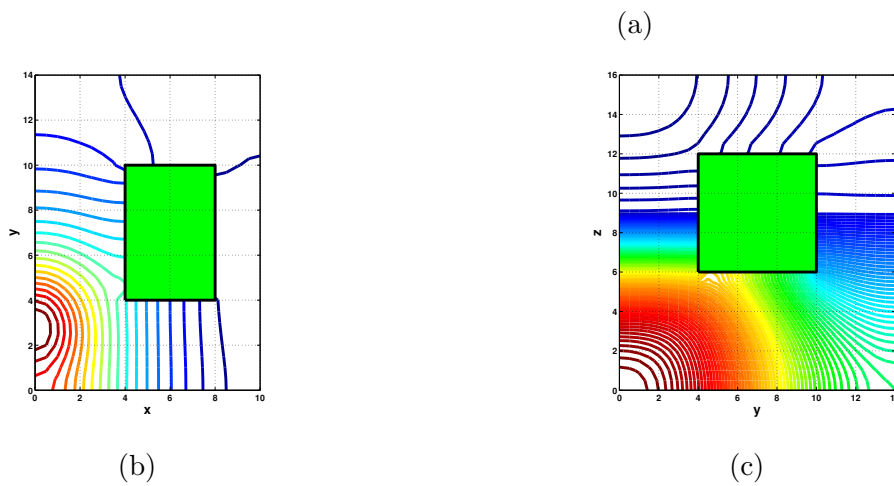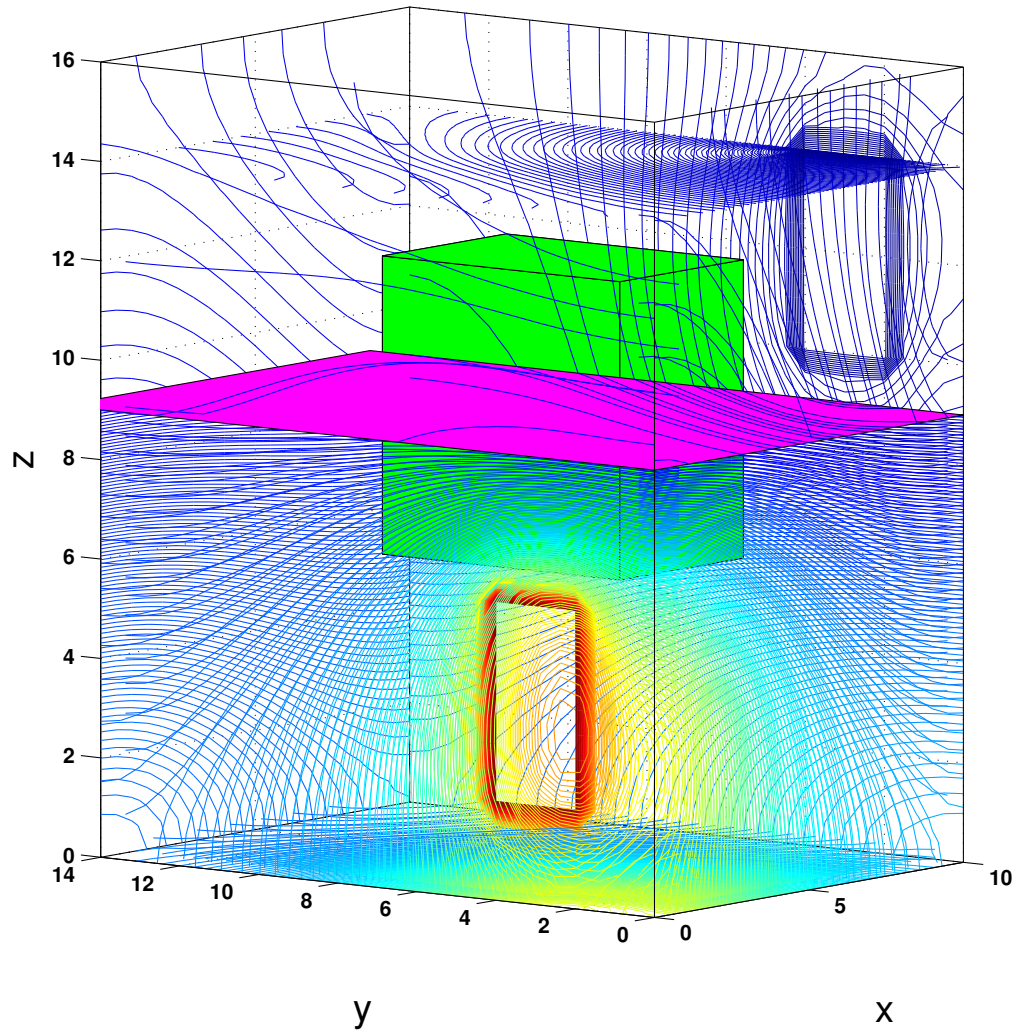
Figure 4.15: *A contour plot of $\phi(x, y, z)$ in a three-dimensional, non-homogeneous porous medium, with $k_1 = 5.3253 \times 10^{-11}$, $k_2 = 10k_1$, with (a) an impermeable cuboidal object embedded in it; (b) an xy-slice at $z = 8$; (c) a yz-slice at $x = 4$.*

Chapter 5

Modelling Groundwater Pollution
Released by Embedded Objects

So far, the purpose of this study was the development of mathematical models for the sake of discussion of fluid flow through aquifers with embedded impervious and pervious objects, overlooking a major factor of interest, namely, groundwater pollution. *Groundwater pollution* or *groundwater contamination* may be defined as the artificially-generated deterioration of natural groundwater quality [52]. Usually, the term *quality* refers to either energy (heat or nuclear radiations) or organic constituents dissolved in groundwater. Sometimes, this dissolved matter reaches up to a certain level, as a result of which water becomes inappropriate for acceptable usage. In this case, we use the term *pollution* for the dissolved constituents whose concentration has definitely increased up to a certain dangerous level.

Pollution can diminish the water usage and can cause hazards to public health due to the spread of diseases and toxicity. Mostly, pollution is generated by wastewater disposal, involving a wide variety of sources, ranging from septic tanks to agricultural irrigation purposes.

Compared with surface water pollution, however, it seems that groundwater is rarely polluted, but it is still subject to pollution, and when the latter occurs, it is difficult to detect and hard to control and may persist underground for a long time. Because of the emerging area of interest for development and management of the water resource system, gradually more efforts are undergoing for the prevention, diminishing, and removal of groundwater pollution.

The number of possible pollutants present in groundwater is countless, however, human water

consumption is considered to be the major source and cause of groundwater pollution.

On the basis of sources and causes, groundwater pollution may be classified into the following four categories:

(i) *Environmental.* When groundwater flows through carbonated rocks, these rocks dissolve in water in small or significant amounts leaving the water polluted. In coastal areas extensive pumping of freshwater may cause salty seawater to enter into the freshwater aquifer, which may disturb the natural equilibrium between the two sources of water, giving an example of environmental pollution.

(ii) *Domestic.* This category includes: biological contaminants, e.g., bacteria and viruses, accidental breaking of sewers, leakage from infected containers, penetration of rain water into clean groundwater, and artificial replenishment of aquifers by sewage.

(iii) *Industrial.* Even though the construction of domestic and industrial pollution is different, it is difficult to differentiate them. Typical examples are: heavy metals, highly toxic compounds, non-decaying materials and radioactive substances.

(iv) *Agricultural.* Irrigation of land with polluted water, rain water, chemical fertilisers, herbicides, pesticides, and salts, etc. seeps through the ground surface and recharges the aquifer [13].

In this chapter, a discussion about the advection-dispersion phenomenon of pollutants released by pervious cylinders (septic tanks, drums of contaminants, etc.) in two- and three-dimensional, isotropic/anisotropic, homogeneous and non-homogeneous porous media is added. The physical system is based on the following assumptions:

1. groundwater aquifer is taken in the form of a porous medium which is connected on left- and right-hand sides with two water reservoirs with different levels of water;

2. inside the porous medium, there is embedded a cylinder/tank, which is completely pervious (leaky), i.e., all sides of the cylinder are equally pervious;

3. the cylinder is full of water and the pressure inside the cylinder is kept constant by a fixed amount of fluid inside. This pressure is different from the pressure of the outside

porous media, as well as from that of the two openings (the places at which the aquifer is connected to the reservoirs);

4. the pollutant concentration inside the box is uniform and constant, and the pollutant advection/dispersion phenomenon depends mainly on the value of pressure inside the box, as well as on the fluid speed and various types of dispersion coefficients.

Based on these assumptions, different results have been compiled in the form of contour as well as surface plots of pollutant concentration for every situation.

5.1 Advective, dispersive, and diffusive fluxes

Consider a fixed component in a single fluid phase or in a multiphase system that occupies the entire void space. The conservation of mass for a solute in a porous medium is considered on the flux of solute into and out of the fixed component of the porous medium [52].

Physical procedures that control flux into and out of the elemental volume are referred to as *advection* and *hydrodynamic dispersion*. Transport of solute as a result of groundwater movement is known as *advection*, whereas, *hydrodynamic dispersion* is caused by *mechanical dispersion* and *molecular diffusion*.

Mechanical dispersion occurs as a result of contamination of contaminated and uncontaminated groundwater. Mechanical dispersion is further composed of two parts: *longitudinal dispersion* and *lateral (transverse) dispersion*. *Longitudinal dispersion* takes place when contamination occurs along the streamline, whereas, *lateral dispersion* lies normal to longitudinal dispersion. Lateral dispersion is a much weaker process as compared to longitudinal dispersion, however, when molecular diffusion is dominant, at lower velocities, coefficients of longitudinal and lateral dispersion become nearly equal.

Diffusion occurs as a result of solute flux from an area of higher concentration to an area of lower concentration caused by Brownian motion of ions and molecules. However, in a porous medium, diffusion is not treated in the same rate as it is treated in water, because in the presence of particles in the solid matrix, ions take a longer route to travel and there may be

ionic adsorption[1] on the solids [52].

5.1.1 Coefficients of dispersion

Various authors (e.g., Nikolaevskii, 1959; Bear, 1961; Scheidegger, 1961; Bear and Bachmat, 1967) established a correspondence between the coefficient D (*coefficient of (mechanical) dispersion*), molecular diffusion, flow velocity, and microscopic porous matrix configuration [13]. The following cases arise for the selection of dispersion coefficients:

Case 1a: Dispersion coefficients for a three-dimensional flow case, when dispersion depends on flow speed and direction, i.e., $\alpha_L \neq \alpha_T$.

We denote fluid velocity $\mathbf{V}$ in a three-dimensional porous medium with the z-axis aligned normal to the xy-plane as

$$\mathbf{V} = u\mathbf{i} + v\mathbf{j} + w\mathbf{k}, \tag{5.1}$$

and the speed is given by

$$V = \sqrt{u^2 + v^2 + w^2}. \tag{5.2}$$

---

[1]Increase in the mass of a substance (pollutant or tracer) on the solid at a fluid-solid interface is known as adsorption [13].

For a *locally isotropic porous medium*, the dispersion coefficients are expressed in the following form

$$
\begin{aligned}
D_{xx} &= \alpha_L \frac{u^2}{V} + \alpha_T V \frac{v^2}{V_1^2} + \alpha_T \frac{u^2 w^2}{V V_1^2}, \\
D_{xy} &= \alpha_L \frac{uv}{V} - \alpha_T V \frac{uv}{V_1^2} + \alpha_T \frac{uvw^2}{V V_1^2}, \\
D_{xz} &= (\alpha_L - \alpha_T) \frac{uw}{V}, \\
D_{yx} &= \alpha_L \frac{uv}{V} - \alpha_T V \frac{uv}{V_1^2} + \alpha_T \frac{uvw^2}{V V_1^2}, \\
D_{yy} &= \alpha_L \frac{v^2}{V} + \alpha_T V \frac{u^2}{V_1^2} + \alpha_T \frac{v^2 w^2}{V V_1^2}, \\
D_{yz} &= (\alpha_L - \alpha_T) \frac{vw}{V}, \\
D_{zx} &= (\alpha_L - \alpha_T) \frac{uw}{V}, \\
D_{zy} &= (\alpha_L - \alpha_T) \frac{vw}{V}, \\
D_{zz} &= \alpha_L \frac{w^2}{V} + \alpha_T \frac{V_1^2}{V},
\end{aligned}
$$

where $V_1 = \sqrt{u^2 + v^2}$, the components α_L [m], and α_T [m], are respectively the *longitudinal dispersivity*, and *transversal dispersivity* of the porous media.

In laboratory experiments in homogeneous sand columns it was found that α_L is of the order of the size of an average sand grain. The transversal dispersivity is approximated as 10- to 20-times smaller than α_L. Very limited information is available for transverse dispersivity α_T in the literature. Ratios of α_L/α_T of $5:1$ to $24:1$ even up to $100:1$ have been published [13]. Based on averaging published data (Gelhar *et al.* [22]), a rough estimation of α_L is [52]

$$
\alpha_L = 0.1L, \tag{5.3}
$$

where L [m] is the length of the flow path. Another approximation is given by Neuman [38], according to whom, for length L less than $3,500$ m,

$$
\alpha_L = 0.0175L^{1.46}. \tag{5.4}
$$

Xu and Eckstein [58] established the following relationship between α_L [m] and L [m] on the basis of published statistical data[2]

$$\alpha_L = 0.83(logL)^{2.414}. \tag{5.5}$$

Case 1b: Dispersion coefficients for two-dimensional flow, when dispersion depends on flow speed and direction, i.e., $\alpha_L \neq \alpha_T$, $v = 0$, $V_1^2 = u^2$, $V = \sqrt{u^2 + w^2}$.

For the two-dimensional case, the three-dimensional dispersion coefficients are reduced to the following form

$$
\begin{aligned}
D_{xx} &= \alpha_L \frac{u^2}{V} + \alpha_T \frac{w^2}{V}, \\
D_{xy} &= 0, \\
D_{xz} &= (\alpha_L - \alpha_T)\frac{uw}{V}, \\
D_{yx} &= 0, \\
D_{yy} &= \alpha_T V, \\
D_{yz} &= 0, \\
D_{zx} &= (\alpha_L - \alpha_T)\frac{uw}{V}, \\
D_{zy} &= 0, \\
D_{zz} &= \alpha_L \frac{w^2}{V} + \alpha_T \frac{u^2}{V},
\end{aligned}
$$

which can be written in matrix form as

$$
\left[D_{ij} \right] =
\begin{bmatrix}
\alpha_L \frac{u^2}{V} + \alpha_T \frac{w^2}{V} & 0 & (\alpha_L - \alpha_T)\frac{uw}{V} \\
0 & \alpha_T V & 0 \\
(\alpha_L - \alpha_T)\frac{uw}{V} & 0 & \alpha_L \frac{w^2}{V} + \alpha_T \frac{u^2}{V}
\end{bmatrix}.
$$

---

[2]The authors who found Equations (5.4) and (5.5) did not non-dimensionalise their units prior to fitting the relationships.

Case 2a: Dispersion coefficients for three-dimensional flow, when dispersion depends on flow speed only, i.e., when $\alpha_L = \alpha_T = \alpha$.

For this case, the following are the dispersion coefficients

$$D_{xx} = \alpha \left(\frac{u^2}{V} + V\frac{v^2}{V_1^2} + \frac{u^2 w^2}{VV_1^2} \right),$$

$$D_{xy} = \alpha \left(\frac{uv}{V} - V\frac{uv}{V_1^2} + \frac{uvw^2}{VV_1^2} \right),$$

$$D_{xz} = 0,$$

$$D_{yx} = \alpha \left(\frac{uv}{V} - V\frac{uv}{V_1^2} + \frac{uvw^2}{VV_1^2} \right),$$

$$D_{yy} = \alpha \left(\frac{v^2}{V} + V\frac{u^2}{V_1^2} + \frac{v^2 w^2}{VV_1^2} \right),$$

$$D_{yz} = 0,$$

$$D_{zx} = 0,$$

$$D_{zy} = 0,$$

$$D_{zz} = \alpha V,$$

which can be written in matrix form $\left[D_{ij} \right] = \alpha \begin{bmatrix} \frac{u^2}{V} + V\frac{v^2}{V_1^2} + \frac{u^2 w^2}{VV_1^2} & \frac{uv}{V} - V\frac{uv}{V_1^2} + \frac{uvw^2}{VV_1^2} & 0 \\ \frac{uv}{V} - V\frac{uv}{V_1^2} + \frac{uvw^2}{VV_1^2} & \frac{v^2}{V} + V\frac{u^2}{V_1^2} + \frac{v^2 w^2}{VV_1^2} & 0 \\ 0 & 0 & V \end{bmatrix}.$

Case 2b: Dispersion coefficients for two-dimensional flow, when dispersion depends on flow speed only, i.e., $\alpha_L = \alpha_T = \alpha$, $v = 0$, $V_1^2 = u^2$, $V = \sqrt{u^2 + w^2}$.

In matrix form, $\left[D_{ij} \right] = \begin{bmatrix} \alpha V & 0 & 0 \\ 0 & \alpha V & 0 \\ 0 & 0 & \alpha V \end{bmatrix}.$

5.2 The fundamental balance equation for a pollutant

Consider a rectangular box in the form of a porous medium with saturated flow, and let inside it be embedded a pervious object as shown in Figure 5.1. This object contains a certain mass of solute, which is described as a *tracer*. Within a porous medium domain, there is a velocity **V** of the fluid at every point and a concentration, C (*C=mass of the substance per*

unit volume of the liquid) of some material under consideration. The average tracer flux of the considered substance is composed of three macroscopic fluxes:

1. An *advective flux*, indicating the flux transported by the water at the latter's average velocity.

2. A *dispersive flux* $= -\mathsf{D} \cdot \nabla C = -D_{ij}\partial C/\partial x_j$, (*ith*-component), where D is a second rank symmetric tensor called the *coefficient of (mechanical) dispersion* and this flux transpires from an area of higher concentration to a lower one [13].

3. A *diffusive flux* $= -\mathsf{D}_{\mathsf{d}}^* \cdot \nabla C$, where $\mathsf{D}_{\mathsf{d}}^*$ is a second rank symmetric tensor called the *coefficient of molecular diffusion* in a porous medium and that demonstrates the influence of the geography of the water holding part of *REV* [13].

As in a groundwater flow, the process of molecular diffusion and mechanical dispersion cannot be separated, the coefficient of hydrodynamic dispersion is considered for both. The coefficient of hydrodynamic dispersion, D_{h}, is given below

$$\mathsf{D}_{\mathsf{h}} = \mathsf{D} + \mathsf{D}_{\mathsf{d}}^*, \tag{5.6}$$

where D is called the coefficient of mechanical dispersion, $\mathsf{D}_{\mathsf{d}}^*$ is the effective (molecular) diffusion coefficient. The longitudinal coefficient of hydrodynamic dispersion, D_L, is given below

$$D_L = \alpha_L \bar{v} + \mathsf{D}_{\mathsf{d}}^*, \tag{5.7}$$

where α_L is the dynamic longitudinal dispersivity, $\bar{v}$ is the average linear groundwater velocity. The total flux (amount of the pollutant passing through a unit area of a porous medium) of a pollutant, by advection. dispersion, and diffusion can be written in the form [13]

$$\mathbf{q_C} = C\mathbf{V} - n\mathsf{D} \cdot \nabla C - n\mathsf{D}_{\mathsf{d}}^* \cdot \nabla C, \tag{5.8}$$

$$\mathbf{q_C} = C\mathbf{V} - n(\mathsf{D} + \mathsf{D}_{\mathsf{d}}^*) \cdot \nabla C, \tag{5.9}$$

where n is the *porosity* of the porous medium. In porous media, if we neglect the effect of the coefficient of molecular diffusion, D_d^*, then Equation (5.9) becomes

$$\mathbf{q_C} \;=\; C\mathbf{V} - n\mathsf{D} \cdot \nabla C. \tag{5.10}$$

A pollutant may be injected (by replenishment through a waste disposal operation) or removed (e.g., by pumping) by the objects embedded in the porous media. Let $C(x, z, t)$ denote the pollutant's concentration within the water. The quantity $\partial(nC)/\partial t$ denotes the rate at which the quantity of the pollutant is increased within a control box. Hence we obtain

$$\frac{\partial(nC)}{\partial t} \;=\; -\nabla \cdot \mathbf{q_C}, \tag{5.11}$$

$$\frac{\partial(nC)}{\partial t} \;=\; -\nabla \cdot (C\mathbf{V} - n\mathsf{D} \cdot \nabla C), \tag{5.12}$$

$$\frac{\partial(nC)}{\partial t} + \mathbf{V} \cdot \nabla C \;=\; \nabla \cdot (n\mathsf{D} \cdot \nabla C), \tag{5.13}$$

$$\frac{\partial C}{\partial t} + \frac{1}{n}(\mathbf{V} \cdot \nabla C) \;=\; \nabla \cdot (\mathsf{D} \cdot \nabla C). \tag{5.14}$$

Three cases arise for the coefficient of mechanical dispersion D, as discussed in Subsection 5.1.1:

1. When dispersion depends on flow speed and direction, then Equation (5.14) becomes

$$\begin{aligned}
\frac{\partial C}{\partial t} + \frac{1}{n}(\mathbf{V} \cdot \nabla C) = {} & \frac{\partial}{\partial x}\left(D_{xx}\frac{\partial C}{\partial x} + D_{xy}\frac{\partial C}{\partial y} + D_{xz}\frac{\partial C}{\partial z} \right) \\
& + \frac{\partial}{\partial y}\left(D_{yx}\frac{\partial C}{\partial x} + D_{yy}\frac{\partial C}{\partial y} + D_{yz}\frac{\partial C}{\partial z} \right) \\
& + \frac{\partial}{\partial z}\left(D_{zx}\frac{\partial C}{\partial x} + D_{zy}\frac{\partial C}{\partial y} + D_{zz}\frac{\partial C}{\partial z} \right).
\end{aligned}$$

   Where x and y are the coordinates in the direction of flow, z is the coordinate normal to flow, $\mathbf{V}$ is fluid velocity.

2. When dispersion depends only on the magnitude of the flow speed, then $\mathsf{D} = D\mathsf{I}$, Equation (5.14) becomes

$$\frac{\partial C}{\partial t} + \frac{1}{n}(\mathbf{V} \cdot \nabla C) \;=\; \nabla \cdot (D\nabla C). \tag{5.15}$$

Writing $D = \alpha V$, Equation (5.15) becomes

$$\frac{\partial C}{\partial t} + \frac{1}{n}(\mathbf{V} \cdot \nabla C) = \frac{\partial}{\partial x}\left(\alpha V \frac{\partial C}{\partial x}\right) + \frac{\partial}{\partial y}\left(\alpha V \frac{\partial C}{\partial y}\right) + \frac{\partial}{\partial z}\left(\alpha V \frac{\partial C}{\partial z}\right). \tag{5.16}$$

3. When dispersion is uniformly constant, then $\mathsf{D} = \bar{D}I = \alpha\bar{V}I$, where, $\bar{V}$=Arithmetic Mean of V, then Equation (5.14) becomes

$$\frac{\partial C}{\partial t} + \frac{1}{n}(\mathbf{V} \cdot \nabla C) = \nabla \cdot (\bar{D}I \cdot \nabla C), \tag{5.17}$$

$$\frac{\partial C}{\partial t} + \frac{1}{n}(\mathbf{V} \cdot \nabla C) = \nabla \cdot (\bar{D}\nabla C), \tag{5.18}$$

$$\frac{\partial C}{\partial t} + \frac{1}{n}(\mathbf{V} \cdot \nabla C) = \bar{D}\left(\frac{\partial^2 C}{\partial x^2} + \frac{\partial^2 C}{\partial y^2} + \frac{\partial^2 C}{\partial z^2}\right). \tag{5.19}$$

To model the problem for the pollutant released by the polluted water from the rectangular object embedded in a porous media, it is assumed that, over reasonable scale of time, C_I is constant and there is no spatial variation of C. Schematic diagram and boundary conditions are shown in Figure 5.1.
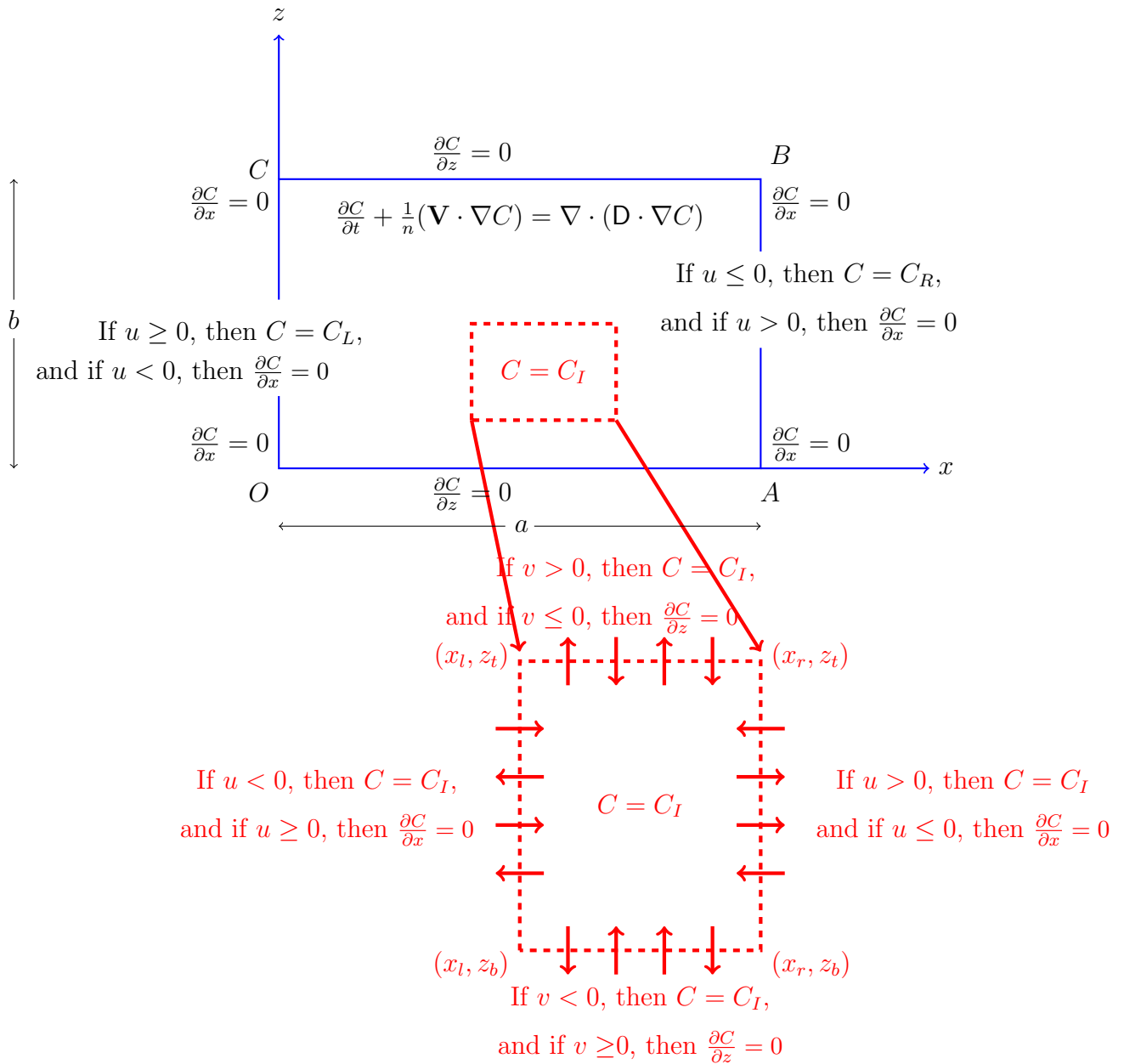
Figure 5.1: *Schematic diagram of the physical domain for concentration C and leaky cylinder embedded in the domain.*

5.2.1 Discussion about the boundary conditions

In the illustration of the schematic diagram of Figure 5.1, thick blue lines of the rectangular porous media are impervious, as no fluid or pollutant can pass across these boundaries so normal components of the gradient of concentration are taken to be zero there. In more detail, the total flux (amount of the pollutant passing through a unit area of a porous medium) of a

pollutant by advection and dispersion can be written in the form

$$\mathbf{q_C} = C\mathbf{V} - n\mathbf{D} \cdot \nabla C, \tag{5.20}$$

where, $\mathbf{q_C} = (q_{Cx}, q_{Cy}, q_{Cz})$.

For assigning boundary conditions on the solid boundaries of the porous medium, the following steps are taken into account.

The pollutant flux component in the z-direction is

$$q_{Cz} = Cw - n\left(D_{zx}\frac{\partial C}{\partial x} + D_{zy}\frac{\partial C}{\partial y} + D_{zz}\frac{\partial C}{\partial z}\right). \tag{5.21}$$

On $z = 0$, and $z = b$, $q_{Cz} = 0$. We have $w = 0$, so $D_{zx} = D_{zy} = 0$ (see Subsection 5.1.1). Using Equation (5.21) gives,

$$q_{Cz} = -n\left(D_{zz}\frac{\partial C}{\partial z}\right) = 0. \tag{5.22}$$

Since $n \neq 0$ and $D_{zz} = \alpha_T\sqrt{u^2 + v^2}$, so by Equation (5.22), on the lower and upper solid boundaries (i.e., on $z = 0$, b), $\partial C/\partial z = 0$.

By a similar argument, on the vertical solid boundaries (i.e., on $x = 0$, and $x = a$), $\partial C/\partial x = 0$.

Boundary conditions on the entrance and exit are assigned in accordance with the value of pressure ϕ_I inside the pervious object (represented by red dotted lines in the Figure 5.1 and discussed in detail in Section 3.7) embedded in the porous medium.

In the entrance, on $x = 0$, the boundary condition is $C = C_L = 0$ only when pressure inside is less than outside the entrance. This is because fresh clean water is entering the domain. On the other hand, the boundary condition, $\partial C/\partial x = 0$ is assigned when the flow is moving through the "entrance" from inside to outside.

Boundary conditions at the "exit" on $x = a$ are assigned similarly.

Boundary conditions on the embedded leaky object are considered in the following way:

Inside the pervious object, there is a constant concentration of pollutant which is represented by $C = C_I$. For the four pervious walls of the object, the boundary conditions are assigned

by considering the velocity of the fluid passing into or out of the object. If the clean water is entering the object, then the boundary conditions on the walls are taken to be $\partial C/\partial n = 0$ (where n is a unit normal vector to a boundary), and if the contaminated water is leaking out from the object, then in this situation, the boundary conditions are assigned to be $C = C_I$.

5.3   Illustrations: homogeneous aquifers

We will discuss the case when pollutants are released from a rectangular pervious object (which is kept at constant pressure) embedded in a homogeneous aquifer. When a pollutant is released from an object, it advects with the fluid flow and disperses in all directions, whose rate depends mainly on the porous structure and fluid speed. First consider the example of a homogeneous porous medium, which is taken in the form of a rectangular box.

5.3.1   When dispersion depends on magnitude and direction

Example 5.3.1 *Consider an aquifer with a running stream of fresh water which is contaminated with a well-mixed pollutant of concentration C_I leaking from a rectangular cylinder embedded in the aquifer. The cylinder is kept at a constant pressure and at a fixed level of pollutant concentration C_I. All the walls of the cylinder are equally pervious. In this example, well sorted sediments are being considered, i.e., fine gravel with a permeability 5.3167×10^{-10} [m^2] is used as the porous material inside the aquifer. Parameters used for the simulations are shown in Table 5.1. The problem is to find a numerical solution of the problem when dispersion depends on magnitude and direction.*

Table 5.1: *Parameters used for the simulations*

Parameters	Values	Units
scaled dynamic pressure in entrance ϕ_L	1	[m]
scaled dynamic pressure in exit ϕ_R	0	[m]
scaled dynamic pressure inside the pervious object ϕ_I	0.5	[m]
constant of proportionality ω_{ps}	1×10^7	[s^{-1}]
measure of resistance of the object's surface to flow through it β_{ps}	1.0224	[m]
porosity n	0.33	[-]
permeability of the porous media k	5.3167×10^{-10}	[m^2]
time step dt	0.001	[-]
maximum allowed real time for simulations T_{max}	2000	[s]
concentration of the injected chloride ions $C_I = mass/volume$	$10.7/12 = 0.8917$	[kg m^{-3}]
density of the groundwater ρ	1000	[kg m^{-3}]
gravitational acceleration g	9.8	[m s^{-2}]
dynamic viscosity of the groundwater μ	1.002×10^{-3}	[kg m^{-1} s^{-1}]
transversal dispersivity α_T	0.01	[m]

The problem under consideration is time-dependent, forced convection pollutant transfer from a leaky cross-section of a cylinder placed in a fairly homogeneous aquifer. After the solution of the fluid flow problem which is already solved in Section 3.7, the fluid velocities are calculated in terms of pressure on the cylinder as well as on the porous medium. The pollutant advection-dispersion phenomenon takes place for the following cases only:

- when the value of pressure inside the cylinder is greater than that in the inlet and in the exit, i.e., $\phi_I > \phi_L$, and $\phi_I > \phi_R$;

- when the value of pressure inside the cylinder is greater than that in the exit, but less than that in the inlet i.e., $\phi_I > \phi_R$, and $\phi_I < \phi_L$;

- when the value of pressure inside the cylinder is greater than that in the exit, but equal to that in the inlet i.e., $\phi_I > \phi_R$, and $\phi_I = \phi_L$;

- when the value of pressure inside the cylinder is less than that in the inlet , but equal to that in the exit i.e., $\phi_I < \phi_L$, and $\phi_I = \phi_R$.

For this model, the value of pressure ϕ_I is taken as an average of the values of pressure in inlet and outlet. To verify the validity of the fluid flow model, flux in, Q_L [m^2 s^{-1}] through inlet; flux out, Q_R [m^2 s^{-1}] through outlet; and flux through the pervious cylinder, Q_I are calculated.

From the Table 5.2, as $Q_{in}=Q_R$ (where, $Q_{in}=Q_L+Q_I$), then the model is verified for further calculations of pollutant transport.

Table 5.2: *Values of the fluid flux through inlet, exit, and pervious cylinder*

Fluxes	Values	Units
flux in Q_L	0.0024	$[\text{m}^2 \text{ s}^{-1}]$
flux through the cylinder Q_I	1.2082×10^{-15}	$[\text{m}^2 \text{ s}^{-1}]$
flux total in Q_{in}	0.0024	$[\text{m}^2 \text{ s}^{-1}]$
flux out Q_R	0.0024	$[\text{m}^2 \text{ s}^{-1}]$

The two-dimensional pollutant transport model, in terms of the transport equation and subject to boundary conditions on the aquifer as well as on the pervious cylinder, is shown in Figure 5.1. In this case, the tracer transport equation for fluid flow in homogeneous aquifer is

$$\frac{\partial C}{\partial t} + \frac{1}{n}(\mathbf{V} \cdot \nabla C) = \frac{\partial}{\partial x}\left(D_{xx}\frac{\partial C}{\partial x} + D_{xz}\frac{\partial C}{\partial z}\right) + \frac{\partial}{\partial z}\left(D_{zx}\frac{\partial C}{\partial x} + D_{zz}\frac{\partial C}{\partial z}\right). \tag{5.23}$$

Following the discussion of Subsection 5.1.1 about dispersion coefficients which further involves two important parameters α_L and α_T, in this part a short discussion about the case in which dispersion depends upon magnitude of speed and direction of flow is included. A list of significant parameters involved in calculations is given in Table 5.1, in which $\beta_{ps} = (\omega_{ps}\mu)/(\rho g)$ is the factor involving the perviousness of the cylinder.

A numerical solution of the time-dependent Equation (5.23) is plotted in Figures 5.2-5.5 for the parametric values listed in Table 5.1. The plots consist of a contour as well as a surface plot for self explanation. As the results are simulated in real situations (i.e., using natural values of the parameters), and the groundwater speed is very slow, so it took a long time to reach the solution near to steady-state form. Results are repeated for a solution near to steady-state with a fixed value of parameter $\alpha_T = 0.01$ [m] and for various values of α_L with a ratio $\gamma = \alpha_L/\alpha_T$ which varies from 1 : 1, 5 : 1, 10 : 1, and 20 : 1.

In these illustrations, as the value of pressure inside the cylinder is $\phi_I = 0.5$ [m], and the stream of water is flowing from left (with $\phi_L = 1$ [m]) to right (with $\phi_R = 0$ [m]) within the aquifer, so very little pollutant can escape towards the upstream entrance and a big pollutant plume moves towards the downstream exit. The white region in all contour plots and blue area in all the surface plots shows the uncontaminated or fresh water, whereas the dark red region in

the surface plots show the polluted water in that region. To know about the impact of various ratios of α_L/α_T on the solution, it is required to calculate the pollutant fluxes through the inlet and exit of the aquifer and through the cylinder.
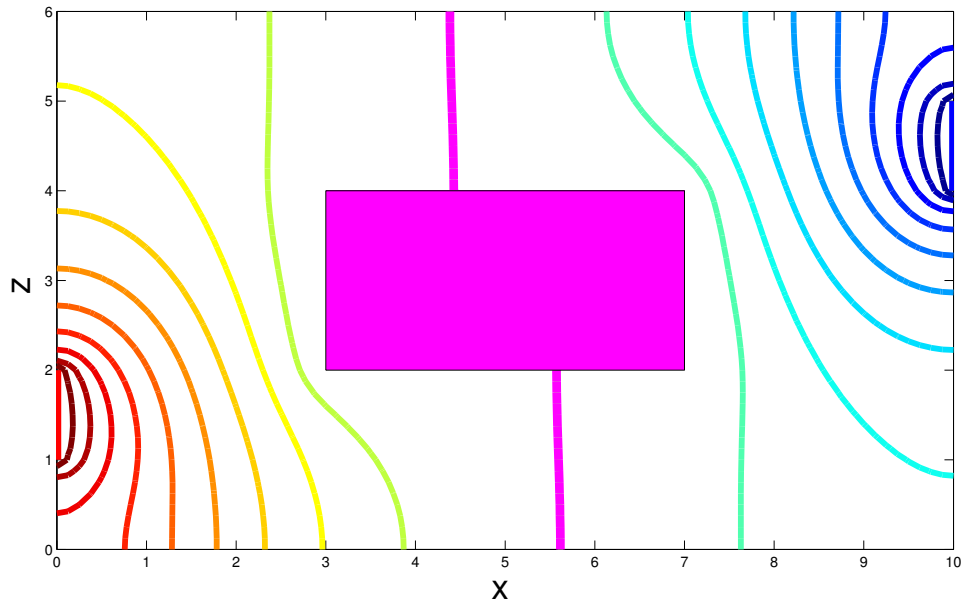
(a) *contour plot for ϕ*
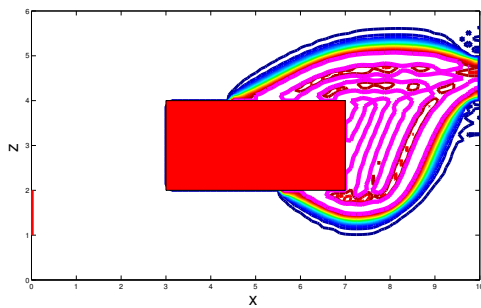
(b) *contour plot for concentration C*
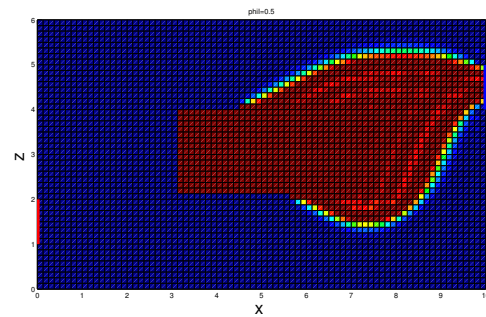
(c) *surface plot for concentration C*

Figure 5.2: *Graphs of a leaky cylinder with rectangular cross-section with $\alpha_L = \alpha_T = 0.01$ (a) a contour plot of ϕ with magenta representing the value of ϕ_I; (b) a contour plot of pollutant concentration, with magenta representing the value of C_I; (c) a surface plot of pollutant concentration.*

121
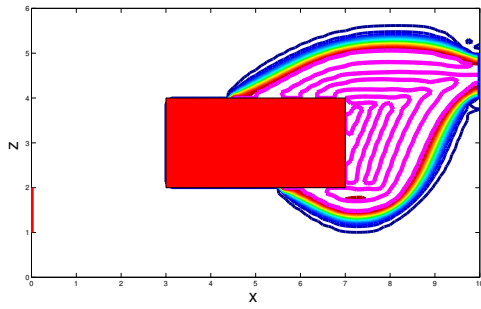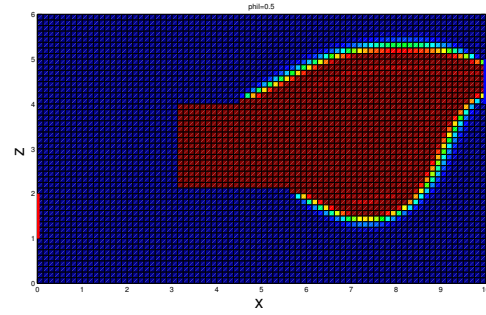
(a) *contour plot for concentration C*   (b) *surface plot for concentration C*

Figure 5.3: *Graphs of a leaky cylinder with rectangular cross-section with $\alpha_L = 0.05$, $\alpha_T = \frac{1}{5}\alpha_L = .01$ (a) a contour plot of pollutant concentration with magenta representing the value of C_I; (b) a surface plot of pollutant concentration.*
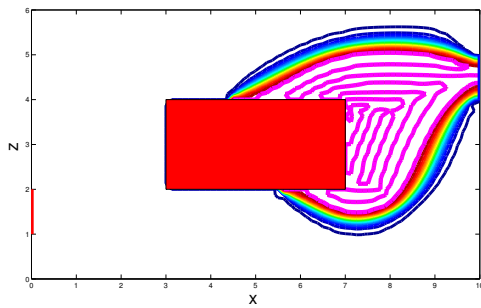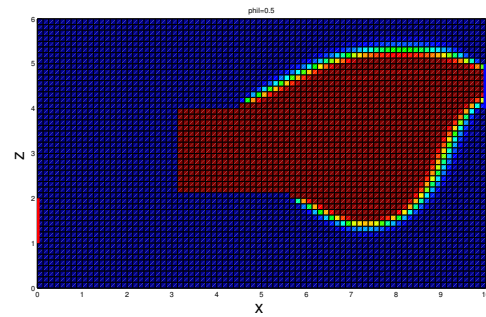
(a) *contour plot for concentration C*   (b) *surface plot for concentration C*

Figure 5.4: *Graphs of a leaky cylinder with rectangular cross-section with $\alpha_L = 0.1$, $\alpha_T = \frac{1}{10}\alpha_L = .01$ (a) a contour plot of pollutant concentration with magenta representing the value of C_I; (b) a surface plot of pollutant concentration.*
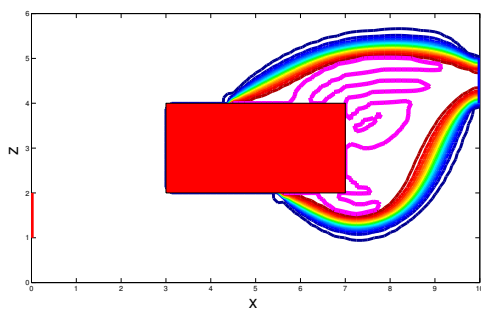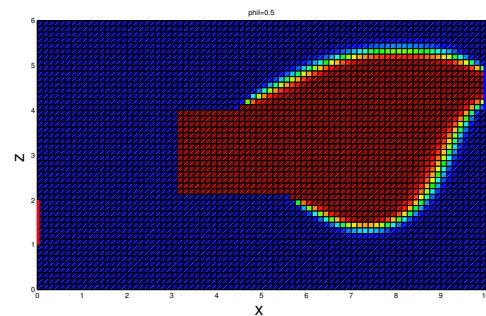
(a) *contour plot for concentration C*   (b) *surface plot for concentration C*

Figure 5.5: *Graphs of a leaky cylinder with rectangular cross-section with $\alpha_L = 0.2$, $\alpha_T = \frac{1}{20}\alpha_L = .01$ (a) a contour plot of pollutant concentration with magenta representing the value of C_I; (b) a surface plot of pollutant concentration.*

Calculations of pollutant fluxes

The advective flux of the pollutant P_L through the entrance (on L.H.S) of the aquifer is calculated as follows.

If $u \geq 0$, then

$$P_L = \int_{b_1}^{b_2} \frac{1}{n} u C_L dz,$$

where, C_L is the value of pollutant concentration outside the entrance (assumed constant).

If $u < 0$, then

$$P_L = \int_{b_1}^{b_2} \frac{1}{n} u C dz.$$

The advective flux of the pollutant P_R through the exit (R.H.S) of the aquifer is calculated as follows.

If $u \leq 0$, then

$$P_R = \int_{b_3}^{b_4} \frac{1}{n} u C_R dz,$$

where, C_R is the value of pollutant concentration outside the exit.

If $u > 0$, then

$$P_R = \int_{b_3}^{b_4} \frac{1}{n} u C dz.$$

The advective flux of the pollutant P_{OL} through the object's lower boundary is given by the following expressions.

If $v \geq 0$, then

$$P_{OL} = \int_{x_l}^{x_r} \frac{1}{n} v C dx.$$

If $v < 0$, then

$$P_{OL} = \int_{x_l}^{x_r} \frac{1}{n} v C_I dx,$$

where, C_I is the value of pollutant concentration inside the cylinder.

The advective flux P_{OT} of the pollutant through the object's top boundary is calculated in this way.

If $v \leq 0$, then

$$P_{OT} = \int_{x_l}^{x_r} \frac{1}{n} v C dx.$$

If $v > 0$, then

$$P_{OT} = \int_{x_l}^{x_r} \frac{1}{n} v C_I dx.$$

The advective flux of the pollutant on the object's L.H.S is given by the following expressions.

If $u \geq 0$, then

$$P_{Oleft} = \int_{z_b}^{z_t} \frac{1}{n} u C dz.$$

If $u < 0$, then

$$P_{Oleft} = \int_{z_b}^{z_t} \frac{1}{n} u C_I dz.$$

The advective flux of the pollutant on the object's R.H.S is given by the following formulae.

If $u \leq 0$, then

$$P_{Oright} = \int_{z_b}^{z_t} \frac{1}{n} u C dz.$$

If $u > 0$, then

$$P_{Oright} = \int_{z_b}^{z_t} \frac{1}{n} u C_I dz.$$

The total amount of advective pollutant flux through the object is:

$P_I = -P_{OL} + P_{OT} - P_{Oleft} + P_{Oright}.$

Values of the three fluxes, viz. P_L, P_R, and P_I are given in Table 5.3. It is evident from the table that as the ratio γ goes to increase, P_R also increases steadily, whereas, P_L decreases gradu-

ally. On the other side, the pollutant flux through the object remains constant for all values of γ.

Table 5.3: *Advective mass flux of a pollutant [kg m^{-1} s^{-1}] through entrance, exit and pervious rectangular cross-section near to steady-state condition for various values of α_L and $\gamma = \alpha_L/\alpha_T$.*

α_L	0.01	0.05	0.1	0.2
α_T	0.01	0.01	0.01	0.01
γ	1	5	10	20
P_L	≈ 0.0000	≈ 0.0000	≈ 0.0000	≈ 0.0000
P_I	0.0037	0.0037	0.0037	0.0037
P_R	0.0031	0.0033	0.0034	0.0035
P_{in}	0.0037	0.0037	0.0037	0.0037

Test for steady-state is: $P_R = P_L + P_I = P_{in}$, but this solution is not in steady-state form. For this model, simulations are done for real values of parameters and due to very slow movement of groundwater, one has to be patient for a long time to get steady-state solution.

5.3.2 When dispersion depends on magnitude only

Example 5.3.2 *Repeat Example 5.3.1 for the case when dispersion depends on magnitude only with the same values of the parameters as listed in Table 5.1.*

In this section, we discuss the case when dispersion depends on magnitude of fluid velocity only. Horizontal and vertical dispersion coefficients are equal and they are proportional to fluid speed V [m s^{-1}], i.e., $D = \alpha V$, where α [m] is the dispersion length (dispersivity) that is dependent on the matrix structure. Two cases arise for the selection of α,

Case 1

when $\alpha_L = \alpha_T = \alpha$, and

Case 2

when α is the geometric mean of (α_L, α_T), i.e., $\alpha = \sqrt{\alpha_L \alpha_T}$.

The average speed $V = \sqrt{u^2 + w^2}$ [m s^{-1}].

For this situation, the pollutant dispersion equation for a two-dimensional, confined and homogeneous aquifer is given by

$$\frac{\partial C}{\partial t} + \frac{1}{n}(\mathbf{V} \cdot \nabla C) = \frac{\partial}{\partial x}\left(\alpha V \frac{\partial C}{\partial x}\right) + \frac{\partial}{\partial z}\left(\alpha V \frac{\partial C}{\partial z}\right). \tag{5.24}$$

125

After the solution of the fluid flow problem, and calculation of Darcy's velocity, Equation (5.24) is solved numerically subject to the boundary conditions as illustrated in Figure 5.1 and discussed in the Subsection 5.2.1. By using the known parameters and varying the value of α [m] as listed in Table 5.4, the transport model is simulated by using chloride ions as a pollutant source leaking from the rectangular cylinder with concentration $(10.7)/(12)$ [kg m^{-3}] and the resulting concentration profile is plotted for a steady-state solution in Figures 5.6-5.12.

Table 5.4: *Parameters used for the simulations.*

Parameters	Values	Units
component of dispersivity α	0.01,	[m]
	$\sqrt{(0.01)(0.05)}{=}0.0224,$	
	$\sqrt{(0.01)(0.1)}{=}0.0316,$	
	$\sqrt{(0.01)(0.2)}{=}0.04472,$	
	0.05, 0.1, 0.2	
coefficient of dispersion	$D = \alpha V$	[m^2 s^{-1}]

A verification between the results of Subsections 5.3.1 and 5.3.2 is when the parameter α_L is equal to α_T. The above argument is validated in the illustrations of Figures 5.2b-5.2c and Figures 5.6a-5.6b, which is further verified by the pollutant fluxes as listed in Tables 5.3 and 5.5 for the value of $\alpha = 0.01$. Moreover, since the dispersion coefficient is equal to the product of α and average speed V, for a very large value of α, the spread of the dispersion plume is large in the transverse direction, however, the mass flux of the pollutant does not change significantly in this direction. The illustrations of this model are given below in Figures 5.6-5.12.

5.3.2.1 Illustrations: When dispersion depends on magnitude only

$\alpha_L = \alpha_T = \alpha = 0.01$ [m]
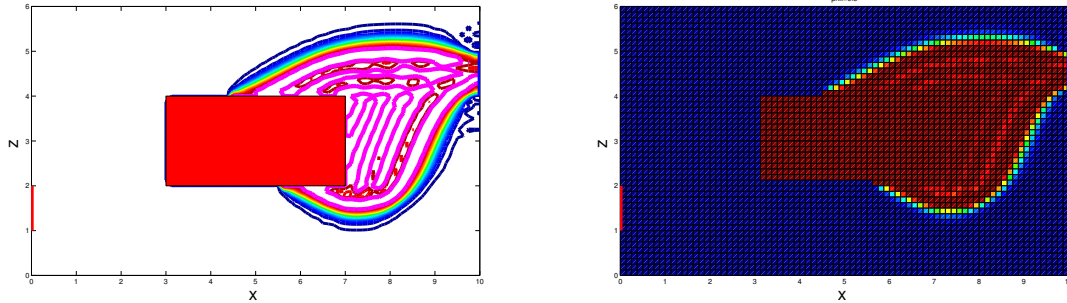
(a) *contour plot for concentration C*   (b) *surface plot for concentration C*

Figure 5.6: *Graphs of a leaky cylinder with rectangular cross-section with $\alpha = 0.01$ (a) a contour plot of pollutant concentration with magenta representing the value of C_I; (b) a surface plot of pollutant concentration.*

α is a geometric mean of $(\alpha_L = 0.05, \alpha_T = 0.01) = 0.0224$ [m]

As discussed in Subsection 5.3.1, the ratio between α_L and α_T, i.e., $\gamma = \alpha_L/\alpha_T$ varies from $1 : 1$, $5 : 1$, $10 : 1$, and $20 : 1$. Results have been conducted already for these ratios in that section. Here, a discussion has been included to view the changes in pollutant concentration profile with varying values of α (which is geometric mean of α_L and α_T) between these ratios. Amongst all other ratios (i.e., arithmetic mean, mode, median, etc.), geometric mean gives the satisfactory results with minimum error of precision. Following are the illustrations for some values of α, when α is a geometric mean of α_L and α_T.
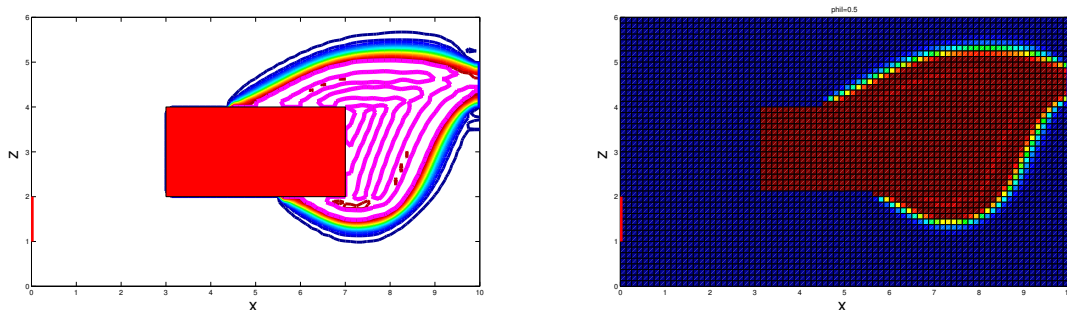
(a) *contour plot for concentration C*   (b) *surface plot for concentration C*

Figure 5.7: *Graphs of a leaky cylinder with rectangular cross-section with $\alpha = 0.0224$ (a) a contour plot of pollutant concentration with magenta representing the value of C_I; (b) a surface plot of pollutant concentration.*

α is a geometric mean of $(\alpha_L = 0.1,\ \alpha_T = 0.01)$=0.0316 [m]
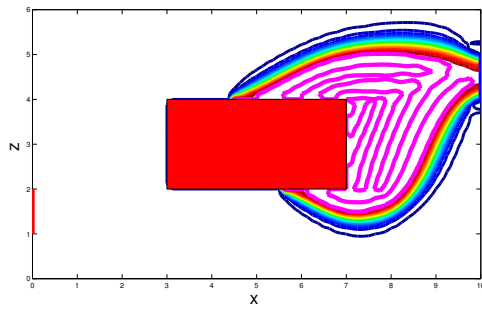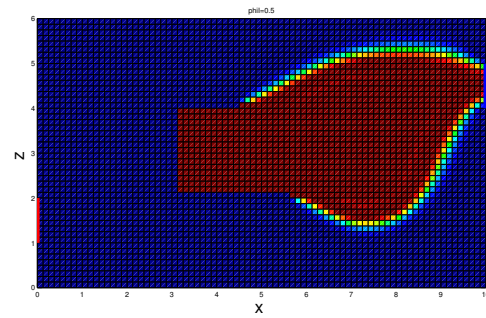
(a) *contour plot for concentration C*   (b) *surface plot for concentration C*

Figure 5.8: *Graphs of a leaky cylinder with rectangular cross-section with $\alpha = 0.0316$ (a) a contour plot of pollutant concentration with magenta representing the value of C_I; (b) a surface plot of pollutant concentration.*

α is a geometric mean of $(\alpha_L = 0.2,\ \alpha_T = 0.01)$=0.04472 [m]
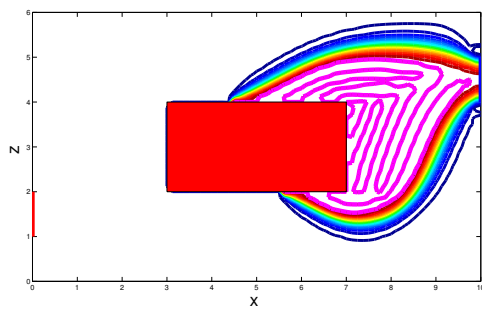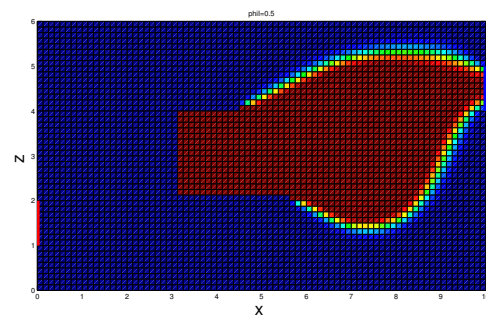
(a) *contour plot for concentration C*   (b) *surface plot for concentration C*

Figure 5.9: *Graphs of a leaky cylinder with rectangular cross-section with $\alpha = 0.04472$ (a) a contour plot of pollutant concentration with magenta representing the value of C_I; (b) a surface plot of pollutant concentration.*

$\alpha_L = \alpha_T = \alpha = 0.05 \ [\mathbf{m}]$
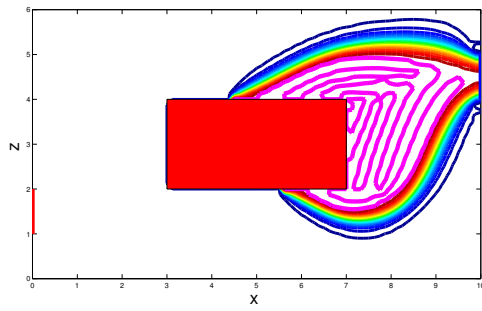
(a) *contour plot for concentration C*
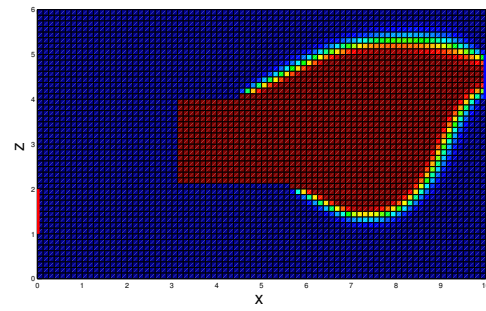
(b) *surface plot for concentration C*

Figure 5.10: *Graphs of a leaky cylinder with rectangular cross-section with $\alpha = 0.05$ (a) a contour plot of pollutant concentration with magenta representing the value of C_I; (b) a surface plot of pollutant concentration.*

$\alpha_L = \alpha_T = \alpha = 0.1 \ [\mathbf{m}]$
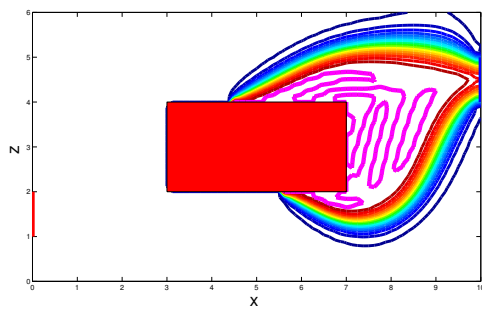
(a) *contour plot for concentration C*
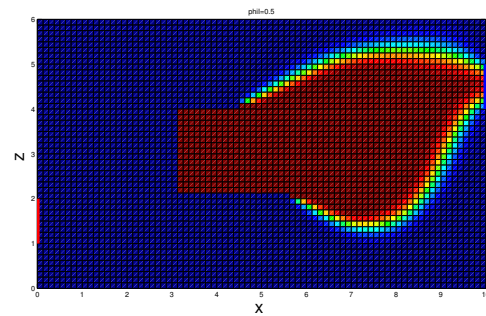
(b) *surface plot for concentration C*

Figure 5.11: *Graphs of a leaky cylinder with rectangular cross-section with $\alpha = 0.1$ (a) a contour plot of pollutant concentration with magenta representing the value of C_I; (b) a surface plot of pollutant concentration.*

$$\alpha_L = \alpha_T = \alpha = 0.2 \; [\mathbf{m}]$$
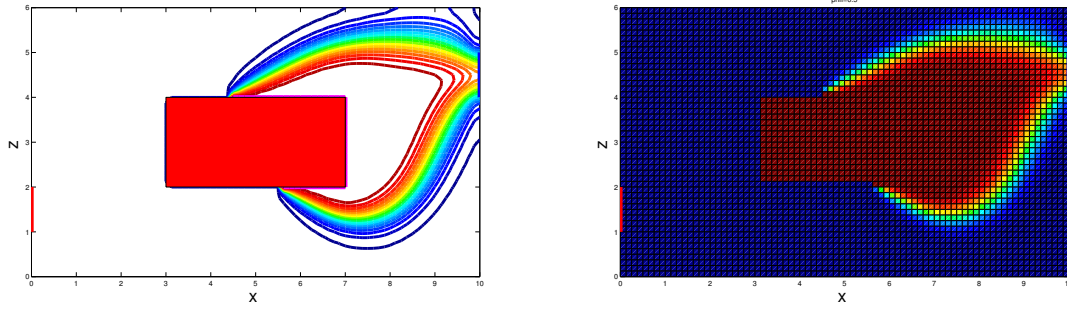
(a) *contour plot for concentration C*   (b) *surface plot for concentration C*

Figure 5.12: *Graphs of a leaky cylinder with rectangular cross-section with $\alpha = 0.2$ (a) a contour plot of pollutant concentration with magenta representing the value of C_I; (b) a surface plot of pollutant concentration.*

For this type of pollutant model, one can observe that the spread of pollutant through the entrance is negligible (i.e., pollutant flux P_L) due to the higher dynamic pressure there, a fresh stream of water is entering the domain, as a result of which little pollutant can escape towards the entrance. On the other hand, the pollutant flux P_R is significantly high due to the lower pressure ϕ_R on the exit. Results are tending to the steady-state level and the test for steady-state is: $P_R = P_L + P_I = P_{in}$.

Table 5.5: *Mass flux of a pollutant [kg m^{-1} s^{-1}] through entrance, exit and pervious rectangular cross-section near to steady-state.*

α	0.01	0.0224	0.0316	0.04472	0.05	0.1	0.2
P_L	≈ 0.0000	≈ 0.0000	≈ 0.0000	≈ 0.0000	≈ 0.0000	≈ 0.0000	≈ 0.0000
P_I	0.0037	0.0037	0.0037	0.0037	0.0037	0.0037	0.0037
P_R	0.0031	0.0033	0.0033	0.0034	0.0034	0.0033	0.0032
P_{in}	0.0037	0.0037	0.0037	0.0037	0.0037	0.0037	0.0037

Table 5.5 shows the values of pollutant fluxes through the entrance, exit, and pervious cylinder. In real situations, average speed of groundwater is very slow and it takes a long time to transport a pollutant leaking from underground buried objects. For this model, since, dispersion coefficient $D = \alpha V$, where, $V = \sqrt{u^2 + w^2}$ [m s^{-1}] is the average fluid speed, the results are not in steady-state form due to the long time consumed for the simulations.

5.3.3 When dispersion is uniformly constant

Example 5.3.3 *Repeat Example 5.3.1 for the case when dispersion is uniformly constant with the same values of the parameters as listed in Table 5.1.*

The transport model for this situation is

$$\frac{\partial C}{\partial t} + \frac{1}{n}(\mathbf{V} \cdot \nabla C) = D \left(\frac{\partial^2 C}{\partial x^2} + \frac{\partial^2 C}{\partial z^2} \right), \tag{5.25}$$

where the constant D is the coefficient of mechanical dispersion. In a geological formation it is due to different flow paths acquired by the water particles. Occasionally, water particles follow a faster flow path which is mainly because of that water flows in a more direct flow or it flows through the larger pores or between the centre of the pores where the friction is negligible. The numerical value of mechanical dispersion is different for each geological material and is equal to the product of advective groundwater velocity and dispersivity. As discussed earlier in Section 5.1, dispersivity is an essential attribute of a geological medium which has two components and is dependent on matrix structure.

The dispersion coefficient D, in this situation is given by $\bar{D} = \alpha \bar{V}$, where α [m] is dispersion length (dispersivity), $\bar{V} = AM(V)$, and V is the average flow speed given by $V = \sqrt{u^2 + w^2}$ [m s^{-1}].

There are various choices for the selection of $\bar{V}$. Arithmetic mean, geometric mean, mode, median, or any other ratio can be considered for $\bar{V}$. In this particular situation, $\bar{V}$ is regarded as the arithmetic mean of average speed V for the purpose of demonstration and to establish an agreement between the two transport models as discussed in Subsections 5.3.1 and 5.3.2.

Two cases arise for the selection of α,

Case 1: when $\alpha_L = \alpha_T = \alpha$, and

Case 2: when α is the geometric mean of $(\alpha_L, \alpha_T) = \sqrt{\alpha_L \alpha_T}$.

Table 5.6 shows a list of parameters used in the simulations.

Table 5.6: *Parameters used for the simulations.*

Parameters	Values	Units
value of $\bar{V}$	3.3276e-04	[m s^{-1}]
component of dispersivity α	0.01,	[m]
	$\sqrt{(0.01)(0.05)}$=0.0224,	
	$\sqrt{(0.01)(0.1)}$=0.0316,	
	$\sqrt{(0.01)(0.2)}$=0.04472,	
	0.05, 0.1, 0.2	
coefficient of dispersion $\bar{D} = \alpha\bar{V}$	3.3276e-06,	[m^2 s^{-1}]
	7.4538e-06,	
	1.0515e-05,	
	1.4881e-05,	
	1.6638e-05,	
	3.3276e-05,	
	6.6552e-05	

A numerical solution for the transport model given by Equation (5.25) is plotted in Figures 5.13-5.19 in the form of a contour as well as a surface plot. In the inlet, exit and inside the pervious body, because $\nabla C = 0$, there is advective flux only, while in the porous medium side we have both advective and dispersive fluxes. We note the spreading of the contaminated water, is not only in the direction of uniform flow (in the longitudinal direction), but also in the transverse direction, and the concentration plume spreads gradually in transverse direction with the increasing value of α. It cannot be due to the fluid flow speed, because in this situation, $\bar{V}$ is taken as the arithmetic mean of fluid speed, and is constant everywhere. Fluid flow is continuous, α may depends upon the porosity and permeability of the porous medium, but it is assumed that the porous medium is homogeneous with uniform porosity.

As α [m] is the dispersion length that depends on matrix structure, so with the increasing value of α, pollutant occupies an ever increasing proportion towards the transversal direction. Hence, the two basic factors that yield this kind of spreading (transverse) are, the fluid flow and the existence of a matrix structure by means of which fluid flow occurs. Graphical representation of this situation is given in Figures 5.13-5.19.

5.3.3.1 Illustrations: When dispersion is uniformly constant

$\alpha_L = \alpha_T = \alpha = 0.01$ [m]
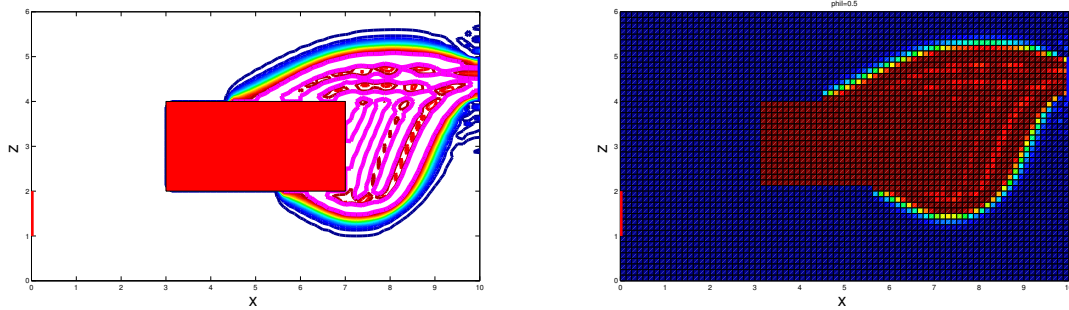
(a) *contour plot for concentration C*   (b) *surface plot for concentration C*

Figure 5.13: *Graphs of a leaky cylinder with rectangular cross-section with $\alpha = 0.01$ (a) a contour plot of pollutant concentration with magenta representing the value of C_I; (b) a surface plot of pollutant concentration.*

α is a geometric mean of ($\alpha_L = 0.05$, $\alpha_T = 0.01$)=0.0224 [m]
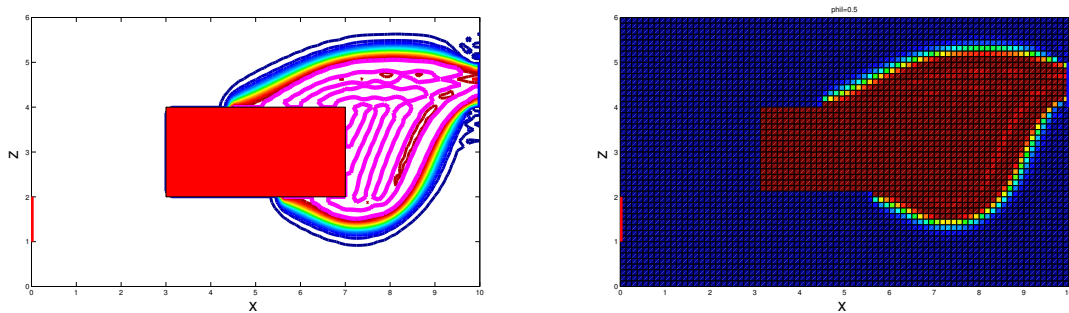
(a) *contour plot for concentration C*   (b) *surface plot for concentration C*

Figure 5.14: *Graphs of a leaky cylinder with rectangular cross-section with $\alpha = 0.0224$ (a) a contour plot of pollutant concentration with magenta representing the value of C_I; (b) a surface plot of pollutant concentration.*

α **is a geometric mean of** $(\alpha_L = 0.1,\ \alpha_T = 0.01)$**=0.0316 [m]**
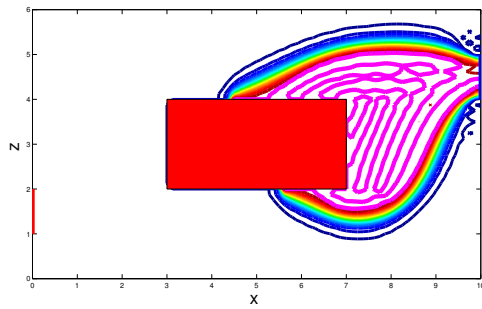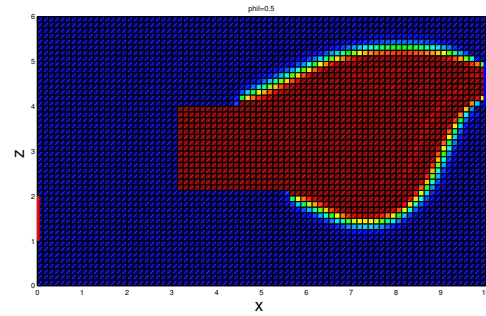
(a) *contour plot for concentration C* (b) *surface plot for concentration C*

Figure 5.15: *Graphs of a leaky cylinder with rectangular cross-section with $\alpha = 0.0316$ (a) a contour plot of pollutant concentration; (b) a surface plot of pollutant concentration.*

α **is a geometric mean of** $(\alpha_L = 0.2,\ \alpha_T = 0.01)$**=0.04472 [m]**
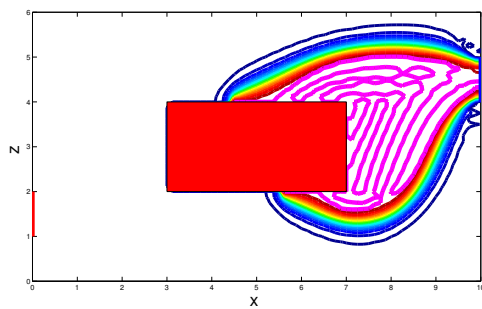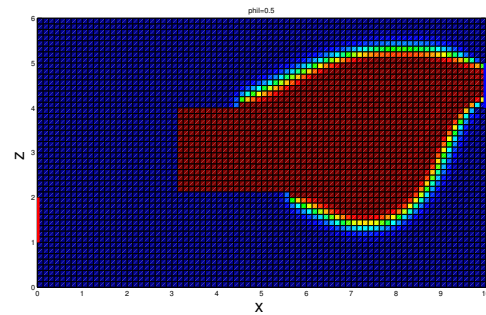
(a) *contour plot for concentration C* (b) *surface plot for concentration C*

Figure 5.16: *Graphs of a leaky cylinder with rectangular cross-section with $\alpha = 0.04472$ (a) a contour plot of pollutant concentration with magenta representing the value of C_I; (b) a surface plot of pollutant concentration.*

$\alpha_L = \alpha_T = \alpha = 0.05 \; [\mathbf{m}]$
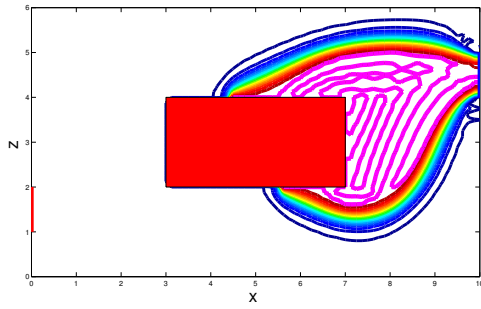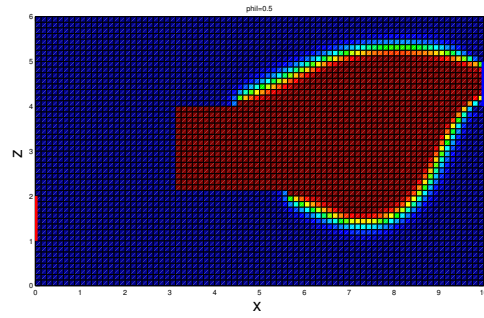
(a) *contour plot for concentration C*   (b) *surface plot for concentration C*

Figure 5.17: *Graphs of a leaky cylinder with rectangular cross-section with $\alpha = 0.05$ (a) a contour plot of pollutant concentration with magenta representing the value of C_I; (b) a surface plot of pollutant concentration.*

$\alpha_L = \alpha_T = \alpha = 0.1 \; [\mathbf{m}]$
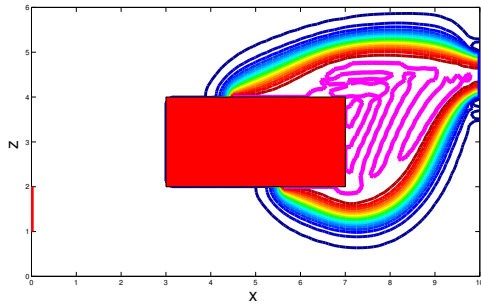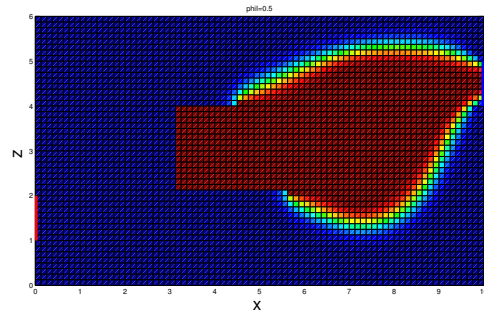
(a) *contour plot for concentration C*   (b) *surface plot for concentration C*

Figure 5.18: *Graphs of a leaky cylinder with rectangular cross-section with $\alpha = 0.1$ (a) a contour plot of pollutant concentration with magenta representing the value of C_I; (b) a surface plot of pollutant concentration.*

$$\alpha_L = \alpha_T = \alpha = 0.2 \ [\mathbf{m}]$$
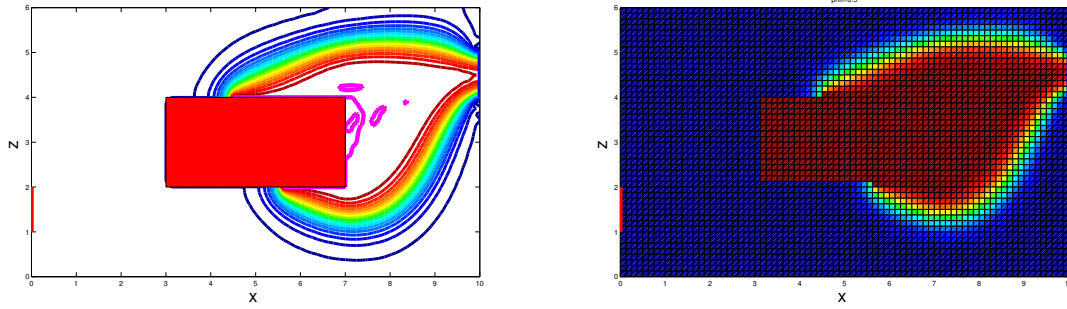
(a) *contour plot for concentration C*

(b) *surface plot for concentration C*

Figure 5.19: *Graphs of a leaky cylinder with rectangular cross-section with $\alpha = 0.2$ (a) a contour plot of pollutant concentration with magenta representing the value of C_I; (b) a surface plot of pollutant concentration.*

Pollutant fluxes are calculated for the inlet, outlet and through the pervious surface in Table 5.7. As according to the boundary conditions (Subsection 5.2.1), on these boundaries there is advective flux only, so for a stationary boundary (solid), there is no transport of pollutant to or from the porous medium domain.

For the nature of the various fluxes, it is noted that in the entrance of the porous medium, there is a running stream of fresh water, therefore very little amount of pollutant can advect through this region, whereas, water is flowing outside from the exit, so with the increasing value of α, the advective flux through this area also increases slowly and becomes equal to the advective pollutant flux through the leaky cylinder in the steady-state condition.

Table 5.7: *Mass flux of a pollutant [kg m^{-1} s^{-1}] through entrance, exit and pervious rectangular cross-section near to steady-state.*

α	0.01	0.0224	0.0316	0.04472	0.05	0.1	0.2
P_L	≈ 0.0000	≈ 0.0000	≈ 0.0000	≈ 0.0000	≈ 0.0000	≈ 0.0000	≈ 0.0000
P_I	0.0037	00.0037	0.0037	0.0037	0.0037	0.0037	0.0037
P_R	0.0030	0.0031	0.0032	0.0033	0.0033	0.0033	0.0033
P_{in}	0.0037	0.0037	0.0037	0.0037	0.0037	0.0037	0.0037

5.3.4 When dispersion is uniformly constant: a case for a larger ϕ_I inside

Example 5.3.4 *Repeat Example 5.3.3 for the case when pressure inside the object is higher than that in the inlet and exit.*

Example 5.3.3 is reconsidered for a higher value of ϕ_I inside the cylinder. Parameters used for the simulations are shown in Table 5.8. As pressure inside is higher than that in the vicinity of the cylinder so inside fluid is ejecting the fluid outside and a part of which is escaping out from inlet and exit; this is visible in Figure 5.20a where red pressure lines are visible in the neighbourhood of the cylinder depicting the fact of higher pressure there. This higher pressure is maintained to be constant inside as a continuous replenishment of water there.

Table 5.8: *Parameters used for the simulations.*

Parameters	Values	Units
scaled dynamic pressure in entrance ϕ_L	1	[m]
scaled dynamic pressure in exit ϕ_R	0	[m]
scaled dynamic pressure inside the pervious object ϕ_I	2	[m]
constant of proportionality ω_{ps}	1×10^7	[s^{-1}]
measure of resistance of the object's surface to flow through it β_{ps}	1.0224	[m]
porosity n	0.33	[-]
permeability of the porous media k	5.3167×10^{-10}	[m^2]
time step dt	0.001	[-]
maximum allowed real time for simulations T_{max}	2000	[s]
concentration of the injected chloride ions $C_I = mass/volume$	$10.7/12 = 0.8917$	[kg m^{-3}]
density of the groundwater ρ	1000	[kg m^{-3}]
gravitational acceleration g	9.8	[m s^{-2}]
dynamic viscosity of the groundwater μ	1.002×10^{-3}	[kg m^{-1} s^{-1}]
component of dispersivity α	0.2	[m]

Table 5.9 shows that flux in Q_L [m^2 s^{-1}] has a negative value -0.0039, which shows that fluid is escaping out through the inlet, whereas, flux through the cylinder Q_I and the exit flux Q_R have respectively the positive values 0.0118 and 0.0081 [m^2 s^{-1}], which indicate fluid inside the cylinder is ejecting the fluid towards the exit as well as in the inlet. The model of fluid flow is verified by the values of fluid fluxes through the inlet, exit and the cylinder, and the check on the model is: $Q_{in} = Q_R$, where $Q_{in} = Q_L + Q_I$.

After the validation of the fluid flow model and calculations of Darcy velocities, the problem

is to find a numerical solution of the pollutant transport model for the case when dispersion is uniformly constant.

Consider a running stream of fresh water which is contaminated with a well-mixed pollutant of concentration C_I leaking from a rectangular cylinder embedded in the aquifer. The cylinder is kept at a constant pressure and at a fixed level of pollutant concentration C_I. All the walls of the cylinder are equally pervious. In this example, well sorted sediments are being considered, i.e., fine gravel with a permeability 5.3167×10^{-10} [m^2] is used as the porous material inside the aquifer.

Figure 5.20b and 5.20c show respectively the concentration contour and surface plots of the problem near steady-state. As pressure inside the cylinder is higher, fluid inside the cylinder pushes the pollutant outside with a great pressure and a pollution plume goes towards the inlet and the exit. When the solution reaches to a steady-state form, all the water will be contaminated by the pollutant which will be visible in the illustration of the surface plot in Figure 5.20c in which whole region will be turned out red.

Table 5.9: *Values of fluid and mass fluxes near the steady-state solution for a larger ϕ_I inside the object.*

Fluxes	Values	Units
flux in Q_L	-0.0039	[m^2 s^{-1}]
flux through the cylinder Q_I	0.0118	[m^2 s^{-1}]
flux total in Q_{in}	0.0080	[m^2 s^{-1}]
flux out Q_R	0.0081	[m^2 s^{-1}]
value of $\bar{V}$	8.9037e-04	[m s^{-1}]
coefficient of dispersion $\bar{D} = \alpha\bar{V}$	1.7807e-04	[m^2 s^{-1}]
mass flux of a pollutant (from entrance) P_L	-0.0088	[kg m^{-1} s^{-1}]
mass flux of a pollutant (through the cylinder) P_I	0.0341	[kg m^{-1} s^{-1}]
total mass flux in of a pollutant P_{In}	0.0254	[kg m^{-1} s^{-1}]
total mass flux out of a pollutant P_R	0.0208	[kg m^{-1} s^{-1}]

A part of the Table 5.9 shows the mass fluxes [kg m^{-1} s^{-1}] of the pollutant through the inlet, exit and the cylinder. As the objective of the illustrations is to elaborate the effect of higher pressure inside the cylinder on concentration profiles, so results of pollutant concentration are restricted near to steady-state form.
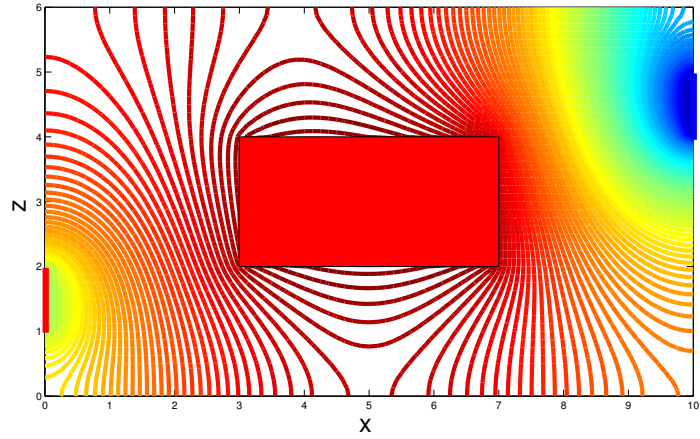
(a)
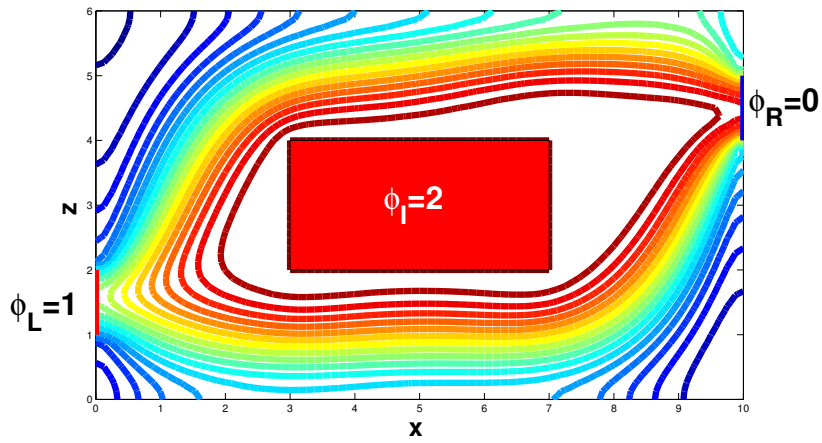
(b)
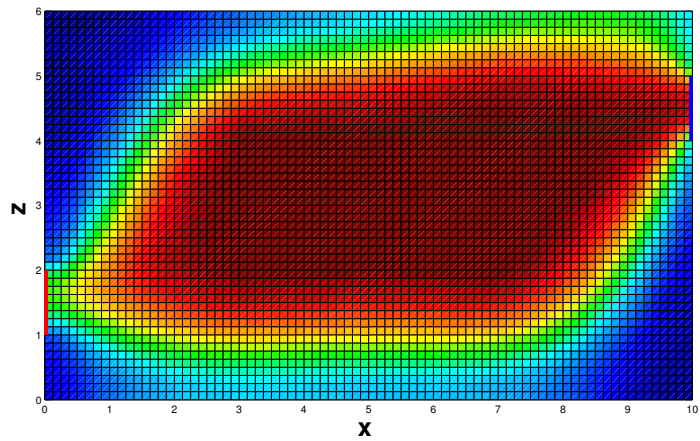
(c)

Figure 5.20: *Graphs for a leaky cylinder with rectangular cross-section placed in a homogeneous aquifer, with $\alpha = 0.2$, $\phi_I = 2$, $\phi_L = 1$, and $\phi_R = 0$ (a) a contour plot of ϕ; (b) a contour plot of pollutant concentration; (c) a surface plot of pollutant concentration.*

5.3.5 Influence of β_{ps} on fluid and pollutant flux rates

The parameter which gives the measure of perviousness of the leaky cylinder is the factor β_{ps} which is discussed in Section 3.7. To find the influence of β_{ps} on pollutant transfer rates, a study is undertaken for three values of pressure (i.e., for $\phi_I = 0.5$, 1, 2) inside the pervious cylinder. It is observed from the Figures 5.21a, 5.21b, and 5.21c that as the perviousness of the cylinder increases from 0 to 1, the value of pollutant concentration flux out also increases abruptly, afterwards the curve increases smoothly.

Moreover, it is also observed that, for a higher value of ϕ_I, the pollutant flux has larger values, as evident from Figure 5.21d, where the pollutant flux curve for $\phi_I = 2$ has the highest values when compared to $\phi_I = 1$ and $\phi_I = 0.5$, and the curve for $\phi_I = 1$ has relatively larger values than for $\phi_I = 0.5$. This comparison is done not only for pollutant fluxes, but is verified for fluid fluxes also, where in Figure 5.22 pollutant and fluid flux curves are shown for $\phi_I = 0.5$, 1, 2 against various values of β_{ps}. It is also shown that as fluid fluxes increase, pollutant fluxes also increase. The relationship between pollutant and fluid fluxes will be discussed later.

(a) $\phi_I = 0.5$

(b) $\phi_I = 1$

(c) $\phi_I = 2$

(d) $\phi_I = 0.5, 1, 2$
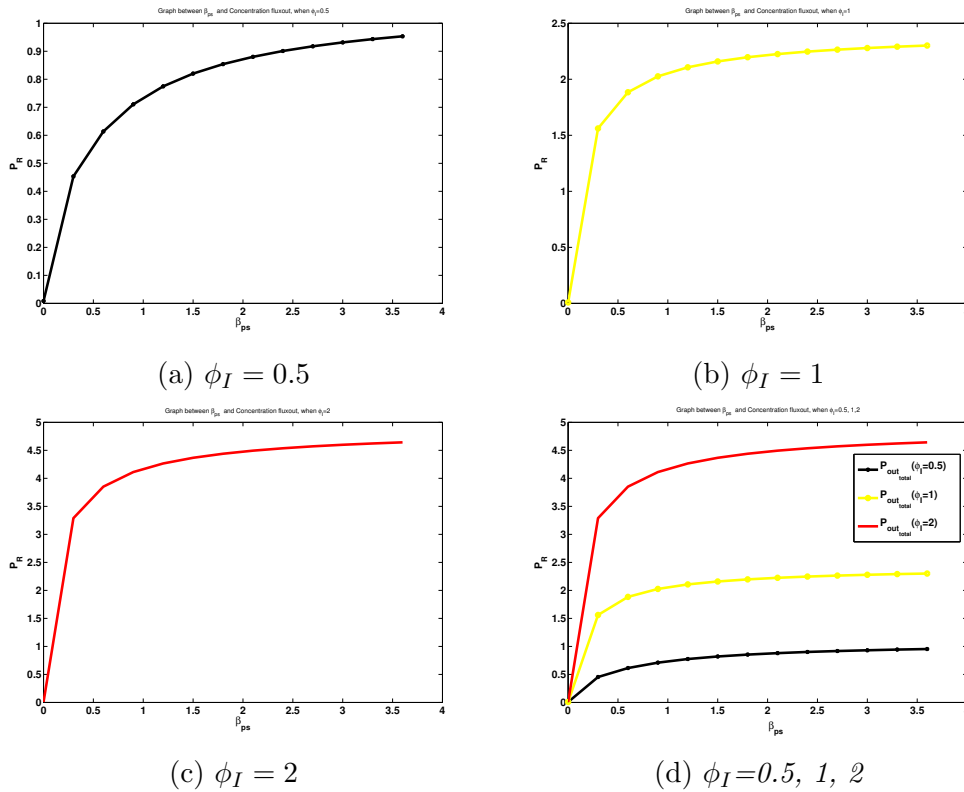
Figure 5.21: *Illustrations of pollutant concentration net flux out plotted against for various values of β_{ps}, for $\phi_L = 1$, $\phi_R = 0$, when (a) $\phi_I = 0.5$; (b) $\phi_I = 1$; (c) $\phi_I = 2$; (d) combined graph of (a), (b), and (c).*
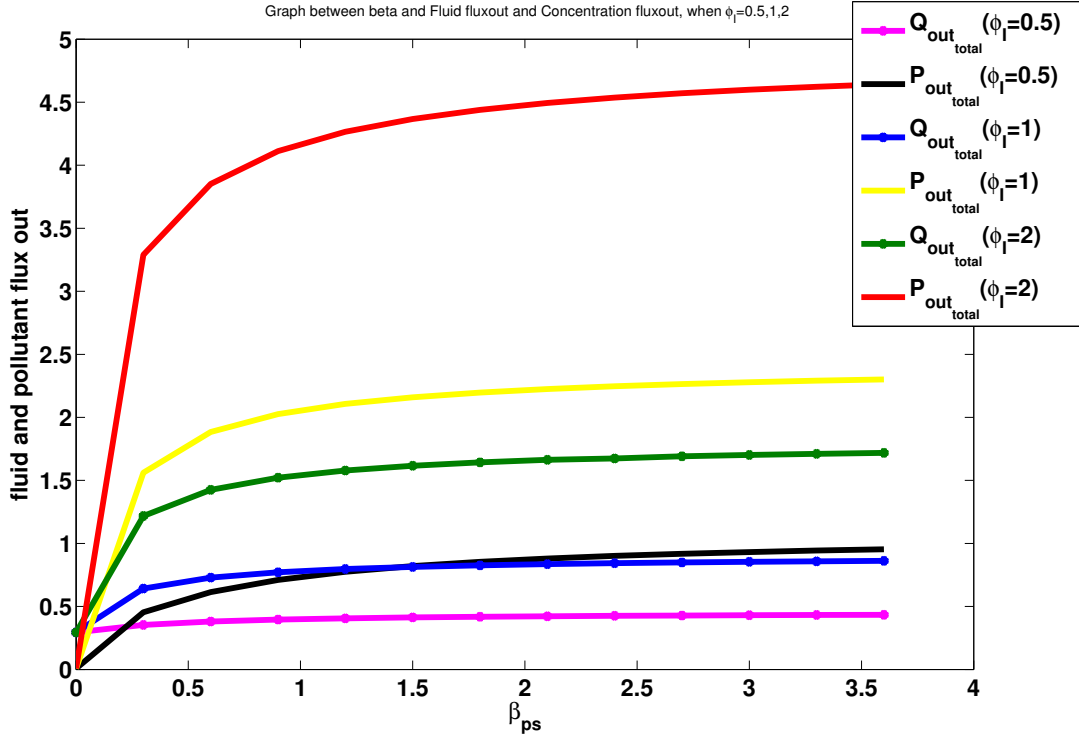
Figure 5.22: *Illustrations of graph of fluid and pollutant concentration net flux out plotted against various values of β_{ps}, for $\phi_L = 1$, $\phi_R = 0$, $\phi_I = 0.5$, 1, 2.*

5.3.6 Influence of ϕ_I on net fluid and pollutant fluxes out

Numerical simulations were performed for total rate of contamination transfer against pressure ϕ_I inside the leaky cylinder for $\beta_{ps} = 0$, 1, 2. Figure 5.23a shows that for $\beta_{ps} = 0$ the total rate of pollutant transfer remains zero against all values of ϕ_I. The reason is that the cylinder is completely impermeable for $\beta_{ps} = 0$, so no transfer of pollutant occurs across the cylinder. However, for $\beta_{ps} > 0$, the total rate of pollutant transfer increases gradually for various values of ϕ_I, as illustrated in Figures 5.23b and 5.23c.

Figure 5.23d gives a comparison for three values of β_{ps} (i.e., for 0, 1, and 2), in which a larger β_{ps} indicates greater perviousness of the cylinder and as a result a relatively greater rate of contamination transfer occurs through the porous medium. Figure 5.24 gives a summary of fluid and contamination flux rates against various values of ϕ_I for $\beta_{ps} = 0$, 1, 2. It is noted that for $\beta_{ps} = 0$, the fluid flux remains at a constant rate of 0.2947 [m^2 s^{-1}], whereas, for $\beta_{ps} > 0$, the fluid flux also increases as the pollutant fluxes do.

(a) $\beta_{ps} = 0$

(b) $\beta_{ps} = 1$

(c) $\beta_{ps} = 2$

(d) $\beta_{ps}=0,\ 1,\ 2$
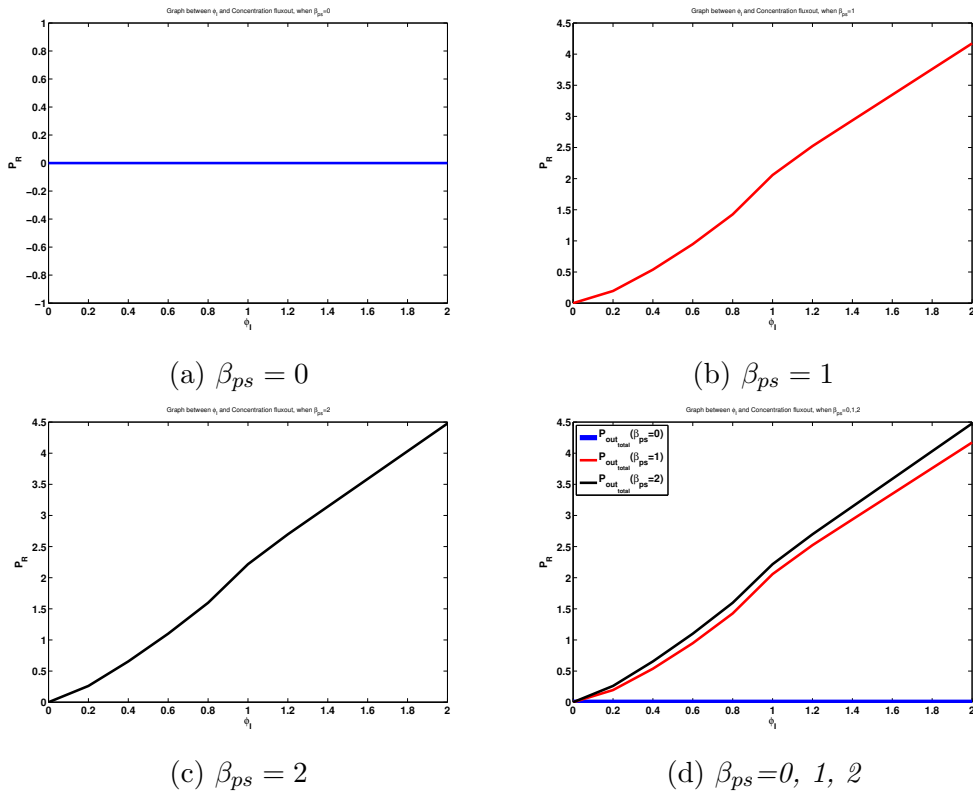
Figure 5.23: *Illustrations of graph of pollutant concentration flux out plotted against various values of ϕ_I, for $\phi_L = 1$, $\phi_R = 0$, when (a) $\beta_{ps} = 0$; (b) $\beta_{ps} = 1$; (c) $\beta_{ps} = 2$; (d) combine graph of (a), (b), and (c).*
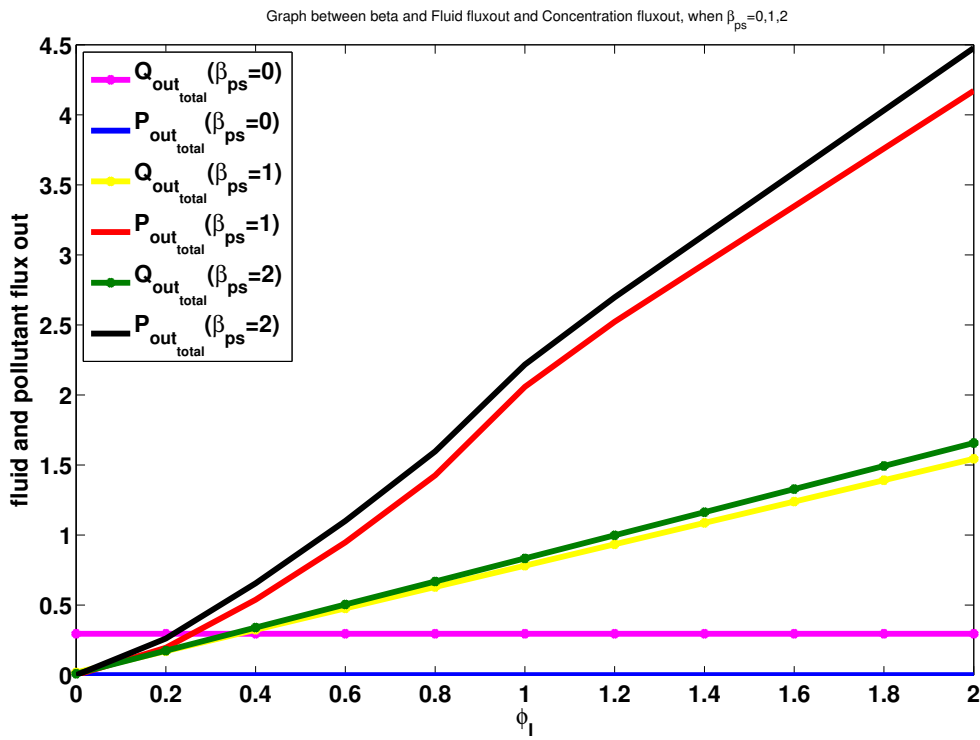
Figure 5.24: *Illustrations of graphs of fluid and pollutant concentration flux out plotted against various values of ϕ_I, for $\phi_L = 1$, $\phi_R = 0$, $\beta_{ps}=0,\ 1,\ 2$.*

5.3.7 Influence of fluid flux on pollutant flux for various values of ϕ_I and β_{ps}

Figures 5.25 and 5.26 gives the rate of total contaminant transfer to the groundwater flow rate, plotted against various parametric values of β_{ps} and ϕ_I, respectively. Before plotting Figure 5.25, fluid fluxes out and contaminant transfer fluxes out are calculated first for various values of parameter β_{ps} by keeping ϕ_I fixed. Afterwards, contaminant fluxes out are plotted against fluid fluxes for three different levels of ϕ_I by selecting its values one by one.

In Figures 5.25a-5.25c, pollutant concentration fluxes are plotted against fluid fluxes for ϕ_I=0.5, 1, and 2. In all these graphs, it is observed that the pollutant contaminant transfer rate increases as the fluid flow rate increases. In addition, Figure 5.25d gives a combined graph of Figures 5.25a-5.25c, which shows that rate of total contaminant transfer is also proportional to ϕ_I. The pollutant concentration flux curve for $\phi_I = 2$ is almost double in length and its rate of increase is twice than that of the curve for $\phi_I = 1$, while the curve for $\phi_I = 1$ is about two times longer (both in length and in value) than for $\phi_I = 0.5$.

(a) $\phi_I = 0.5$ 　　　　 (b) $\phi_I = 1$

(c) $\phi_I = 2$ 　　　　 (d) ϕ_I=0.5, 1, 2
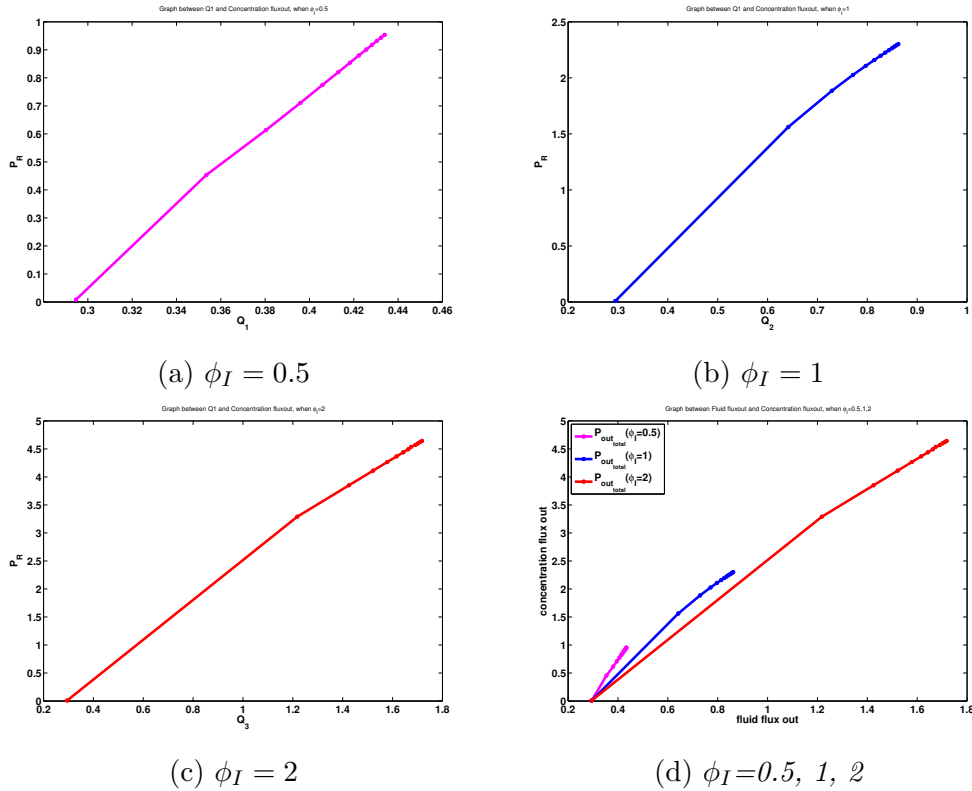
Figure 5.25: *Illustrations of pollutant concentration flux out plotted against fluid flux out, calculated for various values of β_{ps}, for $\phi_L = 1$, $\phi_R = 0$, when (a) $\phi_I = 0.5$; (b) $\phi_I = 1$; (c) $\phi_I = 2$; (d) combined graph of (a), (b), and (c).*

Pollutant or fluid transfer through the embedded groundwater objects occurs only when they are leaky/pervious. The parameter β_{ps} characterises the perviousness of the embedded objects. If β_{ps} is zero, then these objects become completely impermeable and it is not possible for fluid and pollutant to pass through them. Before plotting the graph of Figure 5.26, fluid and pollutant concentration flux out are calculated first for various values of ϕ_I and by keeping β_{ps} fixed. Then, pollutant concentration fluxes out are plotted against fluid fluxes out for $\beta_{ps}=0$, 1 and 2 .

In Figure 5.26a, it is observed that, for $\beta_{ps} = 0$, the pollutant concentration flux rate remains zero against a constant value of fluid flux out. However, for $\beta_{ps} > 0$, as the fluid flux increases, the pollutant concentration flux also increases, as observed in Figures 5.26b and 5.26c. Figure 5.26d gives the comparison for three values of β_{ps}, in this graph, it is shown that the two curves of pollutant fluxes for $\beta_{ps}= 1$, 2 increase at the same rates because for positive values of β_{ps}, as the fluid flux increases, the contamination flux also increases, and vice versa.

(a) $\beta_{ps} = 0$ (b) $\beta_{ps} = 1$

(c) $\beta_{ps} = 2$ (d) $\beta_{ps} =0,\ 1,\ 2$
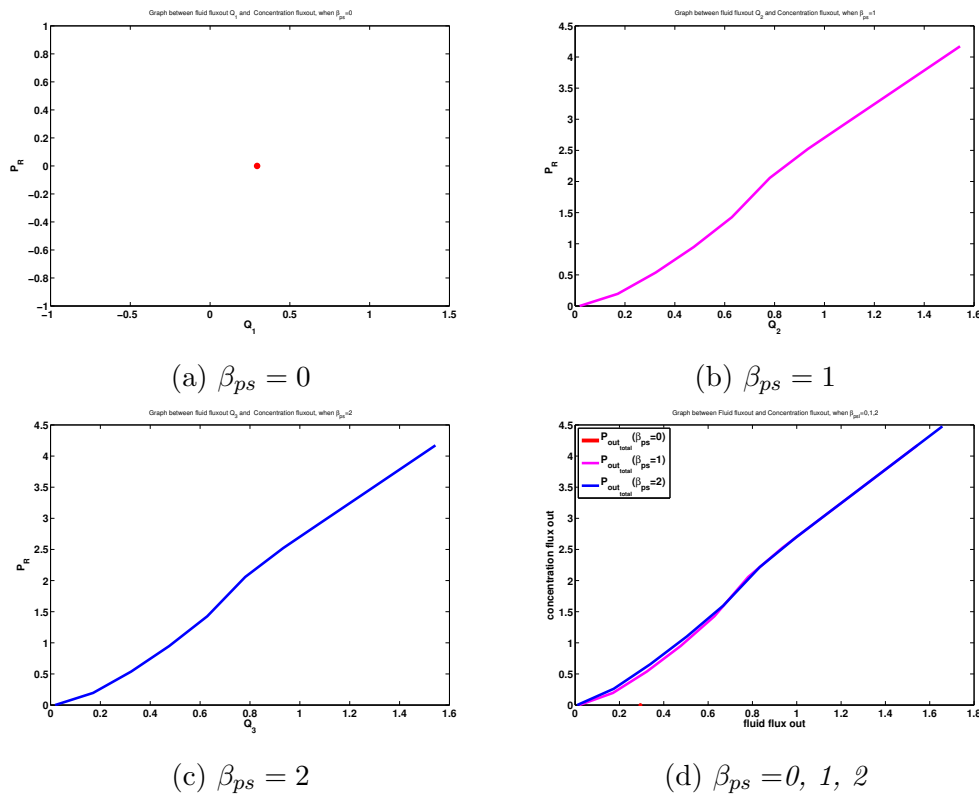
Figure 5.26: *Illustrations of graph of pollutant concentration net flux out plotted against fluid flux out, calculated for various values of ϕ_I, for $\phi_L = 1$, $\phi_R = 0$, when (a) $\beta_{ps} = 0$; (b) $\beta_{ps} = 1$; (c) $\beta_{ps} = 2$; (d) combined graph of (a), (b), and (c).*

5.3.8 Swimming pool problem

Example 5.3.5 *Figure 5.27 shows a three-dimensional homogeneous groundwater aquifer with a rectangular top measuring 14 m by 10 m. The front, back, top and bottom sides of the aquifer are impervious. The system is 14 m deep at both the rectangular ends and water is entering into the aquifer through the entrance $OECD$ and leaving from the exit $AFBG$. Chlorinated water with mass C_I [kg m^{-3}] is leaking from one corner of a swimming pool which is embedded inside the aquifer and is polluting the groundwater. The swimming pool has coordinates: (4, 4, 6), (4,10, 6), (8 ,4, 6), (8, 10, 6), (4, 4, 14), (4, 10, 14), (8, 4, 14), (8, 10, 14). Plot the pollutant concentration profile of the problem.*
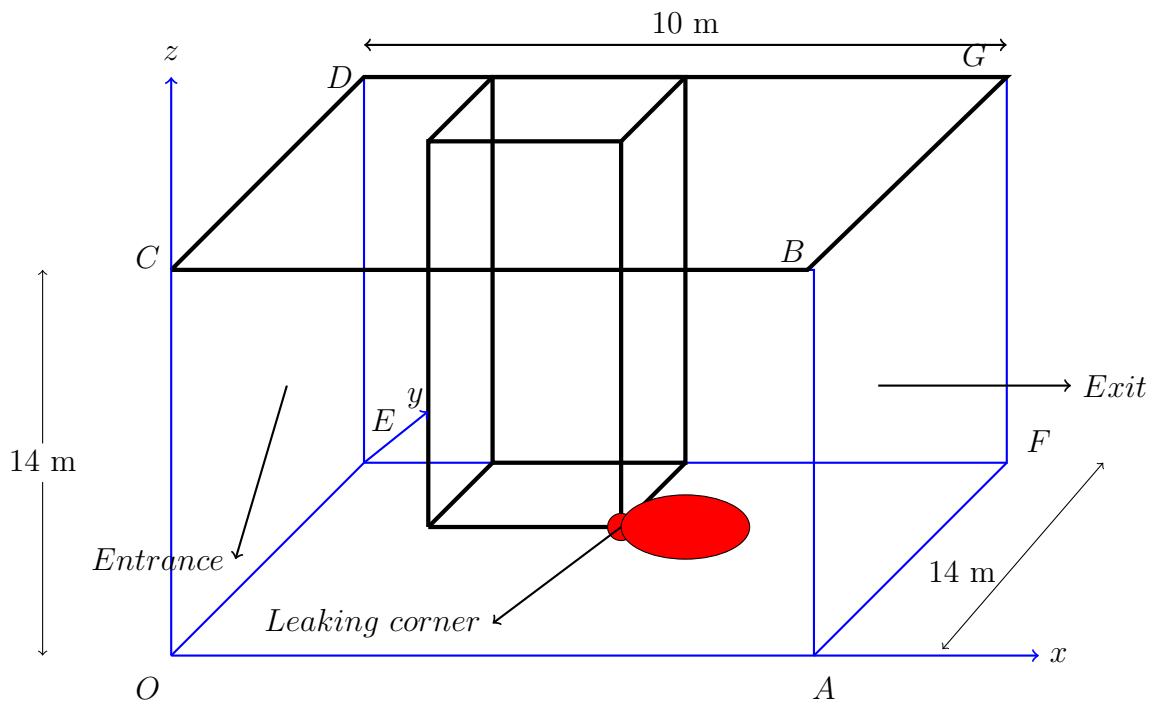
Figure 5.27: *Schematic diagram of a swimming pool problem*

The tracer transport equation for the swimming pool problem is given by

$$\frac{\partial C}{\partial t} + \frac{1}{n}(\mathbf{V} \cdot \nabla C) = D\left(\frac{\partial^2 C}{\partial x^2} + \frac{\partial^2 C}{\partial y^2} + \frac{\partial^2 C}{\partial z^2}\right), \tag{5.26}$$

subject to the boundary conditions on the porous medium which are

$$\frac{\partial C}{\partial y}(x, 0, z) = \frac{\partial C}{\partial y}(x, 14, z) = 0, \quad 0 \le x \le 10, \quad 0 \le z \le 14, \qquad (5.27)$$

$$\frac{\partial C}{\partial y}(x, y, 0) = \frac{\partial C}{\partial y}(x, y, 14) = 0, \quad 0 \le x \le 10, \quad 0 \le y \le 14, \qquad (5.28)$$

$$C_L(0, y, z) = C_R(10, y, z) = 0, \quad 0 \le y \le 14, \quad 0 \le z \le 14. \qquad (5.29)$$

The swimming pool is impervious, except at one point which is the common point of the front, bottom, and right hand sides of the swimming pool (as shown in Figure 5.27 marked by a red circle and pollutant plume is going towards the exit). So, on the solid boundaries, the normal components of the gradient of concentration are assigned to be zero.
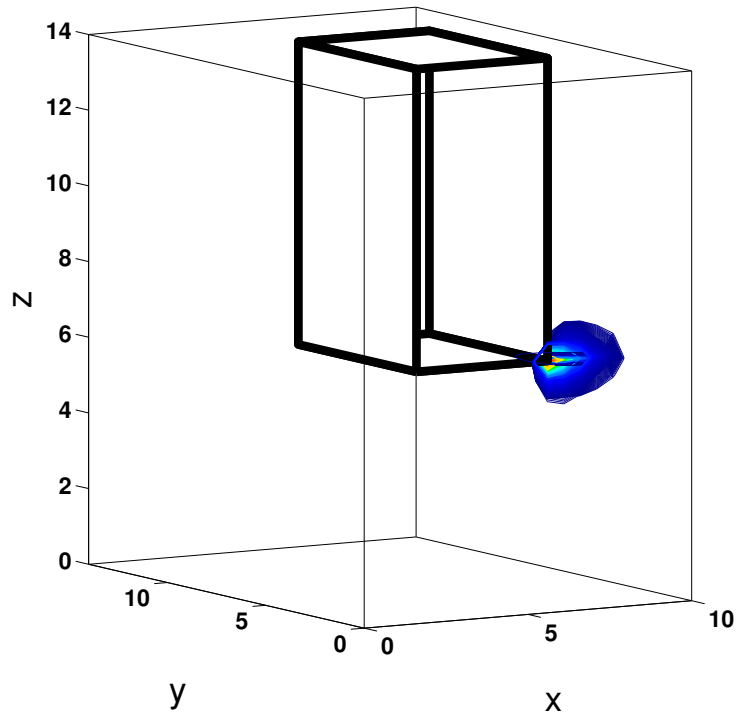
Figure 5.28: *Numerical solution of pollutant concentration in a three-dimensional homogeneous aquifer at time t=5000 [s] after release. Pollutant of concentration $C_I = 20$ [kg m^{-3}] is leaking from the xz-plane's right-bottom corner of a swimming pool. The parametric values are: $n = 0.33$ [-], $D = 0.01$ [$m^2\ s^{-1}$].*

In the earlier discussions of this chapter, it was assumed that the whole surface of the cylinder was leaking, but in this particular problem, the pollutant is leaking from a point source only. After the solution of the fluid flow problem and calculation of Darcy's velocities,

a numerical solution of the Equation (5.26) together with the boundary conditions is plotted in Figure 5.28. Illustration shows that chlorinated water is advecting towards the exit with the incoming groundwater from the entrance and dispersing all around in the neighbouring area. However, in the three-dimensional view, it is difficult to view the exact position of the concentration plume. To overcome this difficulty, two-dimensional slices may help the viewer to understand the problem.

Following are the xy- and yz-slices of the three-dimensional problem. Since, the pollutant is leaking from one corner of the swimming pool, so chopping off these slices should be taken at an appropriate distance from the leaking point. A cutting extremely close or extremely far from the source point may lead to an absurd result.

(a)	(b)
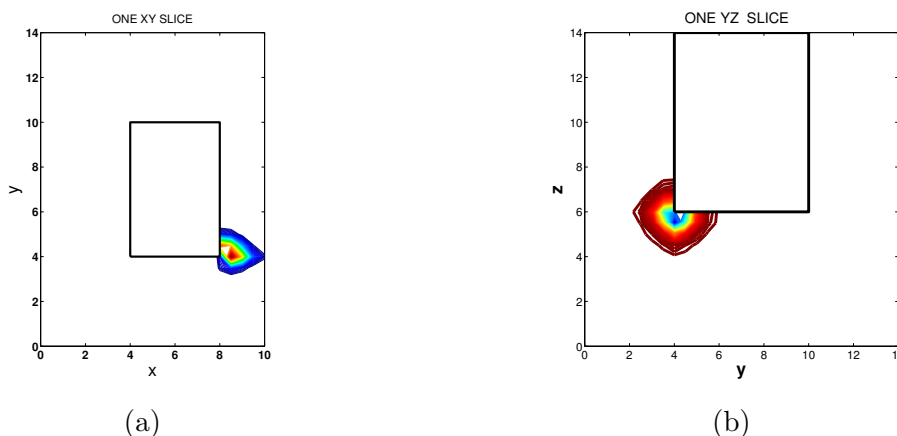
Figure 5.29: *Two-dimensional slices of Figure 5.28 taken in the form of (a) an xy-slice at $z = 8$ [m]; (b) a yz-slice taken at $x = 7$ [m].*

5.4 Illustrations: non-homogeneous aquifers

The fluid flow problem for a two-layer non-homogeneous aquifer with a pervious rectangular cylinder has already been discussed in Section 4.5. Here, a fluid flow problem and pollutant advection-dispersion model for a three-layer non-homogeneous aquifer with different permeabilities, k_i, $i = 1, 2, 3$, with a leaky cylinder (full of some pollutant) is presented. In this three-layer case, the bottom layer is composed of coarse sand ($K_1 = 45$ [m day^{-1}]), the middle layer is composed of fine gravel ($K_2 = 450$ [m day^{-1}]) and the top layer consists of coarse gravel ($K_3 = 150$ [m day^{-1}]), see Table 4.2.

Results are given for three different positions of the entrance while keeping fixed the position of

the exit. Values of the common parameters involved in the calculation are listed in Table 5.10.

For the sake of simplicity, results are calculated for the transport model of pollutant concentration when dispersion is uniformly constant. In this model, the permeability k_1 of the bottom layer is the smallest, while the middle layer is 10 times more permeable than that of the bottom layer and the permeability of the top layer is $3k_1$. Simulations are obtained for results near to the steady-state solution.

Intuitive results are found for the three cases, viz. (a) when the entrance is lying in the lower layer; (b) when the entrance is lying in the middle layer; and (c) when the entrance is lying in the top layer. Graphical representation of these cases is given in Figures 5.30, 5.31, and 5.32.

Table 5.10: *Parameters used for the simulations for a non-homogeneous three-layer system.*

Parameters	Values	Units
scaled dynamic pressure in entrance ϕ_L	1	[m]
scaled dynamic pressure in exit ϕ_R	0	[m]
scaled dynamic pressure inside the pervious object ϕ_I	0.5	[m]
constant of proportionality ω_{ps}	1×10^7	[s^{-1}]
measure of resistance of the object's surface to flow through it β_{ps}	1.0224	[m]
porosity n	0.33	[-]
density of groundwater ρ	1000	[kg m^{-3}]
gravitational acceleration g	9.8	[m s^{-2}]
dynamic viscosity of groundwater μ	1.002×10^{-3}	[kg m^{-1} s^{-1}]
permeabilities (k_1, k_2, k_3) of the layers of the non-homogeneous aquifer (from bottom to top)	$k_1 = 5.3252 \times 10^{-11}$, $k_2 = 10k_1$, $k_3 = 3k_1$	[m^2]
time step dt	0.001	[-]
maximum allowed real time for simulations T_{max}	5000	[s]
concentration of the injected chloride ions C_I	0.8917	[kg m^{-3}]
component of dispersivity α	0.2	[m]

When the entrance is lying in the lower layer

In the illustration of Figure 5.30a, some fluid is going inside the object due to a lower pressure in the pervious object as compared to the inlet and some is leaving because of higher pressure inside as compared to the exit. The pollutant in the higher permeability middle layer of the non-homogeneous aquifer appears to advect and disperse faster due to the highest fluid speed being in that region [7].

Figure 5.30 represents the case when the entrance lies in the bottom sub-layer of lowest permeability, as a result of which fluid as well as pollutant move slower in this area and we can see a lower spread of pollutant concentration there. However, in the top sublayer, pollutant advects and disperses faster due to a higher permeability zone and the position of the exit there.

(a)

(b)

(c)
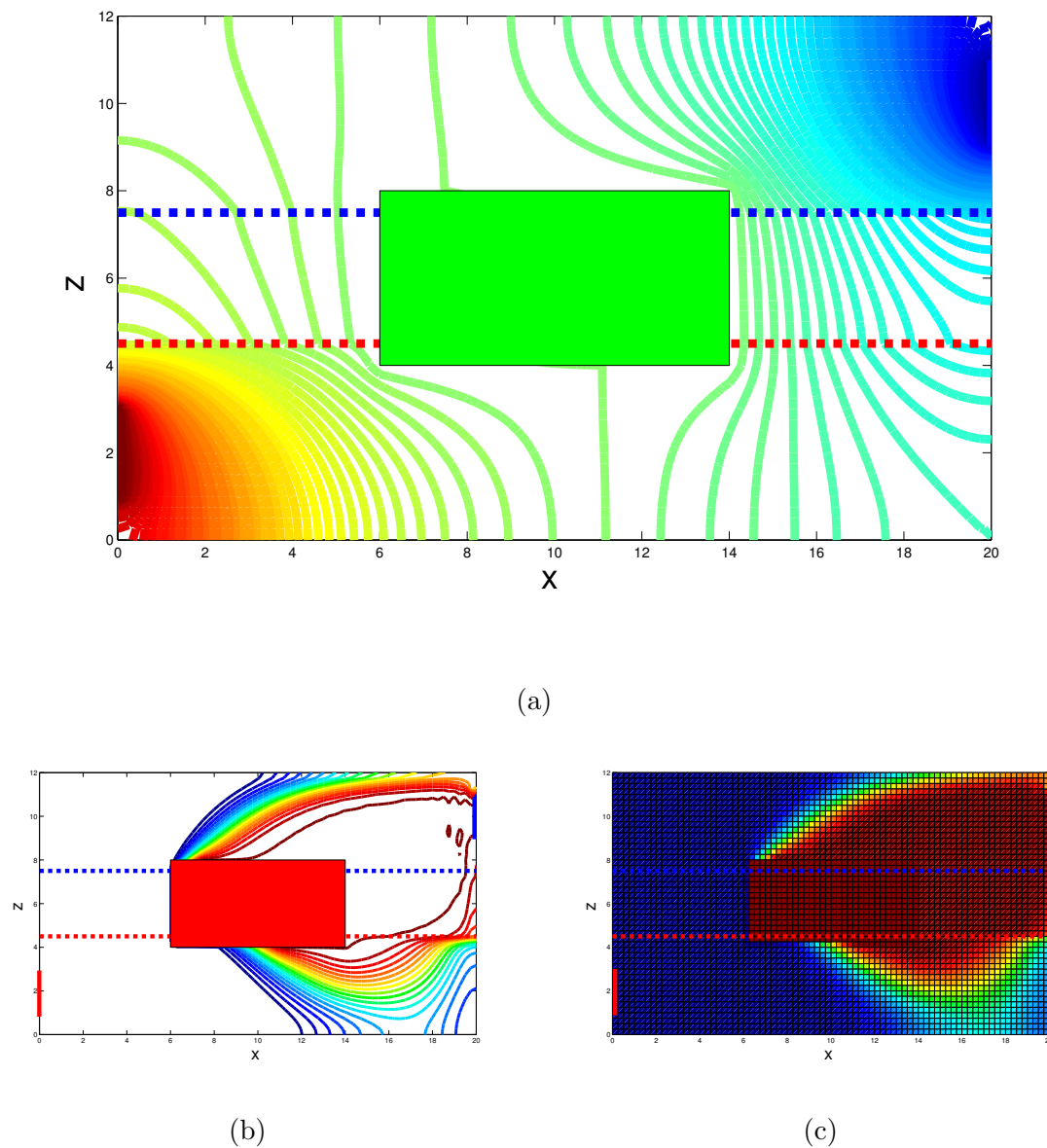
Figure 5.30: *Graphs for a leaky cylinder with rectangular cross-section placed in a non-homogeneous aquifer, with the entrance in the lowest sub-layer (a) a contour plot of ϕ; (b) a contour plot of pollutant concentration; (c) a surface plot of pollutant concentration.*

The fluid and mass fluxes for this first case (i.e., when the entrance lies in the bottom layer), through the inlet, exit, and pervious cylinder are given in Table 5.11, whereas, the fluid and mass fluxes for the remaining two cases are listed in separate tables.

149

For verification of the model, fluid as well as the mass fluxes through the cylinder and entrance should be equal to those of through the exit. However, in this example, the total fluid flux in is 7.6779×10^{-4} [m^2 s^{-1}] which is slightly less than the total fluid flux out which is 8.1846×10^{-4} [m^2 s^{-1}]. Similarly, the total mass flux in of a pollutant is 0.0020 [kg m^{-1} s^{-1}] which is slightly less than the total pollutant mass flux out which is 0.0022 [kg m^{-1} s^{-1}]. This is probably because of the the high permeability difference between the adjacent layering system.

Table 5.11: *Values of fluid and mass fluxes near the steady-state solution, for an entrance lying in the bottom sub-layer; position of entrance between points $b_1 = 1$ [m], $b_2 = 3$ [m], and exit between points $b_3 = 9$ [m], $b_4 = 11$ [m].*

Fluxes	Values	Units
flux in Q_L	2.9510×10^{-4}	[m^2 s^{-1}]
flux through the cylinder Q_I	4.7269×10^{-4}	[m^2 s^{-1}]
flux total in Q_{in}	7.6779×10^{-4}	[m^2 s^{-1}]
flux out Q_R	8.1846×10^{-4}	[m^2 s^{-1}]
value of $\bar{V}$	3.9342×10^{-5}	[m s^{-1}]
coefficient of dispersion $\bar{D} = \alpha \bar{V}$	7.8684×10^{-6}	[m^2 s^{-1}]
mass flux of a pollutant (from entrance) P_L	2.5479×10^{-19}	[kg m^{-1} s^{-1}]
mass flux of a pollutant (through the cylinder) P_I	0.0020	[kg m^{-1} s^{-1}]
total mass flux in of a pollutant P_{In}	0.0020	[kg m^{-1} s^{-1}]
total mass flux out of a pollutant P_R	0.0022	[kg m^{-1} s^{-1}]

When the entrance is lying in the middle layer

Table 5.12 and Figure 5.31 show respectively the recordings and illustration of the case when the entrance lies in the second zone of maximum permeability. Maximum transport of fluid and pollutant is visible in the middle layer of highest permeability and dispersion of the pollutant occurs in the other sub-layers due to the fact of mechanical dispersion from the higher concentration region to the lower one.

Table 5.12: *Parameters used for the simulations, and values of fluid and mass fluxes near the steady-state solution, for an entrance lying in the middle sub-layer; position of entrance between points $b_1 = 5$ [m[, $b_2 = 7$ [m], and exit between points $b_3 = 9$ [m], $b_4 = 11$ [m].*

Parameters	Values	Units
flux in Q_L	16.3479×10^{-4}	$[\text{m}^2 \text{ s}^{-1}]$
flux through the cylinder Q_I	-7.2188×10^{-4}	$[\text{m}^2 \text{ s}^{-1}]$
flux total in Q_{in}	9.1291×10^{-4}	$[\text{m}^2 \text{ s}^{-1}]$
flux out Q_R	8.2034×10^{-4}	$[\text{m}^2 \text{ s}^{-1}]$
value of $\bar{V}$	7.5526×10^{-5}	$[\text{m s}^{-1}]$
component of dispersivity α	0.2	$[\text{m}]$
coefficient of dispersion $\bar{D} = \alpha \bar{V}$	1.5105×10^{-5}	$[\text{m}^2 \text{ s}^{-1}]$
mass flux of a pollutant (from entrance) P_L	4.8784×10^{-16}	$[\text{kg m}^{-1} \text{ s}^{-1}]$
mass flux of a pollutant (through the cylinder) P_I	0.0018	$[\text{kg m}^{-1} \text{ s}^{-1}]$
total mass flux in of a pollutant P_{In}	0.0018	$[\text{kg m}^{-1} \text{ s}^{-1}]$
total mass flux out of a pollutant P_R	0.0020	$[\text{kg m}^{-1} \text{ s}^{-1}]$
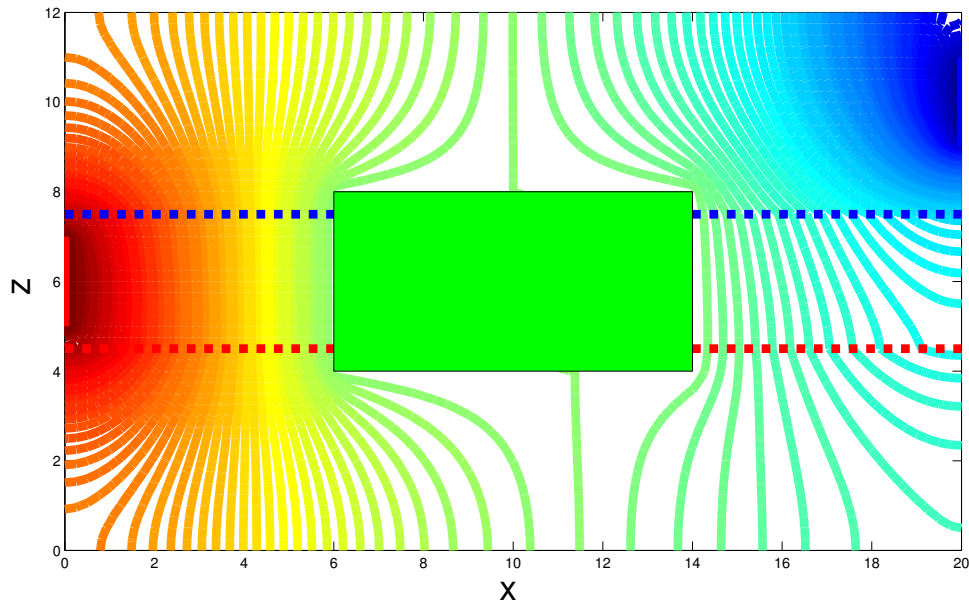
(a)
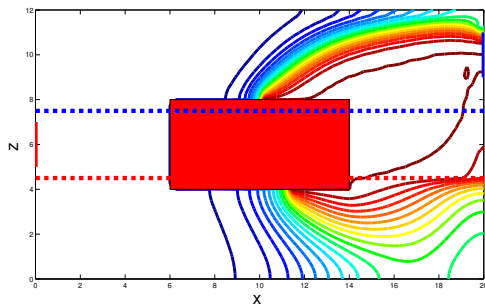
(b)
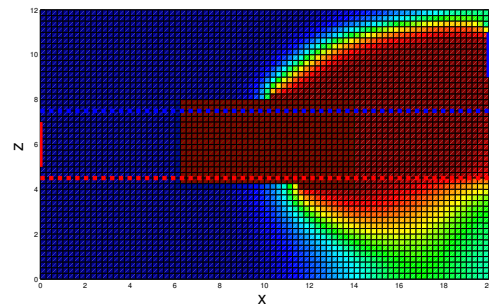
(c)

Figure 5.31: *Graphs for a leaky cylinder with rectangular cross-section placed in a non-homogeneous aquifer, with the entrance in the second sub-layer (a) a contour plot of ϕ; (b) a contour plot of pollutant concentration; (c) a surface plot of pollutant concentration.*

When the entrance is lying in the top layer

Lastly, the fluid flow and pollutant advection-dispersion model for the case when the entrance lies in the top sub-layer, is plotted in Figure 5.32. Surprisingly, more dispersion of pollutant can be seen in the bottom sub-layer of minimum permeability as compared to the top layer of relatively higher permeability. Is this due to the faster fluid speed or is there another mechanism involved for dispersion?

As the movement of fluid as well as pollutant takes place from the region of lower permeability

to the higher one, so more spread and transport of pollutant occurs in the middle sub-layer of highest permeability and then transport of pollutant further extends to the bottom layer of lowest permeability due to the relatively higher value of pressure in the middle layer just past the object.

Table 5.13: *Parameters used for the simulations, and values of fluid and mass fluxes near the steady-state solution, for entrance in the top sub-layer, position of entrance between points $b_1 = 9$ [m], $b_2 = 11$ [m], and exit between points $b_3 = 9$ [m], $b_4 = 11$ [m].*

Parameters	Values	Units
flux in Q_L	8.2021×10^{-4}	$[\text{m}^2\ \text{s}^{-1}]$
flux through cylinder Q_I	4.5024×10^{-16}	$[\text{m}^2\ \text{s}^{-1}]$
flux total in Q_{in}	8.2021×10^{-4}	$[\text{m}^2\ \text{s}^{-1}]$
flux out Q_R	8.2021×10^{-4}	$[\text{m}^2\ \text{s}^{-1}]$
value of $\bar{V}$	5.6944×10^{-5}	$[\text{m}\ \text{s}^{-1}]$
component of dispersivity α	0.2	$[\text{m}]$
coefficient of dispersion $\bar{D} = \alpha\bar{V}$	1.1389×10^{-5}	$[\text{m}^2\ \text{s}^{-1}]$
mass flux of a pollutant (from entrance) P_L	1.6121×10^{-15}	$[\text{kg}\ \text{m}^{-1}\ \text{s}^{-1}]$
mass flux of a pollutant (through the cylinder) P_I	0.0019	$[\text{kg}\ \text{m}^{-1}\ \text{s}^{-1}]$
total mass flux in of a pollutant P_{In}	0.0019	$[\text{kg}\ \text{m}^{-1}\ \text{s}^{-1}]$
total mass flux out of a pollutant P_R	0.0020	$[\text{kg}\ \text{m}^{-1}\ \text{s}^{-1}]$
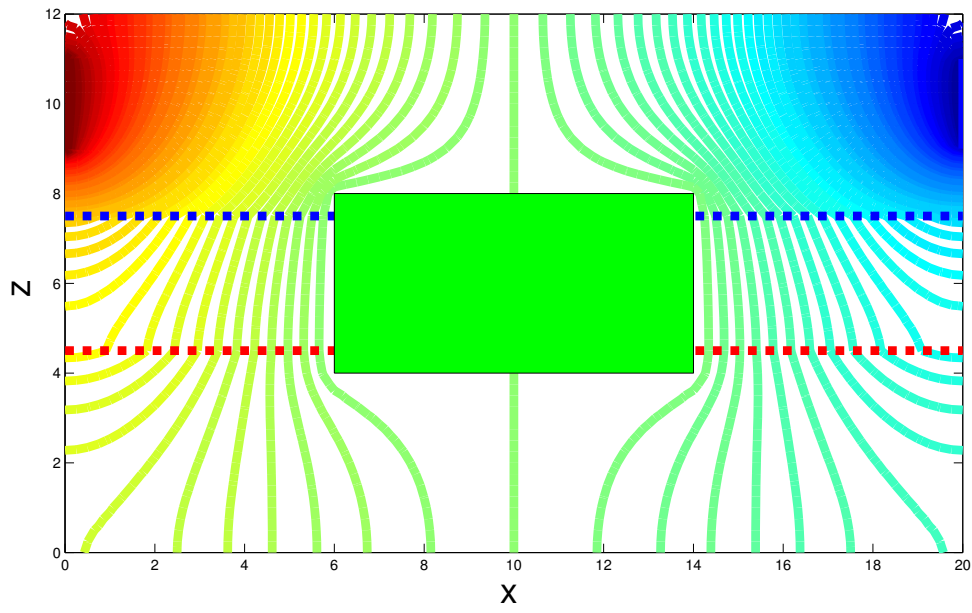
(a)
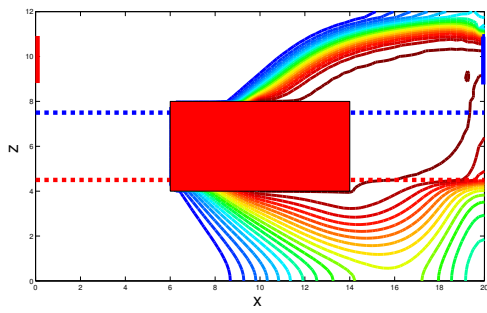
(b)
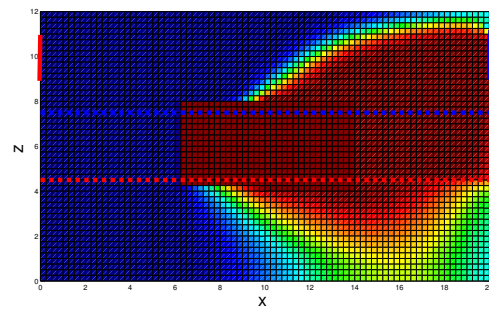
(c)

Figure 5.32: *Graphs for a leaky cylinder with rectangular cross-section placed in a non-homogeneous aquifer, with the entrance in the top sub-layer (a) a contour plot of ϕ; (b) a contour plot of pollutant concentration; (c) a surface plot of pollutant concentration.*

Chapter 6

Modelling Heat Transport in a Porous Medium with Embedded Convex Objects

In this chapter our main aim is to formulate models of heat (which is released by heated bodies embedded in a porous media) transport in groundwater aquifers. Generally, in all transport models, heat as well as fluid transport is taken into account. Perhaps, it is due to the fact that both the fluid's density and viscosity depend on the temperature [12]. However, we shall assume the case when the fluid is incompressible and irrotational, so our model will be restricted to only heat transfer.

Before analysing the basis of convective heat transfer modelling, it is important to know about the historic relationship between fluid mechanics and heat transfer. Particularly, during the past century, both fluid mechanics and heat transfer have completed their journey in successful collaboration [14]. Problems encountered in this area, includes the examples of chemical engineering, geothermal reservoir engineering, storage of nuclear waste material, groundwater flows, pollutant dispersion in aquifers, radioactive waste reservoirs, solar power accumulators, and food industries, etc. [12]. There has been extensive and substantial published research in the field of heat convection, advection and dispersion in porous media.

In contrast with mass transfer, where the solid is considered to be impermeable to mass flux, in the case of heat transfer, the solid matrix is regarded to be a heat conduction source. Due

to the fact that heat may be exchanged between these two phases, the average temperature of solid and fluid(s) need not be the same, However, all our study will be based on the assumption that the system will remain in thermal equilibrium.

Heat that is injected into a groundwater aquifer together with a fluid source that may be associated with the object(s) (e.g., heat from a tank), is dispersed by water flowing within the permeable matrix. It is well-known from the literature that heat transfer can be increased by using porous media with higher thermal conductivity.

This chapter will discuss fluid and heat transport in a homogeneous aquifer. Heated objects which are embedded in the underground aquifers will be taken as elliptic or diamond cross-sections of the cylinder. To discuss the fluid/heat flow model with these objects, first a complex variable technique known as *conformal mapping* will be discussed. In this technique, complicated objects may be transformed into regular objects [18]. The transformed problem then becomes simpler to solve for fluid and heat flow in porous media with embedded convex objects.

After finding the transformation and solving the fluid flow problem in the transformed plane, the heat equation is then solved for steady-state and time dependent cases for some values of thermal diffusion/dispersion and advection coefficients. Validity of the solution is checked by calculating heat fluxes through the cylinders, inlet, and outlet for both original (x, z) and transformed (ξ, η) planes.

6.1 Conformal mapping

It is hard to fit curved objects like circles or ellipse and polygons like diamonds, pentagons, etc., using rectangular mesh in a porous medium. But it is possible to find a mapping using complex variables techniques namely, conformal mappings. The procedure is to find a conformal transformation of a rectangular flow region $((x, z)$ plane) into another rectangular region $((\xi, \eta)$ plane, say) for which the transformed stream function $\hat{\psi}(\xi, \eta)$ and velocity potential $\hat{\phi}(\xi, \eta)$ persist to be harmonic. The problem becomes easy to solve after finding a mapping $x = \hat{x}(\xi, \eta)$, $z = \hat{z}(\xi, \eta)$, as both $\hat{x}(\xi, \eta)$ and $\hat{z}(\xi, \eta)$ are harmonic. So after getting the transformation, $\hat{x}(\xi, \eta)$,

and $\hat{z}(\xi, \eta)$ remain harmonic. i.e.,

$$-\frac{\partial \hat{x}}{\partial \xi} = \frac{\partial \hat{z}}{\partial \eta}, \quad -\frac{\partial \hat{x}}{\partial \eta} = -\frac{\partial \hat{z}}{\partial \xi}. \qquad (6.1)$$

The transformed problem is simpler to solve, but it also requires that the boundary conditions from the (x, z) plane should be mapped across to the (ξ, η) plane. The Laplace's equation in the (x, z) plane is transformed numerically into Laplace's equation in the (ξ, η) plane, provided these two planes are related by a conformal transformation.

Laplace's equation for the coordinates $\hat{x}(\xi, \eta)$ and $\hat{z}(\xi, \eta)$ whose transformation is made using conformal mapping [18] is

$$\hat{\nabla}^2 \hat{x} = \frac{\partial^2 \hat{x}}{\partial \xi^2} + \frac{\partial^2 \hat{x}}{\partial \eta^2} = 0, \qquad (6.2)$$

$$\hat{\nabla}^2 \hat{z} = \frac{\partial^2 \hat{z}}{\partial \xi^2} + \frac{\partial^2 \hat{z}}{\partial \eta^2} = 0, \qquad (6.3)$$

and Laplace's equation for the coordinates $\xi(x, z)$ and $\eta(x, z)$ is

$$\nabla^2 \xi = \frac{\partial^2 \xi}{\partial x^2} + \frac{\partial^2 \xi}{\partial z^2} = 0, \qquad (6.4)$$

$$\nabla^2 \eta = \frac{\partial^2 \eta}{\partial x^2} + \frac{\partial^2 \eta}{\partial z^2} = 0. \qquad (6.5)$$

6.1.1 Some discussion about governing equation and boundary conditions

Figure 6.1 shows the schematic diagram for the governing equation and boundary conditions in terms of (ξ, η) and (x, z) planes for conformal mapping. Figures 6.1a-b show the boundary value problems in the (ξ, η) plane, however, the only difference in these two figures is that Figure 6.1a illustrates the boundary value problem in terms of $\hat{x}(\xi, \eta)$ and Figure 6.1b shows the governing equation and boundary conditions in terms of $\hat{z}(\xi, \eta)$. Figures 6.1c and 6.1d are the original planes in terms of (x, z) for quarter of a diamond and elliptic cylinders.

Numerical solution of Figures 6.1a-b is plotted in Figure 6.2a and the solution of Figures 6.1c-d is given by Figures 6.2b and 6.2c respectively.

Following are the governing equations in terms of $\hat{x}(\xi, \eta)$ and $\hat{z}(\xi, \eta)$ in the $\xi\eta$-plane.

$$\hat{\nabla}^2 \hat{x} = \frac{\partial^2 \hat{x}}{\partial \xi^2} + \frac{\partial^2 \hat{x}}{\partial \eta^2} = 0, \quad 0 < \xi < a', \quad 0 < \eta < b, \tag{6.6}$$

$$\hat{\nabla}^2 \hat{z} = \frac{\partial^2 \hat{z}}{\partial \xi^2} + \frac{\partial^2 \hat{z}}{\partial \eta^2} = 0, \quad 0 < \xi < a', \quad 0 < \eta < b, \tag{6.7}$$

where a' is the length of the rectangle in $\xi\eta$-plane, and is found during the solution process for the mapping. Generally, $a' \neq a$.

With reference to Figure 6.1, the boundary conditions are:

$$\text{on} \quad O'A', \quad \frac{\partial \hat{x}}{\partial \eta} = 0, \quad \hat{z} = 0, \tag{6.8}$$

$$\text{on} \quad A'B', \quad \frac{\partial \hat{x}}{\partial \eta} = 0, \quad \frac{\partial \hat{z}}{\partial \xi} = 0, \tag{6.9}$$

$$\text{on} \quad B'C', \quad \frac{\partial \hat{x}}{\partial \eta} = 0, \quad \hat{z} = b, \tag{6.10}$$

$$\text{on} \quad C'D', \quad \hat{x} = 0, \quad \frac{\partial \hat{z}}{\partial \xi} = 0. \tag{6.11}$$

For the case of a quarter diamond (see Figure 6.1c):

$$\text{on } D'O', \ \hat{x} \text{ and } \hat{z} \text{ are related by } \hat{z} = c - m\hat{x}.$$

Other relationships between $\hat{x}$ and $\hat{z}$ depend on the cylinder shape.

Figure (a):

$\frac{\partial \hat{x}}{\partial \eta} = 0$

C' B'

$\hat{x} = 0$ $\nabla^2 \hat{x}(\xi, \eta) = 0$ $\frac{\partial \hat{x}}{\partial \eta} = 0$

D' O' $\frac{\partial \hat{x}}{\partial \eta} = 0$ A'

(a)

Figure (b):

$\hat{z} = b$

C' B'

$\frac{\partial \hat{z}}{\partial \xi} = 0$ $\nabla^2 \hat{z}(\xi, \eta) = 0$ $\frac{\partial \hat{z}}{\partial \xi} = 0$

D' O' $\hat{z} = 0$ A'

(b)

Figure (c):

C B

D $\hat{z} = c - m\hat{x}$

O A

(c)

Figure (d):

C B

D $\frac{\hat{x}^2}{a^2} + \frac{\hat{z}^2}{b^2} = 1$

O A

(d)
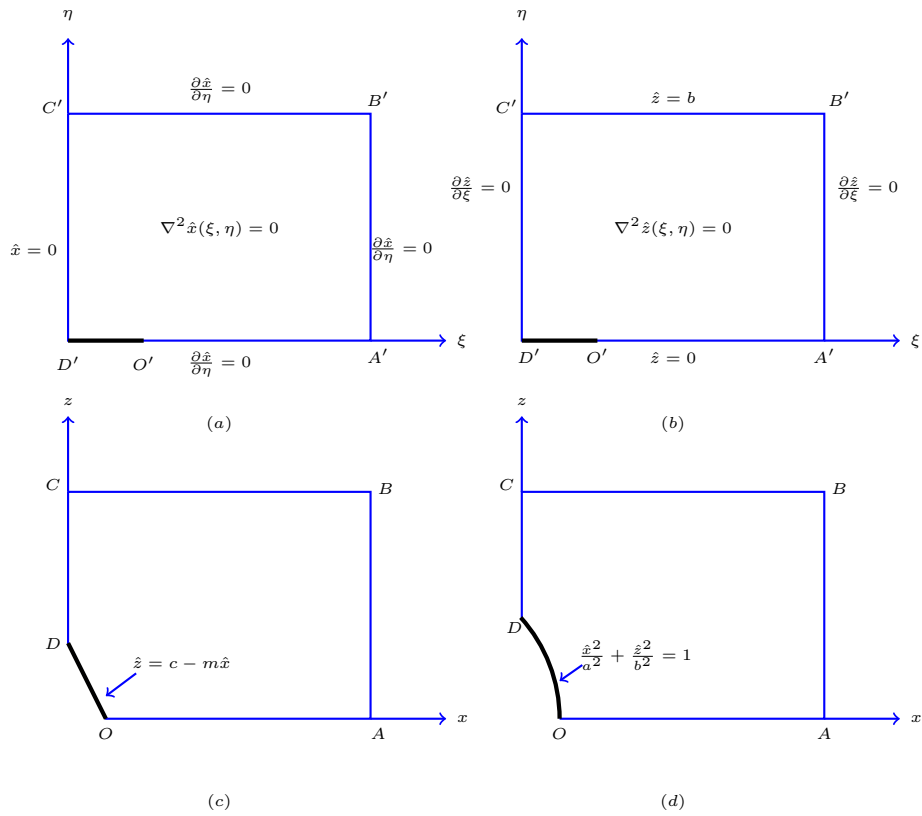
Figure 6.1: *Schematic diagram of the physical domains for conformal mapping in (a) $\xi\eta$-plane (mapped plane), governing equation and boundary conditions are in terms of $\hat{x}(\xi, \eta)$. $D'O'$ is the quarter of a horizontal plate, which is a mapping for DO in (c) and (d); (b) same as (a), but in terms of $\hat{z}(\xi, \eta)$; (c) xz-plane (original plane), DO is the quarter of a diamond, which is mapped on a horizontal plate $D'O'$ in (a) and (b); (d) xz-plane (original plane), DO is the quarter of an ellipse, which is mapped on a horizontal plate $D'O'$ in (a) and (b).*

6.1.2   Illustrations: graphs of conformal transformation

In this study, first a conformal mapping is found in the first quadrant of two planes, in which quarter of a diamond and elliptic shaped cylinders are mapped to a quarter of a horizontal plate, as shown in Figure 6.2.

We are still solving Laplace's equation for the coordinates $\hat{x}(\xi, \eta)$ and $\hat{z}(\xi, \eta)$ whose transformation is made using conformal mapping, which map the quarter of a horizontal plate and the mesh (which is all rectangular), as shown in Figure 6.2a into quarter of a diamond/ellipse and the orthogonal mesh, as shown in Figures 6.2b and 6.2c. If we do the mapping in the right way all the lines of Figure 6.2a become bent around the object and are orthogonal, as shown in Figures 6.2b and 6.2c.

(a)   (b)   (c)
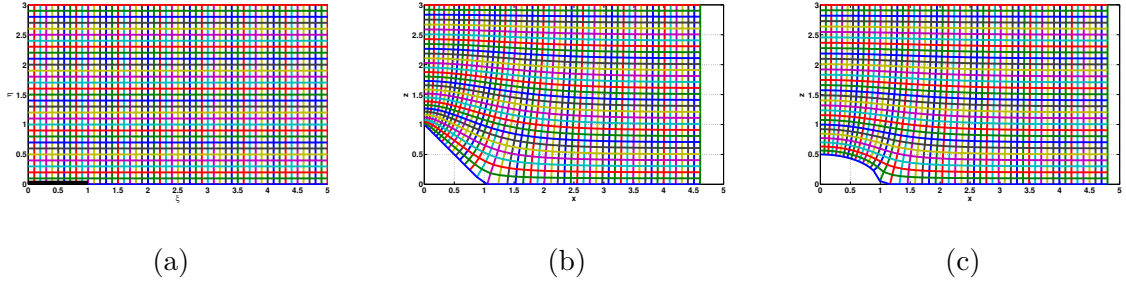
Figure 6.2: *Typical computational domain in quarter of $\xi\eta$- and xz- planes for (a) map of the region into $\xi\eta$-plane. The mapped points on the cylinder are marked by quarter of a horizontal plate; (b) orthogonal mesh in (x, z) plane corresponding to rectangular mesh in the (ξ, η) plane for quarter of a diamond; (c) orthogonal mesh in (x, z) plane corresponding to rectangular mesh in the (ξ, η) plane for quarter of an ellipse.*

After finding a transformation in the first quadrant of the $\xi\eta$- and xz-planes, a transformation for the complete $\xi\eta$- and xz-planes is found by flipping the results into the second quadrant and then in the negative η- and z-axis of the two planes. Figure 6.3a is a complete mapping in the $\xi\eta$-plane, which shows a mapping of a horizontal plate into a diamond/ellipse in the xz-plane, whose graphs are shown in Figures 6.3b-6.3c. In fact, Figure 6.3a is an image of Figure 6.3b and Figure 6.3c.

Moreover, a dilatation in the mesh size of Figure 6.3a is visible in Figures 6.3b and 6.3c, where the mesh size of $\xi\eta$-plane is compacted (shrinkage) by an amount known as the Jacobian of the transformation and is discussed in Appendix A. In some cases of conformal transformation, this dilatation may result in the expansion of the mesh size of the mapped $\xi\eta$-plane.

It should be noted that, in conformal mapping, shrinkage of the $\xi\eta$-plane is different for different shapes, and is visible in both the graphs of the xz-plane. It is also observed that the length of the xz-plane in the case of an elliptic cylinder is greater than that of diamond shaped cylinder, even though we have mapped a plate of the same length to the diamond and ellipse, and verified the results with the same length and width of horizontal plate in the $\xi\eta$-plane for both types of cylinders. Because of the different geometric shapes, the shrinkage is different due to the conformal mapping. The diamond shape cylinder has a very sharp edge, which reduces the length of the xz-plane.
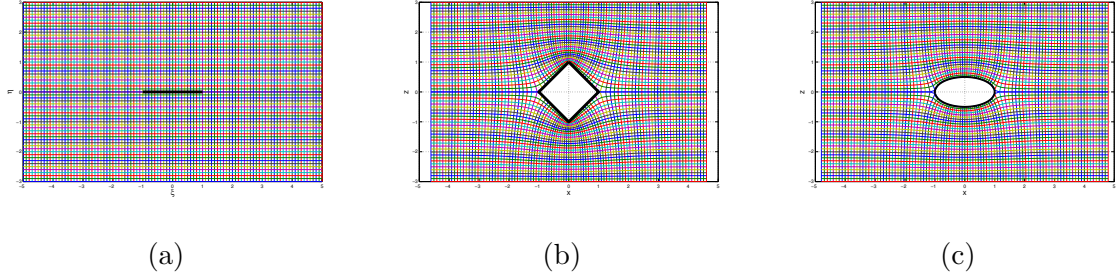
Figure 6.3: *Typical computational domain for (a) map of the region into (ξ, η)-plane. Lines correspond to constant x and z. The mapped points on the cylinder are marked by a horizontal plate; (b) orthogonal mesh in (x, z) plane corresponding to rectangular mesh in the (ξ, η) plane for diamond; (c) orthogonal mesh in (x, z) plane corresponding to rectangular mesh in the (ξ, η) plane for ellipse.*

6.2 Numerical solution of $\phi(\xi, \eta)$, $\phi(x, z)$, $\psi(\xi, \eta)$, and $\psi(x, z)$

After conformal transformation, our next goal is the discussion of fluid flow through a homogeneous porous medium with embedded bluff bodies. Mathematical modelling starts with the assumption that the fluid is incompressible and Darcy's law is applicable, so, as discussed before in Section 3.3 both $\phi(x, z)$ and $\psi(x, z)$ are harmonic functions in the xz-plane. Since under conformal mapping harmonic functions remain harmonic, so both $\hat{\phi}(\xi, \eta)$, and $\hat{\psi}(\xi, \eta)$ are still harmonic in the (ξ, η) plane.

The approach is to find a conformal mapping of the flow region to a rectangular region in the (ξ, η) plane where the transformed functions $\hat{\phi}(\xi, \eta)$ and $\hat{\psi}(\xi, \eta)$ remain harmonic. The basis of the complex potential is that both velocity potential ϕ and stream function ψ have to satisfy Laplace's equation. If we want to see the effects of conformal transformation on complex potentials, it is fair enough to investigate their effect on Laplace's equation. In order to show this, we have only to transform the first and second derivative of variables ψ and ϕ with respect to x and z into derivatives with respect to the transformed variables ξ and η. Then considering ψ and ϕ to be functions of ξ and η, we can easily calculate the Laplace's equation for both ψ and ϕ.

In the context of Darcy's law, the components of velocity in terms of $\phi(x, z)$ and $\psi(x, z)$ are

$$u(x,z) = -\frac{\rho g k}{\mu}\frac{\partial \phi}{\partial x}, \quad w(x,z) = -\frac{\rho g k}{\mu}\frac{\partial \phi}{\partial z}, \tag{6.12}$$

$$u(x,z) = \frac{\rho g k}{\mu}\frac{\partial \psi}{\partial z}, \quad w(x,z) = -\frac{\rho g k}{\mu}\frac{\partial \psi}{\partial x}, \tag{6.13}$$

and the corresponding velocity components in the (ξ, η) plane are

$$\hat{u}(\xi,\eta) = -\frac{\rho g k}{\mu}\frac{\partial \hat{\phi}}{\partial \xi}, \quad \hat{w}(\xi,\eta) = -\frac{\rho g k}{\mu}\frac{\partial \hat{\phi}}{\partial \eta}, \tag{6.14}$$

$$\hat{u}(\xi,\eta) = \frac{\rho g k}{\mu}\frac{\partial \hat{\psi}}{\partial \eta}, \quad \hat{w}(\xi,\eta) = -\frac{\rho g k}{\mu}\frac{\partial \hat{\psi}}{\partial \xi}. \tag{6.15}$$

One special feature of the harmonic functions is that they satisfy Laplace's equation, so the following are Laplace's equations for $\phi(x,z)$ and $\psi(x,z)$

$$\nabla^2 \phi = \frac{\partial^2 \phi}{\partial x^2} + \frac{\partial^2 \phi}{\partial z^2} = 0, \tag{6.16}$$

$$\nabla^2 \psi = \frac{\partial^2 \psi}{\partial x^2} + \frac{\partial^2 \psi}{\partial z^2} = 0, \tag{6.17}$$

and the corresponding Laplace's equations for $\hat{\phi}(\xi,\eta)$ and $\hat{\psi}(\xi,\eta)$ are

$$\hat{\nabla}^2 \hat{\phi} = \frac{\partial^2 \phi}{\partial \xi^2} + \frac{\partial^2 \phi}{\partial \eta^2} = 0, \tag{6.18}$$

$$\hat{\nabla}^2 \hat{\psi} = \frac{\partial^2 \psi}{\partial \xi^2} + \frac{\partial^2 \psi}{\partial \eta^2} = 0. \tag{6.19}$$

The boundary conditions on the porous media and on the body in terms of $\phi(x,z)$ and $\psi(x,z)$ are similar to the Sections 3.5 and 3.6. The respective boundary conditions in terms of $\hat{\phi}(\xi,\eta)$ and $\hat{\psi}(\xi,\eta)$ in the (ξ,η) plane are same as for $\phi(x,z)$ and $\psi(x,z)$ in the xz-plane.

As the bodies embedded in the porous media are impervious, so in terms of the velocity potential ϕ, the normal components of velocity are taken to be zero and in terms of the stream function, ψ is taken constant all over the body. It is evident from the Figures 6.4a-6.4c, that all pressure lines strike normally to the impermeable horizontal wall placed in the (ξ, η) plane and the solid walls of the diamond-shaped and elliptic cross-sections of the cylinder in the xz-plane.

Lastly, in Figures 6.4d-6.4f streamlines are wrapping around the impermeable horizontal wall

placed in the (ξ, η) plane and around the two cross-sections of the cylinder placed in a uniform stream of water flowing inside the rectangular xz- porous media with one entrance and one exit. So in this case, we can see two layers of streamlines are separated above and below the bodies.

(a) (b) (c)

(d) (e) (f)
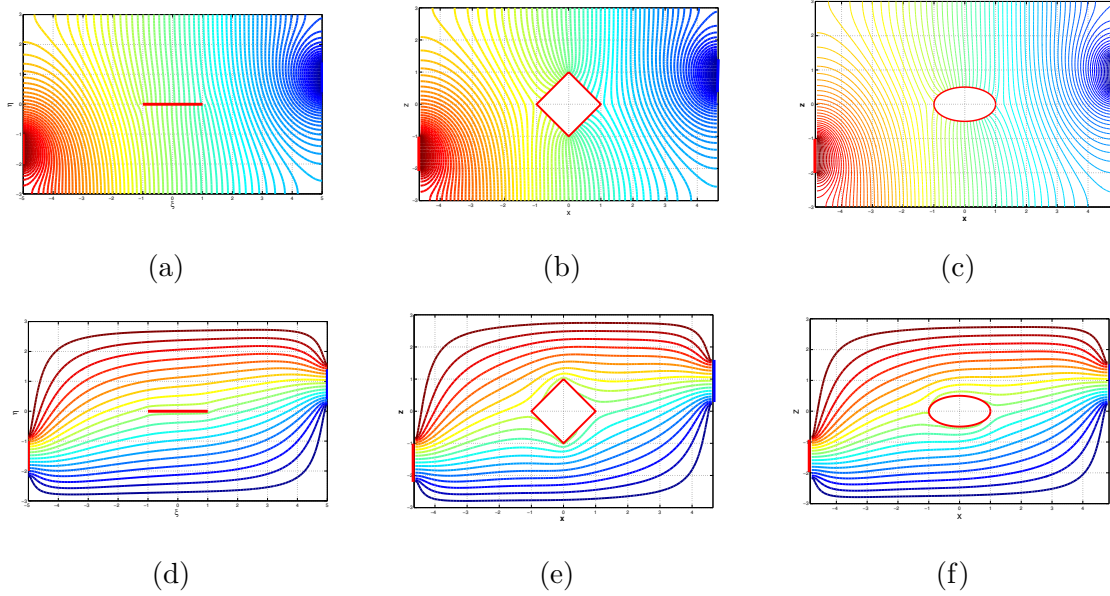
Figure 6.4: *Graphs of the numerical solution of (a) isobars for the impermeable horizontal line embedded in (ξ, η) plane; (b) isobars for the impermeable diamond embedded in the (x, z) plane; (c) isobars for impermeable elliptic body embedded in the (x, z)-plane; (d) streamlines for the impermeable horizontal line embedded in the (ξ, η) plane; (e) streamlines for the impermeable diamond embedded in the (x, z) plane; (f) streamlines for the impermeable elliptic body embedded in the (x, z) plane.*

6.3 Balance equation of two-dimensional heat advection-dispersion in a porous medium

The problem under consideration is steady/unsteady forced convective flow over a diamond/elliptic shape cylinder embedded in a rectangular domain, as illustrated in Figures 6.5 and 6.7. The cylinder is isothermally heated at a constant temperature T_I and cooled by the incoming external flow at temperature T_{in}. The confining horizontal walls have the same temperature T_b and T_t which is equal to the temperature of the flow at the inlet. The confining vertical walls are kept insulated. The fluid is incompressible. Thermal expansion and fluid buoyancy effects are neglected. No heat generation occurs inside the porous medium. Based on this setup there is both steady/unsteady heat advection and conduction.

6.3.1 Governing equations for steady heat advection-conduction

The 2D governing equations for forced convection flow past a cylinder embedded in a porous medium are based on the conservation of mass, momentum and thermal energy. It is assumed that flow in the porous media is governed by Darcy's law, and therefore inertial, thermal expansion, and fluid buoyancy effects are negligible. The total heat flux, by advection, mechanical dispersion, and thermal diffusion can be written in the form

$$q_h = (\rho c)_{water} T \mathbf{V} - \mathsf{D}\nabla T - \kappa_{\mathsf{ms}}\nabla T, \tag{6.20}$$

where T [K] is the temperature, D is a second rank symmetric tensor called the coefficient of mechanical dispersion, κ_{ms} [W m^{-1} K^{-1}] is the thermal conductivity (diffusion), c [J kg^{-1} K^{-1}] is the specific heat, and ρ [kg m^{-3}] is the density of water. For the isotropic case, we have $\mathsf{D} = DI$, so Equation (6.20) becomes

$$q_h = (\rho c)_{water} T \mathbf{V} - (DI + \kappa_{ms}I)\nabla T, \tag{6.21}$$

$$q_h = (\rho c)_{water} T \mathbf{V} - (D + \kappa_{ms})I\nabla T, \tag{6.22}$$

$$q_h = (\rho c)_{water} T \mathbf{V} - (D + \kappa_{ms})\nabla T, \tag{6.23}$$

$$q_h = (\rho c)_{water} T \mathbf{V} - D_h\nabla T, \tag{6.24}$$

where $D_h = (D + \kappa_{ms})$.

It is assumed that the mixture values are just weighted proportional to the component values, i.e., porosity, thermal conductivity, density of water and the specific heat. In terms of the component values, κ and (ρc) are written in the form:

$$\kappa_{ms} = (1 - n)\kappa_{rock} + n\kappa_{water},$$

$$\text{also} \quad (\rho c)_{ms} = (1 - n)(\rho c)_{rock} + n(\rho c)_{water},$$

where the subscript m denotes mixture values for the fluid-saturated porous medium (subscript s), and n is the porosity of the medium. The thermal energy equation of the porous media in

steady-state form [14] is:

$$\nabla \cdot q_h = 0, \tag{6.25}$$

$$\nabla \cdot ((\rho c)_{water} T \mathbf{V} - D_h \nabla T) = 0. \tag{6.26}$$

Hence we have,

$$\mathbf{V} \cdot \nabla T = \frac{D_h}{(\rho c)_{water}} \nabla^2 T, \quad \text{implies} \quad \mathbf{V} \cdot \nabla T = D_{th} \nabla^2 T, \tag{6.27}$$

where the (constant) thermal diffusivity $D_{th} = D_h/(\rho c)_{water}$. We are left with

$$\frac{\rho g k}{\mu} \nabla \phi \cdot \nabla T + D_{th} \nabla^2 T = 0, \quad \text{where} \quad \mathbf{V} = (u, w) = -\frac{\rho g k}{\mu} \nabla \phi. \tag{6.28}$$

The temperature in terms of the mapped coordinates is $T = \hat{T}(\xi, \eta)$. The transformed equation is:

$$\frac{\rho g k}{\mu} \hat{\nabla} \hat{\phi} \cdot \hat{\nabla} \hat{T} + D_{th} \hat{\nabla}^2 \hat{T} = 0. \tag{6.29}$$

Hence the steady-state problem with fluid velocity components written in terms of $\hat{\phi}$ and $\hat{T}$ is:

$$\frac{\rho g k}{\mu} \left(\frac{\partial \hat{\phi}}{\partial \xi} \frac{\partial \hat{T}}{\partial \xi} + \frac{\partial \hat{\phi}}{\partial \eta} \frac{\partial \hat{T}}{\partial \eta} \right) + D_{th} \left(\frac{\partial^2 \hat{T}}{\partial \xi^2} + \frac{\partial^2 \hat{T}}{\partial \eta^2} \right) = 0, \tag{6.30}$$

or

$$\frac{\partial^2 \hat{T}}{\partial \xi^2} + \frac{\partial^2 \hat{T}}{\partial \eta^2} = \frac{1}{D_{th}} \left(\hat{u} \frac{\partial \hat{T}}{\partial \xi} + \hat{w} \frac{\partial \hat{T}}{\partial \eta} \right), \tag{6.31}$$

subject to the boundary conditions:

$$\hat{T}(x,0) = \hat{T}_b \;\; = \;\; 10, \qquad \hat{T}(x,b) = \hat{T}_t = 10, \quad 0 \le x \le a, \qquad (6.32)$$

$$\hat{T}_I \;\; = \;\; 20, \quad (\text{on the cylinder}), \qquad\qquad\qquad (6.33)$$

$$\hat{T}_{in} \;\; = \;\; 10, \quad b_1 \le z \le b_2, \qquad\qquad\qquad (6.34)$$

$$\frac{\partial \hat{T}}{\partial x}(0,z) \;\; = \;\; 0, \quad 0 \le z \le b_1, \quad b_2 \le z \le b, \qquad (6.35)$$

$$\frac{\partial \hat{T}}{\partial x}(a,z) \;\; = \;\; 0, \quad 0 \le z \le b_3, \quad b_4 \le z \le b. \qquad (6.36)$$
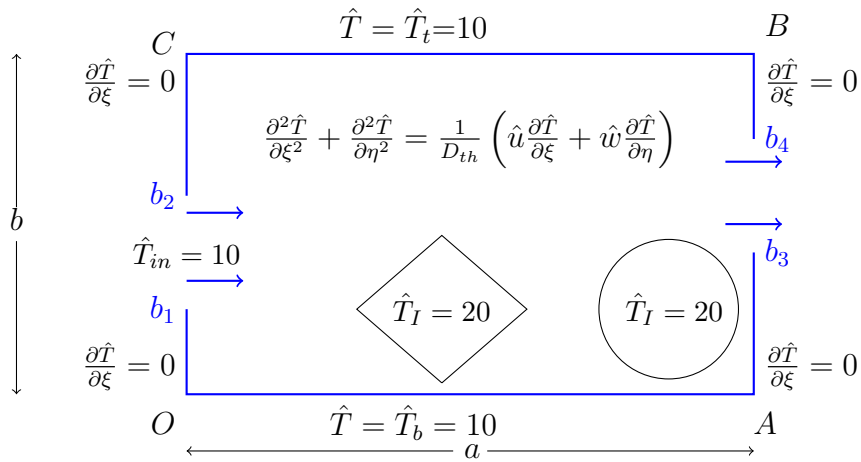
Figure 6.5: *Schematic diagram of the physical domain for heat flow in the steady-state case.*

6.3.2 Illustration: numerical solution for steady heat advection-conduction

Steady-state Equations (6.31)-(6.36) have been solved numerically by using a relaxation technique. Figures 6.6a-6.6b and Figures 6.6c-6.6d contain sample contour and surface plots of the typical shapes of dimensionless fluid temperature for both, plate (in the (ξ, η) plane) and diamond shape cylinders (in the (x,z) plane) respectively. Moreover, similar results are found for different shapes of the cylinder.

From the illustration of the Figures 6.6c-6.6d, it can be noticed that the region in front of the diamond shaped cylinder seems to be cooled, actually, there is present a very thin boundary layer of heat and this is because the main flow from the entrance sweeps the hot fluid near the

cylinder towards the exit. The regions behind the the cylinder have the highest temperatures because of the separation point between cylinder and porous media.

(a)   (b)

(c)   (d)
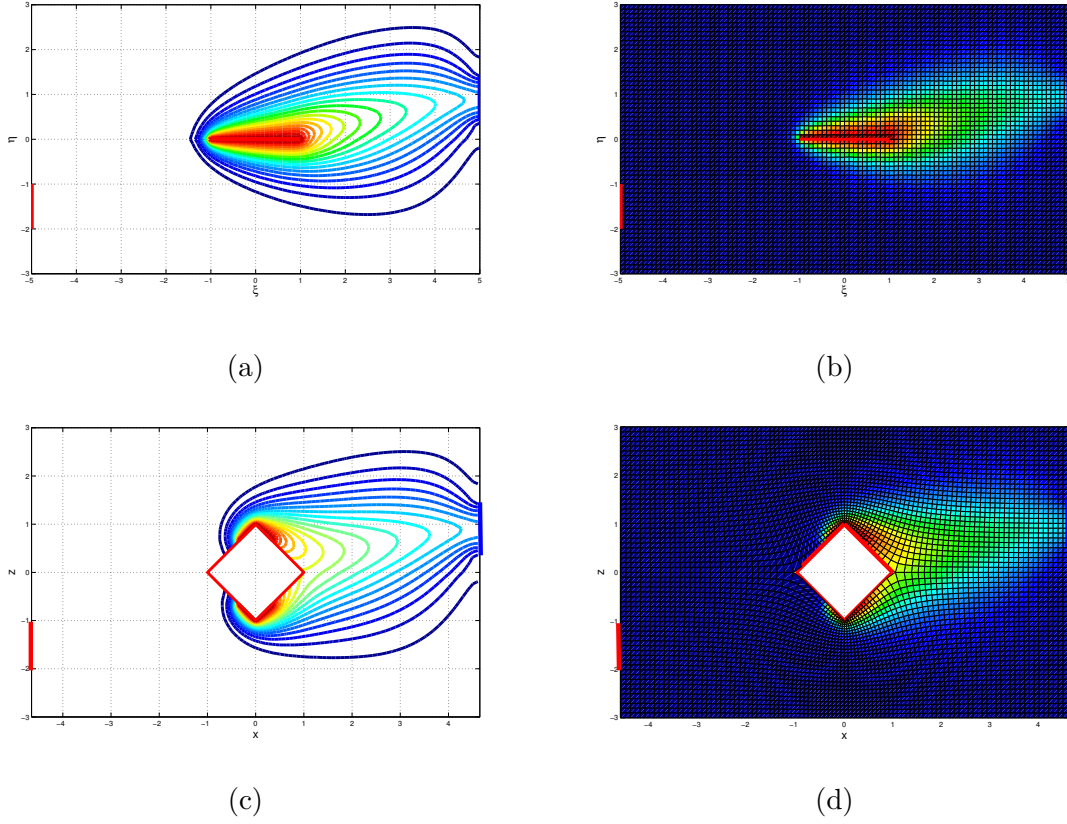
Figure 6.6: *Representation of the solution of steady-state heat dispersion-advection with heated objects inside a homogeneous porous medium with top and bottom boundaries at constant temperature, $\hat{T}_b = \hat{T}_t = 10\,°C$, with inlet temperature $T_{in} = 10\,°C$, object $T_I = 20\,°C$, contours at $0.5\,°C$ intervals, in the form of: (a) contour plot for plate; (b) surface plot for plate; (c) contour plot for diamond; (d) surface plot for diamond.*

6.3.3   Governing equations for non-steady heat advection-conduction

The system is shown in Figure 6.7. A two-dimensional rectangular box of height b and length a is taken in the form of a fluid filled porous media. In accordance with the homogeneous porous media model, the first law of thermodynamics reduces to the 2D time dependent governing equations of the system as [14]:

$$\frac{\partial}{\partial t}((\rho c)_{ms}T) = -\nabla \cdot ((\rho c)_{water}\mathbf{V}T - D_h\nabla T). \tag{6.37}$$

$$\text{Hence} \quad \frac{\partial T}{\partial t} + \frac{(\rho c)_{water}}{(\rho c)_{ms}}\mathbf{V} \cdot \nabla T = \frac{D_h}{(\rho c)_{ms}}\nabla^2 T. \tag{6.38}$$

Which can be written as

$$\frac{\partial T}{\partial t} + \sigma \mathbf{V} \cdot \nabla T = \alpha_{th} \nabla^2 T, \tag{6.39}$$

where

$$\sigma = \frac{(\rho c)_{water}}{(\rho c)_{ms}} \quad \text{and} \quad \alpha_{th} = \frac{D_h}{(\rho c)_{ms}}. \tag{6.40}$$

In Appendix A

$$\frac{\partial T}{\partial t} = \sigma \frac{\rho g k}{\mu} \nabla \phi \cdot \nabla T + \alpha_{th} \nabla^2 T, \tag{6.41}$$

where

$$\mathbf{V} = (u, w) = -\frac{\rho g k}{\mu} \nabla \phi. \tag{6.42}$$

The temperature in terms of the mapped coordinates is $T = \hat{T}(\xi, \eta)$. The transformed equation is:

$$\frac{1}{J} \frac{\partial \hat{T}}{\partial t} = \sigma \frac{\rho g k}{\mu} \hat{\nabla} \hat{\phi} \cdot \hat{\nabla} \hat{T} + \alpha_{th} \hat{\nabla}^2 \hat{T}, \tag{6.43}$$

where

$$J = \left(\frac{\partial \xi}{\partial x}\right)^2 + \left(\frac{\partial \xi}{\partial z}\right)^2. \tag{6.44}$$

Hence the unsteady problem with fluid velocity components written in terms of the velocity potential is:

$$\frac{1}{J} \frac{\partial \hat{T}}{\partial t} = \sigma \frac{\rho g k}{\mu} \left(\frac{\partial \hat{\phi}}{\partial \xi} \frac{\partial \hat{T}}{\partial \xi} + \frac{\partial \hat{\phi}}{\partial \eta} \frac{\partial \hat{T}}{\partial \eta}\right) + \alpha_{th} \left(\frac{\partial^2 \hat{T}}{\partial \xi^2} + \frac{\partial^2 \hat{T}}{\partial \eta^2}\right), \tag{6.45}$$

$$\text{implies} \quad \frac{1}{J} \frac{\partial \hat{T}}{\partial t} = -\sigma \left(\hat{u} \frac{\partial \hat{T}}{\partial \xi} + \hat{w} \frac{\partial \hat{T}}{\partial \eta}\right) + \alpha_{th} \left(\frac{\partial^2 \hat{T}}{\partial \xi^2} + \frac{\partial^2 \hat{T}}{\partial \eta^2}\right). \tag{6.46}$$
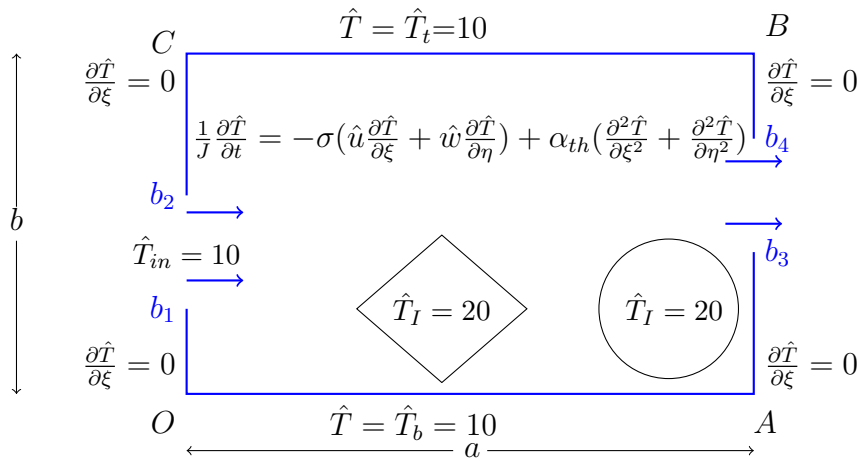
Figure 6.7: *Schematic diagram of the physical domain for heat in the unsteady case.*

6.3.4 Illustrations: solution for the non-steady heat equation

Example 6.3.1 *A stream of $10\,^{\circ}\mathrm{C}$ water enters in a rectangular porous duct, the temperature of the horizontal wall is uniform and equal to $10\,^{\circ}\mathrm{C}$, whereas the vertical solid walls of the duct are kept insulated. The duct cross-section is a 10 cm $\times$ 6 cm rectangle. An elliptic shaped hot cylinder is embedded in the centre of the duct with a constant temperature of $20\,^{\circ}\mathrm{C}$. The major axis of the ellipse has a length of 2 cm, and the minor is 1 cm long. Water is flowing through the duct over the hot cylinder and leaves out from another opening.*

(a) *Plot the heat transfer from the duct, until the system becomes in a state of steady-state. Assume that the thickness of the boundary layer that lines the inner surface of the duct is much smaller than 10 cm.*

(b) *What are the effects of α_{th} and σ on heat transfer?*

(c) *What are the other factors influencing the fluid flow and heat transfer through the porous duct?*

Mathematically, we have to solve the equation

$$\frac{1}{J}\frac{\partial \hat{T}}{\partial t} = -\sigma\left(\hat{u}\frac{\partial \hat{T}}{\partial \xi} + \hat{w}\frac{\partial \hat{T}}{\partial \eta}\right) + \alpha_{th}\left(\frac{\partial^2 \hat{T}}{\partial \xi^2} + \frac{\partial^2 \hat{T}}{\partial \eta^2}\right), \tag{6.47}$$

169

subject to the boundary conditions:

$$\hat{T}(x,0) \;=\; \hat{T}_b = 10, \qquad \hat{T}(x,b) = \hat{T}_t = 10, \qquad 0 \le x \le a, \tag{6.48}$$

$$\hat{T}_I \;=\; 20, \qquad \text{(on the cylinder)}, \tag{6.49}$$

$$\hat{T}_{in} \;=\; 10, \qquad b_1 \le z \le b_2, \tag{6.50}$$

$$\frac{\partial \hat{T}}{\partial x}(0,z) \;=\; 0, \qquad 0 \le z \le b_1, \quad b_2 \le z \le b, \tag{6.51}$$

$$\frac{\partial \hat{T}}{\partial x}(a,z) \;=\; 0, \qquad 0 \le z \le b_3, \quad b_4 \le z \le b. \tag{6.52}$$

(a) For the numerical solution, first of all a conformal mapping is found, which maps a horizontal plate in the $\xi\eta$-plane into the elliptic cylinder in the (x,z) plane, as shown in Figure 6.3a and 6.3c, then the fluid flow equation is solved in terms of ϕ and ψ. Darcy velocities are calculated all across the duct and over the cylinder by using one sided finite difference and central difference formulae in terms of ϕ. After calculation of the Darcy velocities, the non-steady heat Equation (6.47) subject to boundary conditions (6.48)-(6.52) has been solved numerically by using finite difference methods and the results are similar to the steady-state case, as discussed above in Subsection 6.3.2.

Figures 6.8a-6.8b show the temperature contour and surface plots around the plate and Figures 6.8c-6.8d show the temperature contour and surface plots for the elliptic cylinder.
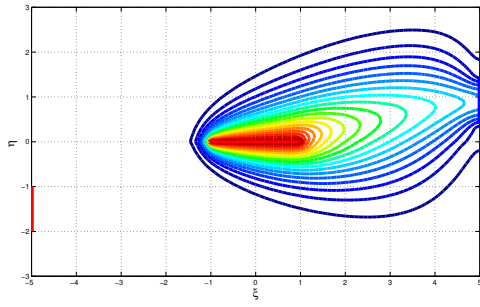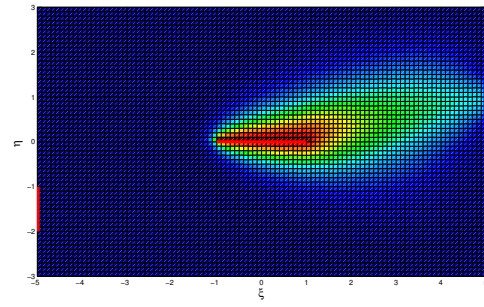
(a)   (b)
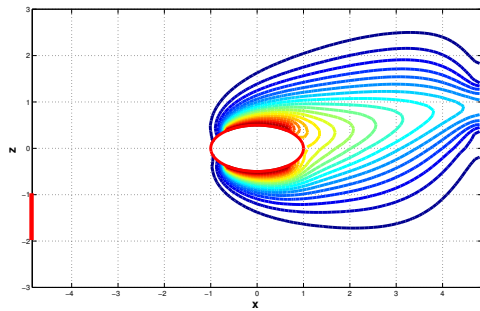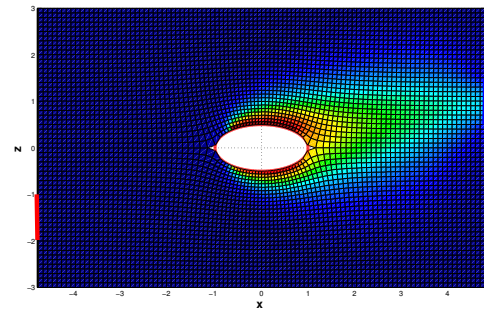
(c)   (d)

Figure 6.8: *Representation of the solution of the unsteady heat dispersion-advection equation, with $\alpha_{th} = 0.01$, $\sigma = 1$, with heated objects inside a homogeneous porous medium with temperature contours the same as in Figures 6.6, in the form of (a) contour plot for plate; (b) surface plot for plate; (c) contour plot for ellipse; (d) surface plot for ellipse.*

(b) Now to show the effect of σ and α_{th} on heat advection-conduction, consider the following graphs.
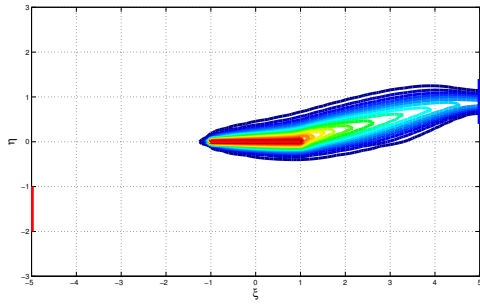
(a)
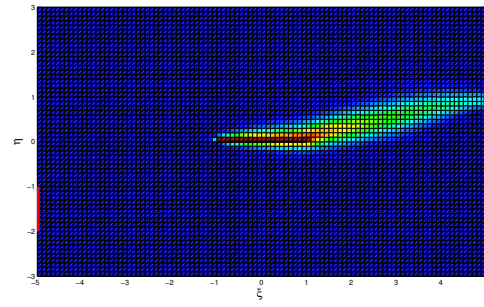
(b)
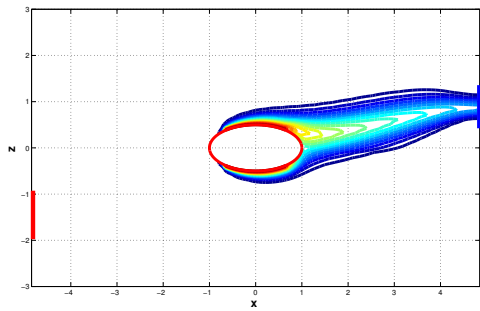
(c)
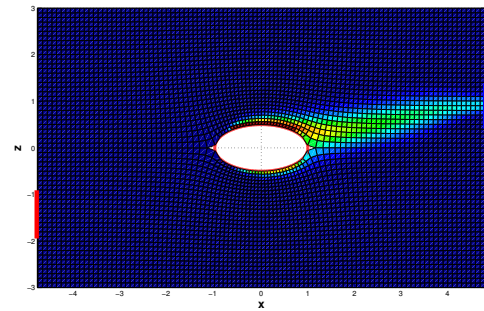
(d)

Figure 6.9: *Representation of the solution of the unsteady heat dispersion-advection equation, with $\alpha_{th} = 0.001$, $\sigma = 1$, with heated objects inside a homogeneous porous medium with temperature contours the same as in Figures 6.6, in the form of: (a) contour plot for plate; (b) surface plot for plate; (c) contour plot for ellipse; (d) surface plot for ellipse.*

172

(a)

(b)

(c)

(d)
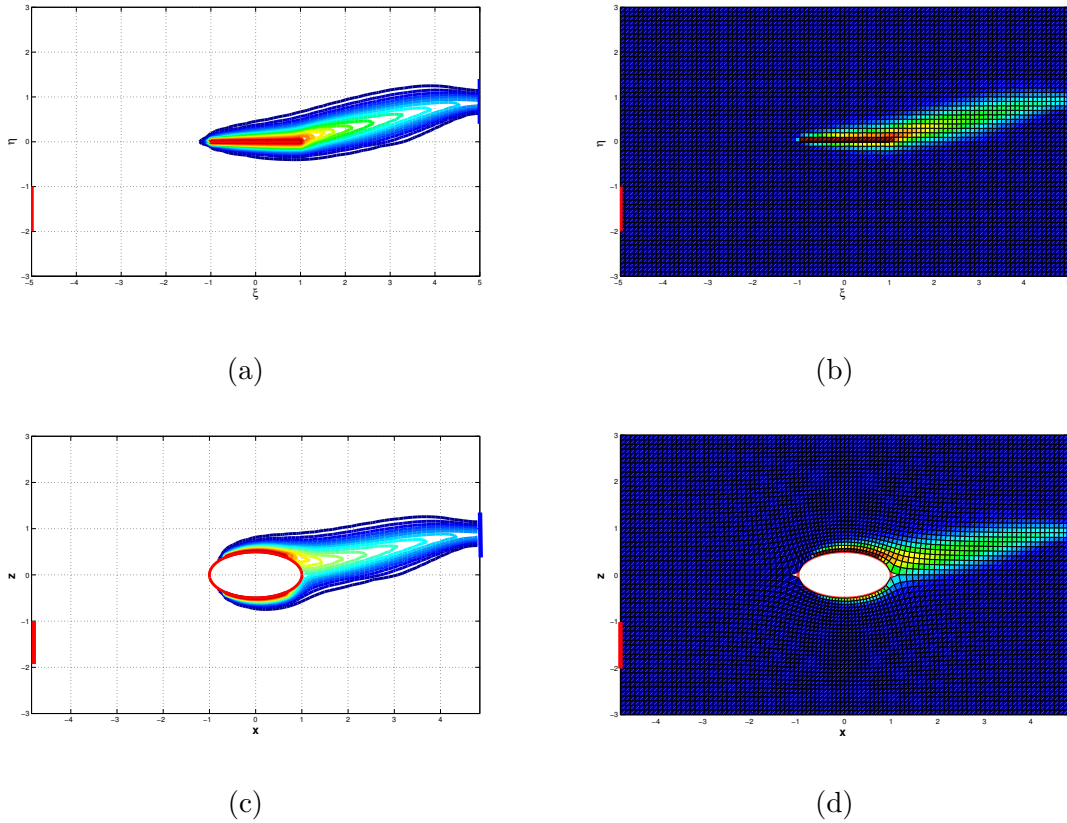
Figure 6.10: *Representation of the solution of the unsteady heat dispersion-advection equation, with $\alpha_{th} = 0.01$, $\sigma = 10$, with heated objects inside a homogeneous porous medium with temperature contours the same as in Figures 6.6, in the form of: (a) contour plot for plate; (b) surface plot for plate; (c) contour plot for ellipse; (d) surface plot for ellipse.*

For a very small value of α_{th}, and/or for a very large value of σ, the dispersion of heat is very low, and most of the heat transfer is due to advection, as is clear from Figures 6.9, and 6.10, where in the former, the value of α_{th} is taken 10 times smaller than that in Figure 6.8 and in the latter, the value of σ is taken 10 times larger than that in Figure 6.8.

Figure 6.11 gives a quantitative analysis of the importance of α_{th} and σ in the observed long-time plume behaviour. The graph of Figure 6.11a shows that, for a fixed value of σ, the width of the heat plume increases gradually as the parametric value of α_{th} increases steadily. However, Figure 6.11b illustrates that for a fixed value of α_{th}, the width of the plume decreases suddenly when σ increases from 0.5 to 2, then the spread of plume decreases slowly as σ increases further.
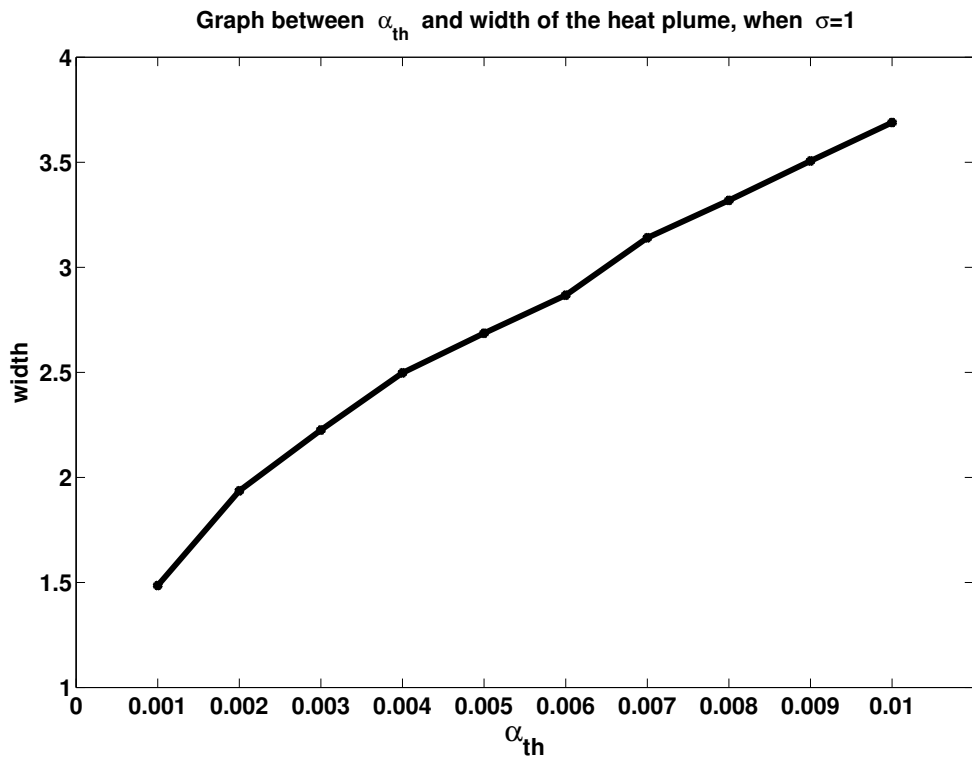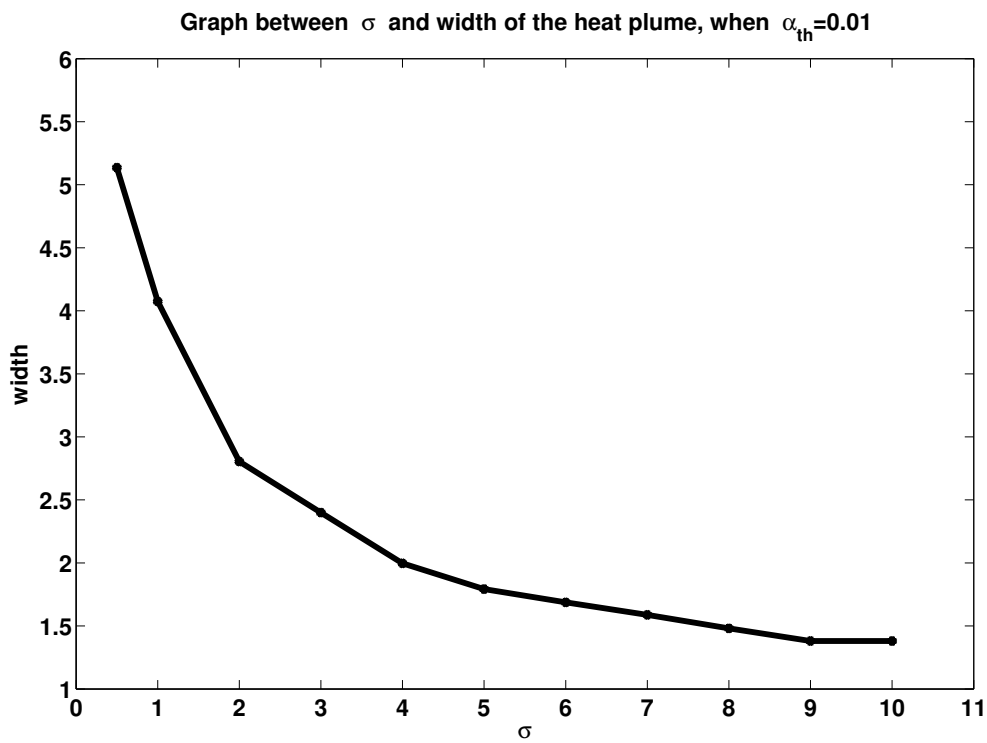
Figure 6.11: *Representation of the relationship between (a)* α_{th} *and the width of the heat plume when* $\sigma = 1$; *(b)* σ *and the width of the heat plume when* $\alpha_{th} = 0.01$.

(c) It is also observed that the size, shape and burial depth of the cylinder affect the pressure drop, as well as the pollutant and/or the heat transfer. Moreover, the rate of dis-

174

persion/advection and pressure drop depends on the permeability structure and the fluid speed.

Example 6.3.2 *Repeat part (a) of Example 6.3.1 with all solid boundaries insulated.*

In this case, the mathematical formulation of the problem is given below.

Unsteady heat Equation (6.46) subject to boundary conditions will be solved numerically:

$$\frac{\partial \hat{T}}{\partial z}(x,0) \;=\; 0, \qquad \frac{\partial \hat{T}}{\partial z}(x,b) = 0, \qquad 0 \leq x \leq a, \tag{6.53}$$

$$\hat{T}_I \;=\; 20, \qquad \text{(on the cylinder)}, \tag{6.54}$$

$$\hat{T}_{in} \;=\; 10, \qquad b_1 \leq z \leq b_2, \tag{6.55}$$

$$\frac{\partial \hat{T}}{\partial x}(0,z) \;=\; 0, \qquad 0 \leq z \leq b_1, \quad b_2 \leq z \leq b, \tag{6.56}$$

$$\frac{\partial \hat{T}}{\partial x}(a,z) \;=\; 0, \qquad 0 \leq z \leq b_3, \quad b_4 \leq z \leq b. \tag{6.57}$$

Provided the boundaries of the aquifer are not very close to the object, non-steady heat Equation (6.46) subject to boundary conditions (6.53)-(6.57) have been solved numerically by using finite difference methods. It is observed that the constant temperature boundaries (as discussed in Example 6.3.1 and illustrated in Figure 6.8) and insulated boundaries in Figure 6.12 effectively give the same results, as the boundaries are far away from the cylinder.

Figures 6.12a-6.12b show the temperature contour and surface plots around the plate and Figures 6.12c-6.12d show the temperature contour and surface plots for the elliptic cylinder. Moreover, after a long time of numerical simulation, the steady-state solution of both the systems is equivalent.
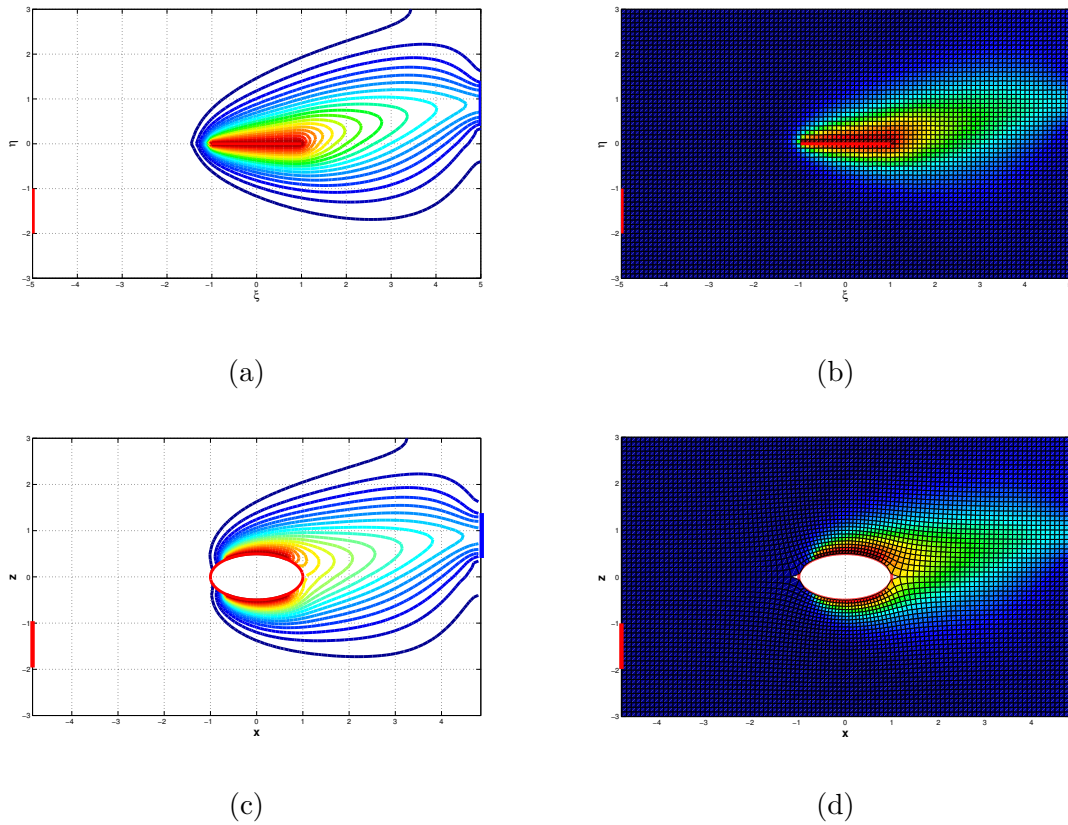
Figure 6.12: *Representation of the solution of the unsteady heat dispersion-advection equation, with $\alpha_{th} = 0.01$, $\sigma = 1$, with heated objects inside a homogeneous porous medium with insulated boundaries. The temperature contours are the same as in Figures 6.6, in the form of: (a) contour plot for plate; (b) surface plot for plate; (c) contour plot for ellipse; (d) surface plot for ellipse.*

Due to the fact that there are a number of parameters involved to consider, only a general review of heat transfer study has been discussed here. Moreover, because so many options for the boundary conditions on the porous medium as well as on the hot body are possible, a complete analysis of all of them is not practicable in this study.

Chapter 7

Summary and Conclusions

The present study has numerically investigated the characteristics of fluid flow rates, pollutant and heat transport from objects embedded in groundwater aquifers. This includes a fully numerical two- and three-dimensional modelling to determine:

- the effects of size and shape of an object or set of solid or partially pervious objects embedded in a porous medium on the local speed and shape of the flow;

- when heat and/or a pollutant is released from, or removed by the object(s), the dependence of subsequent dispersal through a groundwater aquifer on the various parameters involved (e.g., the object size, object's burial depth, the aquifer's depth, the fluid flow rates, etc.);

- the effect of the non-homogeneity in matrix properties (e.g., permeability or hydraulic conductivity) in the case of layered aquifers.

The work included in this thesis is based on the following assumptions:

- the groundwater, which is in a single liquid phase, is assumed to be incompressible, irrotational and at low temperature;

- the flow domain which is rigid and non-deformable is considered to be a rectangle in the two-dimensional case and in the case of a three-dimensional domain, it is regarded as cuboidal;

- the parameters that contribute to the governing Laplace's equation with initial and boundary conditions in the flow domain are assumed to be ϕ (3D) and ψ (2D);

- the objects embedded in the groundwater aquifer are impermeable and pervious, which mainly depend on two parameters, β_{ps}, and a constant inside pressure, ϕ_I;

- non-homogeneous aquifers have a horizontal as well as a vertical layered structure;

- the pollutant advection-dispersion equation that models the transport problem is in linear and non-linear form;

- in the case of the heat advection-dispersion phenomenon, the modelling includes a complex variable technique, namely conformal mapping to map simple geometries on complex configurations.

Following is a short discussion about the above objectives and assumptions.

7.1 Effect of presence of impermeable objects

When modelling fluid flow and heat transport in groundwater aquifers, one needs to observe the influence of the presence of solid (impermeable) objects embedded in underground aquifers. These objects may be due to natural occurrences such as deep geological formations, or some man-made constructions, like engineering reservoirs, etc.

The results presented in Chapters 3, 4 and 6 provide a better understanding of fluid and heat flow rates in the presence and absence of impermeable objects embedded in groundwater aquifers. It is found that the presence of these objects alters significantly the steady/unsteady hydrodynamic and thermal behaviour in the aquifers.

In spite of the fact that in this thesis, the results have been calculated with finite differences for fluid flow in groundwater aquifers for some regular shaped objects, its results can be used and generalized for any kind of numerical method, shape of embedded objects and porous media.

7.2 Effect of presence of pervious objects

When it is a matter of pollutant leaking from some underground buried formations, there is a need to formulate the geometrical configurations, suitable boundary conditions and a list of parameters/variables that will be used to describe the state of the system.

In this thesis, a mixture of Neumann- and Dirichlet-type boundary conditions is used to describe the boundary conditions on the pervious walls of rectangular objects. In these boundary conditions, normal components of pressure gradient, $\partial\phi/\partial n$ are assumed to be proportional to the constant inner pressure ϕ_I of the object. ϕ_I is the parameter involved in the calculations, whose value describes the injection or removal of groundwater from the embedded objects.

The non-negative parameter β_{ps} is supposed to be a proportionality constant, whose value specifies the perviousness of the object; a zero value of β_{ps} indicates the object is impermeable. A detailed discussion about the influence of β_{ps} on fluid flow for a pervious wall has been included in Chapters 3 and 4. It is noted that, for a larger value of β_{ps}, the fluid ignores the presence of the wall.

7.3 Effect of layering

Generally, the porous media comprising groundwater aquifers are rarely homogeneous with respect to their permeability. Layered systems have evolved after centuries during continuous geological eruptions/processes and can be differentiated with varying thicknesses. Physical properties (like porosity, permeability, hydraulic conductivity, etc.) are assumed to be constant within each sub-layer, but can be different in each of the various layers of the system.

In a multi-layered system, fluid flows faster in a region of higher permeability. Results for fluid flow have been presented in Chapter 4 for impermeable and pervious objects embedded in non-homogeneous aquifers. It was observed that, for a multi-layer system (with varying permeabilities), parallel to the plane of the flow, fluid flow occurs under the influence of the varying pressure gradient. For a system perpendicular to the plane of flow, the flow is assumed to be nearly uniform.

In the advection-dispersion model, for pollutant leaking from embedded bodies in the aquifers, transport of pollutant across layer interface may take place due to different permeability struc-

ture within adjacent layers. Some results have been discussed in Chapter 5 for three-layer aquifers for pervious objects.

7.4   Effect of dispersion coefficients

The coefficient of mechanical dispersion D appearing in the advection-dispersion equation that models the transport problem of pollutant concentration C has been studied by many researchers. It is found that D mainly depends on flow patterns (e.g., velocity) and on some basic medium properties, like porosity, permeability and hydraulic conductivity, etc.

Across any cross-section of a pore, the velocity of fluid varies in both magnitude and direction, with the greatest velocity at some internal point. Due to the shape of the interconnected pore space, the maximum velocity itself varies according to the pore size.

Thus spreading of pollutant in an aquifer depends on two factors, flow and a pore system through which the flow takes place [13]. In spite of the fact that spreading takes place in both the longitudinal (in the direction of average flow) and transverse (normal to average flow) directions, it is mostly in the former direction. In the transverse direction, very little spreading can occur by only velocity variation. Moreover, this velocity variation is not the only factor responsible for spreading normal to the direction of flow. In order to explain this latter spreading, we have to go into more detail. A number of researchers (e.g., Nikolaevskii; 1959; Bear, 1961; Scheidegger, 1961; Bear and Bachmat, 1967) derived a relationship between the coefficient D, flow velocity and porous matrix formation.

In Chapter 5, a detailed discussion about the dispersivity of the porous medium (α_L, and α_T) has been included. The parameter α_L, which is the *longitudinal dispersivity* of the isotropic porous medium, is responsible for the longitudinal spreading and α_T, which is the *transverse dispersivity* of the isotropic porous medium, is the parameter responsible for the lateral spreading. Moreover, a short study about the cases when α_L is equal to α_T and when both have some averaged relationship has also been included. It was also found that, for a significantly high speed of fluid, the spread of pollutant concentration plume in the transverse direction becomes more prominent and greater.

7.5 Conformal mapping

A procedure has been developed for mapping simple geometries (in the $\xi\eta$-plane) on complex configurations (in the xz-plane) by using a complex variable technique, namely conformal mappings. In Chapter 6, an analytical derivation of steady-state and time-dependent heat equations for the transformed $\xi\eta$-plane has been added by using conformal mappings. Later, to find a mapping, solution of the fluid flow problem and heat transport, a numerical algorithm has been developed using finite differences.

In the first step of numerical simulations, a mapping of a horizontal line into complex shapes, such as diamond and elliptic cylinders, has been formed. Secondly, a solution has been found for Laplace's equation for fluid flow in a homogeneous aquifer. Following the solution of fluid flow, steady-state as well as time-dependent heat equations have been solved for these objects in the $\xi\eta$-plane and then in the xz-plane.

It is found that transformed domains as well as heat transfer rates are different for both the bodies. In the case of a diamond-shaped cylinder, the dimensions of the transformed domain are slightly less than that of elliptic cylinder; probably it is due to the sharper edges of the diamond. The work is still in progress due to the limitation of conformal mapping to 2D objects.

7.6 Effect of boundary conditions

Boundary conditions play a vital role in the solution of differential equations. Although in this model aquifers are assumed to be rectangular with finite dimensions, in real situations, they are usually situated over a scale of kilometres.

The scope of this thesis is to elaborate general features of some real situations, so in some places only the effect of boundary conditions has been discussed. In Chapter 6, for example, for heat transfer from a heated cylinder, insulated and constant temperature boundaries give the same steady-state solutions because of the boundaries which are located far away from the hot object.

Appendix A

A.1 Derivation of the non-steady state heat advection-conduction equation for the (ξ, η)-plane

If we need to find the non-steady state heat equation in terms of the mapped coordinates ξ and η, we proceed as follows:

In a fluid-saturated porous media, transport of heat (released by embedded hot objects) occurs by conduction and advection. The model is based on the assumptions that the fluid speed is very slow and fluid buoyancy and thermal effects are negligible. The unsteady heat equation in the xz-coordinate system is:

$$\frac{\partial T}{\partial t} = \sigma \frac{\rho g k}{\mu} \left(\frac{\partial \phi}{\partial x} \frac{\partial T}{\partial x} + \frac{\partial \phi}{\partial z} \frac{\partial T}{\partial z} \right) + \alpha_{th} \left(\frac{\partial^2 T}{\partial x^2} + \frac{\partial^2 T}{\partial z^2} \right), \tag{A.1}$$

where $\phi(x, z)$ is a velocity potential for the flow. Now temperature in fluid region $T(t, x, z)$ is expressed in terms of the mapped coordinates as

$$
\begin{aligned}
T(t, x, z) &= T(t, \hat{x}(\xi, \eta), \hat{z}(\xi, \eta)), \tag{A.2} \\
&= \hat{T}(t, \xi, \eta). \tag{A.3}
\end{aligned}
$$

Transformation of the heat equation

For a steady flow, the Darcy velocity vector is $\mathbf{V} = (u, w)$. In terms of $\phi(x, z)$, $u = -(\rho g k/\mu)\partial\phi/\partial x$, $w = -(\rho g k/\mu)\partial\phi/\partial z$. Then, for the conformal mapping $(x, z) = (\hat{x}(\xi, \eta), \hat{z}(\xi, \eta))$:

$$\frac{\partial\xi}{\partial x} = -\frac{\partial\eta}{\partial z}, \quad \text{and} \quad \frac{\partial\xi}{\partial z} = \frac{\partial\eta}{\partial x}, \tag{A.4}$$

also

$$\frac{\partial^2\xi}{\partial x^2} + \frac{\partial^2\xi}{\partial z^2} = 0, \quad \text{and} \quad \frac{\partial^2\eta}{\partial x^2} + \frac{\partial^2\eta}{\partial z^2} = 0. \tag{A.5}$$

Writing $T(x, z) = \hat{T}((\xi, \eta))$, and $\phi(x, z) = \hat{\phi}((\xi, \eta))$, differentiation gives:

$$\frac{\partial\phi}{\partial x} = \frac{\partial\xi}{\partial x}\frac{\partial\hat{\phi}}{\partial\xi} + \frac{\partial\eta}{\partial x}\frac{\partial\hat{\phi}}{\partial\eta}, \tag{A.6}$$

$$\frac{\partial\phi}{\partial z} = \frac{\partial\xi}{\partial z}\frac{\partial\hat{\phi}}{\partial\xi} + \frac{\partial\eta}{\partial z}\frac{\partial\hat{\phi}}{\partial\eta}, \tag{A.7}$$

$$\frac{\partial T}{\partial x} = \frac{\partial\xi}{\partial x}\frac{\partial\hat{T}}{\partial\xi} + \frac{\partial\eta}{\partial x}\frac{\partial\hat{T}}{\partial\eta}, \tag{A.8}$$

$$\frac{\partial T}{\partial z} = \frac{\partial\xi}{\partial z}\frac{\partial\hat{T}}{\partial\xi} + \frac{\partial\eta}{\partial z}\frac{\partial\hat{T}}{\partial\eta}. \tag{A.9}$$

Further differentiation of (A.8) and (A.9) gives:

$$\frac{\partial^2 T}{\partial x^2} = \frac{\partial\hat{T}}{\partial\xi}\frac{\partial^2\xi}{\partial x^2} + \left(\frac{\partial\xi}{\partial x}\right)^2\frac{\partial^2\hat{T}}{\partial\xi^2} + \frac{\partial\hat{T}}{\partial\eta}\frac{\partial^2\eta}{\partial x^2} + \left(\frac{\partial\eta}{\partial x}\right)^2\frac{\partial^2\hat{T}}{\partial\eta^2}, \tag{A.10}$$

and

$$\frac{\partial^2 T}{\partial z^2} = \frac{\partial\hat{T}}{\partial\xi}\frac{\partial^2\xi}{\partial z^2} + \left(\frac{\partial\xi}{\partial z}\right)^2\frac{\partial^2\hat{T}}{\partial\xi^2} + \frac{\partial\hat{T}}{\partial\eta}\frac{\partial^2\eta}{\partial z^2} + \left(\frac{\partial\eta}{\partial z}\right)^2\frac{\partial^2\hat{T}}{\partial\eta^2}. \tag{A.11}$$

Adding Equations (A.10) and (A.11) and simplification using Equations (A.4) and (A.5) leaves:

$$\frac{\partial^2 T}{\partial x^2} + \frac{\partial^2 T}{\partial z^2} = \left[\frac{\partial^2\hat{T}}{\partial\xi^2} + \frac{\partial^2\hat{T}}{\partial\eta^2}\right]\left[\left(\frac{\partial\xi}{\partial x}\right)^2 + \left(\frac{\partial\xi}{\partial z}\right)^2\right]. \tag{A.12}$$

Putting the values of Equations (A.6), (A.7), (A.8), (A.9) and (A.12) into Equation (A.1)

we get:

$$\frac{\partial \hat{T}}{\partial t} = \left[\left(\frac{\partial \xi}{\partial x}\right)^2 + \left(\frac{\partial \xi}{\partial z}\right)^2\right] \left[\sigma \frac{\rho g k}{\mu}\left(\frac{\partial \hat{T}}{\partial \xi}\frac{\partial \hat{\phi}}{\partial \xi} + \frac{\partial \hat{T}}{\partial \eta}\frac{\partial \hat{\phi}}{\partial \eta}\right) + \alpha_{th}\left(\frac{\partial^2 \hat{T}}{\partial \xi^2} + \frac{\partial^2 \hat{T}}{\partial \eta^2}\right)\right],$$

which implies

$$\frac{\partial \hat{T}}{\partial t} = J\left[\sigma \frac{\rho g k}{\mu}\left(\frac{\partial \hat{T}}{\partial \xi}\frac{\partial \hat{\phi}}{\partial \xi} + \frac{\partial \hat{T}}{\partial \eta}\frac{\partial \hat{\phi}}{\partial \eta}\right) + \alpha_{th}\left(\frac{\partial^2 \hat{T}}{\partial \xi^2} + \frac{\partial^2 \hat{T}}{\partial \eta^2}\right)\right], \tag{A.13}$$

$$\text{where} \qquad J = \left(\frac{\partial \xi}{\partial x}\right)^2 + \left(\frac{\partial \xi}{\partial z}\right)^2 \qquad \text{is the Jacobian.} \tag{A.14}$$

Hence Equation (A.13) becomes

$$\frac{1}{J}\frac{\partial \hat{T}}{\partial t} = \sigma \frac{\rho g k}{\mu}\left(\frac{\partial \hat{T}}{\partial \xi}\frac{\partial \hat{\phi}}{\partial \xi} + \frac{\partial \hat{T}}{\partial \eta}\frac{\partial \hat{\phi}}{\partial \eta}\right) + \alpha_{th}\left(\frac{\partial^2 \hat{T}}{\partial \xi^2} + \frac{\partial^2 \hat{T}}{\partial \eta^2}\right),$$

which implies

$$\frac{1}{J}\frac{\partial \hat{T}}{\partial t} = -\sigma\left(\hat{u}\frac{\partial \hat{T}}{\partial \xi} + \hat{w}\frac{\partial \hat{T}}{\partial \eta}\right) + \alpha_{th}\left(\frac{\partial^2 \hat{T}}{\partial \xi^2} + \frac{\partial^2 \hat{T}}{\partial \eta^2}\right). \tag{A.15}$$

Equation (A.15) is the unsteady heat advection-conduction equation in the (ξ, η)-plane.

A.2 Derivation of the steady-state heat advection-conduction equation for the (ξ, η)-plane

Putting $\partial \hat{T}/\partial t = 0$ in Equation (A.15) we get:

$$\alpha_{th}\left(\frac{\partial^2 \hat{T}}{\partial \xi^2} + \frac{\partial^2 \hat{T}}{\partial \eta^2}\right) = \sigma\left(\hat{u}\frac{\partial \hat{T}}{\partial \xi} + \hat{w}\frac{\partial \hat{T}}{\partial \eta}\right), \tag{A.16}$$

which implies

$$\frac{\partial^2 \hat{T}}{\partial \xi^2} + \frac{\partial^2 \hat{T}}{\partial \eta^2} = \frac{\sigma}{\alpha_{th}}\left(\hat{u}\frac{\partial \hat{T}}{\partial \xi} + \hat{w}\frac{\partial \hat{T}}{\partial \eta}\right), \tag{A.17}$$

which leads to

$$\frac{\partial^2 \hat{T}}{\partial \xi^2} + \frac{\partial^2 \hat{T}}{\partial \eta^2} = \frac{1}{D_{th}} \left(\hat{u} \frac{\partial \hat{T}}{\partial \xi} + \hat{w} \frac{\partial \hat{T}}{\partial \eta} \right), \tag{A.18}$$

where $1/D_{th} = \sigma/\alpha_{th}$.

In terms of $\hat{u} = -(\rho g k/\mu)\partial\hat{\phi}/\partial\xi$, and $\hat{w} = -(\rho g k/\mu)\partial\hat{\phi}/\partial\eta$, Equation (A.18) gives:

$$\frac{\partial^2 \hat{T}}{\partial \xi^2} + \frac{\partial^2 \hat{T}}{\partial \eta^2} = -\frac{1}{D_{th}} \frac{\rho g k}{\mu} \left[\frac{\partial \hat{T}}{\partial \xi} \frac{\partial \hat{\phi}}{\partial \xi} + \frac{\partial \hat{T}}{\partial \eta} \frac{\partial \hat{\phi}}{\partial \eta} \right], \tag{A.19}$$

which implies

$$\frac{\rho g k}{\mu} \hat{\nabla} \hat{\phi} \cdot \hat{\nabla} \hat{T} + D_{th} \hat{\nabla}^2 \hat{T} = 0. \tag{A.20}$$

Equation (A.20) is the steady-state heat advection-conduction equation in the (ξ, η)-plane.

Appendix B

1. Numerical solution of the time-dependent heat equation

Example B.0.1 *Consider a thin rectangular plate $OABC$, with length a and width b as shown in Figure B.1. The edges of the plate are kept at zero temperature, while the initial temperature of the plate is given by $f(x, z)$. Let $T(x, z, t)$ be the temperature at any point (x, z) of the plate at any time t. Compute the solution by separation of variables and compare with the numerical solution.*

In this case, the mathematical formulation of the problem is given below.

Unsteady heat Equation (6.46) subject to boundary conditions will be solved numerically:

$$\frac{\partial T}{\partial t} = \alpha_{th}\left(\frac{\partial^2 T}{\partial x^2} + \frac{\partial^2 T}{\partial z^2}\right), \quad 0 < x < a, \quad 0 < z < b, \quad t > 0, \quad \text{(B.1)}$$

$$T(x, 0, t) = 0, \quad 0 < x < a, \quad t > 0, \quad \text{(B.2)}$$

$$T(x, b, t) = 0, \quad 0 < x < a, \quad t > 0, \quad \text{(B.3)}$$

$$T(0, z, t) = 0, \quad 0 < z < b, \quad t > 0, \quad \text{(B.4)}$$

$$T(a, z, t) = 0, \quad 0 < z < b, \quad t > 0, \quad \text{(B.5)}$$

$$T(x, z, 0) = f(x, z), \quad 0 < x < a, \quad 0 < z < b. \quad \text{(B.6)}$$
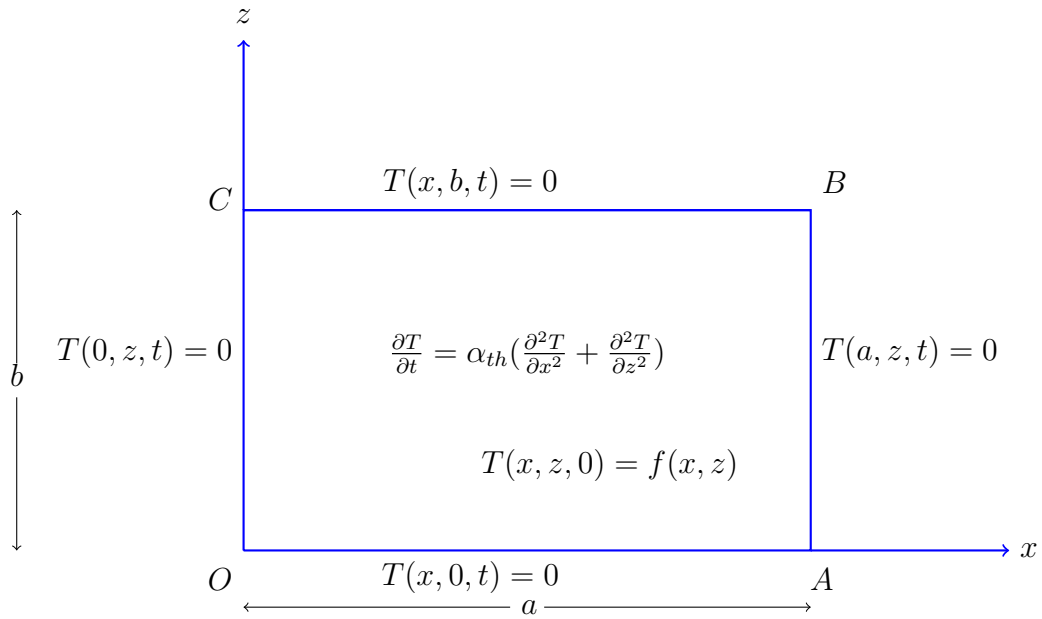
Figure B.1: *Schematic diagram of the physical domain for heat in the unsteady case.*

First, we solve the problem by separation of variables and then we will compare the analytic and numerical solutions.

Let $T(x, z, t) = X(x)Z(z)T(t)$, then Sturm-liouville systems in $X(x)$ and $Z(z)$ are obtained as

$$X'' + \lambda^2 X = 0, \quad 0 < x < a, \quad X(0) = 0 = X(a),$$

$$Z'' + \mu^2 Z = 0, \quad 0 < z < b, \quad Z(0) = 0 = Z(b).$$

Eigenpairs of these systems may be written as

$$\lambda_n^2 = \frac{n^2 \pi^2}{a^2}, \quad X_n(x) = \sqrt{\frac{2}{a}} \sin \frac{n\pi x}{a},$$

$$\mu_m^2 = \frac{m^2 \pi^2}{b^2}, \quad Z_m(z) = \sqrt{\frac{2}{b}} \sin \frac{m\pi z}{b},$$

where m and n are positive integers.

What remains is an ODE in $T(t)$, namely,

$$T' + \alpha_{th}(\lambda_n^2 + \mu_m^2)T = 0, \quad t > 0,$$

with general solution

$$T_{mn}(t) = A_{mn}e^{-\alpha_{th}(\lambda_n^2 + \mu_m^2)t}.$$

To satisfy the initial condition $T(x, z, 0) = f(x, z)$, the separated functions are superposed in the form

$$T(x, z, t) = \sum_{n=1}^{\infty}\sum_{m=1}^{\infty} \left[A_{mn}e^{-\alpha_{th}(\lambda_n^2 + \mu_m^2)t}\sqrt{\frac{2}{a}}sin\frac{n\pi x}{a}\sqrt{\frac{2}{b}}sin\frac{m\pi z}{b} \right], \tag{B.7}$$

and according to the initial temperature $f(x, z)$ at $t = 0$, it requires that

$$f(x, z) = T(x, z, 0) = \sum_{n=1}^{\infty}\sum_{m=1}^{\infty} \left[A_{mn}\sqrt{\frac{4}{ab}}sin\frac{n\pi x}{a}sin\frac{m\pi z}{b} \right], \quad 0 < x < a, \quad 0 < z < b. \tag{B.8}$$

To find out the value of A_{mn}, we multiply (B.8) successively by $\sqrt{\frac{2}{a}}sin\frac{M\pi x}{a}$ and $\sqrt{\frac{2}{b}}sin\frac{N\pi z}{b}$, then integrate with respect to x and z and use orthogonality conditions. Hence the value of A_{mn} is

$$A_{mn} = \frac{4}{ab}\int_0^b\int_0^a f(x, z)sin\frac{n\pi x}{a}sin\frac{m\pi z}{b}dxdz.$$

Hence, inserting the value of A_{mn} into (B.7) gives the required solution. For example, we set the value of $f(x, z)$ to be

$$f(x, z) = T(x, z, 0) = Rsin\frac{\pi x}{a}sin\frac{\pi z}{b}. \tag{B.9}$$

$$A_{mn} = \frac{4R}{ab} \int_0^b \int_0^a sin\frac{\pi x}{a} sin\frac{\pi z}{b} sin\frac{n\pi x}{a} sin\frac{m\pi z}{b} dx dz, \tag{B.10}$$

$$= \frac{4R}{ab} \left[\int_0^a sin\frac{\pi x}{a} sin\frac{n\pi x}{a} dx \right] \left[\int_0^b sin\frac{\pi z}{b} sin\frac{m\pi z}{b} dz \right], \tag{B.11}$$

$$= R, \quad \text{when } m = 1 \text{ and } n = 1, \tag{B.12}$$

and $A_{mn} = 0$ when $m \neq 1$ or $n \neq 1$.

Hence the required solution is

$$T(x, z, t) = R\sqrt{\frac{4}{ab}} sin\frac{\pi x}{a} sin\frac{\pi z}{b} e^{-\alpha_{th}(\frac{\pi^2}{a^2} + \frac{\pi^2}{b^2})t}. \tag{B.13}$$
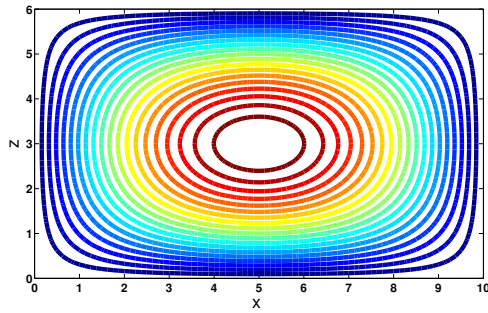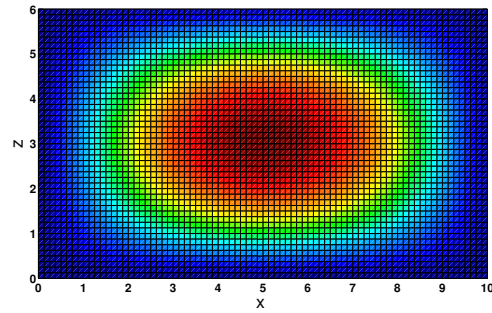
(a) (b)

Figure B.2: *Representation of the analytical solution of the unsteady heat equation, with $\alpha_{th} = 0.01$, $R = 5$, in the form of: (a) contour plot; (b) surface plot.*
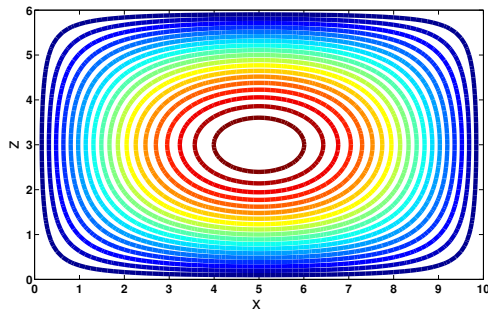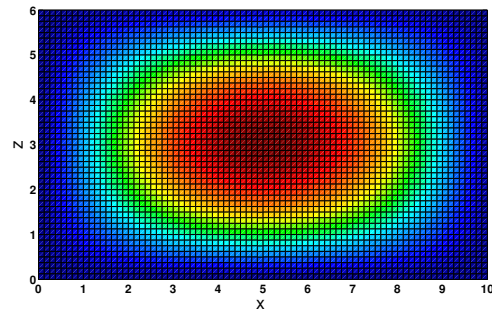
(a) (b)

Figure B.3: *Representation of the numerical solution of the unsteady heat equation represented in Example B.0.1, with $\alpha_{th} = 0.01$, $R = 5$, in the form of: (a) contour plot; (b) surface plot.*

From Figure B.2 and Figure B.3, it is clear that the analytical and numerical solutions are in good agreement. Moreover, as all the four boundaries of the plate have zero temperature,

189

so temperature contours move in an elliptical way from the centre of the plate towards outer boundaries.

2. Numerical methods to solve the equations

In this thesis, a standard second order finite difference scheme with a uniform square mesh is used. The finite difference formulae given below are based on the following assumptions [23]:

- The numerical derivatives will be computed on a grid of $n + 1$ equispaced points: e.g. in the x-direction, x_1, $x_2 = x_1 + h$, $x_3 = x_1 + 2h$,..., $x_n = x_1 + (n-1)h$, $x_{n+1} = x_1 + nh$.

- Due to lack of space, the function values will be written shortly as: $f(x_k) = f_k$, $f(x_{k+3}) = f_{k+3}$, $f(x_{k-2}) = f_{k-2}$ and so on.

Table B.1: *Finite difference formulae for $f'(x)$.*

Type	Difference Formula	LTE
Forward	$\frac{-3f_k + 4f_{k+1} - f_{k+2}}{2h}$	$O(h^2)$
Backward	$\frac{f_{k-2} - 4f_{k-1} + 3f_k}{2h}$	$O(h^2)$
Centered	$\frac{-f_{k-1} + f_{k+1}}{2h}$	$O(h^2)$

Table B.1 gives the finite difference formulae in standard form. One can use them according to the need of the problem. For example, for a one-dimensional problem, the one-sided forward difference formula can be written as:

$$f_1' = \frac{-3f_1 + 4f_2 - f_3}{2h}.$$
(B.14)

Similarly, in terms of second derivatives, Table B.2 gives some formulae

Table B.2: *Finite difference formulae for $f''(x)$.*

Type	Difference Formula	LTE
Forward	$\frac{2f_k - 5f_{k+1} + 4f_{k+2} - f_{k+3}}{h^2}$	$O(h^2)$
Backward	$\frac{-f_{k-3} + 4f_{k-2} - 5f_{k-1} + 2f_k}{h^2}$	$O(h^2)$
Centered	$\frac{f_{k-1} - 2f_k + f_{k+1}}{h^2}$	$O(h^2)$

Here, some part of computer code is included for the sake of explanation. For convenience, a numerical code for $\nabla^2 \phi(x, z) = 0$ subject to boundary conditions (as discussed in Subsection 3.5.3 and for Figure 3.8a only) is given as follows:

$\star$ For the interior of the domain, $\partial^2\phi/\partial x^2 + \partial^2\phi/\partial z^2 = 0$ is solved by a second-order central difference formula, which is in fact a truncated Taylor's series, i.e.,

for $j = 2 : M$

for $k = 2 : N$

$$\phi(j, k) = \frac{\left(\frac{\phi(j,k-1) + \phi(j,k+1)}{dx^2} + \frac{\phi(j-1,k) + \phi(j+1,k)}{dz^2} \right)}{\frac{2}{dx^2} + \frac{2}{dz^2}}; \tag{B.15}$$

end

end

$\star$ on the left-hand side, $\partial\phi/\partial x = 0$ is solved by a second order, one-sided forward difference formula, i.e.,

for $j = [1 : j_{b_1} - 1 \quad j_{b_2} + 1 : M + 1]$

$$\phi(j, 1) = \frac{4\phi(j, 2) - \phi(j, 3)}{3};$$ (B.16)

end

★ on the right-hand side, $\partial\phi/\partial x = 0$ is solved by a second order, one-sided backward difference formula, i.e.,

for $j = [1 : j_{b_3} - 1 \quad j_{b_4} + 1 : M + 1]$

$$\phi(j, N + 1) = \frac{4\phi(j, N) - \phi(j, N - 1)}{3};$$ (B.17)

end

★ on the top, $\partial\phi/\partial z = 0$ is solved by a second order, one-sided backward difference formula, i.e.,

for $k = M + 1, 2 : N$

$$\phi(M + 1, k) = \frac{4\phi(M, k) - \phi(M - 1, k)}{3};$$ (B.18)

end

★ on the bottom, $\partial\phi/\partial z = 0$ is solved by a second order, one-sided forward difference formula, i.e.,

for $k = 1, \quad 2 : N$

$$\phi(1, k) = \frac{4\phi(2, k) - \phi(3, k)}{3};$$ (B.19)

end

$\star$ and lastly, the values of the scaled dynamic pressure in the entrance, $b_1 b_2$ and exit, $b_3 b_4$ are assigned in this way:

$\phi(j_{b_1} : j_{b_2}, \quad 1) = \phi_L;$

$\phi(j_{b_3} : j_{b_4}, \quad N + 1) = \phi_R.$

Similarly, the computer code could be generated for steady-state as well as time-dependent heat and pollutant equations by using finite difference formulae as discussed in Tables B.1 and B.2.

a. A discussion of the relaxation method

In a system of linear equations with some specified boundary conditions, we have to find the solution of the system, which is unknown. The overall idea of relaxation method is that, first we have to guess the unknown solution of the system, which may contain all trivial values. Then we use some kind of repeated iterative process to improve the solution.

Now in the case of linear equations, we know that all of the equations would be satisfied. We also know how to solve them all simultaneously, so, in theory, we can set it up as an massive linear algebra problem. Then we just do an inversion of large matrix and just check the equations straight away. Most of the time, if we cannot get the determinant or we cannot find the inverse of this matrix, then the problem is called ill-conditioned.

In our case, we may have thousands of lines in the matrix, so the idea is that, at each point, we have found some way of relating the values at that point to nearby values. If we take the Laplace's equation in the start, we have written down the equation in terms of finite differences at each point. What we have to do next, is to go through iteratively in an organised way, so using the formula and the present values we put in there, we calculate new values for all of these; we call them improved values or new values. We did not do the instant replacement of the old values in terms of new values, but we are using

all the old values and calculating a new set of improved values and then taking some weighting of the old and new values to calculate an update. That is called relaxation and that's the way a relaxation factor r comes along. The relaxation technique is:

improved values=$(1 - r)$ new values +r old values.

If $r = 1$, then we calculate all the improved values by just plugging them all in and replacing them all at once and then do it all again. But if we relax it, then we take a bit of the old values and build the new values getting it slowly to improve each time. That's why when we have a very small relaxation factor, it takes a long time because we only take a little change every time. Sometimes, if we take r too big, then it goes unstable.

b. A discussion of how the system is linear and why the iterative method is chosen over the direct computation of the system

The system of finite difference equations is linear, but the boundary conditions, and the layering of the porous medium make it a non-homogeneous problem, the set of equations to solve is very complicated. So, it is difficult to solve using separation of variables and therefore the iterative method is chosen over direct computation of the underlying system of linear equations.

A detailed discussion about solution of linear equations and their convergence will come in Section B.1.

c. How the time domain solution is calculated by time stepping methods

The time stepping method is the same as the relaxation method. It is just we use the all old values and then we take a little time step and calculate a new set of values and then do it again and again. If we continue to do this, eventually it will converge and it is called "steady-state". So, the time stepping method is just like relaxation and if we are looking for steady-state, we can think about it as time stepping or we can think about it as relaxation. However, in time stepping we think about what the time was at each step.

So, the time stepping method is essentially the same as the relaxation method, that we are just advancing the solution by a small amount at each time.

B.1 Solution of a system of linear equations

Problems involving linear systems of equations play a prominent role in engineering, physics, chemistry, computer science, and economics. Consider an $N \times N$ real matrix A and a real N-vector b. The problem is to find $x \in R^N$ such that

$$Ax = b. \tag{B.20}$$

Equation (B.20) is a linear system, A is the coefficient matrix, b is a right-hand side constant vector and x is a vector of unknowns.

There are two main methods for solving linear systems: direct elimination and iterative techniques. Direct methods are also known as exact methods, which enable the finding of an exact solution of the system in a finite and predictable number of operations. This number depends on the order of the system and in general, a nonsparse $N \times N$ system of matrix is considered [31]. These methods includes Cramer's rule, the Gaussian method, LU decomposition, the method of principal elements, the method of square roots, etc.

Iterative methods, which are also known as indirect methods give only approximate solutions and within the available limit of accuracy, this approximation can be made as fine as we wish. The number of iterations may depend strongly on the quality of the initial guess of the solution. Moreover, the number of iterations depends on the values of the coefficients in the equations which specify the rate of convergence per iteration. The number of operations per iteration corresponds to N^2.

Among the iterative methods, there are the Jacobi iterative method, the Gauss-Seidel iterative method and relaxation methods. The rate of convergence of the Jacobi and Gauss-Seidel iterative methods is usually slow, particularly for large systems of equations. Detailed study of Jacobi and Gauss-Seidel iterative methods can be found in any numerical analysis books, here, a small discussion of relaxation methods is given below.

Relaxation methods were developed for solving large sparse linear systems, which arose as finite difference discretizations of Elliptic Partial Differential Equations [59, 55]. In this scheme, the general i^{th} equation is given by

$$x_i^{(m+1)} = \frac{1}{a_{ii}} \left[b_i - \sum_{j=1}^{i-1} a_{ij} x_j^{(m+1)} - \sum_{j=i+1}^{N} a_{ij} x_j^{(m)} \right], \quad i = 1, 2, 3, ...N. \tag{B.21}$$

Suppose we let x_i^* denote the ith component of the solution obtained by the Gauss-Seidel method (Equation (B.21)). Let r be the so-called *relaxation parameter* or *relaxation factor*. The convergence rate of iterations can be improved by defining the weighted average

$$x_i^{(m+1)} = (1-r)x_i^{(m)} + rx_i^*, \tag{B.22}$$

$$= x_i^{(m)} + r(x_i^* - x_i^{(m)}), \tag{B.23}$$

$$= x_i^{(m)} + r\Delta x_i. \tag{B.24}$$

Then replacing x_i^* by Equation (B.21) gives the general i^{th} equation:

$$x_i^{(m+1)} = x_i^{(m)} + r \left[\frac{1}{a_{ii}} \left(b_i - \sum_{j=1}^{i-1} a_{ij} x_j^{(m+1)} - \sum_{j=i+1}^{N} a_{ij} x_j^{(m)} \right) - x_i^{(m)} \right], \quad i = 1, 2, 3, ...N. \tag{B.25}$$

Relaxation methods include Successive Over-Relaxation (SOR) and Successive Under-Relaxation (SUR) methods. These methods differ only in the value of the relaxation factor r. If $0 < r < 1$, the procedure is called under-relaxation and if $1 < r < 2$, this technique is called over-relaxation, and if $r = 1$, the system becomes similar to the Gauss-Seidel method. So this method is merely a developed version of the Gauss-Seidel method, which is in turn is just a modification of the Jacobi iterative method [31]. The rate of convergence of relaxation methods depends on the choice of relaxation factor; if r is chosen properly, then the system may converge faster than the other two iterative methods [1]. While writing the numerical code for relaxation methods, one should always consider the relaxation parameter as an input.

Finally in this discussion, there are two separate criteria on which the algorithm for relaxation methods can be stopped: (i) satisfaction of iteration convergence tolerance, and (ii) exceeding the maximum permitted number of iterations. The second of these is more important, because

no one knows ahead of time whether the convergence to the required tolerance level can be obtained. If due to round off errors, it cannot be achieved, then iterations would continue forever unless they are forcefully stopped because of exceeding the maximum designated allowed number [31].

B.1.1   Convergence of linear methods

In this subsection, a short summary about the convergence of iterative methods is given in the form of a table. In Table B.3, the preferred solution method is given with the required storage for a typical implementation, and total floating-point arithmetic required to obtain the solution and presented in terms of N, the order of the system.

It is known [31] that the convergence rate of relaxation methods is highly dependent on the optimal value of relaxation factor r. Clearly, this is an disadvantage. For an optimal value of r, only $O(N^{1.5}) \sim O(N)$ arithmetic operations are required in $2D$. But for other than optimal values of r, as many as $O(N^2)$ arithmetic operations are needed.

On the other hand, it is important to note that the number of operations per iteration of relaxation methods is far less than that for essentially any other method. Although its rate of convergence may be smaller than any other method, it is often still used because of its simple numerical coding.

Analytically, the optimal value of r can be derived for Poisson/Dirichlet problems in a rectangular domain [31]. Thus the treatment of relaxation methods is mainly efficient for constant coefficient Dirichlet problems.

Table B.3: *Summary for convergence of linear systems.*

System matrix	Preferred method	Storage	Arithmetic
Nonsparse	Direct elimination	$O(N^2)$	$O(N^3)$
Sparse	Iteration, e.g., SOR	$O(N^2)$	$O(N^{1.5}) \sim O(N)$
Sparse, compactly banded	Sparse band LU decomposition	$O(N^2)$	$O(N)$

Bibliography

[1] F. Ahmad and M. A. Rana. *Elements of numerical analysis*. National Book Foundation, Islamabad, Pakistan, 1998.

[2] G. F. Al-Sumaily. Forced convection heat transfer from a bank of circular cylinders embedded in a porous medium. *Journal of Heat Transfer*, 136:1–11, 2014.

[3] G. F. Al-Sumaily, J. Sheridan, and M. C. Thompson. Analysis of forced convection heat transfer from a circular cylinder embedded in a porous medium. *International Journal of Thermal Sciences*, 51:121–131, 2012.

[4] A. Ali, R. McKibbin, and W. L. Sweatman. Fluid flow and solute transport in un-evenly-stratified groundwater aquifers. In K. Vafai, editor, *Proceedings of Porous Media and its Applications in Science, Engineering, and Industry, Fourth International Conference (ICPM4), Potsdam, Germany*, volume 1453, pages 11–16. American Institute of Physics, 17-22, June 2012.

[5] A. Ali, R. McKibbin, and W. L. Sweatman. Simplified modelling of pollutant transport in stratified groundwater aquifers. In R. Seppelt, A. A. Voinov, S. Lange, and D. Bankamp, editors, *Proceedings of International Environmental Modelling and Software Society (iEMSs), International Congress on Environmental Modelling and Software Managing Resources of a Limited Planet, Sixth Biennial Meeting, Leipzig, Germany*, pages 2739–2746, 2012.

[6] A. Ali, R. McKibbin, and W. L. Sweatman. A simplified model for transport in aquifers. In *Proceedings of the 5th International Conference on Porous Media and its Applications in Science and Engineering ICPM5, Kona, Hawaii*, pages 6–25, 22-27, June 2014.

[7] A. Ali, W. L. Sweatman, and R. McKibbin. Pollutant transport and its alleviation in groundwater aquifers. In M. Fontes, M. Günther, and N. Marheineke, editors, *Progress in Industrial Mathematics at ECMI 2012, Mathematics in Industry*, volume 19, pages 53–58. Springer, 2014.

[8] A. Azizullah, M. N. K. Khattak, P. Richter, and Donat-Peter Hader. Water pollution in Pakistan and its impact on public health − A review. *Environment International*, 37:479–497, 2011.

[9] H. M. Badr and I. Pop. Combined convection from an isothermal horizontal rod buried in a porous medium. *International Journal of Heat and Mass Transfer*, 31(12):2527–2541, 1988.

[10] G. K. Batchelor. *An introduction to fluid dynamics.* Cambridge University Press, 1967.

[11] J. Bear. *Dynamics of fluids in porous media.* Constable, United Kingdom, 1972.

[12] J. Bear and Y. Bachmat. *Introduction to modeling of transport phenomena in porous media*, volume 4th. Kluwer, Dordrecht, The Netherlands, 1991.

[13] J. Bear and A. Verruijt. *Modeling groundwater flow and pollution.* D. Reidel, Dordrecht, Holland, 1978.

[14] A. Bejan. *Convection heat transfer.* J. Wiley and Sons, Hoboken, New Jersey, 4th edition, 2013.

[15] D. T. Burr, E. A. Sudicky, and R. L. Naff. Nonreactive and reactive solute transport in three-dimensional heterogeneous porous media: Mean displacement, plume spreading, and uncertainty. *Water Resources Research*, 30:791–815, 1994.

[16] P. Cheng. Heat transfer in geothermal systems. *Adv. Heat Transfer*, 14:1–105, 1978.

[17] P. Cheng. Mixed convection about a horizontal cylinder and a sphere in a fluid-saturated porous medium. *International Journal of Heat and Mass Transfer*, 25(8), 1982.

[18] I. G. Currie. *Fundamental mechanics of fluids.* McGraw-Hill, United States of America, 1974.

[19] M. P. Dalwadi, D. O'Kiely, S. J. Thomson, T. S. Khaleque, and C. L. Hall. Mathematical modeling of chemical agent removal by reaction with an immiscible cleanser. *SIAM Journal on Applied Mathematics*, 77(6):1937–1961, 2017.

[20] H. Darcy. Flow through porous media. *Les Fontaines Publiques de La Ville de Dijon, Victor Dalmont, Paris*, 1856.

[21] S. V. Garimella and D. J. Schlitz. Heat transfer enhancement in narrow channels using two and three- dimensional mixing devices. *Journal of Heat Transfer*, 117:590–596, 1995.

[22] L. W. Gelhar, C. Welty, and K. R. Rehfeldt. A critical review of data on field-scale dispersion in aquifers. *Water Resources Research*, 28(7):1955–1974, 1992.

[23] C. F. Gerald and P. O. Wheatley. *Applied Numerical Analysis*. Addison-Wesley Publishing Company, 5th edition, 1994.

[24] D. B. Ingham and I. Pop. Transport phenomenon in porous media. *Pergamon, Oxford*, 2, 1979.

[25] D. B. Ingham and I. Pop. Natural convection about a heated horizontal cylinder in a porous medium. *Journal of Fluid Mechanics*, 184:157–181, 1987.

[26] A. Jourak, J. Gunnar, I. Hellstrm, T. Staffan Lundstrm, and V. Frishfelds. Numerical derivation of dispersion coefficients for flow through three-dimensional randomly packed beds of monodisperse spheres. *Transport Phenomena and Fluid Mechanics*, 60:749–761, 2014.

[27] S. Kakac, B. Kilkis, F. A. Kulacki, and F. Arine. Convective heat and mass transfer in porous media. *Kluwer, Dordrecht*, 1991.

[28] K. Kannan and K. R. Rajagopal. Flow through porous media due to high pressure gradient. *Applied Mathematics and Computation*, 199:748–759, 2008.

[29] S. Kimura. Transient forced convection heat transfer from a circular cylinder in a saturated porous medium. *International Journal of Heat and Mass Transfer*, 32(1):192–195, 1989.

[30] M. Layeghi and A. Nouri-Borujerdi. Fluid flow and heat transfer around circular cylinders in the presence and no-presence of porous medium. *Journal of Porous Media*, 7(3):239–247, 2004.

[31] J. M. McDonough. *Lectures in basic computational numerical analysis.* 2007.

[32] R. McKibbin. Groundwater pollutant transport: Transforming layer models to dynamical systems. *An. St. Univ. Ovidius Constanta, Ser.Mat*, 17(3):183–196, 2009.

[33] R. McKibbin. Some aspects of modelling pollutant transport in groundwater aquifers. In L. H. Weiranto and S. R. Pudjaprasetya, editors, *Proceedings of CIAM, Conference On Industrial and Applied Mathematics*, pages 9–16. Institut Teknologi Bandung, Indonesia, 6-8, July 2010.

[34] R. McKibbin and S. Kimura. Heat flow from a buried cylindrical tank partially submerged in groundwater. In *Proceedings of the 5th International Conference on Porous Media and its Applications in Science and Engineering ICPM5*, Kona, Hawaii, 22-27, June 2014.

[35] J. H. Merkin. Free convection boundary layers on axisymmetric and two-dimensional bodies of arbitrary shape in a saturated porous medium. *International Journal of Heat and Mass Transfer*, 22(10):1461–1462, 1979.

[36] S. V. S. S. N. V. G. Krishna Murthy, B. V. Rathish Kumar, and M. Nigam. A parallel finite element study of $3D$ mixed convection in a fluid saturated cubic porous enclosure under injection/suction. *Applied Mathematics and Computation*, 269:841–862, 2015.

[37] V. D. Murty, M. P. Camden, C. L. Clay, and D. B. Paul. A study of non-darcian effects on forced convection heat transfer over a cylinder embedded in a porous medium. *Journal of Heat Transfer*, pages 201–206, 1990.

[38] S. P. Neuman. *Universal scaling of hydraulic conductivities and dispersivities in geological media*, volume 26. Water Resources Research, 1990.

[39] D. A. Nield and A. Bejan. *Convection in porous media*. Springer-Verlag, New York, 3rd edition, 2006.

[40] C. Orndorff, S. Ponomarev, W. Dai, and A. Bejan. Thermal analysis in a triple-layered skin structure with embedded vasculature, tumor, and gold nanoshells. *International Journal of Heat and Mass Transfer*, 111:677–695, 2017.

[41] I. Pop and P. Cheng. Flow past a circular cylinder embedded in a porous medium based on the brinkman model. *International Journal of Engineering Science*, 30(2):257–262, 1992.

[42] I. Pop and D. B. Ingham. Convective heat transfer: Mathematical and computational modelling of viscous fluids and porous media. *Pergamon, Oxford*, 2001.

[43] I. Pop and B. Yan. Forced convection flow past a circular cylinder and a sphere in a darcian fluid at lage peclet numbers. *International Communications in Heat and Mass Transfer*, 25(2):261–267, 1998.

[44] T. A. Prickett. Modelling techniques for groundwater evaluation. *In Advances in Hydroscience*, pages 1–113, 1975.

[45] D. A. S. Rees, A. P. Bassom, and I. Pop. Forced convection past a heated cylinder in a porous medium using a thermal non-equilibrium model: boundary layer analysis. *European Journal of Mechanics, B/Fluids*, 22(5):473–486, 2003.

[46] N. H. Saeid. Analysis of free convection about a horizontal cylinder in a porous media using a thermal non- equilibrium model. *International Communications in Heat and Mass Transfer*, 33(2):158–165, 2006.

[47] T. Sano. Unsteady heat transfer from a circular cylinder immersed in a darcy flow. *Journal of Engineering Mathematics*, 14(3):177–190, 1980.

[48] M. K. Singh and P. Das. Analytical solution for solute transport modeling along the unsteady groundwater flow in porous medium. *Journal of the Geological Society of India*, (4):130–135, 2016.

[49] M. K. Singh, V. P. Singh, and P. Das. Mathematical modeling for solute transport in aquifer. *Journal of Hydroinformatics*, pages 481–499, 2016.

[50] J. Thevenin and D. Sadaoui. About enhancement of heat transfer over a circular cylinder embedded in a porous medium. *International Communications in Heat and Mass Transfer*, 22(2):295–304, 1995.

[51] C. L. Tien and K. Vafai. Convective and radiative heat transfer in porous media. *Adv. Appl.Mech*, 27:225–281, 1990.

[52] D. K. Todd and L. W. Mays. *Groundwater hydrology*. J. Wiley and Sons, Hoboken, New Jersey, 3rd edition, 2005.

[53] K. Vafai. *Handbook of porous media*. Marcel Dekker, New York, 2000.

[54] O. A Van Herwaarden. Spread of pollution by dispersive groundwater flow. *SIAM Journal of Applied Mathematics*, 54:26–41, 1994.

[55] R. S. Varga. *Matrix Iterative Analysis*. Springer-Verlag, 2nd edition, 2002.

[56] H. F. Wang and M. P. Anderson. *Introduction to groundwater modelling, finite difference and finite element methods*. W. H. Freeman and Company, 1982.

[57] W. S. Wong, D. A. Rees, and I. Pop. Forced convection past a heated cylinder in a porous medium using a thermal non-equilibrium model: finite peclet number effects. *International Journal of Thermal Sciences*, 43(3):213–220, 2004.

[58] M. Xu and Y. Eckstein. Use of weighted least squares method in evaluation of the relationship between dispersion and field scale. *Ground Water*, 33(6):905–908, 1995.

[59] D. M. Young. *Iterative Solution of Large Linear Systems*. Dover, 2003.

[60] M. J. Zhou and R. C. Lai. Aiding and opposing mixed convection from a cylinder in a saturated porous medium. *Journal of Porous Media*, 5(2):103–111, 2002.